Co-operative degradation in thin films of poly(methyl methacrylate) and poly(ethyleneterephthaiate): a c[methyl methacrylate) and Poly(ethyl(

Mark Russell Hodgson

Co-operative Degradation in Thin Films of Poly(methyl methacrylate) and Poly(ethylene terephthalate)

Mark Russell Hodgson

A thesis submitted for the degree of Doctor of Philosophy at the University of Durham

September 2000

Table of Contents

Abstract

Co-operative degradation in Thin Films of Polymethyl methacrylate and Polyethylene terephthalate.

Mark Hodgson, PhD thesis, September 2000

The interaction between thin films of polymethyl methacrylate and polyethylene terephthalate is reported. Studies of bulk PET/PMMA blends reveal that a direct ester exchange reaction occurs between the two polymers, and this information is used in the investigation of thin film interfaces between PET and PMMA. Discrete wavelength ellipsometry has been used to study the thermal decomposition of thin films of PMMA , and the crystallisation of thin films of PET. It is found that, below ~ 74.5 nm ($6 \times R_g$), the rate of degradation of PMMA (M_N ~ 44,000), increases with decreasing film thickness. For films < 100 nm , the rate of crystallisation of PET (M_N ~ 23,000), is found to decrease with decreasing film thickness. Using data obtained from neutron reflectometry, the equilibrium interfacial width between PET and dPMMA is measured. At an annealing temperature of 493K, the interface is broadened by crystalline roughness in the PET phase, and the maximum interfacial width is found to be ~7.7nm. At 573K, despite extensive degradation of dPMMA, an equilibrium interfacial width of ~5nm is achieved. Capillary wave broadening and the effects of asymmetry are considered. A detailed analysis of Interfacial Marker Movements, reveals that there is an asymmetric broadening of the gold markers towards the PMMA side of the interface, indicative of a grafting reaction between PET and PMMA or a crosslinking reaction within the residual PMMA layer. The degradation of PET films, treated with acrylic based coating formulations has been studied by GPC, UV-vis spectrophotometry, and weight loss techniques. The rate of chain scission at 563K is seen to be dependant on the the concentration of tri methoxy methyl melamine (TMMM), the coating crosslinking agent.

Acknowledgements

I owe a huge debt of gratitude towards my supervisor, Professor Randal Richards. Without his support, patience, understanding and wisdom this thesis would not have been possible. I am also grateful to the assistance I have received from other residents of the Durham IRC, past and present, particularly, Professor Jim Feast, Dr. Stella Peace and Dr. Richard Thompson.

I would also like to thank my industrial supervisors, Bill MacDonald and Julian Robinson for guiding me through the logistical minefield of combining part - time study and full - time employment. Several others in DuPont Teijin Films have helped me in many ways and of honourable mention are Bill Brennan, Steve Sankey, Duncan Mackerron, and Steve Restorick.

I would also like to thank Dr Neil Everall and Alan Titerton of ICI plc for their tutelage and encouragement throughout the course of my research.

Finally I would like to thank my family for their unending support. To David, and Emma, for not complaining too much, and most importantly to Helen, without whom I would never have started, and could never have finished.

Memorandum

The work reported in this Thesis was carried out at the interdisciplinary Research Centre in Polymer Science and Technology at the University of Durham, and the Wilton Materials research Centre, between October 1994 and September 1999. The work has not been submitted for any other degree and is the original work of the author except where acknowledged by an appropriate reference.

Financial Support

I gratefully acknowledge the funding provided by EPRSC for neutron beam time, and DuPont Teijin Films Inc.

For Helen, David and Emma, who all deserve so much more;
and for my parents in the hope that I might make them proud.

Chapter 1

Introduction.

1.1. Background to Project.

In order to enhance their performance, poly(ethylene terphthalate) (PET) films are routinely coated with materials which impart desirable properties to the surface of these films [1]. These coatings are often used as adhesive layers to inks, lacquers and dyes; barrier layers for packaging applications [2], or intermediary layers in the construction of photographic films [3]. Although the performance of these coated products is well understood in terms of the functionality of the surface treatment, the interactions of the components of a typical coating with the base film have rarely been investigated. For instance, the adhesion of the coating to the PET film itself is a poorly understood phenomena, much of the knowledge is taken from the results of work conducted in the paint industry [4].

On a more general level, the burgeoning interest in the properties of polymer / polymer interfaces has, to some extent, ignored commodity polymers such as PET and nylon, presumably because of their relative insolubility and semi-crystalline nature, factors which complicate the analysis of interfacial studies [5]. A greater understanding of interfaces between PET and other polymers is therefore desirable from an academic and an industrial perspective.

It has been known for many years that the coatings applied to poly(ethylene terephthalate) film have an adverse effect on the reclaimability of the film; i.e. the quality and colour of the recycled material is compromised by the presence of a surface coating [1]. The reasons for this are still poorly understood, despite the extensive work that has been undertaken on the degradation of PET itself [6]. Investigation of this apparent increase in degradation is therefore necessary in order that the recycling of PET films can be fully optimised in terms of product performance and manufacturing economics. This thesis describes research that addresses the issues described above.

1.2. Poly(ethylene terephthalate).

1.2.1. Properties of PET.

Poly(ethylene terephthalate) (PET), was first prepared in 1941 by J.R. Whinfield and J.T. Dickson [7] of the Calico Printers Association, and despite the complex nature of its polymerisation, was rapidly commercialised as a synthetic fibre and a biaxially orientated film. PET has the repeat unit shown in figure 1.1.

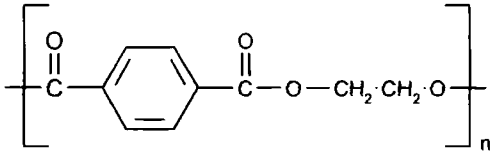

Figure 1.1 Repeat unit of PET.

The linear character of its structure gives the polymer a high propensity for crystallisation when cooled from the melt phase (~528K) or heated above it's glass transition temperature (~350K). The degree of crystallinity that PET can exhibit determines many properties that have direct consequences on its processing and performance.

The rate of crystallisation and maximum degree of crystallinity obtainable, increase with temperature up to a maximum at about 443K. The density of PET increases with crystallinity; amorphous material has a density of ~1.33g/cm^3 while prolonged crystallisation at 443K yields polymer with a maximum density of ~1.4g/cm^3 [8].

Film produced from PET has excellent mechanical and thermal stability, particularly when the film is biaxially orientated. Biaxially orientated material is also produced by the 'blowing' process, which is particularly effective in the preparation of beverage bottles [9]. The combination of high mechanical strength, good thermal stability and a controllable morphology have established PET as one of the most important thermoplastics in world production today.

1.2.2. Synthesis of PET.

PET is formed by the polycondensation of oligomeric bis-hydroxy ethyl terephthalate (BHET), which is itself formed by the condensation of ethylene glycol (EG) with dimethyl terephthalate (DMT), or terephthalic acid (TA). For many years the transesterification of DMT was the only commercially viable large scale production route, but with the advent of bulk production of pure terephthalic acid, the direct esterification process has taken on much more significance. The advantages and drawbacks of both processes will now be reviewed briefly.

BHET from transesterification of DMT and EG.

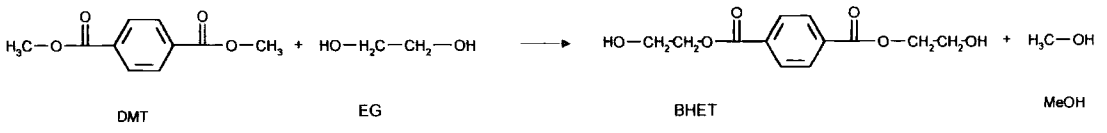

Scheme 1.1 Transesterification of DMT / EG

Scheme 1.1 outlines the general process. The progress of the reaction is monitored by the distillation of methanol; i.e. when the theoretical yield for 100% transesterification has been distilled the reaction is assumed to have reached completion. Although molar ratios of unity should be adequate, in reality a molar ratio of 1:2.2 DMT:EG is used in order to drive the reaction forwards. In all practical circumstances the reaction is accelerated catalytically; a vast number of metals and their derivatives having been claimed to be effective [10,11]. However only salts of Mn, Pb, Co, Zn are usually used.

BHET from esterification of TA by EG

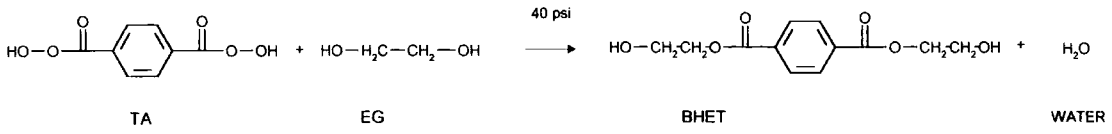

Scheme 1.2. Direct Esterification of TA / EG

Scheme 1.2. outlines the general process. The reaction is monitored by the distillation of water, and can also be catalysed [13], but does not need to be; the reaction proceeds at an adequate rate using a molar ratio of 1:1.5 TA:EG. The carboxylic acid groups of the TA catalyse the reaction , which is carried out under pressure (~40psi) and high temperature (~523K) [1,11,14].

The choice of first stage reaction in PET production is dependant on local raw material supply economics and regional health and safety regulations. Until recently the production of PET in the USA was almost exclusively by the DMT route. However, TA direct esterification is becoming the preferred route because of three primary factors;

1) Higher reaction rate and lower ethylene glycol consumption.
2) Reduced catalytic requirements.
3) Elimination of methanol as distillation product.

The advantages of a faster reaction are obvious and lower consumption of EG is financially more favourable. It has been suggested that the transesterification catalysts used in the DMT route have an adverse effect on the thermal and thermoxidative stability of PET [11,12], as they are thought to catalyse the thermal degradation of PET. The toxicity of methanol is also a factor in the selection of the route to be used.

It must be noted, however, that a major disadvantage of PET produced from TA is that it contains higher amounts of copolymeric diethylene glycol (DEG) than polymer produced from DMT [11]. DEG severely effects the thermal, thermoxidative, photo and

mechanical stability of PET [11,12,15], and has also been shown to influence the morphology of the solid polymer [16].

Polymerisation of BHET

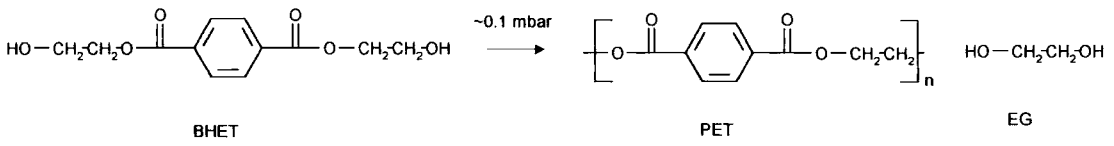

Scheme 1.3. Polycondensation of PET

The reaction proceeds with the loss of ethylene glycol (scheme 1.3), and an increase in melt viscosity (and therefore molecular weight), of the reaction vessel contents. This is usually monitored via the power load on the vessel agitator or stirrer, which, in commercial processes, is calibrated against resultant intrinsic viscosity (i.v.) of the polymer. Consequently the reaction end point can be determined, for a desired final molecular weight.

The melt condensation of BHET is also accelerated catalytically [11,12,14]. The catalysts used in the polycondensation of PET have been shown to exhibit a detrimental effect on the polymer stability [10,12], presumably in the same manner as the transesterification catalysts previously discussed.

Stevenson and Nettleton [17], have shown that, using antimony trioxide as catalyst, only oligomeric BHET is actually converted to PET, claiming that monomeric BHET and antimony trioxide form an inactive complex. Their study is based heavily on work by Challa [18], who studied uncatalysed polymerisations to establish kinetic expressions for the forward (polycondensation), reverse (glycolysis), and redistribution (transesterification) reactions occurring during melt condensation of BHET. The assumption that the polycondensation reaction is second order with respect to end groups was made by both parties. Further work by Santacesaria *et al*, has shown that, assuming monomeric BHET is the starting point for polycondensation is inadequate when describing the complex kinetics of polymerisation [19].

The elimination of the known degradative character of the transesterification and polycondensation catalysts, has received much attention in the literature [20,21]. It has been shown that the addition of phosphorous based 'stabilisers' at the end of the first stage of PET manufacture, yields polymer with increased thermal stability and sometimes a more aesthetically pleasing appearance [11,12,20]. Commonly, phosphoric acid, triphenyl phosphate and triphenyl phosphite are used [20,21].

There is still uncertainty over the mechanism by which phosphorous based additives enhance thermal stability. It has been suggested that the transesterification and/or polycondensation catalysts are rendered inactive by the formation of phosphate complexes [11,12,20]. However, other processes have been considered including a chain extension mechanism, and a reduction of DEG content [21].

1.3. PET Film.

1.3.1. General Film Process.

Several different processes have been developed for film manufacture [22]. This reflects the diversity of polymers used for films and also the variety of end uses of and properties of these films. Currently films can be produced by slit die extrusion (polyether sulphone, polyether-ether ketone), calendering (polyvinyl chloride), solvent casting (cellulose actate), blow extrusion (polypropylene), or the stenter process (polystyrene, polyethylene). PET is routinely produced as a biaxially orientated film via the stenter process; although increasing demands for ultra thin films (<5μ) has seen the advent of a variation of this process, namely the simultaneous biaxial stenter (SBS)[23].

Polymer processing by the stenter process can be achieved in one of two ways. Polymer can be cast into the filming process by extrusion, or nascent polymer can be cast immediately after manufacture from a continuous polymerisation operation. If the later process is used then the film line is said to be 'coupled'. The advantage of using an extrusion fed line is that different polymer types and grades can be interchanged rapidly, creating a flexible manufacturing asset. The advantage of a coupled process is the increase in product uniformity created by using 'as manufactured' polymer. The films and processes considered in this thesis are all derived from an extrusion fed, stenter

process, and hence this is the process which will now be described. This process is described diagramattically in figure 1.2.

1.3.2. Extrusion and Casting.

PET chip is first dried in order to eliminate any sorbed water from the polymer. Dry polymer is essential as thermal melt hydrolysis has been shown to occur [24], even at very low water concentrations. The particular conditions of drying are also important in the subsequent processing of the polymer [25], and care is taken not to dry the polymer for too long, as additional chemical and physical processes can occur [26]. Dry polymer is then extruded through a slot die and rapidly quenched on a cold casting drum (~283K) to yield an amorphous sheet. If the quenching rate is too slow during casting, crystallites will start to form in the polymer [27], resulting in a brittle cast which cannot be processed further.

1.3.3. Forward Draw Stage.

Cast amorphous sheet is then reheated to approximately 358K, i.e. above the glass transition temperature, (T_g ~ 350K), allowing the film to be drawn along the machine direction. This stage is known as the 'forward draw' stage and induces some stress crystallisation (10-20%) in the film [28]. Forward drawing is physically achieved by increasing the speed of transport rolls after the heating stage relative to the transport rolls stationed before the heating stage. A forward draw ratio can be defined;

$$\text{FWD ratio} = \frac{v_f}{v_s} \tag{1.1}$$

where v_s is the speed of the rolls before the draw point, and v_f is the speed of the rolls after the draw point. Immediately after the draw, the film is quenched by means of a chilled roller. The film is said to be uni-axially orientated, whereby the main axes of the crystallites formed, are aligned in the direction of draw [1,23]. This process increases the mechanical strength of the film in the machine direction (MD).

1.3.4. Transverse Stretching and Film Annealing.

The forward drawn film is again heated above T_g and drawn in the direction perpendicular or transverse, to the machine direction by a similar factor to the forward draw process. Additional stress induced crystallisation occurs (25-40%), and the film is said to be biaxially orientated, with the crystallite axes orientated about an axis normal to the plane of the film, but dependant upon the web position [29]. The alignment of the main crystallite axes with the draw stress produces a 'bow angle' in the film, and the film is therefore anisotropic, and for optically transparent films, 3 refractive index values can be measured (2 in the plane of the film, MD and TD, and 1 normal to the plane of the film) [30] The mechanical properties of the film are said to be balanced.

The sideways draw is effected by two sets of chain driven clips which grab the edges of the film, pulling the film forwards and, as the chains diverge the film is stretched sideways. A sideways draw ratio can be defined by the following relationship

$$\text{SWD ratio} = \frac{d_s}{d_i} \tag{1.2}$$

where d_s is the width of the film immediately after draw, and d_i is the width of the film as it enters the draw station. This process produces an edge to the film which has not experienced the sideways draw and hence, has a different morphology to the rest of the film. This edge is usually removed during the winding of the film. After the sideways draw the film is annealed to increase the crystallinity still further (~50%), reducing the tendency of the film to shrink on heating (by further crystallisation), and producing a tough, dimensionally stable and relatively inert, flat film.

1.3.5. Film Winding.

After heat setting, film exits the stenter and enters the winding station. Here the edge trim is removed from the film and sent directly for recovery. This recovery operation is effected by a flake cutter [31], which produces material which can be dried, and re-fed to the polymer feedstock. The film can either be slit to the correct width during winding or is wound as one reel, the full width of the production unit, called a

mill roll. The rolls produced are checked in quality control tests and then taken for further conversion or packaged for dispatch.

Winding is an important stage in film production, and care has to be taken to avoid film from creasing, folding and puckering. Tension control and roller alignment are therefore paramount factors in producing reels of high quality.

1.4. Film Coating.

1.4.1. Coating PET Films.

Coatings can be applied to films in a variety of ways and at various stages during and after manufacture. Off line coating operations are common and offer cheap and flexible options for enhancing film performance. In line coating processes i.e. treatment of the film during the production of the film itself, are somewhat limited with respect to the type and thickness of coating which can be sustained by the film making process. The high temperatures (~493K), which stenter ovens operate at during film production, negate the use of volatile and flammable organic solvents as media for in-line coating formulations; generally only water based systems can be used in pre-stenter or inter-draw coating operations. However, the availability and ever expanding range of water based resins and polymers has ensured a strong research and development basis for this process [4, 32].

The preferred design of an in-line coater varies between film producers, but the basic principle of application remains then same. One of the most popular methods of in-line coating is the 'kiss coating' method [33]. In this procedure the coating is applied to the film by an applicator roll which kisses the film and thus transfers a coating to the film surface. One configuration of for an in-line coater for 2 side coating is shown in figure 1.3. The applicator roll is itself wetted by a gravure roll, which has 'cells' engraved or etched into its surface. The size, depth and shape of these cells determines the amount of solution which can be held by the gravure, and hence determines the amount of solution transferred to the applicator roll and then the film.

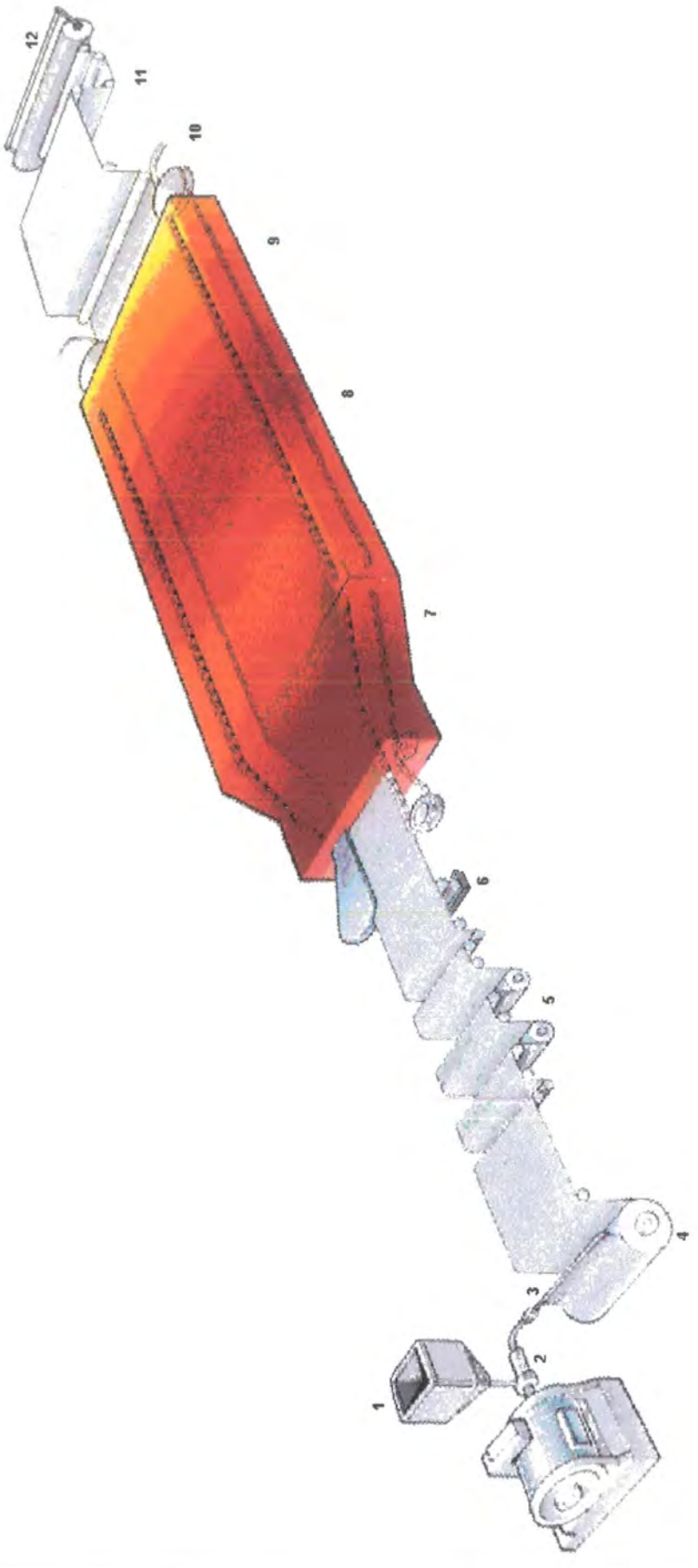

Figure 1.1. Standard extrusion fed, sequential draw stenter process for flat PET film manufacture. 1. Polymer delivery. 2. Extruder. 3.Die. 4. Casting drum. 5. Forward draw section. 6. In-line coating station. 7. Transvers draw. 8. Heat set zones. 9. Quench zone. 10.Edge trim. 11. Transport section. 12 Winding.

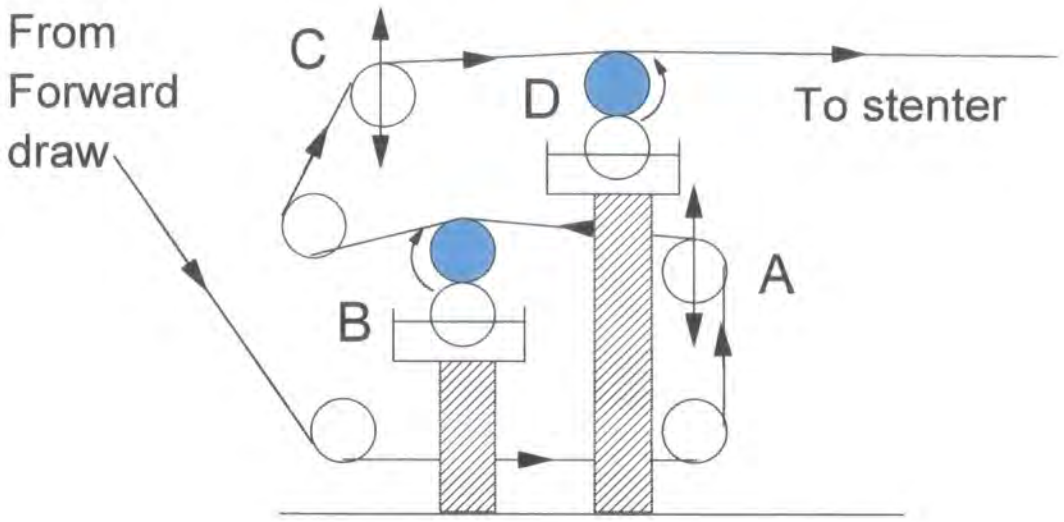

Figure 1.3. Two side coater configuration. A and C, height adjustable transport rollers for moving film onto and off coating heads as required. B, bottom head coater; D, top head coater.

1.4.2. Coating Formulation Chemistry.

Here, only the coatings applied during film manufacture to Melinex® will be discussed. These coatings are all aqueous based, and have finished dimensions of 10 - 100 nm typically. The particular nature of the coating will depend upon the application into which the film will be sold. For instance, a film offering static protection will have a surface coating comprised of chemical species which have the ability to dissipate static charge [34]. Films intended for the food packaging applications may have a coating which provides a mechanical barrier to the transport of oxygen and other gaseous species through the film [2].

As all of the coatings applied during film manufacture are deposited from aqueous solution, then the components of these coatings must be water soluble or water dispersable. For this reason many of the coatings used are in the form of aqueous emulsions and latexes of addition polymers.

Another requirement of the coatings is that they provide continuous surface coverage, (there are some specific applications which require a discontinuous coating

but these will not be discussed here). To do this the coating must be formulated to wet the surface of the film, hence a wetting agent or surfactant is normally required. The coating must not crack or fracture during the drying and winding operations, and must be able to flow with the sideways draw procedure. Therefore, if the major coating component is polymeric, it must exhibit a T_g below the draw temperature of the film, (typically 383K, see figure 1.2).

Further requirements of a coating formulation are made depending upon the application and type of film. For instance, many coatings will need to display a high degree of optical clarity when applied to unfilled (transparent) films. Other requirements for coatings are their influence on gloss, slip, abrasion resistance, colour and regulatory approvals for food contact.

A typical coating formulation may be listed as follows (all as % solids in volume);

1) Functional component (anti-stat, latex, etc)	~5%
2) Wetting agent (surfactant)	~0.2%
3) Cross-linking agent	~0.5%
4) Cross-linker initiator	~0.05%

As already stated, the selection of a functional component depends upon the required effect and application. The surfactants used must be able to fully wet the PET surface in the short time before the coating dries (see figure 1.2). Common surfactants are of the alkyl phenol ethoxylates (APE's), which have the general chemical structure shown in figure 1.4.

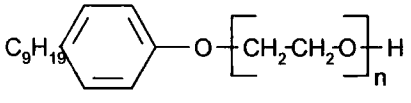

Figure 1.4. Structure of alkyl phenol ethoxylates.

The effectiveness of these surfactants plays an important role in the coating process. If complete wetting is not achieved then the coating defects such as poor adhesion and retraction spots will be in evidence. This in turn will lead to product

failure. Hence, the formulation of coatings for PET depends critically upon matching the surface tension of the coating solution with the surface energy of PET[35]. Further complications arise if the coating is in latex form, where factors controlling the film formation of such a system need to be considered [36]. The overall process of latex film formation has been researched in considerable detail [37], but a detailed discussion lies outside the scope of this thesis.

Crosslinkers are needed to effect adhesion between the coating and the film, and to impart the necessary durability to the coating required for the subsequent handling of the film. Many coating formulations use melamine formaldehyde based resins as cross linkers, commonly used in a water based paints and coatings, decorative emulsions, and automative coatings [38]. The general structure is based upon Hexamethoxy-methyl melamine (figure 1.5), although variations with different levels of alkylation are also used [39].

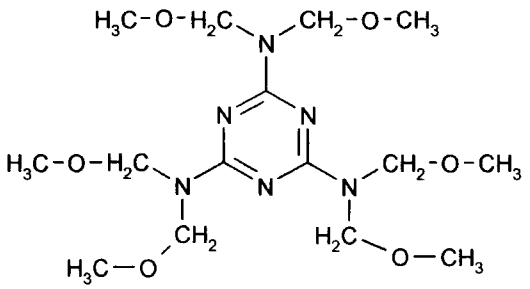

Figure 1.5. structure of hexamethoxy methyl melamine (HMMM).

The reaction of HMMM and related resins is known to be acid catalysed (scheme 1.4), hence the inclusion of acid based initiators within coating formulations [38]. Derivatives of HMMM have methoxy groups replaced by hydroxyl functionality's [38,39], and many have been shown to react with carboxyl and hydroxyl functionality's, as shown in scheme 1.5. Acrylic based coatings in particular, are well suited to curing with melamine formaldehyde resins, and much work has been conducted on the chemistry of melamine / acrylic coatings [40].

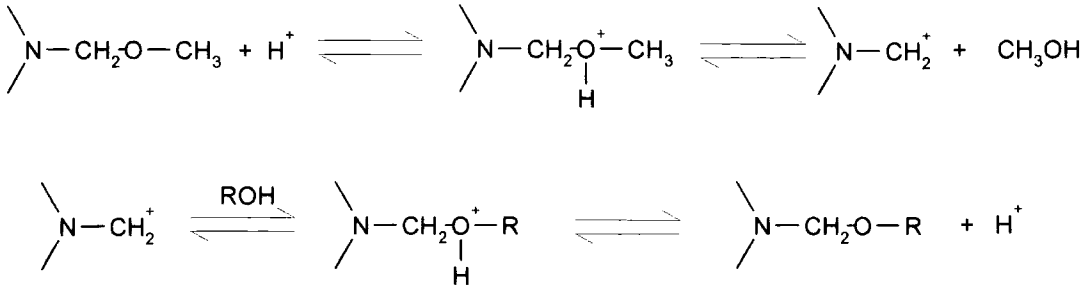

Scheme 1.4. Acid catalysis of HMMM resins with hydroxyl containing polymer.

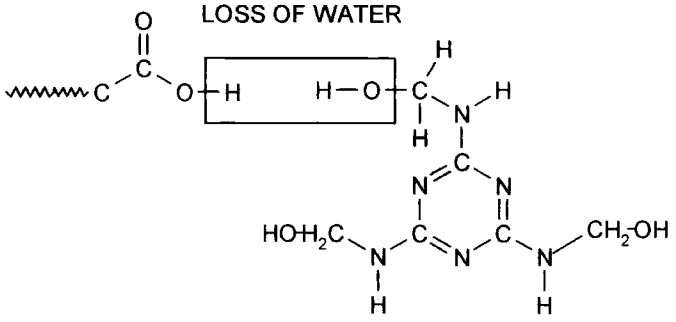

Scheme 1.5. Reaction of carboxyl functionality with MF derivative. The reaction proceeds via the elimination of water.

The effectiveness of any given coating depends upon many factors; the interaction of the individual components with each other; the possible interactions with the base film; the conditions of draw and heat set in the stenter oven and overall thickness of the coating.

1.5. Film Recovery / Reclaimability.

Not all film made during production is suitable for distribution or sale. As already mentioned edge 'trim' is removed from the film as it has a different morphology and thickness to the rest of the web, and would therefore compromise film performance

and hinder proper reel formation during winding. Scrap film from start up and shut down procedures is also of no commercial use, as are reels which have failed the quality control assessment. All this material is potentially useful as recycled feedstock, i.e. the film is converted to a form where it can be used as polymer feedstock. This conversion can be achieved in several ways. One way is to hydraulically fold and crush the film into a ribbon which can then be cut into a process able form. a process known as direct palletising. A more common reclaim procedure is to first 'flake' the film in large rotary cutters [31], and then to either convert the flake to conventional PET chip via re-extrusion or to feed the flake directly into the polymer feed for the film process.

All these recycling procedures lead to PET of inferior quality, i.e. yellow discolouration, lower molecular weight, higher propensity for gel formation etc. [41], and the amount of reclaimed PET in any product therefore needs careful monitoring and control. The problem is further pronounced when the film being recycled has been coated [1]. Some coatings render the film totally unacceptable for reclaim [42]; the level of discolouration produced is too great, and the aesthetic quality of the resultant film is too low, even at very low reclaim loading. This can be of great inconvenience to film producers as some coatings can be made in virgin only processes, any scrap is of no use and has to be disposed of in other ways. Therefore, one of the main criteria in the selection of a coating for PET film is its 'reclaimability'. and this is usually measured as a function of the colour generated by the recycled film. Direct colour measurements are a primary quality control parameter on most film production units.

1.6. Aims of the Project.

There are 3 primary aims of this project. Firstly, to investigate the physical and chemical parameters of the PET / coating interface by means of reflection techniques. Secondly, to examine the behaviour of the presumed incompatibility between PET and PMMA. And thirdly, to asses the effect of model coating formulations upon the melt degradation of PET films.

1). In order to understand fully the interface formed between PET and another polymer it is necessary to characterise thin layers of the polymers and observe the surface and dimensional behaviour in response to the conditions of interest, in this case

the temperatures seen in the film making process (493K), and the temperatures of extrusion processes used in reclaim operations (573K). Using this knowledge of thin film behaviour, a thorough investigation of polymer / polymer interfaces can then be conducted using ellipsometry, X-ray reflectometry and neutron reflectometry. The equilibrium interfacial width can be determined by the correct use of model fitting procedures, and hence a value for the Flory-Huggins interaction parameter can be derived. The exact nature of interfacial broadening can be deciphered by comparing the results of different interfacial measurement techniques, yielding information pertaining to the chemical as well as physical interactions between PET and the model polymers used.

2). Blends of PET and model polymers can be studied to support the information garnered from the interfacial studies. Furthermore, the study of these blends is relevant to the study of mixed reclaimed systems, whereby consideration is given to the effect of polymeric contamination in recycled PET. To this effect the phase behaviour of model blends of PET / PMMA will be studied, and the extent of any chemical interaction between the polymers investigated by thermal, optical and spectroscopic techniques.

3). The influence of individual coating components upon the degradation of coated PET films is important in establishing a comprehensive knowledge of the ability of PET to be recycled. Laboratory and industrial scale experiments can determine the components of a coating which lead to the observed detrimental phenomena such as yellowing and gelation. Kinetic expressions for the degradation of PET with respect to the concentrations of these components need to established, and the overall degradation mechanisms need to be reviewed in light of experimental evidence.

1.7. References.

[1] Werner, E., Janocha, S., Hopper, M. J. and Mackenzie, K. J., in *Encyclopaedia of Polymer Science and Technology, Vol. 12,* 1985, John Wiley, New York.

[2] Barnes, J. A., Brennan, W. J. and Meredith, W. N., Patent; UK 0463740
Harrison, A. G., Meredith, W. N. and Higgins, D. E., Patent; UK 0498569.
Crocker, C., Patent; US 4,786,560.
Hart, C. R., Patent; UK 0429179.

[3] Elmes, T. D. J. and McGrail, P. T., Patent; US 4,339,531.
Robinson, J. N., Patent; US 5,411,845.

[4] Padget, J. C., *J. Coat. Tech.,* 1994, **66**, pp 89 - 105.

[5] Wehrum, A., PhD thesis, 1998, St Catherines College, University of Cambridge.

[6] Carlsson, D. J. and Wiles, D. M., in *Encyclopaedia of Polymer Science and Technology,* 1985, John Wiley, New York.

[7] Whinfield, J. R. and Dickson, J. T., Patents; US 2,465,319. and UK 578,079.

[8] Birks, J. B., *Modern Dielectric Materials,* 1960, Heywood & Co., London, UK.

[9] Jadhav, J. Y. and Kantor, S. W., in *Encyclopaedia of Polymer science and Technology, Vol. 12.,* 1985, John Wiley, New York.

[10] Tomita, K. and Ida, H., *Polymer,* 1975, **16**, pp 185 - 190.

[11] Pillati, F., in *Comprehensive Polymer Science, Vol. 5,* 1989, Pergamon Press. London, UK.

[12] Zimmerman, H., in *Developments in Polymer Degradation, Vol. 5.,* 1985, Ed. Grassie, N., Elsevier Applied Science.

[13] Fradet, A. and Marechal, E., *Adv. Polym. Sci.,* 1982, **43**, pp 51.

[14] Cowie, J. M. G., *Polymers; Chemistry and Physics of Modern Materials, 2nd Ed.,* 1991, Blackie, Glasgow, UK.

[15] Hergenrother, W. L., *J. Polym. Sci., Polym. Chem. Ed.,* 1974, **13**, pp 875 - 883.
Militký, J., Vanícek, J., Dostál, J., Jansa, J. and Cáp, J., *J. Appl. Polym. Sci.,* 1980, **25**, pp 1195 - 1208.

[16] Droscher, M., *J. Appl. Polym. Sci., Appl. Polym. Symp.*, 1981, **36**, pp 217 - 230.
Fakirov, S., Seganov, I. and Kurdowa, E., *Makromol. Chem,* 1981, **182**, pp 185 - 197.
Yu, T., Bu, H. and Chen, J., *Makromol. Chem.*, 1986, **187**, pp 2697 - 2709.

[17] Stevenson, R. W. and Nettleton, H. R., *J. Polym. Sci., Polym. Chem. Ed.,* 1968, **6**, pp 889 - 900.

[18] Challa, G., *Makromol. Chem.*, 1960, **38**, pp 105 - 122.
Challa, G., *Makromol. Chem.*, 1960, **38**, pp 123 - 137.
Challa, G., *Makromol. Chem.*, 1960, **38**, pp 138 - 145.

[19] Santacesaria, E., Trulli, F., Minervini, L., Di Serio, M., Tesser, R. and Contessa, S., *J. Appl. Polym. Sci.*, 1994, **54**, pp 1371 - 1384.

[20] Kamatani, H., Konagaya, S. and Nakamura, Y., *Polym. J.*, 1980, **12**, pp 125 - 130.
Karayannidis, G., Sideridou, I., Zamboulis, D., Stalidis, G., Bikiaris, D. and Wilmes, A., *Die Angew. Makromol. Chem.*, 1993, **208**, pp 117 - 124.

[21] Chang, S., Sheu, M.-F. and Chang, N.-H., *J. Polym. Sci., Polym. Chem. Ed.*, 1982, **20**, pp 2053 - 2061.
Aharoni, S. M., Forbes, C. E., Hammond, W. B., Hindenlang, D. M., Markes, F., O' Brien, K. and Sedgwick, R.D., *J. Polym. Sci., Polym. Chem. Ed.*, 1986, **24**, pp 1281 - 1296.

[22] Briston, J. H., *Plastic Films,* Plastics Institute Monographs, 1974, Illiffe Books, London.

[23] Schuur, G. and Van Der Vegt, A. K., in *Structure and Properties of Orientated Polymers,* 1975, Ed. Ward, I. M., Applied Science Publishers, London.

[24] Zimmerman, H. and Kim, N. T., *Polym. Eng. Sci.*, 1980, **20**, pp 680 - 683.

[25] Jabarin, S. A. and Lofgren, E. A., *Polym. Eng. Sci.*, 1984, **24**, pp 1056 - 1063.

[26] Halek, G. W., *J. Polym. Sci., Polym. Symp.*, 1986, **74**, pp 83 - 92.

[27] Tan, S., Su, A., Li, W. and Zhou, E., *Macromol. Rapid Commun.*, 1998, **19**, pp 11 - 14.

[28] Alfrey, T., *J. Polymeric. Mater.*, 1979, **7**, pp 83 - 92.
Blundell, D. J., Oldman, R. J., Fuller, W., Mahendrasingam, A., Martin, C., MacKerron, D. H., Harvie, J. L. and Rickel, C., *Polym. Bulletin*, 1999, **42**, pp 357 - 363.
Yeh, G. S. Y. and Geil, P. H., in *Cryogenic Properties of Polymers*, 1968, Ed. Serafini, T. T. and Koenig, J. L., Marcel Dekker, New York.

[29] Faisant de Champchesnel, J. B., Tassin, J. F., Bower, D. I., Ward, I. M. and Lorentz, G., *Polymer*, 1994, **35**, pp 4092 - 4102.

[30] Gedde, U. W., *Polymer Physics*, 1995, Chapman and Hall, London, UK.
Stein, R. S., in *Structure and Properties of Polymer Films*, 1973, Ed. Lenz, R. W. and Stein, R. S., Plenum Press, New York.

[31] Sun, Y., Lai, F. and Chen. S., *J. Plast. Film Sheet.*, 1989, **5**, pp 154 - 166.

[32] Clarke, J. B. and Alston, E., in *Waterborne Coatings and Additives*, 1995, Ed. Karsa, D. R. and Davies, W. D., Royal Society of Chemistry, Cambridge, UK.

[33] Booth, G. L., *Coating Equipment and Processes*, 1970, Lockwood, New York.

[34] Brennan, W. J., Brabbs, N. S. and Wright, M., Patent; US 5,882,800.

[35] Lipatov, Y. and feinerman, A., *Adv. Colloid Polym. Sci.*, 1979, **11**, pp 195 - 234.

[36] Vandezande, G. A. and Rudin, A., *J. Coat. Tech.*, 1996, **68** (860), pp 63 - 71.

[37] Keddie, J. L., Meredith, P., Jones, R. A. L. and Donald, A. M., *Macromolecules*, 1995, **28**, pp 2673 - 2682.

[38] Bauer, D. R. and Dickie, R. A., *Org. Coat. Plast, Chem.*, 1979, **41**, pp 451 - 456.
Bauer, D. R. and Dickie, R. A., *Org. Coat. Plast, Chem.*, 1979, **41**, pp 457 - 462.
Bauer, D. R., *J. Coat. Tech.*, 1994, **66**, pp 57 - 64.
Blank, W. J., *J. Coat. Tech.*, 1979, **51**, pp 61 - 70.
Nicholson, J. W., in *Waterborne Coatings and Additives*, 1995, Ed. Karsa, D. R. and Davies, W. D., Royal Society of Chemistry, Cambridge, UK.

[39] Ebdon, J. R., Hunt, B. J. and O' Rourke, W. T. S., *Brit. Polym. J.*, 1987, **19**, pp 197 - 203.

[40] Bauer, D. R. and Mielewski, D. F., *Polym. Deg. Stab.*, **40**, 1993, pp 349 - 355.
Bauer, D. R., *J. Appl. Polym. Sci.*, 1982, **27**, pp 3651 - 3662.
Bauer, D. R. and Dickie, R. A., *J. Polym. Sci., Polym. Phys. Ed.*, 1980, **18**, pp 2015 - 2025.
English, A. D., Chase, D. B. and Spinelli, H. J., *Macromolecules*, 1983, **16**, pp 1422 - 1427.
Collette, J. W., Corcoran, P., Tannenbaum, H. P. and Zimmt, W. S., *J. Appl. Polym. Sci.*, 1986, **32**, pp 4209 - 4228.

[41] Müller, A. J., Feijoo, J. L., Alvarez, M. E. and Febles, A. C., *Polym. Eng. Sci.*, 1987, **72**, pp 796 - 803.
Abu-Isa, I. A., Jaynes, C. B. and O' Gara, J. F., *J. Appl. Polym. Sci.*, 1996, **59**, pp 1957 - 1971.

[42] Subramanian, P. M., Mehra, V., *Antec '93*, 1993, pp 3206 - 3207.
Davies, C., Naoush, H. F. and Rees, G. J., *Polym. Internat.*, 1996, **41**, pp 215 - 225.

Chapter 2

Theory and Literature Review.

2.1. Polymer Interfaces.

2.1.1. Introduction.

Polymer surfaces and interfaces are important in many areas of technology. For instance, the study of plastics fracture, healing and welding requires an acute knowledge of polymer chain dynamics at interfaces [1]. Mechanical properties of polymer composites, blends and alloys are strongly influenced by the strength and width of the interface between the separate polymer phases [2], and in the coating and paint industry, film formation by polymer emulsions is dependant upon the interfacial development between individual latex particles [3].

During the pre-treatment of polymer films, the strength of adhesion between the coating and the film ultimately depends upon the extent of interactions, (chemical and physical), between the coating substituents and the polymer film [4,5]. Strong interactions may lead to well adhered systems with superior end use performance, but reclamation of this film may be complicated by the presence of diffuse and intractable interfaces. Hence, an understanding of the fundamental nature of polymer interfaces is necessary for the development of new, improved coating / film systems, and by the necessity of improving the quality of recycled material [6]

2.1.2. Estimating Interfacial Tensions Between Polymers.

An estimate of the strength of interaction between two polymers can be gained by direct measurement of the interfacial tension in the molten state, and this has proven to be a successful and popular technique [7,8]. However, for a bicomponent system such as PET and PMMA, in which there exists a high degree of thermal incompatibility, -

PET melt process temperatures are ~548K, a temperature at which PMMA is known to degrade [9];- direct measurement of interfacial tensions becomes extremely difficult.

Despite this practical difficulty, we can still predict the interfacial tension between PET an PMMA by assessing their measured surface tension values and interpolating for the temperatures of interest. There exists a set of rules, that allow the estimation of interfacial tension, of which Antonoff's rule [10], is the oldest and simplest but generally invalid for polymers. Good and Girifalco [11], used an approach based on an interaction parameter,.

$$\gamma_{12} = \gamma_1 + \gamma_2 - 2\phi(\gamma_1\gamma_2)^{\frac{1}{2}} \tag{2.1}$$

where γ designates a surface tension value, and ϕ is the aforementioned interaction parameter. However, the theories most applicable to polymer/polymer interfaces are those based on fractional polarity, whereby consideration is given to the polar and dispersive components of surface tension values;

$$\gamma = \gamma^d + \gamma^p \tag{2.2}$$

where γ^d and γ^p are the dispersive and polar components respectively. This approach is used in the geometric mean and the harmonic mean approximations (equations 2.3 and 2.4).

$$\gamma_{12} = \gamma_1 + \gamma_2 - 2(\gamma_1^d\gamma_2^d)^{\frac{1}{2}} - 2(\gamma_1^p\gamma_2^p)^{\frac{1}{2}} \tag{2.3}$$

$$\gamma_{12} = \gamma_1 + \gamma_2 - \frac{4\gamma_1^d\gamma_2^d}{\gamma_1^d+\gamma_1^d} - \frac{4\gamma_1^p\gamma_2^p}{\gamma_1^p+\gamma_2^p} \tag{2.4}$$

The harmonic mean approximation has been shown to yield accurate predictions for polymers [12]. Using these equations and the tabulated values often found in literature [8], we can interpolate values for the interfacial tension between PET and PMMA. (see table 2.1)

Table 2.1 Measured and interpolated values of surface energies for PET and PMMA

Temp. (K)	Poly(ethylene terephthalate)			Poly(methyl methacrylate)		
	γ^d	γ^p	γ	γ^d	γ^p	γ
293	9.86	34.74	44.60 [a]	11.55	29.55	41.10 *
413	8.13	28.66	36.79	8.99	23.01	32.00 *
453	7.55	26.63	34.18	8.12	20.78	28.90 *
493	6.98	24.60	31.58	5.71	20.13	25.84
543	6.25	22.05	28.30 [a]	6.19	15.84	22.03
573	5.83	20.57	26.40 [a]	5.55	14.19	19.74

*from [8]

[a] from [13]

According to Wu [8], the interfacial tension and interfacial width can be simply related;

$$\gamma_{12} = 55 w_I^{-0.86} \tag{2.5}$$

or,

$$\gamma_{12} = 102 w_I^{-1} \tag{2.6}$$

and either of these two equations can be used to estimate interfacial thickness. For a PET/PMMA system the interfacial parameters are shown in table 2.2.

Table 2.2 Interfacial parameters for PET / PMMA.

Temp. (K)	Interfacial Tension (dynes/cm²)	Calculated interfacial width (Å)
293	0.55	184.66
413	0.66	155.25
453	0.74	136.99
493	0.84	120.86
543	1.01	100.58
573	1.18	86.59

Hence, we now have an estimate of the interfacial width between PET and PMMA, at a range of temperatures, and without prior knowledge of the fundamental parameters of the polymers, such as statistical step length, molecular weight, or chain mobility. However, these methods of estimation for interfacial tensions are crude and

rely upon broad and sometimes inadequate assumptions, and hence we must resort to a more detailed and thorough thermodynamic treatment to gain a more meaningful insight.

2.1.3. The Flory-Huggins Theory.

Any thermodynamic description of polymer interfaces is dominated by factors which influence the miscibility of a given pair of polymers. Unlike small organic molecules, most polymers are mutually immiscible and form definable (measurable) interfaces. In general terms, two species A and B will mix if the free energy of the mixture is lower than the free energy of the individual species in isolation; i.e.

$$F_{MIX} = F_{A+B} - (F_A + F_B) \tag{2.7}$$

determined by the composition and temperature of the mixture. The treatment of miscibility in polymers has been encapsulated in the Flory-Huggins model [14], although we must also acknowledge the work of Hildebrand and Scott [15]. The Flory-Huggins model is not a complex or rigorously precise theory, but has been shown to predict qualitatively the correct trends in mixed polymer systems, and provides us with a tool for quantifying phenomena such as the morphology of polymer blends, and the extent of interfacial mixing between two separate polymer phases.

Bulk polymers in the amorphous or melt state are isotropic and have unperturbed dimensions. If we consider two such polymers in a mixture we need to know if the resultant blend is still spatially homogenous with respect to time, temperature and the composition ratio, i.e. is the system mixed at a molecular level.

If we are working at constant pressure, then the parameter in which we are interested is the free energy of the system, and for a two component blend it can be shown that,

$$\Delta F_m = RT\left(\frac{\phi_A}{X_A}\ln\phi_A + \frac{\phi_B}{X_B}\ln\phi_B + \chi\phi_A\phi_B\right) \tag{2.8}$$

which is the Flory-Huggins free energy of mixing and χ is the Flory-Huggins interaction parameter, and as originally defined, is an entirely enthalpic term. The phase diagrams for two component systems can now be calculated. The simplest case for these polymer phase diagrams is to consider polymers with equivalent degrees of polymerisation (see figure 2.1)

The shape of the phase diagram is determined by the value of χ. As can be seen from Figure 2.1, at certain higher values of χ the phase behaviour becomes more complex and two free energy minima can be discerned. If we plot the phase diagrams for several values of χ we can define the coexistence curve, where $df/d\phi = 0$ i.e. the *minima* of the curve; and the spinodal curve, where $d^2f/d\phi^2 = 0$, i.e. the point of inflexion between maxima and minima. (see figure 2.2)

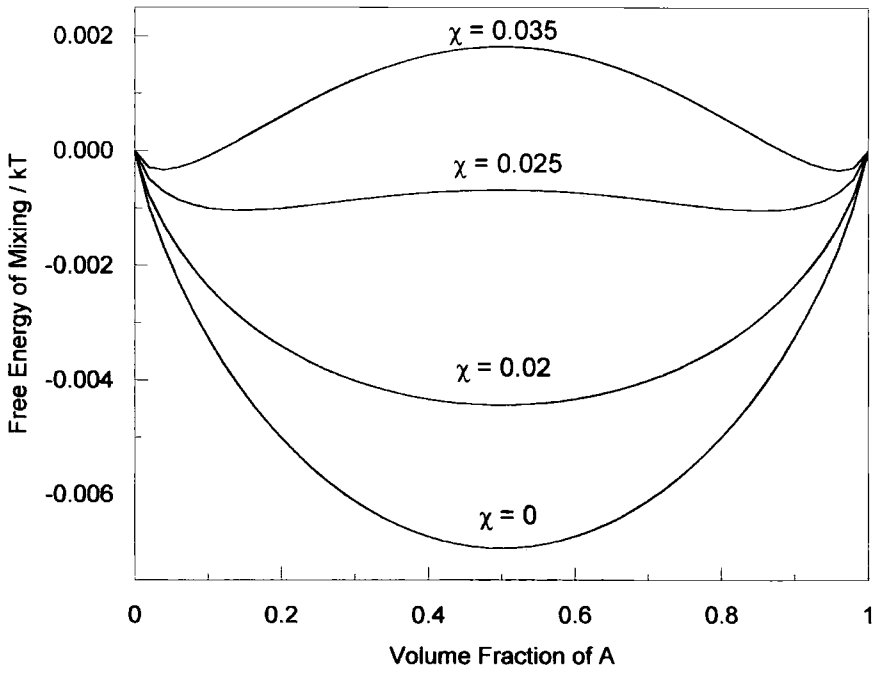

Figure 2.1. Phase diagram for a two component polymer system, where N=100. Note how the free energy response becomes increasingly complex as χ is increased. In experimental situation the phase behaviour would be measured as a function of temperature, and as $\chi \sim 1/T$, then the phase portrait will be inverted.

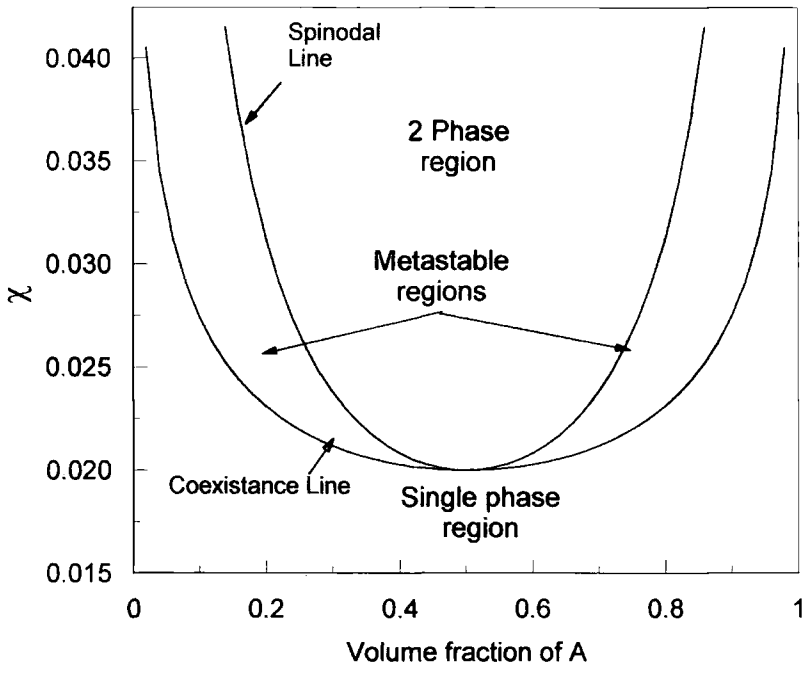

Figure 2.2. Spinodal and coexistence lines for increasing values of the Flory-Huggins interaction parameter.

The spinodal line defines the limit of stability of the mixture, whereas the coexistence line predicts the limit at which both polymers will be mixed in a single phase. The region between the spinodal line and the coexistence line is the region in which the mixture may phase separate i.e. the mixture is metastable. The equation for the coexistence line in terms of the values of χ, is;

$$\chi coex = \frac{1}{N}\frac{1}{2\phi-1}\ln\left(\frac{\phi}{1-\phi}\right) \tag{2.9}$$

and the equation for the spinodal line is;

$$\chi spinodal = \frac{1}{N}\left(\frac{1}{2\phi}+\frac{1}{2(1-\phi)}\right) \tag{2.10}$$

The point at which the coexistence line and the spinodal line coincide tangentially is known as the critical point and for a pair of homopolymers with identical degrees of polymerisation it can be shown that,

$$\chi_c = \frac{2}{N} \tag{2.11}$$

i.e. phase separation occurs at all values of $\chi > \chi_c$.

When the two polymers do not have the same degree of polymerisation, we can identify a critical volume fraction:

$$\phi_c = \frac{N_B^{1/2}}{N_A^{1/2}+N_B^{1/2}} \tag{2.12}$$

A mismatch in molecular weights generates asymmetric free energy curves, and the spinodal temperatures and the critical volume fraction are shifted to lower values.

The Flory-Huggins model is an attractive theory because of the simplicity of the equations which define fundamental concepts, as can be seen from equations 2.8 - 2.12. Phase behaviour is effectively reduced to a function of temperature and composition, and both of these can usually be defined exactly.

However, the Flory-Huggins theory has been shown to have many flaws, and these flaws can be attributed to some of the assumptions made in the derivation of the theory. For instance, the Flory-Huggins model assumes 'incompressibility', i.e. there is no change of volume on mixing the two species. Experimentally, this has been shown to be incorrect for highly incompatible polymers, whereby a system will lower it's density slightly in order to reduce the number of unfavourable contacts. The Flory-Huggins theory also assumes that polymer chains always behave as random walks, but it is known that a polymer chain will collapse in a thermodynamically unfavourable environment, such as a poor solvent, or an incompatible blend [16].

Despite these limitations, the Flory-Huggins model remains a popular starting point in the description of the thermodynamics of polymer systems, and the Flory-Huggins interaction parameter has become a powerful tool in the process of describing polymer interfaces.

2.1.4. Incompatible Polymer Interfaces.

The application of the thermodynamic theory of polymer mixing to interfacial phenomena requires the consideration of concentration gradients. For polymers in the weak segregation limit we apply the random phase approximation (RPA). This treatment is valid in the limit that the concentration gradients are small compared to the chain dimensions of the polymers (i.e. the radius of gyration R_g).

The RPA has been described by de Gennes [17] and has been shown to be applicable for those polymers which develop broad interfaces [18]. However, we also need to consider the case when the concentration gradients are large compared to R_g, a situation in which the RPA is not applicable. This is the case for the interface between strongly immiscible polymer pairs, in the so-called strong segregation limit.

The interfacial energy between two polymers can be considered to be comprised of two thermodynamic factors, the statistics of chain conformation (entropic), which will favour a broad interface; and the energy of interaction between the two polymers (enthalpic), which favours a narrow interface. This balance was first proposed by Helfand and co-workers [19,20,21], who attempted to formalise an estimation of the interfacial width based on the fundamental dimensions of polymer chains in the limit of infinite molecular weight, i.e. chain end effects are ignored.

They considered a system comprising two strongly immiscible polymers A and B (whose fundamental characteristics were nevertheless, considered equivalent). A chain of polymer B has a loop with N units which protrudes into the side of the interface dominated by polymer A (see figure 2.3), so there will be an unfavourable energy due to the protrusion of this loop, i.e.

$$U_{loop} \sim N_{loop} \chi kT \tag{2.13}$$

If the interface is at equilibrium this equation is reduced to

$$N_{loop} \chi = 1 \tag{2.14}$$

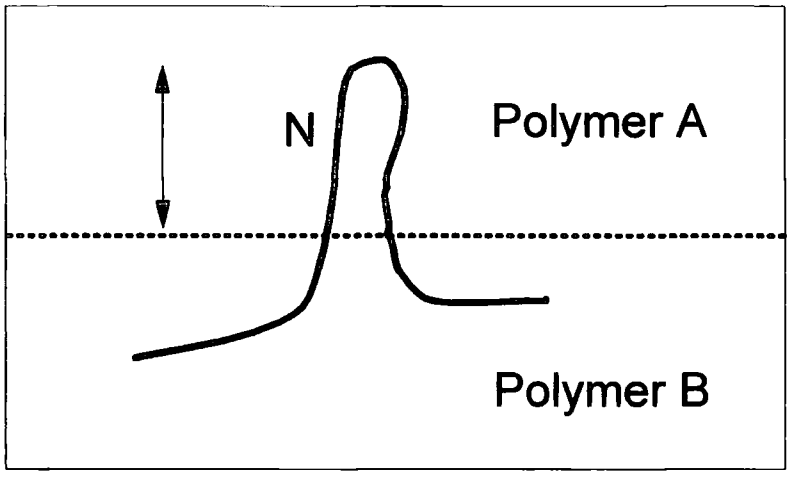

Figure 2.3. Protrusion of chain loop across A / B interface.

statistically, the protruding loop is a random walk, and therefore the width of this interface is the size of this random walk, so,

$$w \sim a\sqrt{N_{loop}} \tag{2.15}$$

or, in terms of the interaction parameter;

$$w \sim \frac{a}{\sqrt{\chi}} \tag{2.16}$$

The interfacial energy can be estimated by counting the number of unfavourable contacts per unit area, each of which has associated with it an energy χkT, i.e.

$$\frac{\gamma}{kT} \sim \varrho a \sqrt{\chi} \tag{2.17}$$

where ϱ is the density. By applying a self - consistent field approach to the problem of random walks (polymer chains), affected by a spatially varying chemical potential, Helfand found that the interfacial width in the limit of infinite molecular weight is,

$$W_I = \frac{2a}{\sqrt{6\chi}} \tag{2.18}$$

and the interfacial tension is,

$$\frac{\gamma}{kT} = \rho a \sqrt{\frac{\chi}{6}} \tag{2.19}$$

The interfacial profile is given by,

$$\phi_A(z) = \tfrac{1}{2}\left\{1 + \tanh\left(\tfrac{z}{w_I}\right)\right\} \tag{2.20}$$

where z is the distance away from the interface.

These expressions have been modified to account for asymmetry in the statistical segment length and densities of the polymers (21), and to rationalise for real systems, with finite molecular weights and high polydispersity ratios (22). Tang and Freed (23) have proposed a modified version of equation 2.18 based on interpolation of numerical tests. Their expression gives the interfacial width as

$$w_I(N) = \frac{a}{\sqrt{6\chi}}\left\{\tfrac{3}{4}\left(1 - \frac{2}{\chi N}\right) + \tfrac{1}{4}\left(1 - \frac{2}{\chi N}\right)^2\right\}^{-\frac{1}{2}} \tag{2.21}$$

Expressions such as 2.18 and 2.21, permit quantitative predictions for the widths of polymer / polymer interfaces to be made, provided that the interaction parameter, χ for the system is known, (or can be estimated). Table 2.3 shows the calculated interfacial dimensions for several polymer pairs, using equations 2.18, 2.21 and other such expressions from literature.

Table 2.3. Calculated interfacial dimensions for Incompatible polymer pairs [19,20,21].

Polymer Pair	Interfacial width (Å)	Interfacial tension (dynes / cm²)
PS / PVA	31	1.9
PE / PS	15	4.7
PE / PMMA	14	5.1

As we can see the interfacial widths are small ($<R_g$), and consequently will require highly resolved techniques, such as neutron reflectivity, to measure them directly. For this reason many workers [7,8], have chosen to measure the interfacial tension between polymers to obtain free energy functionals for incompatible systems. Fernandez *et al* [24], and Russell *et al* [25], have measured the interfacial width between poly(methyl methacrylate) and polystyrene by neutron reflectivity, and both have found the interfacial width to be 50Å, which is in excellent agreement with the prediction of Helfand and Tagami [19], although the value for χ has subsequently been refined.

Further experimental verification of theoretical values has yielded interfacial widths broader than those predicted by theory. This discrepancy can be accounted for by consideration of many factors. Firstly, Helfand and Tagami's result is found in the limit of infinite molecular weight, which approximates well for high degrees of polymerisation, but nevertheless fails to account for the polydispersity and chain end effects. Broseta *et al* [22], and Mills *et al* [26], have considered the effect of finite molecular weights and differing chain lengths on the polymer interface. They concluded that short chains had a surfactant like effect at the interface reducing the interfacial tension and broadening the interface between the two polymers..

Secondly, interfacial broadening may be compounded by the presence of capillary waves at the interface (see figure2.4). Capillary waves arise as a result of thermal fluctuations at the polymer surafaces, and broaden the interface by a factor of ~ 1.7. Capillary wave broadening has been accounted for in several studies [27,28], and offers an appealing reason for the increased interfacial width between polymers.

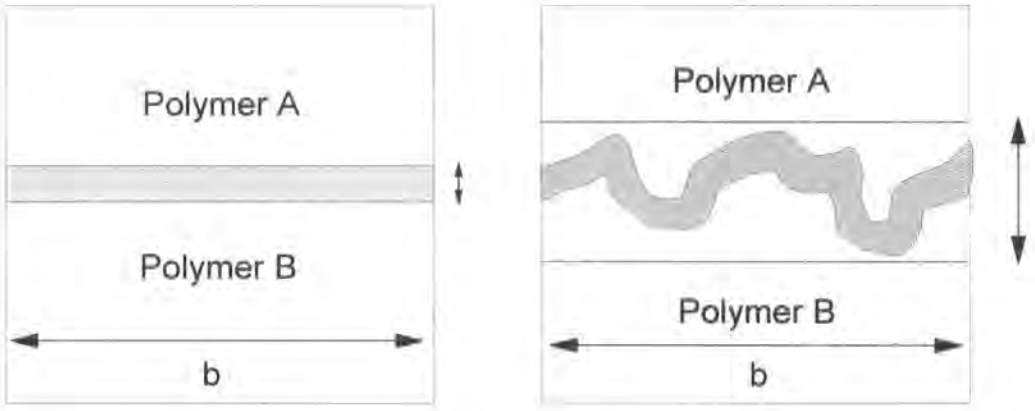

Figure 2.4. Capillary wave broadening of polymer / polymer interfaces. A pair of polymers displays an intrinsic interfacial width as in the diagram on the left. This width can appear to be broadened by the presence of thermally stimulated capillary waves, as on the right. An analysis technique which measures over a nominal distance, b, will average the waves as a broader interface, than that predicted by theory.

2.1.5. Formation of Polymer / Polymer Interfaces.

The thermodynamic description of polymer interfaces is restricted to those systems that have reached equilibrium. However, in real systems the amount of time in which any two polymers may form an interface is limited to the processing conditions employed in rapid manufacturing regimes.

For two miscible polymers, an initially sharp interface will broaden by mutual diffusion of the two types of polymer chains. Interfacial widths of the order of mm can be achieved if rapid Fickian diffusion occurs [29]. For immiscible polymers, with sharp (i.e.$<R_g$) interfaces, the exact nature of this interfacial broadening is complicated by the hierarchy of length scales in which a polymer chain moves, and several theories of chain dynamics have been proposed. The most influential and abiding theories are now reviewed.

a) Rouse dynamics

In 1953 P.G. Rouse proposed a model for chain dynamics, in which the chain was composed of a series of solid beads, connected together linearly by springs [30].

The motion of such a construct depends on many factors but the polymer effectively acts as a complex harmonic oscillator, (see figure 2.5a).

This model is found to adequately describe the behaviour of low molecular weight polymers, but breaks down at the molecular weights encountered in most commercially viable plastics. The model becomes inadequate because it fails to account for entanglement, and the limiting molecular weight is known as the entanglement molecular weight M_e. The value of this molecular weight has been determined for many polymers [31]. However, the Rouse model is still valid when considering the motion of segments of polymer chains below M_e.

b) Polymer Mode-Coupling dynamics

This model was proposed by Schweizer [32], and is similar to the Rouse theory in that the motion of a single polymer chain in the bulk is described by the Brownian motion of a Gaussian chain. However, the friction coefficient for each 'bead' is determined by the position and velocity of all the other beads in the system, whereas the friction coefficient for a bead in the Rouse model is effectively constant. Despite this difference the time and molecular weight dependencies for this model are very similar to the Rouse model.

c) Reptation Dynamics

De Gennes [33], and Edwards [34] proposed a new model for entangled (i.e. high molecular weight) polymers, whereby topological constraints are placed around a single polymer chain by the presence of other polymer chains in a random orientation. These constraints define an imaginary tube in which a polymer chain can move or 'reptate' (from the Latin 'reptare', - to crawl). This tube describes the same topology as the polymer chain, and its central axis can be defined as the 'primitive path' (see figure 2.5c). This is an elegant theory, and has generated much experimentation and discussion. Recently, Wool et al [35], claim to have shown that repatation is the correct model for polymer chain dynamics in concentrated melts, by use of neutron reflectivity and dynamic secondary ion mass spectrometry (SIMS), on precisely constructed tri-block copolymers. This theory seems to be the most abiding in current literature.

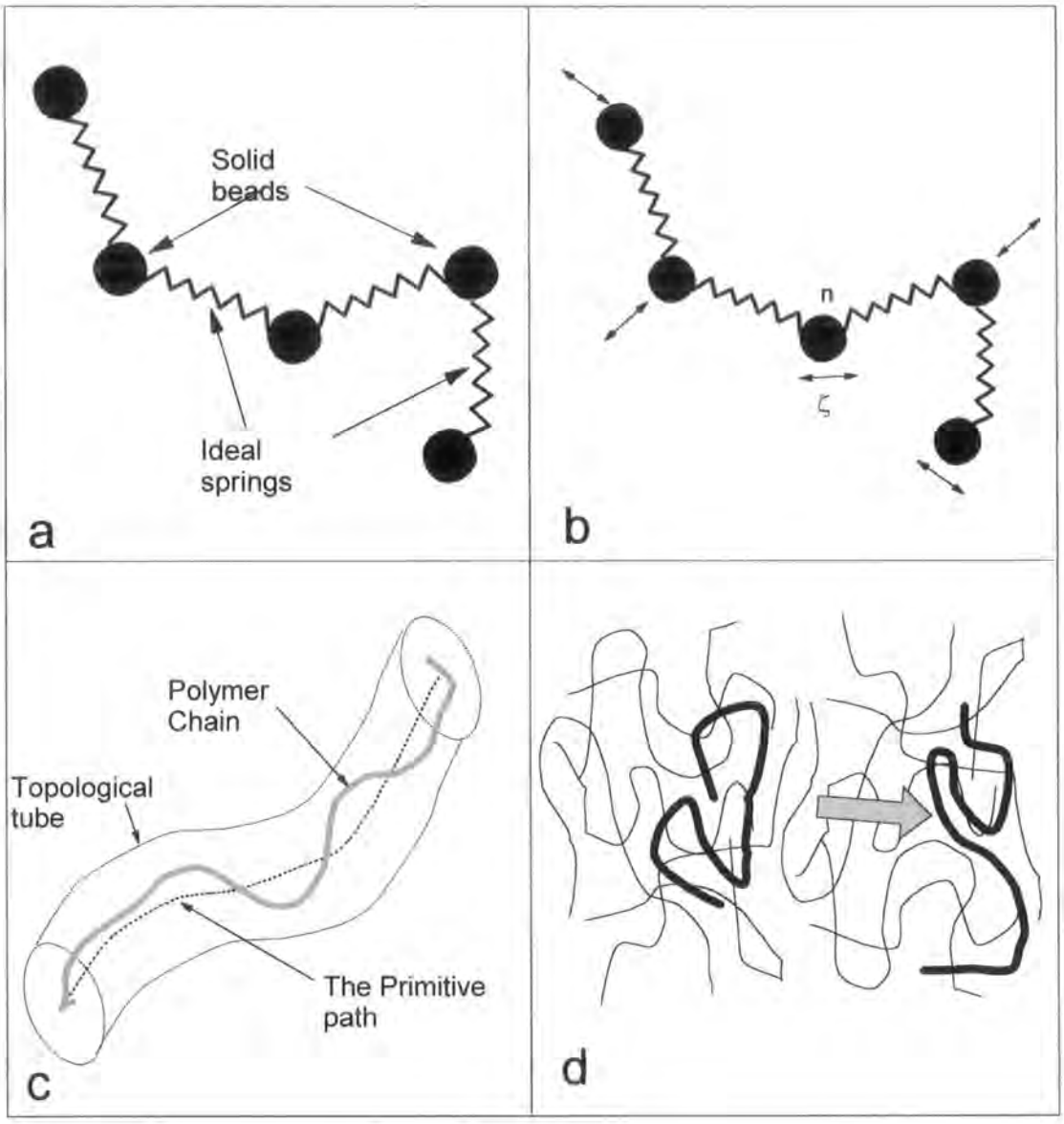

Figure 2.5. Polymer chain dynamics. a) The Rouse model. Each bead experiences a constant isotropic friction. b) Polymer Mode Coupling. Each bead experiences a friction generated by the position and movement of all other beads. c) Reptation tube model . Polymer chain is constrained by the topological tube. d) Fickian diffusion. The polymer chain undergoes centre of mass movement over distances greater than R_g

d) Hairpin Model

The Hairpin model has been suggested by Herman [36]. In this model, high molecular weight polymers move by the propagation of the loops associated with the chain conformation. On a simple statistical basis, this motion will dominate because the

chain will have many more loops than ends, despite the increased energy of loop propagation over end movement.

e) Other models

Other models of polymer dynamics can be classified as tube models (reptation modified) or tubeless (Rouse modified). There are several tubeless models, including those by Skolnick and Kolinski [37], Ngai *et al* [38], and Agarwal *et al* [39]. Reptation modified proposals have been made by Graessley [40], Doi [41], and Fixman [42].

f) Fickian Diffusion

Fickian diffusion is the classical diffusion of polymers over length scales greater than the radius of gyration of the polymers in question. i.e. the polymer chains undergo centre of mass movement and are displaced from their original positions. This centre of mass movement is governed by classical diffusion and obeys Fick's second law [43].

As already intimated, these dynamic models are applicable to different length scales, and can be assumed therefore, to operate on accordingly different time scales. It may at first seem a complex and intractable procedure to normalise the plethora of theories into a common framework, but this has been accomplished elegantly by Doi and Edwards [44], (see figure 2.6). By combining the short (Rouse), medium (Reptation), and long (Fickian) motions, we now have a complete model of polymer dynamics which we can use in the description of interdiffusion at polymer / polymer interfaces.

Statistical segments

At very short times chain motion is limited to the movement of single statistical segments (Kuhn segments). This motion is molecular weight independent, as these segments feel neither the topological constraints nor the chain connectivity. The end of this period is defined as the segment relaxation time τ_0. Interfacial width due to segmental relaxation are of the order of 5-10Å.

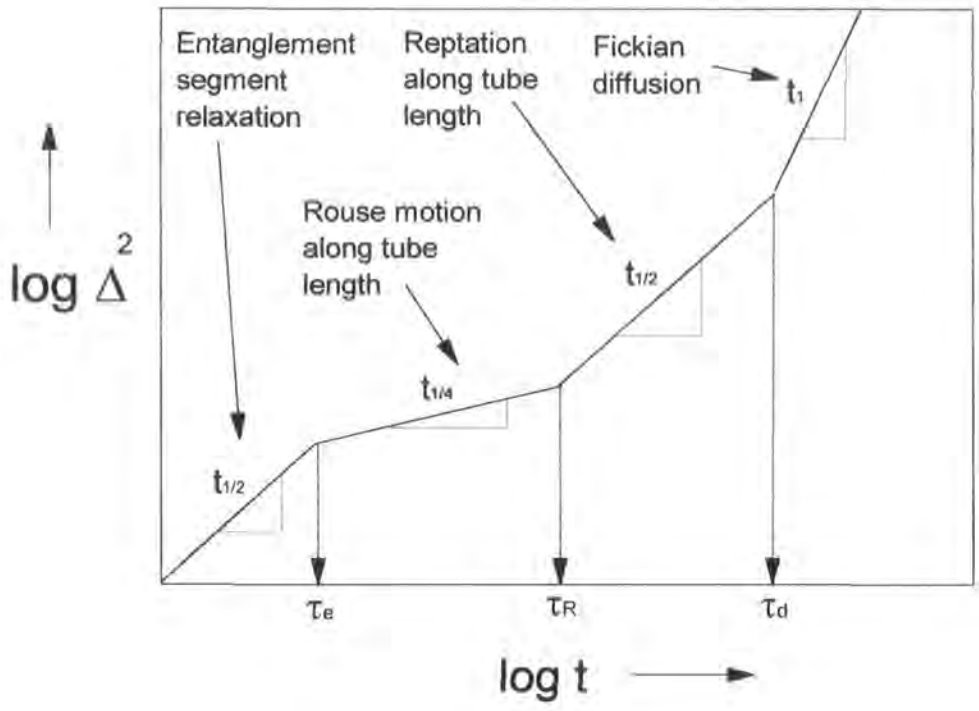

Figure 2.6. Time regimes of polymer dynamics after Doi and Edwards (ref. 90) Δ^2 is the mean squared displacement of the polymer chain

Entanglement Segments

At $t >$ the Rouse relaxation time for the entanglement chain length, the motion of the chain propagates further along the polymer backbone. In this time regime we must consider, at least to some degree, the chain connectivity and chain segments with a length approximating that of the entanglement length. At the end of this time period, the entanglement relaxation time, τ_e, is reached, and the diffusion of the polymer across the interface will be of the order of R_{ge} , the radius of gyration of the entanglement length. The time dependency is;

$$\Delta^2 \sim t^{\frac{1}{2}} \tag{2.22}$$

The Rouse Chain

After the relaxation of the entanglement lengths, further relaxations are propagated along the chain as far as the chain ends. However, the chain is still restricted by the topological constraints of the tube, i.e. the monomers cannot diffuse further than

the tube wall. The end of this time regime is defined as the Rouse relaxation time, τ_R. The motion is independent of molecular weight and the time dependence is now;

$$\Delta^2 \sim t^{\frac{1}{4}} \tag{2.23}$$

Chain Motion by reptation

In this time period the polymer chain reptates along the topological tube , and eventually disengages from the original tube , describing a new tube in the process. At the end of this time period the reptation time, τ_d, is reached and lateral movement of the order of R_g has occurred. As the whole chain is undergoing lateral movement molecular weight becomes important and the time and molecular weight dependencies are;

$$\Delta^2 \sim t^{\frac{1}{2}} M^{-1} \tag{2.24}$$

Centre of Mass Motion of the chains

When the chains disengage from the tube movement is random, and as a result the motion can be described by Fickian diffusion. Time and molecular weight dependencies are;

$$\Delta^2 \sim t M^{-2} \tag{2.25}$$

The motion of polymer chains at interfaces can be quantified using the time scale criteria set out above. Implicit in this convolution of polymer chain dynamic modes is the assumption that the interface is symmetrical with respect to the fundamental characteristics of the polymers. This is not always case, and we must also consider asymmetrical interfaces.

2.1.6. Asymmetric Interfaces; Fast and Slow Diffusion.

Asymmetric interfaces arise when two polymers are brought together whose, chemical and physical compositions are intrinsically different. These differences may be

due to mismatches in molecular weight, statistical dimensions, viscosity, density or thermal relaxations, such as glass transition temperature. In this situation, the overriding question is, which polymer exerts the greatest influence over the dynamics of interfacial diffusion? This question has propagated many experimental and theoretical studies [45,46].

In general, the mutual diffusion coefficient of a polymer couple can be expressed as,

$$D_M = D_0 F \tag{2.26}$$

where D_0 is the dynamic term and F the thermodynamic term. F is non controversial and is simply;

$$F = \frac{1-\phi}{N_i} + \frac{\phi}{N_2} - 2\chi\phi(1-\phi) \tag{2.27}$$

D_0 however, has been the subject of some debate. The 'slow' mode theory of de Genne [47] and Brochard *et al* [48], assumes that the fluxes of the two types of diffusing chains are equal and opposite, and therefore the interdiffusion is controlled by the slowest moving species in the couple. We then have;

$$D_0 = \left[\frac{1-\phi}{D_1^* N_1} + \frac{\phi}{D_2^* N_2}\right]^{-1} \tag{2.28}$$

where D_i* is the self diffusion coefficient for species I, and N and ϕ have their usual assignations.

Kramer *et al* [49,50] have proposed an alternative theory for interdiffusion by invoking the Kirkendall effect, evident in brass alloys. This approach intoduces vacancies into the diffusion model and assumes that,

$$J_1 + J_2 + J_v = 0 \tag{2.29}$$

where $J_{1/2}$ is the flux of the polymers in the couple and J_v is the flux of the vacancies. (Note: this reduces to the 'slow' theory if $J_v = 0$). This is the aptly named 'fast' theory because the diffusion of the couple is determined by the faster moving component. D_0 for the fast theory is;

$$D_0 = D_1 N_1 (1 - \phi) + D_2 N_2 \tag{2.30}$$

where the assignations are the same as in equation 2.28.

In the 'slow' theory, the slower component acts as a barrier to the diffusion of the faster component. In the 'fast, theory, the fast moving component penetrates the slow component, and so the material density of the couple rises. To offset this, there is a bulk flow of slower moving material in the opposite direction, which results in an interfacial movement towards faster component. Some experimentation has supported the 'slow' theory [51], but the majority of literature work has supported the 'fast' theory [52].

More recent proposals on mutual diffusion have tended towards hybrid theories, comprising elements of both the 'fast' and 'slow' models. Most notable are the theories of Akcasu *et al* [53], Brereton [54], and Jabbari and Peppas [55].

2.2. Polymer Mixtures and Interpolymer Reactions.

2.2.1. Polymer Alloys and Blends.

In the previous section we have seen that the interface formed between two polymers is one of the most important factors which determine the properties of these blends and alloys. In this section we will discuss the aspects of polymer mixtures associated with these interfaces, but not the interface itself. One such aspect will be the chemical reactions which may occur between polymers. Another aspect will be the compatability of these blends with respect to composition and temperature The thermodynamic treatments according to Flory-Huggins theory have already been

discussed in the context of polymer interfaces and as such these conjectures do not need to be repeated.

The principle interest in polymer mixtures arises from the enhanced properties which may be evident when certain polymers are alloyed at certain composition ratios [56,57]. A typical example would be the increase in toughness seen of polybutylene terephthalate (PBT), when it is blended with epoxidised ethylene propylene rubber [58]. However, the interest in the current study, is in mixtures of polymers as an impurity problem during plastics recycling. Contaminated reclaim streams are of great concern because incompatible mixtures will lead to reclaimed material of inferior quality and of little or no value [59,60]

2.2.2. Mixtures and Compatibility.

By inspection of the Flory-Huggins theory of polymer miscibility, (see previous section), it is apparent that the principal factor affecting the compatibility of polymers is the molecular weight of the separate phases, given a fixed value of χ. In a general sense, we can see that polymers, by nature of their large molecular size, are incompatible. However, certain specific interactions between particular polymers have been found to reduce the thermodynamic barrier to mixing, resulting in blends which appear to be miscible [45,61]. It is these interactions which are of interest in the study of polymer blends.

The compatibility of a given polymer pair is often studied as a function of composition, and temperature of mixing. The blends are often tested for properties such as increased mechanical strength, chemical and thermal resistance and improved optical characteristics, compared to the homopolymers in the blend [58,61,62].

Outside the scope of the Flory-Huggins theory, which as already stated in the previous section is somewhat limited, there are many instances in which polymers are seen to be compatible. As a general rule, an increase in compatibility may be expected whenever hydrogen bonding is possible [63]. Further predictions are based upon the relative solubility of the polymers in the blend. This approach led to the prediction of polymer miscibility based upon group molar attraction constants first proposed by Small [68], using the equation;

$$\delta = \rho \Sigma \frac{F_i}{M} \tag{2.31}$$

where δ is the solubility parameter, ρ is the polymer density, ΣF_i is the sum of the group molar attraction constants for all groups in the repeat unit of the polymer, and M is the molecular weight of the repeat unit of the polymer.

Tables of group molar attraction constants have been given by several authors [8,64]. This solubility approach to estimating the miscibility of polymers was verified in a remarkable experiment by Iyengar and Erickson who showed that the interfacial adhesion between PET films and other polymers was dependant on the solubility of the other polymer. When the solubilities were very similar the polymers adhered well to each other, whereas when the solubilities were mismatched then little adhesion was present. An approximately linear relationship was seen between the log of interfacial strength (peel strength), and the difference in solubility (see figure 2.7).

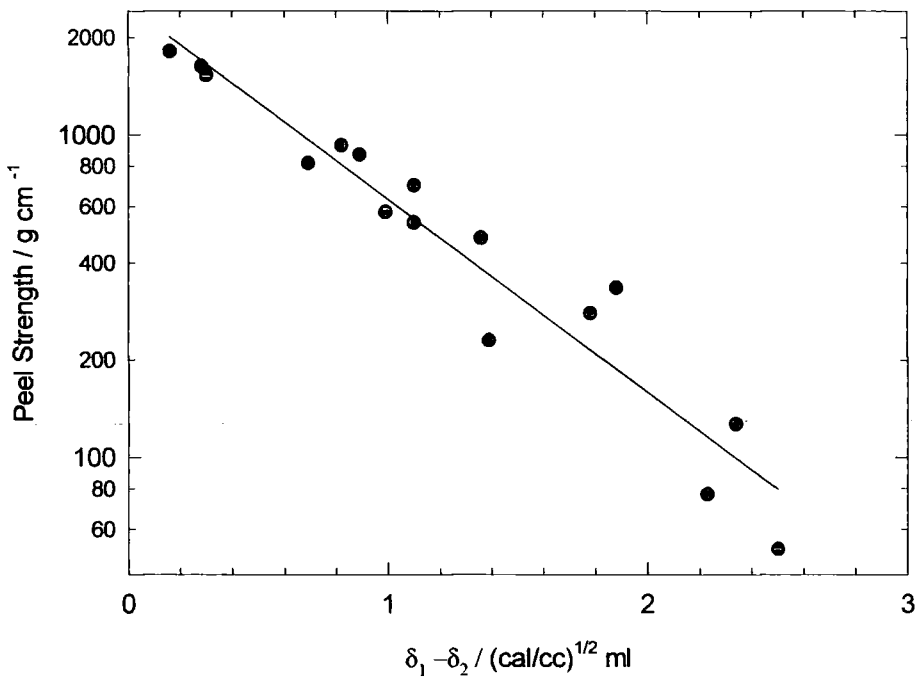

Figure 2.7. Peel strength vs. difference in solubility parameter for various polymers adhered to PET film (ref. 65). The highest peel strengths are seen when the difference between the two phases is at a minimum.

2.2.3. Phase Separation and Wetting.

One of the most significant physical effects of incompatible polymer blends is the phenomena of macroscopic phase separation [66]. This phenomena results in the gross segregation of the two polymers into distinct regions as determined by the Flory-Huggins theory (see section 2.1.3). If the surface of immiscible polymer blends is considered (either as a hard wall or the polymer / air interface) then 'wetting' becomes an important factor in the concentration profile through the sample. by changing the temperature of the blend then one component may separate preferentially to the surface of the sample, yielding a surface excess of the low surface energy component. The phenomena of complete wetting is defined when the contact angle between two phases is zero, and this can be determined by use of the Young - Dupre equation,

$$\gamma_{AB}\cos\theta_c + \gamma_{AB} = \gamma_B \tag{2.32}$$

where, γ_{AB} is the interfacial tension between the two polymers. When θ_C is finite, then the condition of partial wetting exists; when $\theta_C = 0$, then complete wetting is seen, (see figure 2.8).

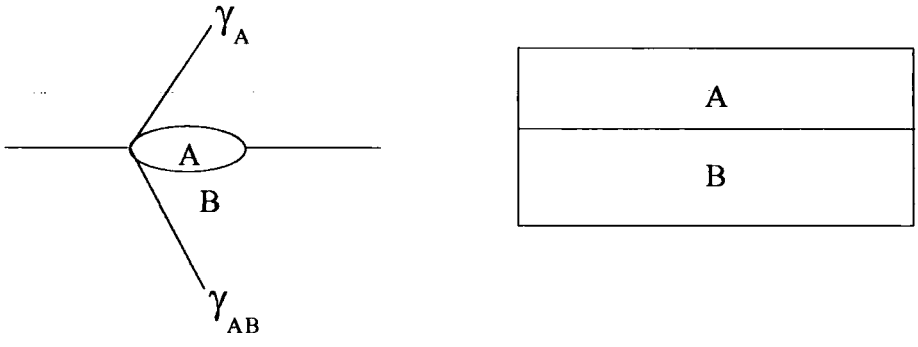

Figure 2.8. Partial and complete wetting for a two -phase system. Partial wetting $\theta_C \neq 0$, complete wetting, $\theta_C = 0$

From an examination of the situations shown in figure 2.8, it is apparent that a certain concentration profile can exist in a system, and this can be expressed using the Cahn square gradient theory adapted by Jones and Kramer and Nakanishi and Pincus [67].

$$\frac{F}{k_B T} = f_S(\phi_S) + \int_0^{\infty} dz \left[\Delta G(\phi) - (\Delta\mu)\phi + \frac{a^2}{24\phi(1-\phi)} \left(\frac{d\phi}{dz} \right)^2 \right] \quad (2.33)$$

where ϕ_s is the surface volume fraction, $f_s(\varphi_s)$ is the surface free energy, $\Delta G(\varphi)$ is the Flory -Huggins free energy of mixing, $\Delta\mu$ is the exchange chemical potential, and he term $a^2/24\varphi(1-\varphi)$ is the gradient coefficient. At equilibrium the volume fraction profile, z, is given by;

$$z = \frac{a}{6} \int_{\phi(s)}^{\phi(z)} \frac{d\phi}{\{\phi(1-\phi)[\Delta G(\phi) - \Delta G(\phi_\infty) - \Delta\mu(\phi - \phi_\infty)]\}^{1/2}} \quad (2.34)$$

so if ϕ_s is known then equation 2.34 can be solved numerically to yield the volume fraction profile of the surface enriching component.

This volume fraction profile is approximated well by the function;

$$\phi(z) = \phi_\infty + (\phi_1 - \phi_\infty) \exp\left(\frac{z}{-\xi} \right) \quad (2.35)$$

where, ξ is the characteristic decay length of the profile, and z can be approximated to the layer height of the surface enriching component.

The phase separation of PET / other polymer systems is important when considering the recycle of coated and coextruded films, as these articles will experience melt phase processing, and the extent to which the non PET component remains mixed with PET determines such factors as extrusion efficiency, melt stability and product quality.

2.2.4. PET and Transesterification

PET can react with other polymers in the polyester family by transesterification [69]. These reactions, with such polymers as PBT and PEN result in copolymers, whose architecture is dependant upon the extent to which the polymers have reacted (time and temperature) [69,70]. Transesterification has been used to produce copolymers of varying degrees of randomness with many polymers including liquid crystalline polyesters [71].

The mechanisms of transesterification have been well reviewed by various authors, and the term now includes all possible reactions such as alcoholysis, acidolysis and ester exchange (see scheme 2.1).

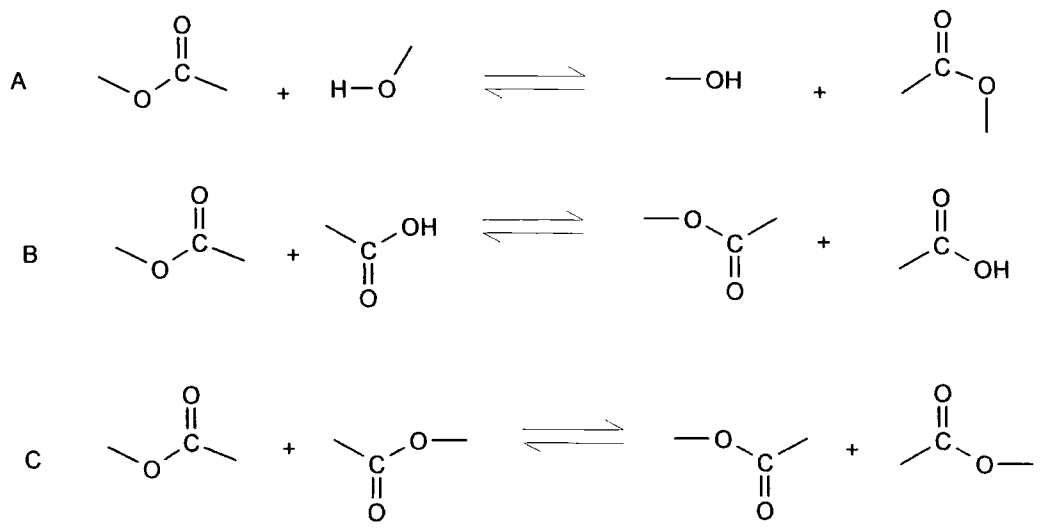

Scheme 2.1. Mechanisms involved in ester exchange reactions. A, Alcoholysis. B, Acidolysis. C, Direct ester exchange.

Overall transesterification between main chain polyesters has been shown to be a second order reversible reaction [72] but is dependant upon the particular polymers used in the reaction. Reactions with other polymers are less well understood. PET / polycarbonate blends have been studied by several workers, and contradictory conclusions have been reached. for instance, Paul, Barlow and co-workers [73], have stated that there is no significant interchange reaction between these two polymers at

melt temperature, whereas Godard *et al* have found evidence of transesterification reactions when PET catalyst residues are present, or specific catalysts are added to the mixture [74].

Transesterification between PET and other aromatic polyesters has been shown for many systems. PET / PEN systems have recently been studied principally because of the industrial importance of these two polymers [75]. PET / PBT has been studied by NMR and DSC and has been shown to be a miscible system [76].

2.2.5. PET and other Polymers.

PET has been shown to be highly incompatible with polyolefins [77]. However, useful materials have been produced from blends of these two polymers by the selected use of compatabilsers, which reduce interfacial tensions between these polymers and so aid the formation of continuous polymer matrix [78]. Chemical grafting of vinyl based polymers onto PET has also been shown to be successful in producing modified surfaces in PET [79]. However, these processes require highly active initiators such as tetravalent cerium or high energy UV irradiation. These interactions are all radical based, i.e., require proton abstraction from the PET backbone followed by reaction with a vinyl group of the polymer to be grafted. Currently, the commercial opportunities for these grafted PET copolymers remains minimal.

2.2.6. Evidence for a PET - PMMA Reaction.

The general characteristics of PET / PMMA blends have not been studied extensively. Nadkarni and Jog have studied PET / PMMA blends at low PMMA concentration and have shown that the peak crystallisation temperature of the blends is shifted to a higher temperature compared to PET homopolymer [80]. In the absence of any specific chemical reaction between the two polymers this is the most notable effect in PET / PMMA alloys.

However, chemical interactions have been observed between PETG (copolymer of PET and cyclo-hexane dimethanol), and an ethylene vinyl acetate (EVA) copolymer by Legros *et al* [81] (see scheme 2.2.), in the presence of a di-butyl tin catalyst. In this

study the amount of catalyst was a critical factor in producing blends with enhanced properties; high levels of catalyst induced higher degrees of transesterification which precipitated undesirable levels of crosslinking within the blend.

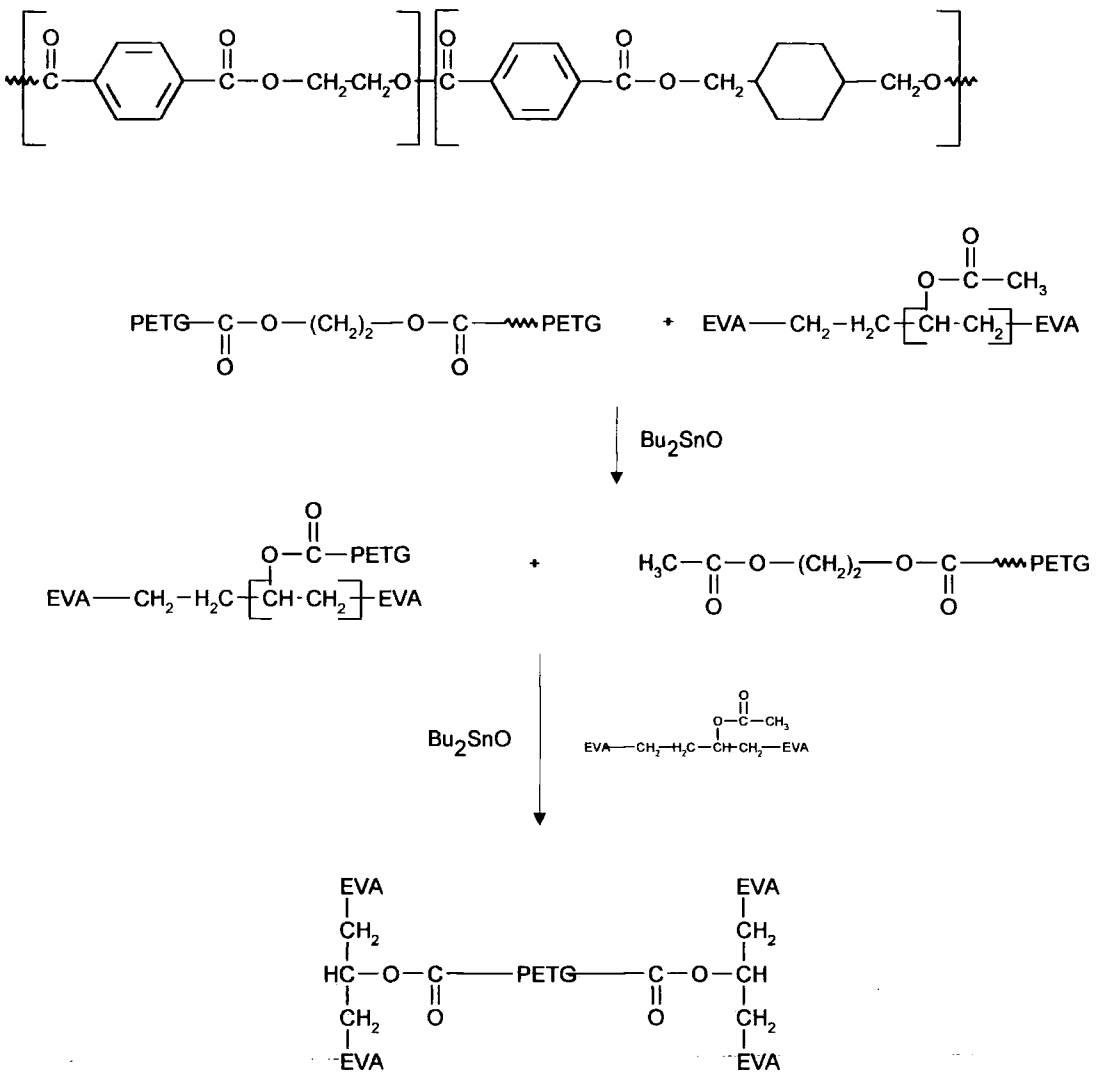

Scheme 2.2. Transesterification between PETG and EVA copolymer, after Legros et al [80]

In another study, Craun *et al* [82] proposed that acrylics and polyesters can be transesterified by using an epoxy nucleophile catalyst system, although the polyester was the minor phase component (~33%). Improved impact resistance was seen for these transesterified blends.

Jha and Bhowmick [83], claim that transesterification is observable in blends of PET and an acrylate rubber, although this acrylate rubber is not defined in their report. The acrylate rubber and PET were transesterified at 573K under 10MPa pressure, which resulted in blends with increased crystallinity, increased tensile strength and a lower glass transition temperature of the plastic phase as measure by dynamic mechanical thermal analysis.

Work carried out on blends of PMMA and PC (which has ester linkages within its chain structure), have shown that transesterification reactions can occur between these two polymers by an ester exchange mechanism. For instance, Raboney *et al* [84], have shown the phase morphology of a blend of these two polymers is influenced by ester - ester exchange reaction above 473K (see scheme 2.3). Evidence of this interaction has also been shown by Yoon and Han [85]. Alternatively Montaudo *et al* [86], have claimed that during the thermal annealing of the PMMA / PC blend, interchange reactions between the polymers do not occur, but instead methyl methacrylate monomer, produced by the thermal depolymerisation of PMMA at the reaction temperature (503K), reacts with the carbonate groups of PC, producing low molecular weight PC oligomers, with MMA end groups.

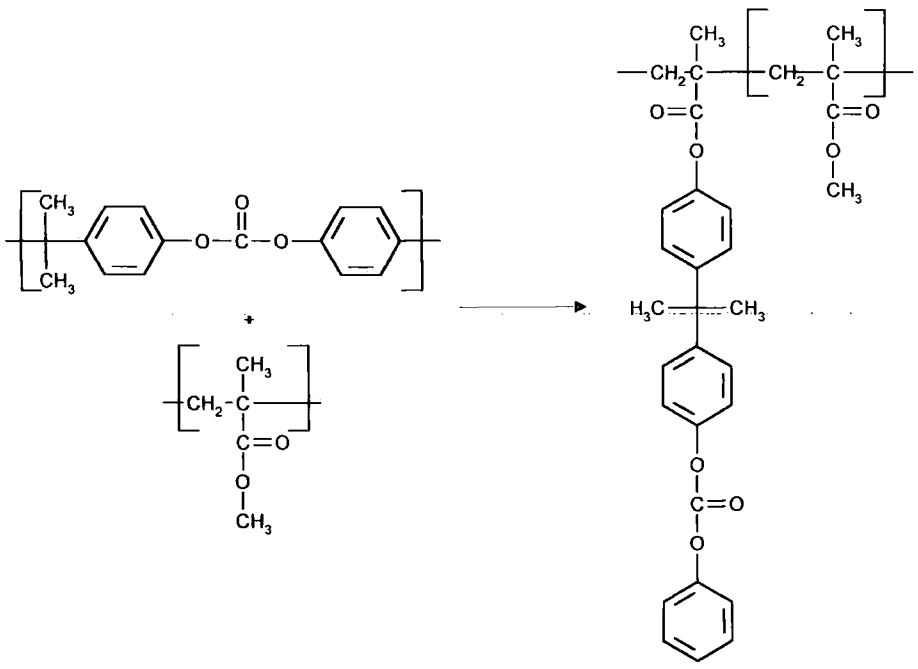

Scheme 2.3. Transesterification of PMMA and PC. After Raboney et al [84].

Therefore there is a body of information which suggests that PMMA could transesterify with PET, and this reaction could produce material which could disrupt the PET film manufacturing process.

2.3. Degradation of PET and PMMA

2.3.1. Fundamentals of Degradation

According to Grassie [87], the first important publication concerned with the degradation of polymeric material appeared in the Journal of the Chemical Society in 1861 [88]; A. W. Hoffmann reported on the deterioration of telegraph cable sheaths in East India. His work showed that heat, light and oxidation were all factors leading to the observed loss of polymer properties.

The study of polymer degradation has increased in tandem with the ever expanding field of polymer science, and today it is a major discipline in itself. The reasons for this are self evident. It is essential that the details of chemical and physical mechanisms leading to the measurable loss in polymer properties are fully understood, in order that polymer manufacturers may make accurate lifetime predictions for polymer articles, and formulate materials with increased stability by inclusion of additives or by post polymerisation treatments.

In actual service conditions it is uncommon for a polymer to experience only one of these phenomena, and usually the article will undergo degradation by a combination of two or more agents, e.g. photoxidation, thermal hydrolysis etc. However, in order to understand the contribution each makes to the overall scheme, laboratory experiments frequently focus on one phenomenon in isolation. Hence, many results need to be treated with caution when attempting to extrapolate these results into actual service or processing situations. Here, the modes of degradation relevant to this study will be described.

2.3.2. *Degradation of PET*

Thermal Degradation

The thermal degradation of PET has been extensively studied over the past five decades. The volume of literature is profuse, and much work has been repeated, sometimes several times; so it is somewhat surprising that controversy still exists over certain aspects of the thermolytic cleavage of PET. However, there does seem to be general agreement that the polymer undergoes main chain scission during thermolysis, primarily at an ester linkage, yielding a carboxylic acid end group and a vinyl end group.

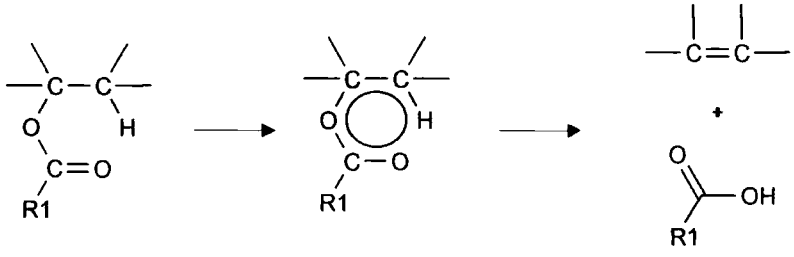

Scheme 2.4. Pyrolyis of simple esters.

This chain scission mechanism is in accordance with the known pyrolysis of simple esters, which have a βH atom, as studied by Hurd, Blades and DuPey and King [89].

Marshall and Todd [90], Goodings [91], Ritchie [92], Buxbaum [93] have all reported the random scission of PET at an ester linkage by the mechanism described in scheme 2.4. This random scission process has been shown to follow 1st order rate law, and activation energies for these processes have been calculated in the range 32 - 62 Kcal/mol, depending upon the parameter used to follow degradation.

Goodings [91] systematically identified four observable chemical effects in the thermal breakdown of PET e.g.

(1) The evolution of gaseous products.

(2) The formation of low molecular weight materials.

(3) The formation of different functional groups in the polymer.

(4) The discoloration of the polymer matrix.

As (1) and (2) both contribute towards a mass reduction of the sample, measuring weight loss with respect to time and temperature is a convenient and simple method for following the thermal degradation of PET.

Goodings also noticed that stirred polymer was significantly less degraded than equivalent unstirred samples. He attributed this to the release of acetaldehyde, necessary in promoting the transesterification of vinyl end groups, a product of degradative chain scission (scheme 2.5), with hydroxyl end groups; therefore maintaining the degree of polymerisation of the polymer. He then postulates that trapped acetaldehyde may self condense to a polyene aldehyde to which he attributes the role of colour formation. No evidence was given for this self condensation reaction.

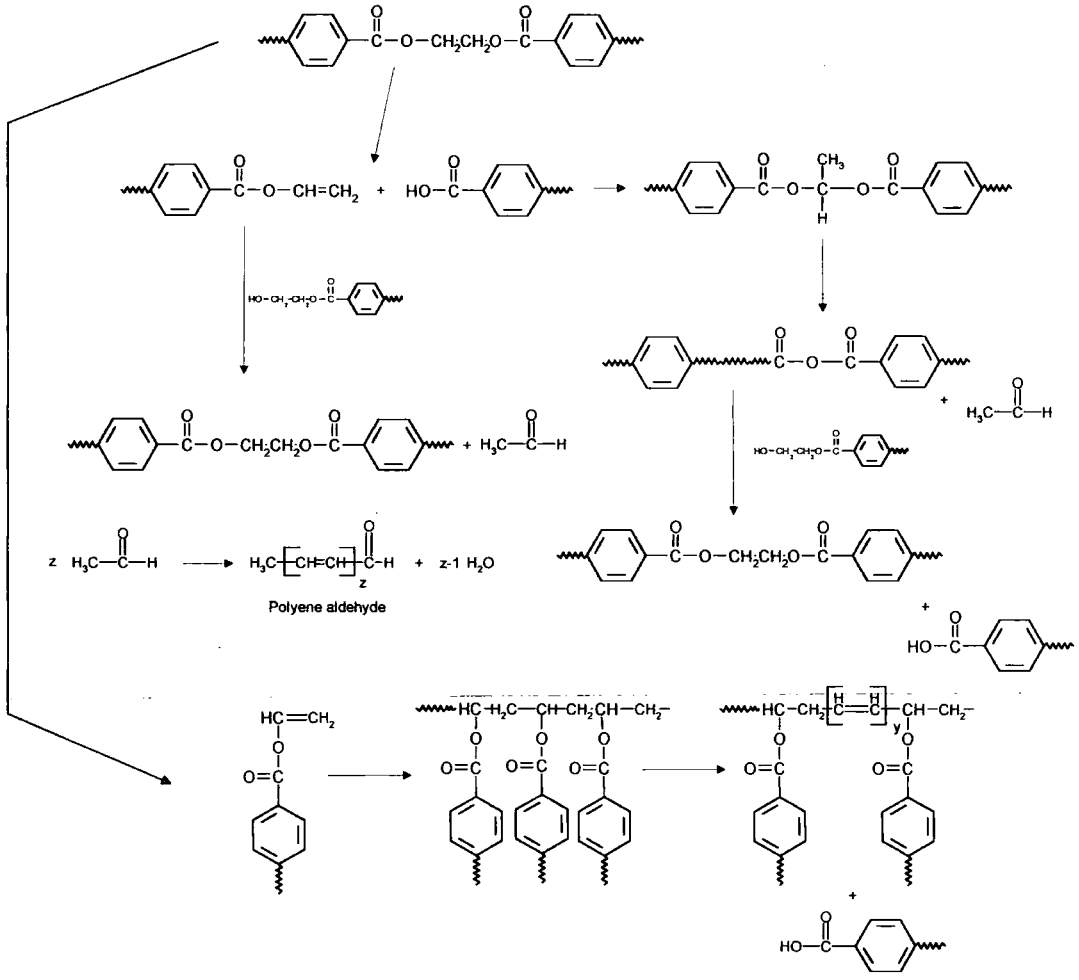

Scheme 2.5. Thermal degradation of PET, after Goodings ref. 91.

Zimmermann's thorough investigation of PET degradation [94], paid particular attention to the role of polymerisation catalysts in the thermal degradation of PET.

Zimmermann claimed that the type and level of transesterification and polycondensation catalyst used during the manufacture of the polymer were the primary thermal degradation parameters.

McNeill and Bounekhel [95] have recently challenged the accepted theory on the nature of the ester cleavage by proposing a homolytic mechanism, although one not part of a free radical cascade (scheme 2.6).

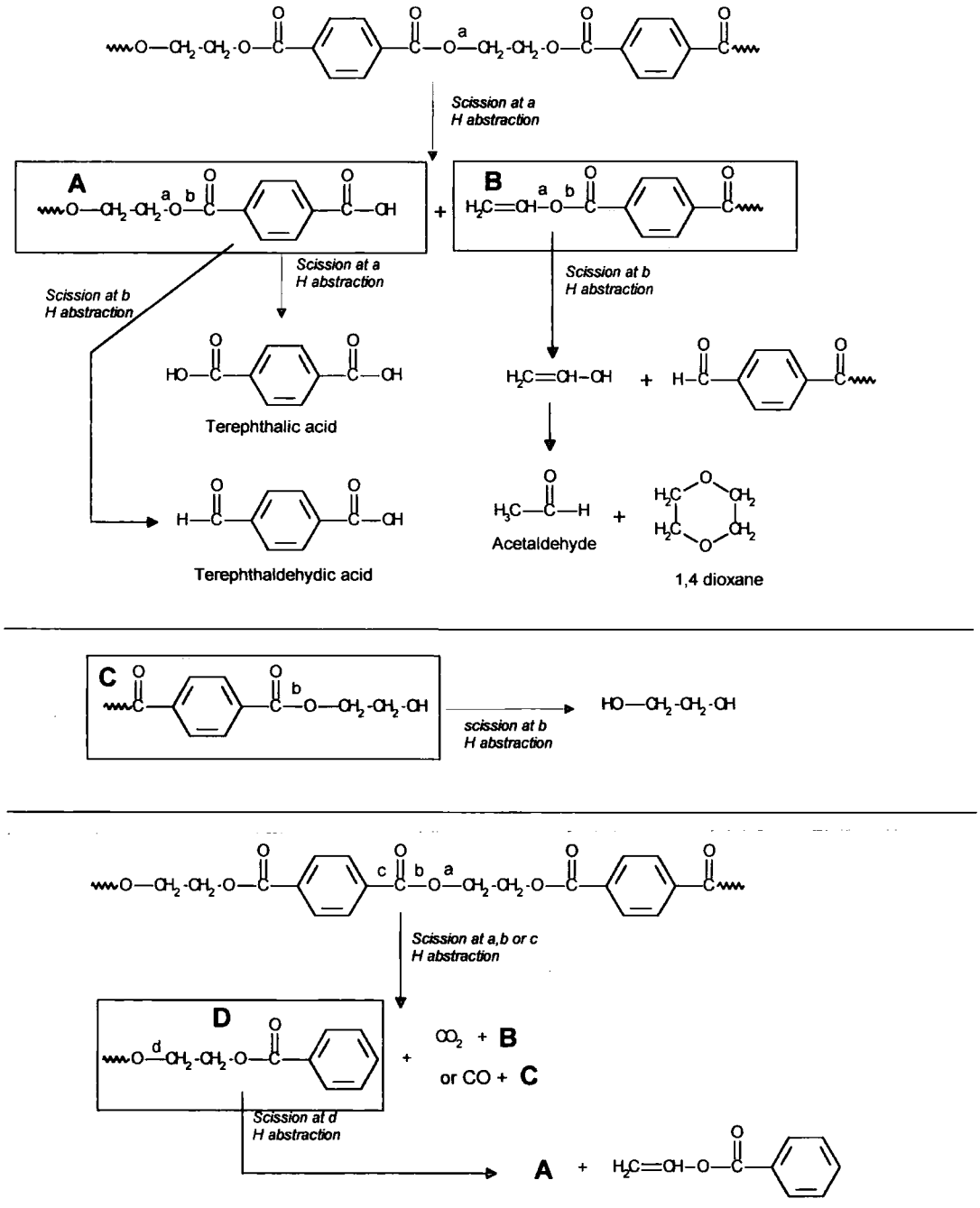

Scheme 2.6 Homolytic thermal degradation of PET after McNeill and Bounkhel [95].

Thermoxidative Degradation.

The thermal oxidation of PET is a very important process when air ingresses into the processing machinery and interacts with the melt. Marshall and Todd [90] noted that random chain scission was accelerated by oxygen. They showed that a significant relationship existed between the molten PET and the concentration of O_2 in the degradation environment, but drew no significant kinetic conclusions.

Degradation under thermoxidative conditions is not fully understood, due to the complex nature and variety of observed degradation products. However, Zimmerman [94] identified key steps to the overall process:

(1) Formation of hydroperoxide at a methylene site.
(2) Homolytic chain scission.
(3) Formation of macro radicals, carboxyl and vinyl end groups.
(4) Crosslinking (gel formation)

Earlier, Buxbaum's study of model compounds [93] led him to propose a reaction scheme for the thermoxidation of PET. (scheme 2.7). It should be noted that both Buxbaum and Zimmermann were studying the thermoxidative degradation of PET below the melt temperature, i.e. in the solid phase, although subsequent work has shown that there the same mechanism applies to the melt phase thermoxidation.

From scheme 2.7. it can be seen that thermoxidation starts with peroxidation at a methylene site in the glycol segment of the PET repeat unit. In this respect, it can be seen that the methylene protons in a diethylene glycol (DEG) unit are even more susceptible to oxidation, and hence the level of DEG in PET is an important factor in the thermoxidative stability of the polymer.[95]

Yoda *et al* [96], Nealy and Adams [97], Zimmerman [94], and Spanninger [98], have all shown that insoluble gel is formed during thermoxidative degradation of PET in the melt state, and this gel formation is attributed to macroradical termination reactions. Large amounts of gel are formed above 573K (~80% by mass). The effect of gel formation upon polymer processing in general, and film manufacture in particular are catastrophic [99].

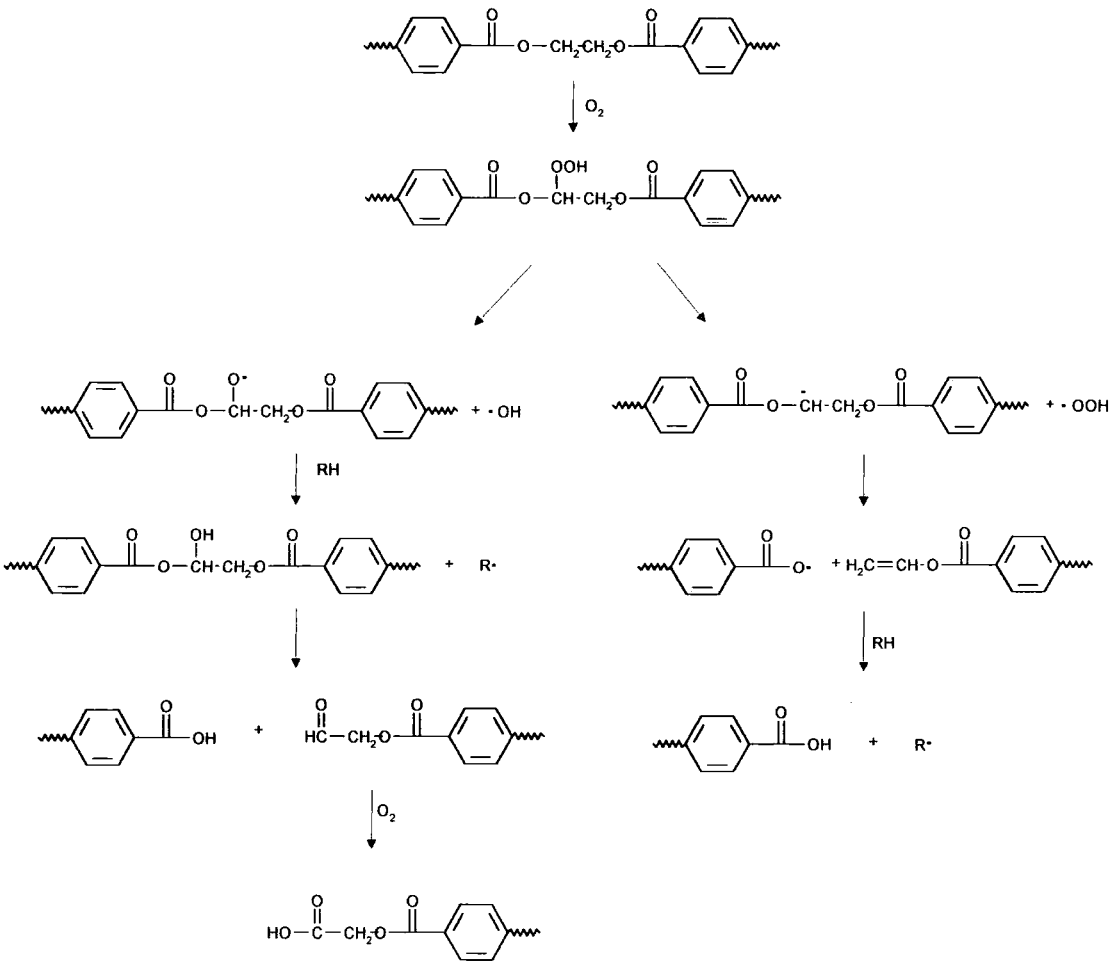

Scheme 2.7. Thermoxidation of PET, after Buxbaum[93].

Hydrolysis and Chemical Degradation.

The hydrolysis of PET is of great interest, as it pertains to 'in service' conditions experienced by polymer articles (films, fibres, mouldings etc.). Much work has been undertaken on thermal hydrolysis at temperatures both above and below the polymer melting point. [100]

McMahon *et al* [101], found that the rates of hydrolysis were very much greater than those found for thermal and oxidative degradations [89], for PET in the solid phase. Golike and Lasoski hydrolysed PET films and claimed that the rate of hydrolysis was diffusion controlled [102]. This was refuted by Davies *et al* who showed that activation energy of diffusion was much lower than the activation energy of hydrolysis at 373K and 100% relative humidity [103]. Subsequently, a number of different kinetic

models have been proposed [101,102,103,104], but it is believed that hydrolysis occurs at ester linkages via the mechanism shown in scheme 2.8.

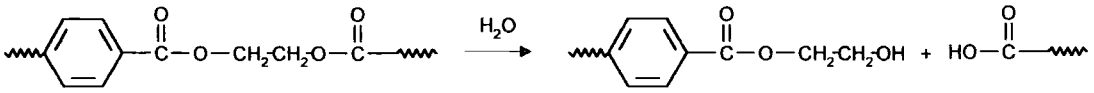

Scheme 2.8. Hydrolysis of PET.

The acid catalysed hydrolysis shown is particularly insidious as one of the products is a carboxylic acid, and the process is therefore autocatalytic. Base-catalysed hydrolysis proceeds via a similar mechanism [105]. Although the hydrophilicity of PET is low, absorption of water can be rapid at low concentrations [94,103]. It is believed that water passes through the amorphous regions of the polymer, where initial hydrolytic attack occurs. Many workers have shown that the resistance to hydrolysis of PET depends significantly on the degree of crystallinity of the polymer sample [103,104,106,107].

The degradation of PET by other chemicals has also been extensively investigated. Chemical degradation by aqueous NaOH [108], CsOH [109], methylamine [110], have all been shown to proceed by the rupture of an ester linkage. These reactions are important when considering the surface treatment and coating of PET films, (see Chapter 1). Indeed, many workers have used chemical etching procedures to enhance the surface functionality of PET [111].

Discolouration

PET discolours upon degradation, particularly under thermal and photo-oxidation conditions. This discolouration is observed as a 'yellowing' of the polymer. Goodings [91] attributed the change in colour to the formation of polyenes in the degraded matrix (see scheme 2.5), however, it is now generally accepted that the species responsible for the increase in colour formation are mono- and di- substituted hydroxy terephthalate moeities, formed by the oxidative free radical mechanisms associated with the mechanisms described in scheme 2.7. These chromophores have been characterised by UV / visible spectroscopy [112], and fluorescence spectroscopy [113].

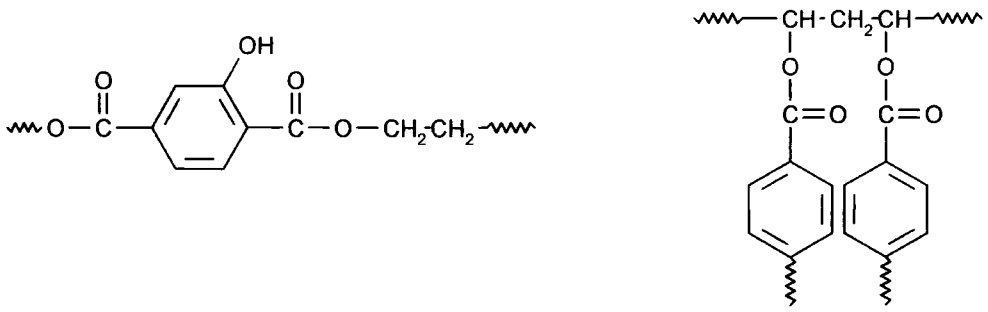

Figure 2.8. Chromophores responsible for yellowing of PET. LHS monosubstituted hydroxy terephthalate [112], RHS polyene structure from polymerisation of vinyl ends, formed during thermal and thermoxidative degradation of PET [91].

2.3.3. Degradation of PMMA.

As much of the work in this thesis concerns the interaction of PET and PMMA at elevated temperatures (i.e. above T_g), it would be prudent to discuss the mechanisms of degradation of PMMA.

Under thermal conditions PMMA is known to undergo depolymerisation to yield almost 100% of MMA monomer in the temperature range 423 - 773K [9]. It has been shown that factors such as tacticity, end group specificity, comonomer concentration, blend ratio, initial molecular weight and chain microstructure all influence the extent and rate of depolymerisation [114].

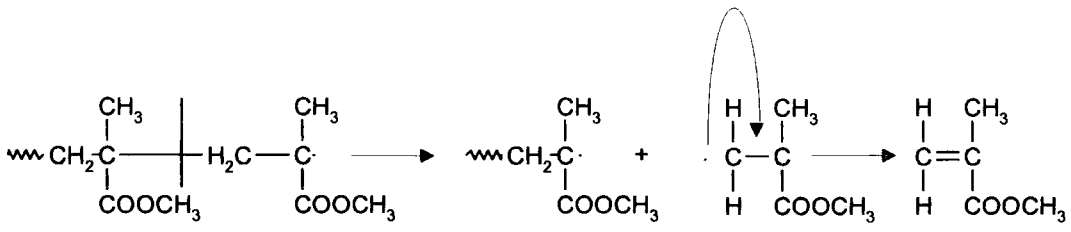

Figure 2.9. Depolymerisation of PMMA to form monomer.

The cleavage of a C-C bond is the first stage of depolymerisation followed by rearrangement to unsaturated monomer and a new chain of lower molecular weight (see figure 2.9). In this way the chain 'unzips' to monomer.

The universality of this mechanism during the depolymerisation of PMMA, allows the reaction to be followed by simple techniques such as weight loss, and intrinsic viscosity measurements. There exists some debate as to whether the initial stages of depolymerisation are dominated by chain end reactions or by a random scission process, with evidence for both being present in the literature [9,115].

Of particular interest in this study is the degradation of PMMA in the presence of other materials, particularly polymers. This has been the subject of many literature reports; for instance Grassie *et al* have shown that the type of degradation products of PMMA are influenced by the presence of poly(acrylonitrile) [116]. Here the low temperature degradation reactions hindered although the monomer is still the main degradation product. Deng *et al* have shown that blending PMMA with a flame regardant, propyl ester phospazene, has no major effect upon the thermal unzipping reaction [117].

Of further interest is the degradation of PMMA in the form of a thin film., as this approximates an acrylic coated PET film product. Grassie and Melville studied PMMA samples of varying thickness in the temperature range 493 - 523K, and found that the degradation rate was independent of thickness up to ~0.8 mm [118]. Working at higher temperatures (> 613K), Barlow *et al* found that the rate of degradation was independent of sample dimensions, only below 400Å thickness [119]. McNeill and Mohammed have shown that PMMA of thickness 3000Å, displays a different degradation characteristic, as measured by thermal volatilisation analysis (TVA) [120]. Thin films were more stable than bulk samples at temperatures below 593K, i.e. exhibited less weight loss.

2.4. Experimental Techniques.

2.4.1. Reflection of light, X-rays and Neutrons.

The principle techniques used in this study to characterise polymer / polymer interfaces are all based on the concept of reflection. Ellipsometry (light), neutrons and X-rays all obey the same fundamental laws of optics. The physical laws governing these phenomena are reveiwed The following description of the theory is based upon the reviews of Russell [121], Higgins and Benoît [122], Bertin [123], Greef [124] and Paik [1125].

Radiation will undergo refraction and reflection at the interface separating two different media, provided that the refractive indices of the media in question are different. This is shown in Figure 2.11.

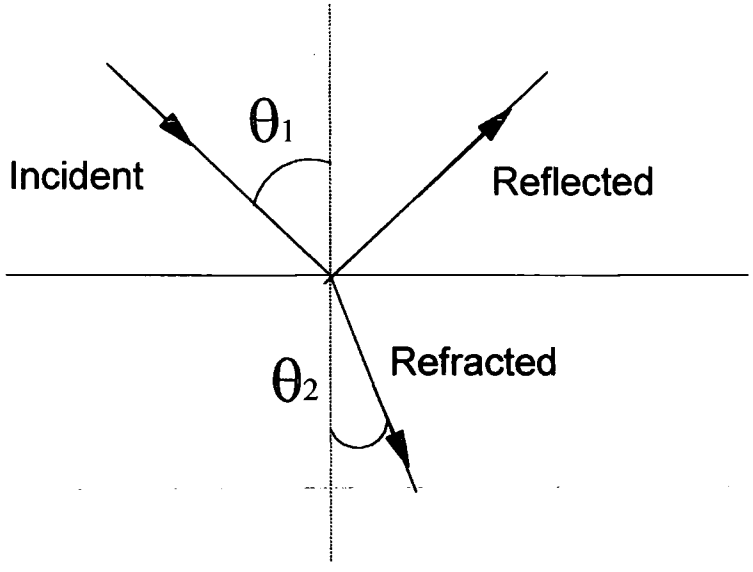

Figure 2.11. Reflection and refraction at an interface.

At the interface the angle by which the incident radiation is refracted is determined by the ratio of the refractive indices of the media. From figure 2.11 Snell's law is given by;

$$n_1 \sin\theta_1 = n_2 \sin\theta_2 \qquad (2.36)$$

where n_1 and n_2 are the refractive indices of the two media on either side of the interface and θ_1 and θ_2 are the angles of incidence and refraction respectively (see figure 2.11). The condition for specular reflection is for $\theta_i = \theta_r$ i.e. the incident and reflected angle are the same. The refractive index of a material can be described by the following equation,

$$n_0 = n - ik \tag{2.37}$$

where n is the real part of the refractive index and k is the complex absorption coefficient. This equation has its counterpart in X-ray and neutron optics; for X-rays

$$n = \delta = \frac{\lambda^2 \rho_e r_0}{2\pi} \tag{2.38}$$

and

$$k = \beta = \frac{\mu\lambda}{4\pi} \tag{2.38}$$

where λ is the X-ray wavelength, ρ_e is the electron density of the material, r_0 is the electron radius (2.82×10^{-15} m), and μ is the mass absorption coefficient. For non-magnetic substances, the neutron refractive index is given by equation 2.37, where

$$n = \delta_N = \frac{\lambda^2}{2\pi} N_A \sum \frac{\rho_i}{A_i} b_i \tag{2.39}$$

where N_A is Avogadro's number, ρ_i is the density of component I with atomic weight A and scattering length b. The second term in equation 2.37 is ignored because, for nearly all practical cases with polymers, the neutron absorption is several orders of magnitude lower than δ_N, and can be safely neglected.

It can also be shown that for radiation incident on a planar surface, a critical glancing angle of incidence exists, at which total internal reflection occurs, if N_0, the refractive index of the medium is greater than N_1, the refractive index of the surface, this angle is given by,

$$\theta_C = \arcsin\frac{N_1}{N_0} \tag{2.40}$$

If this condition exists, i.e. $N_0 > N_1$ then there will be no refracted component, and only an evanescent wave will penetrate the surface. For X-ray and neutron reflection, it can be shown that, to a very good approximation,

$$\theta_C = (2\delta)^{\frac{1}{2}} \tag{2.41}$$

and hence the critical angle is only dependant upon the wavelength of the incident radiation, and the electron density, in the case of X-ray reflectivity, and the scattering length density, in the case of neutron reflectivity. For the case of light (ellipsometry), the studies described in this thesis, generally have an air / sample / substrate geometry. In most cases, $N_0 < N_1 < N_2$, where N_2 is the refractive index of the substrate (silicon), and as such total external reflection will not occur.

Radiation can be described as an oscillating electromagnetic field. If we limit our discussion to non-magnetic materials then we need only consider the electric vector and the polarisation of light can now be defined in terms of this electric vector. For radiation incident on a plane surface, the conventional co-ordinate system is based on this plane of incidence and we define the direction parallel to this plane the *p* direction. The perpendicular to this plane is called the *s* direction (after the German word, 'senkrecht').

The measurement of reflectance is reflectivity and this may be conveniently determined in terms of the Fresnel coefficients for reflection (there are analogous terms for transmission (refraction)). For the case of ellipsometry we must consider both the *s and p* polarisation; - it will be seen that the term 'ellipsometry' is derived from a consideration of these two vectors; whereas X-rays and neutrons are unpolarised in common use, and a more general term to describe reflectivity can be used (see later).

The Fresnel equations can be stated in many forms but most commonly by,

$$r_p = \frac{N_2\cos\theta_1 - N_1\cos\theta_2}{N_2\cos\theta_1 + N_1\cos\theta_2} \tag{2.42}$$

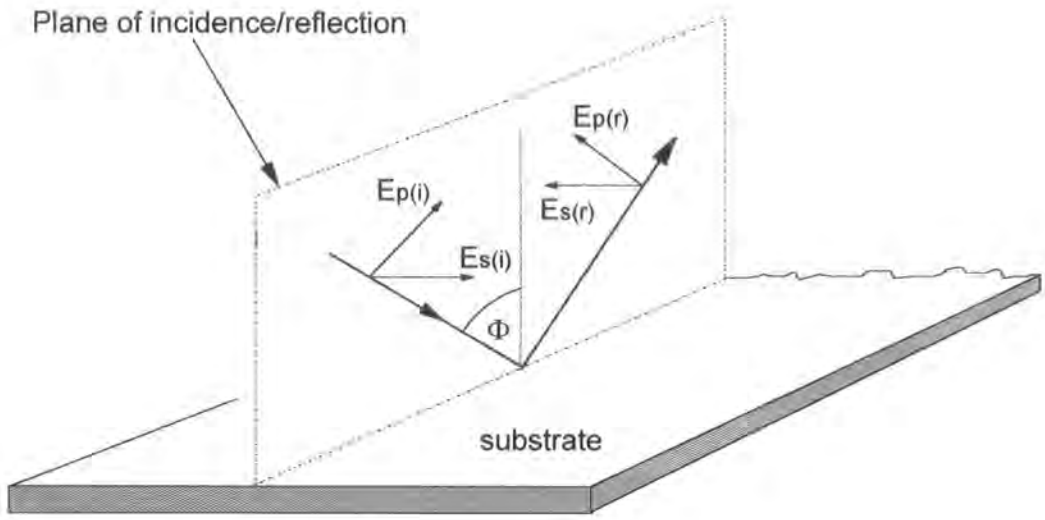

Figure 2.12. Schematic representation of the electric vectors of light undergoing reflection at a plane interface (substrate).

for the electric vector parallel to the plane of incidence

$$r_s = \frac{N_1 \cos\theta_1 - N_2 \cos\theta_2}{N_1 \cos\theta_1 + N_2 \cos\theta_2} \tag{2.43}$$

for the electric vector perpendicular to the plane of incidence.

For the general case of an isotropic thin layer deposited on a semi-infinite substrate we have

$$R_S = \frac{r_{12s} + r_{23s} e^{-2i\beta}}{1 + r_{12s} r_{23s} e^{-2i\beta}} \tag{2.44}$$

and

$$R_P = \frac{r_{12p} + r_{23p} e^{-2i\beta}}{1 + r_{12p} r_{23p} e^{-2i\beta}} \tag{2.45}$$

where β is a function of the film thickness and wavelength, and is defined by

$$\beta = 2\pi\left(\frac{d}{\lambda}\right)N_2 \cos\theta \qquad (2.46)$$

and the r terms are the Fresnel coefficients for the phase boundaries. This equation illustrates how the film phase thickness is wavelength dependent

For ellipsometry, the Fresnel coefficients for both s and p polarisation are important (in fact absolute), whereas for the neutron and X-ray reflectivity, one can consider a more general Fresnel coefficient if the incident radiation is unpolarised (as is the case in our experiments (see chapter 3 and 4). The treatment of reflectivities in the three techniques will now be considered.

2.4.2. Ellipsometry

Ellipsometry is an often underrated technique which is applicable to many problems in the physical sciences. It is particularly useful in characterising thin layers deposited on solid surfaces and as such its popularity within polymer research is growing rapidly [10]. The principles behind ellipsometry have been known for many years, being first propounded by Drude [100]. The fundamental ellipsometric equation is:

$$\rho = \frac{R_P}{R_S} = (\tan\Psi)e^{i\Delta} \qquad (2.47)$$

where ρ is the complex reflectance ratio, R_p and R_S are the reflectivities of the p and s components respectively, and ψ and Δ are the ellipsometric parameters, the phase amplitude and phase difference of the reflected light. Ellipsometry differs from other reflectance spectroscopy techniques because the phase of the reflected light is important in the characterisation.

When the s and p polarisations depicted in figure 2.12 are in phase, the radiation is linearly polarised. however, if the two component vectors are out of phase, the resultant electric vector will trace out an ellipse in space when looking along the direction of propagation. If the phase difference between the s and p components is 90°, then the light

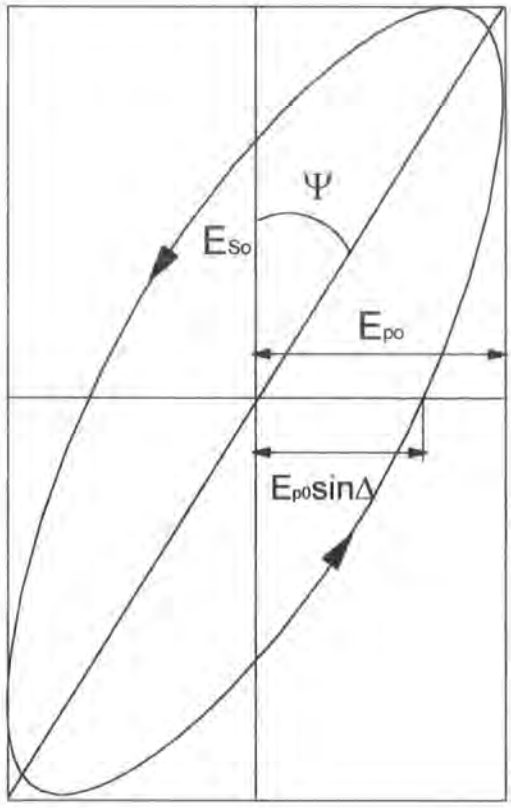

Figure 2.13. representation of elliptically polarised light, the most general form of the polarisation of light.

is circularly polarised, hence the most general form of polarisation of the electric vector is an ellipse and light is said to be elliptically polarised, see figure 2.13.

This most general form of the polarisation of light is the basis of ellipsometry, whereby the relative phase of the two components is measured after reflection from a planar surface. The reflected intensity, refractive index, layer thickness are all used to calculate the fundamental elleipsometric parameters.

Figure 2.14 shows a schematic illustration of a manual, or nulling ellipsometer, which requires direct observation to extract the null points in terms of polariser and analyser settings, in order that a manual calculation can be made. Modern ellipsometers are automated and interfaced directly to a PC for rapid calculation of the ellipsometric parameters. Automated ellipsometers differ from nulling ellipsometers in that a compensator (quarter wave plate) is not required because the analyser is constantly

rotating, and therefore the photodetector will measure a sinusoidally varying light intensity from which the parameters Ψ and Δ can be determined.

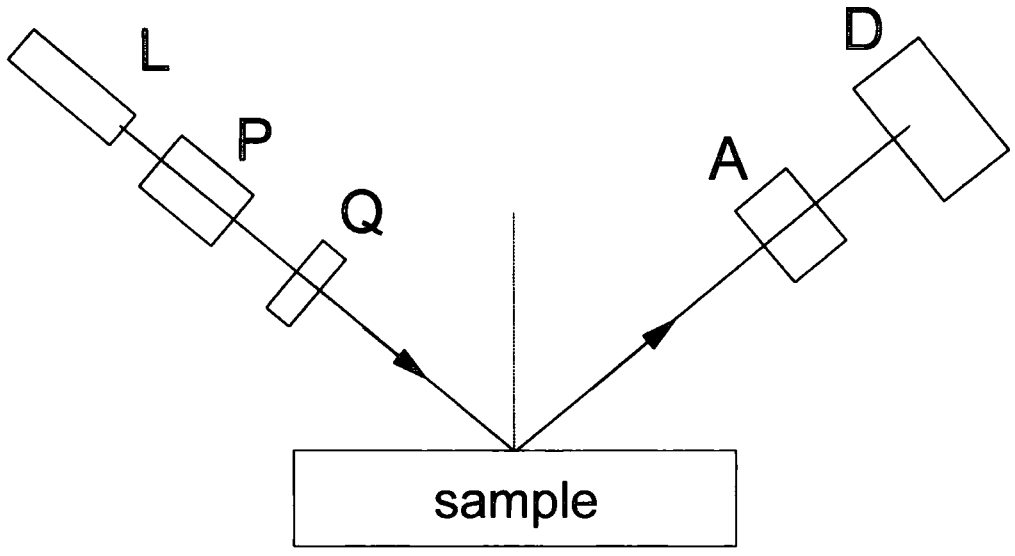

Figure 2.14. Manual (nulling) ellipsometer. L, light source (laser). P, Polariser. Q, Quarter wave plate (compensator). A, Analyser (another polariser). D, Detector.

Ellipsometric parameters are most sensitive to changes in thickness or refractive index when the measurement is made at, or very near to, the angle known as the Brewster angle [2], of the reflecting surface. The Brewster angle is given by,

$$\phi_B = \arctan\left(\frac{N_1}{N_0}\right) \tag{2.48}$$

where N_0 is the refractive index of the medium and N_1 is the refractive index of the material. The Brewster angle is calculated as ~75° for silicon in air, and ~58° for PET in air.

For a single layer system on a substrate of known refractive index, Ψ and Δ can be measured using a single measurement at one angle and at a single wavelength. For more complex systems, i.e. information about the variation in refractive index perpendicular to the plane of the sample, then another parameter must be included. Here the angle of incidence or the incident wavelength, or both can be varied and measurements taken. Measurements in the variation of wavelength are accomplished

using a spectroscopic ellipsometer, whereas multiple angle measurements require a goniometer to be fitted to the light source and detector of an ellipsometer. This allows a sample to be measured in three parameters, Psi, Delta and Phi (incident angle) and as such materials will have a Psi / Delta signature for a given Phi. Figure 2.15 shows the simulated Psi and Delta curves for a 50 nm material of $n = 1.5$ on a silicon substrate.

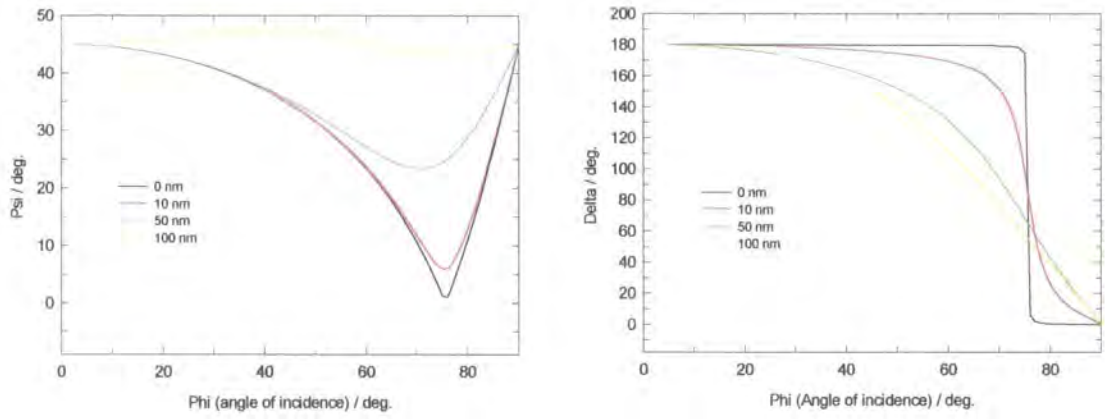

Figure 2.15. Simulated ellipsometric response for a material of N = 1.5, d = 0-100nm, on a silicon substrate. Incident wavelength = 632.8 nm. Note the change in response of both Psi and Delta at ~75°, i.e. the Brewster angle for Silicon.

Ellipsometry is becoming an increasingly important technique in the field of polymer surfaces and interfaces. For instance, the technique has been used to determine the interfacial width between PMMA and styrene acrylonitrile (SAN) copolymers [126]. Habicht *et al* [127], and Chen *et al* [128], have used ellipsometry to study the swelling of macromolecular structures by solvents. Beaucage *et al* have measured the glass transition temperature of thin films of polystyrene by ellipsometry [129], and Wehrum has measured the ellipsometric response of dimensional changes in thin PET films, when subjected to a programmed heating ramp [130].

Many other applications of ellipsometry in polymer science can be found in the literature, and there are many excellent reviews of the theory and practice [124,125,131].

2.4.3. X-Ray and Neutron Reflectivity.

The reflection of X-rays and neutrons from surfaces can be treated with a generalised form of the Fresnel reflection equations, because polarisation does not need to be considered. It is also more convenient to use the wave vector k of the incident radiation for the construction of these reflectivities.

$$k = \frac{2\pi}{\lambda} \sin\theta \tag{2.49}$$

where k is the measured wave vector, perpendicular to the plane of the sample. The scattering vector Q can also be used;

$$Q = \frac{4\pi}{\lambda} \sin\theta \tag{2.51}$$

Using this wave vector, the Fresnel reflectivity can be described using the equation

$$r_{0,1} = \frac{k_0 - k_1}{k_0 + k_1} \tag{2.52}$$

and

$$R = r.r^* \tag{2.53}$$

where r^* is the complex conjugate of r, which reduces to an equivalent expression to equation 2.x or 2.x when expanded.

In neutron reflectivity, refractive index contrast is achieved via selective isotopic substitution, (usually deuterium). Most organic polymers are comprised of carbon, hydrogen and oxygen and hence all have similar scattering length densities. However, replacing the hydrogen with deuterium increases the scattering length density of these polymers significantly.

In X-ray reflectivity, the important parameter is the electron density [121,123], again this will be very similar for many important organic polymers and little contrast will be provided. This can be overcome by the use of labelling with species with high electron densities such a halogens. Halogenated polymers, such as PVC are therefore useful specimens for investigation via X-ray reflectometry.

The dependence of k upon the angle θ and the wavelength λ, results in two modes of measurement for reflectometers. The angle of incidence can be fixed and the wavelength of the neutrons can be scanned, or a fixed wavelength of neutrons can be used and the angle θ can be scanned. The CRISP reflectometer, shown in figure 2.16, located at the ISIS spallation source at the Rutherford Aplleton laboratories, Didcot, UK, is a time of flight spectrometer based on scanning the neutron wavelength.

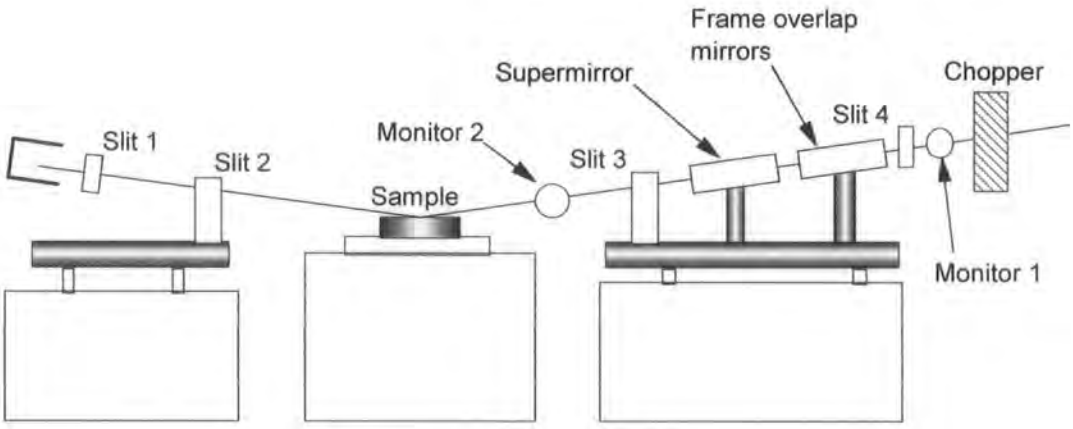

Figure 2.16. Schematic representation of the CRISP reflectometer at the ISIS pulsed neutron source, Rutherford Aplleton Laboratories, UK.

X-ray reflectometers are fixed wavelength machines which scan through a given angular range in order to obtain variation in the scattering vector k. The major advantage of X-ray reflectometers is their commercial availabilty, (many diffractometers can be fitted with a reflection stage); the disadvantages of X-ray reflection experiments are in the need for labelling of samples, and the possibility that the specimens under investigation will be degraded by the incident X-ray radiation.

Neutron reflectivity of polymers has proven to be a powerful and robust technique for the analysis of polymer / polymer interdiffusion, surface structure and polymers arranged at solid / liquid phase boundaries. Neutron reflectivity is particularly useful in the analysis of incompatible interfaces, whereby the interfacial width is comparable to the dimensions of the polymer chains being investigated, i.e. $\sim R_g$. As examples, Fernandez *et al* and Russell *et al* have measured the PMMA / PS interface and have both found a value of 50Å for the interfacial width. Wehrum [130], has used neutron reflectometry to study the polymer mobility in thin films of PS and Lin *et al* [132] have measured the interdiffusion of d-PMMA into PMMA as a function of R_g and lower film thickness.

X-ray reflectometry has been employed in the study of interdiffsuion, by use of marker movements [34,35,133]. This technique will be further described in chapter 4. Tronin *et al* have used x-ray reflectometry to study the self assembly of alternating layers of electrolytes deposited from solution in combination with ellipsometry [134]. Daillant *et al* have used X-ray reflectometry to study the spreading behaviour of polydimethyl siloxane (PDMS) on flat silicon substrates [121].

2.4.4. Analysis and Fitting of Reflectivity data.

Reflection data of thin layers and interfacial phenomena can be analysed in several ways. The kinematic approximation can be used for data collected well above the critical angle, but this method does not provide accurate evaluations of reflectivity profiles near the critical angle, θ_c [122].

When multiple layers are present on a semi-infinite substrate the reflections from each layer need to be considered. A recursive technique such as the Parret method can be employed [135], but much more elegant and popular is the exact optical matrix method as described by Born and Wolf [136].

In describing the interfacial roughness between layers, arising from, for instance, the interdiffusion of two polymers, the interface can be divided into slices turning the interface into a histogram of discrete layers. The reflection from each of these layers is calculated and the total sum of all these reflected waves have to be added together to

obtain the total reflectivity. A convenient solution to handling this data is to use a matrix for each layer,

$$M = \begin{bmatrix} \cos\beta_j & -i/p_j \sin\beta_j \\ -ip_j \sin\beta_j & \cos\beta_j \end{bmatrix} \tag{2.54}$$

where β has been described in equation 2.46. and $p_j = n_j sin\theta_j$. The matrix for the entire assembly can now be obtained by multiplying the matrix for each layer together;

$$M_R = [M_1][M_2][M_3].....[M_N] = \begin{bmatrix} M_{11} & M_{12} \\ M_{21} & M_{22} \end{bmatrix} \tag{2.55}$$

the reflectivity is now given by;

$$R = \left[\frac{(M_{11}+M_{12}p_s)p_a - (M_{21}+M_{22})p_s}{(M_{11}+M_{12}p_s)p_a + (M_{21}+M_{22})p_s} \right]^2 \tag{2.56}$$

However, it is apparent that this method becomes mathematically unwieldy when there are many layers in the system of interest, or an interface needs to be described by a large number of slices.

In X-ray and neutron reflectivity particular use has been made of the Abeles method for constructing these optical matrices [137]. This has been achieved by convoluting the particular form of the approximate scattering function with term which includes the mean squared roughness and the functional form of the interface.

Roughness of any interface can be taken into account by use of a Debye-Waller factor such that;

$$R_r = R_0 \exp(-q_0 q_1 \langle \sigma^2 \rangle) \tag{2.57}$$

where $\langle \sigma^2 \rangle$ is the mean squared roughness, $q_0 = 2k\sin\theta_0$, $q_1 = 2k\sin\theta_1$, θ_0, θ_1 are the glancing angles of incidence and refraction respectively. Cowley and Ryan [138] have

also shown that Gaussian roughness can be incorporated for each layer by use of a modified fresnel coefficient, provided the Abeles method is used, i.e.

$$r_{ij} = \frac{(n_i \sin\theta_i - n_j \sin\theta_j)}{(n_i \sin\theta_i + n_j \sin\theta_j)} \exp\left(-0.5 q_i q_j \langle \sigma^2 \rangle\right) \qquad (2.58)$$

In the analysis of reflectivity profiles, it is necessary to first establish a model against which the measured data can be compared. For the analysis of interfacial profiles, this may include the trial and error of different functional forms, such as a hyperbolic tangent or an error function, although for a given interfacial overlap, certain functional forms are very similar, (see figure 2.17). Alternatively the analysis may rely simply upon a roughness of a characteristic width, with no further extrapolation of the data.

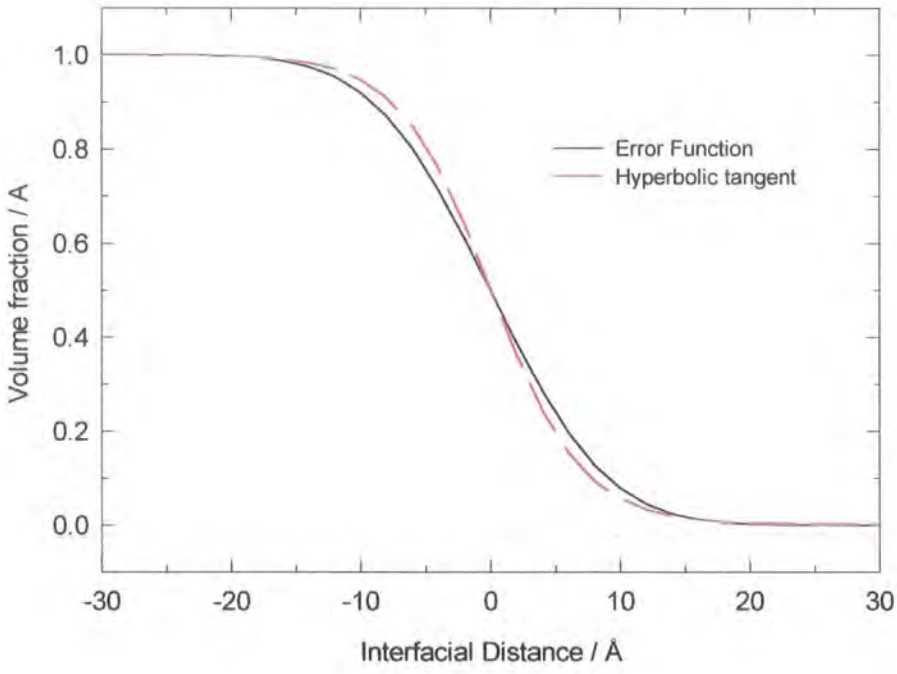

Figure 2.17. Theoretical interfacial profiles for an A / B interface. The tanh and erf profiles have been fixed to occupy the same dimensions in terms of total overlap.

The fitting of these model values to experimentally observed results is usually via iterative routines minimising the residual or fit index. Simplex or Levenberg -

Marquardt algorithms have been used for this purpose, although other mathematical formalisms have also been employed.

In practical use, these methods of data manipulation and model fitting are embedded into computer software which will run recursive algorithms to obtain the least squared fit to data. In normal circumstances the practitioner needs only to specify initial values of the parameters he wishes to fit, such as specimen thickness, roughness and density, which will modify the chosen model to minimise the residual or 'fit index'. This is given by equation 2.59.

$$R_e = \frac{1}{N-p} \sum \left(R_{\exp}(Q) - R_{calc}(Q) \right)^2 \tag{2.59}$$

where N is the number of data points, p is the number of parameters in the model and $R_{exp}(Q)$ and $R_{calc}(Q)$ are the experimental and calculated reflectivities at scattering vector Q.

2.5. References.

[1] Wool, R. P., Yuan, B.-L. and Mcgarel, O.J., *Polym. Eng. Sci.,* 1989, **29**, pp 1340 - 1367.

[2] Schlumpf, H. P., in *Plastics Additives, 3rd Ed.,* 1990, Ed. Gächter, R. and Müller, H., Hanser, Munich.

Maréchal, P., PhD thesis, 1993, Université Catholique de Louvain.

[3] Richard, J. and Wong, K., *J. Polym. Sci., Polym. Phys. Ed.,* 1995, **33**, pp 1395 - 1407.

Hoy, K.L., *J. Coat. Tech.,* 1996, **68**, pp 33 -39.

Keddie, J. L., Meredith, P., Jones, R. A. L. and Donald, A. M., *Macromolecules,* 1995, **28**, pp 2673 - 2682.

[4] Zosel, A., *J. Adhesion*, 1991, **34**, pp 201 - 209.

Loukis, M. J. and Aravas, N., *J. Adhesion,* 1991, **35**, pp 7 - 22.

Lee, L.-H., *J. Adhesion*, 1991, **36**, pp 39 - 54.

[5] Cherry, B. W. and Evely, P. B., *J. Adhesion*, 1987, **22**, pp 171 - 182.

Gutowski, W. S., *J. Adhesion*, 1987, **22**, pp 183 - 196.

Gent, A. N. and Lin, C.-W., *J. Adhesion,* 1990, **32**, pp 113 -125.

[6] Subramanian, P. M. and Mehra, V., *Antec '93,* 1993, pp 3206 - 3207.

[7] Anastasiadis, S. H., Gancarz, I. and Koberstein, J. T., *Macromolecules*, 1988, **21**, pp 2980 - 2987.

Lee, H. S. and Jo, W. H., *Polymer*, 1998, **39**, pp 2489 - 2493.

[8] Wu, S., *Polymer Interface and Adhesion,* 1982, Marcel Dekker, New York.

[9] Madorsky, S. L., *Thermal Degradation of Organic Polymers,* 1964, John Wiley, Interscience, New York.

[10] Antonoff, G., *J. Phys. Chem.,* 1942, **46**, p 497.

[11] Girifalco, L. A. and Good, R. J., *J. Phys. Chem.,* 1957, **61**, p 904.

[12] Wu, S., *J. Polym. Sci., Polym. Lett.,* 1971, **34**, p 19.

[13] Wu, S., *J. Phys. Chem.,* 1970, **74**, p 632.

[14] Flory, P.J., *Principles of Polymer Chemistry.,* 1953, Cornell Univ. Press, Ithaca, New York.

[15] Hildebrand, J. and Scott, R. L., *Regular Solutions,* 1962, Prentice Hall, Englewood Cliffs, N. J.

[16] De Gennes, P.-G., *C. R. Acad. Aci., (Paris),* 1991, **313**, p 1117.

[17] De Gennes, P.-G., *Scaling Concepts in Polymer Physics,* 1979, Cornell Univ. Press, Ithaca, New York.

[18] Dudowicz, J. and Freed, K. F., *Macromolecules,* 1990, **23**, pp 1519 - 1526.

[19] Helfand, E. and Tagami, Y., *J. Polym. Sci., Polym. Phys. Ed.*, 1971, **9**, pp 741 - 746.

[20] Helfand, E. and Tagami, Y., *J. Chem. Phys.,* 1972, **56**, pp 3592 - 3601.

[21] Helfand, E. and Sapse, A. M., *J. Chem. Phys.*, 1975, **62**, pp 1327 - 1331.

[22] Broseta, D., Fredrickson, G. H., Helfand, E. and Leibler, L., *Macromolecules,* 1990, **23**, pp 132 - 139.

[23] Tang, H. and freed, K. F., *J. Chem. Phys.,* 1991, **94**, pp 6307 - 6322.

[24] Fernandez, M. L., Higgins, J. S., Penfold, J., Ward, R. C., Shackleton, C. and Walsh, D. J., *Polymer,* 1988, **29**, pp 1923 - 1928.

[25] Anastasiadis, S. H., Russell, T. P., Satija, S. K. and Majkrzak, C. F., *J. Chem. Phys.* 1990, **92**, pp 5677 - 5691.

[26] Mills, P. J., Green, P. F., Palmstrøm, C. J., Mayer, J. W. and Kramer, E. J., 1984, *MSC Report # 5381.* Department of Materials Science and Engineering and the Materials Science Center, Cornell University. Ithaca, New York.

[27] Sferrazza, M., Xiao, C., Jones, R. A. L., Bucknall, D. G., Webster, J. and Penfold, J., *Phys. Rev. Lett.,* 1997, **78**, p 3693.

[28] Lacasse, M.-D., Grest, G. S. and Levine, A. J., *Phys. Rev. Lett.,* 1998, **80**, pp 309 - 312.

[29] Jordan, E. A., Ball, R. C., Donald, A. M., Fetters, L. J., Jones, R. A. L. and Klein, J., *Macromolecules,* 1988, **21**, pp 235 - 239.

[30] Rouse, P. E., *J. Chem. Phys.,* 1953, **21**, p 1272.

[31] Fetters, L. J., Lohse, D. J., Milner, S. T. and Graessley, W. W., *Macromolecules,* 1999, **32**, pp 6847 - 6851.

[32] Schweizer, K. S., *J. Chem. Phys.,* 1989, **91**, p 5822.

[33] De Gennes, P.-G., *J. Chem. Phys.,* 1971, **55**, p 572.

[34] Edwards, S. F., in *Molecular Fluids,* Ed. Balain, R. and Weill, 1976, Gordon and Beach, New York.

[35] Welp, K. A., Wool, R. P., Satija, S. K., Pispas, S. and Mays, J. W., *Macromolecules,* 1998, **31**, pp 4915 - 4925.

[36] Herman, M. F., *Macromolecules,* 1992, **25**, p 4925.
Herman, M. F., *Macromolecules,* 1992, **25**, p 4931.

[37] Skolnick, J. and Kolinski, A., *Adv. Chem. Phys.,* 1990, **78**, p 223

[38] Ngai, K. L., *Comments Solid State Phys.*, 1979, **9**, p 1651.

[39] Agrawal, G., Wool, R. P., Dozier, W. D., Felcher, G. P., Zhou, J., Pispas, S., Mays, J. W. and Russell, T. P., *J. Polym. Sci., Polym. Phys. Ed.*, 1996, **34**, p 2919.

[40] Graessley, W. W., *Adv. Polym. Sci.,* 1982, **47**, p 68.

[41] Doi, M., *J. Polym. Sci., Polym. Lett. Ed.,* 1981, **19**, p 265.
Doi, M., *J. Polym. Sci., Polym. Lett. Ed.,* 1983, **21**, p 667.

[42] Fixman, M., *J. Chem. Phys.*, 1988, **89**, p 3892.
Fixman, M., *J. Chem. Phys.*, 1988, **89**, p 3912.

[43] Crank, J., *The Mathematics of Diffusion, 2nd. Ed.*, 1975, Oxford University Press, Oxford, U.K.

[44] Doi, M. and Edwards, S.F., *The Theory of Polymer Dynamics,* 1986, Oxford University Press, New York.

[45] Jones, R. A. L., 1987, PhD thesis, University of Cambridge.

[46] Composto, R. J., Kramer, E. J. and White, D. M., *Macromolecules,* 1988, **21**, pp 2580 - 2588.

[47] De Gennes, P.-G., *J. Chem. Phys.,* 1980, **72**, p 4756

[48] Brochard, F., Jouffroy, J. and Levinson, P., *Macromolecules,* 1983, **16**, pp 1638 -1641.
Brochard, F., Jouffroy, J. and Levinson, P., *Macromolecules,* 1984, **17**, pp 2925 - 2927.

[49] Kramer, E. J., Green, P. F. and Palmstrøm, C. J., *Polymer,* 1984, **25**, pp 473 - 480.

[50] Green, P.F., Palmstrøm, C. J., Mayer, J. W. and Kramer, E. J., *Macromolecules,* 1985, **18**, pp 501 - 507.

[51] Shearmur, T. E., Clough, A. S., Drew, D. W., van der Grinten, M. G. D. and Jones, R. A. L., *Polymer,* 1998, **39**, pp 2155 - 2159.

[52] Composto, R. J. and Kramer, E. J., *J. Mater. Sci.,* 1991, **26**, pp 2815 - 2822.
Mills, P. J., Green, P. F., Palmstrøm, C. J., Mayer, J. W. and Kramer, E. J., *Appl. Phys. Lett.,* 1984, **45**, pp 957 - 959.
Bucknall, D. G., Butler, S. A. and Higgins, J. S., *Macromolecules,* 1999, **32**, pp 5453 - 5456.

[53] Akcasu, A. Z., *Macromol. Theory Simul.,* 1997, **6**, pp 679 - 702.

[54] Brereton, M. P., *Prog. Colloid. Polym. Sci.,* 1993, **91**, p 8.

[55] Jabbari, E. and Peppas, N. A., *Polymer,* 1995, **36**, pp 576 - 586.

[56] Cook, W. D., Zhang, T., Moad, G., Van Deipen, G., Cser, F., Fox, B. and O'Shea, M., *J. appl. Polym. Sci.,* 1996, **62**, pp 1699 - 1708.

[57] Zhou, Z., Wu, X. and Yu, M., *Intern. Polym. Processing,* 1990, **1**, pp 37 - 41.

[58] Wang, X.-H., Zhang, H.-X., Wang, Z.-G. and Jiang, B.-Z., *Polymer,* 1997, **38**, pp 1569 - 1572.

[59] La Mantia, F. P., *Polym. Deg. Stab.,* 1993, **42**, pp 213 - 218.

[60] Sitek, F. A., *Mod. Plast. Int.* 1993, **23**, No. 10. pp 74 - 79.

[61] Fox, D. W. and Allen, R. B., in *Encyclopaedia of Polymer science and Engineering,* 1985,

[62] Baker, W. E. and Saleem, M., *Polym.Eeng. Sci.,* 1987, **27**, pp 1634 - 1641.

[63] Porter, R. S. and Wang, L.-H., *Polymer,* 1992, **33**, pp 2019 - 2030.

[64] Kwei, T. K. and Wang, T. T., in *Polymer Blends,* 1978, Ed. Paul, D. R. and Newman, S., Academic Press, New York.

[65] Iyengar, Y. and Erickson, D., *J. Appl. Polym. Sci.,* 1967, **11**, p 2311.

[66] Krause, S., in *Polymer Blends,* 1978, Ed. Paul, D. R. and Newman, S., Academic Press, New York.

[67] Cahn, J. W., *J. Chem. Phys.* 1963, **42**, p 93.
Cahn, J. W. and Hilliard, J. E., *J. Chem. Phys.,* 1958, **28**, p 258.
Nakanishi, H. and Pincus, P., *J. Chem. Phys.* 1983, **79**, pp 997 - 1003.
Jones, R. A. L., Kramer, E. J., *Polymer,* 1993, **34**, pp 115 - 118.

[68] Small, P. A., *J. Appl. Chem.,* 1953, **3**, p 71.

[69] Kotliar, A. M., *J. Polym. Sci., Macromol. Rev.,* 1981, 16, pp 367 - 395.

[70] Ha, W. S., Chun, Y. K., Jang, S. S., Rhee, D. M. and Park, C. R., *J. Polym. Sci., Polym. Phys. Ed.,* 1997, **35**, pp 309 - 315.

[71] Jin, J.-I., Chang, J.-H., Hatada, K., Ute, K. and Hotta, M., *Polymer,* 1992, **33**, pp 1374 - 1378.

Kricheldorf, H. R., Gerken, A. and Karhinen, H., *J. Polym. Sci., Polym. Chem. Ed.,* 1998, **36**, pp 1813 - 1820.

McCullagh, C. M., Blackwell, J. and Jamieson, A. M., *Macromolecules,* 1994, **27**, pp 2996 - 3001.

[72] Devaux, J., Goddard, P. and Mercier, J. P., *J. Polym. Sci., Polym. Phys. Ed.,* 1982, **20**, pp 1895 - 1900.

[73] Nassar, T. R., Paul, D. R. and Barlow, J. W., *J. Appl. Polym Sci.,* 1979, **23**, p 85.

Murff, S. R., Paul, D. R. and Barlow, J. W., *J. Appl. Polym Sci.,* 1984, **29**, p 3231.

[74] Godard, P., Dekoninck, J. M., Devlesaver, V. and Devaux, J., *J. Polym. Sci., Polym. Chem. Ed.,*1986, **24**, pp 3301 - 3313.

[75] Ihm, D. W., Park, S. Y., Chang, C. G., Kim, Y. S. and Lee, H. K., *J. Polym. Sci., Polym. Chem. Ed.,* 1996, **34**, pp 2841 - 2850.

Stewart, M. E., Cox, A. J. and Naylor, D. M., *Polymer,* 1993, **34**, p 4060.

[76] Backson, S. C. E., Kenwright, A. M. and Richards, R. W., *Polymer,* 1995, **36**, pp 1991 - 1998.

[77] Ihm, D. J. and White, J. L., *J. Appl. polym. Sci.,* 1996, **60**, pp 1 - 7.

[78] Lepers, J.-C., Favis, B. D. and Kent, S. L., *Polymer,* 2000, **41**, pp 1937 - 1946.

Papadopoulou, C. P. and Kalfoglou, N. K., *Polymer,* 2000, **41**, pp 2543 - 2555.

[79] Pradhan, A. K., Pati, N. C. and Nayak, P. L., *J. Appl. Polym. Sci.,* 1982, **27**, pp 1873 - 1881.

Sanli, O. and Pulat, E., *J. Appl. Polym. Sci.,* 1993, **47**, pp 1 - 6.

[80] Nadkarni, V. M. and Jog, J. P., *Polym. Eng. Sci.,* 1987, **27**, pp 451 - 457.

Nadkarni, V. M., Shingankuli, V. L. and Jog, J. P., *J. Appl. Polym. Sci.,* 1992, **46**, pp 339 - 351.

[81] Legros, A,., Carreau, P. J., Favis, B. D. and Michel, A., *Polymer*, 1994, **35**, pp 758 - 764.

[82] Graun, G. P., Kuo, C.-Y. and Neag, C. M., *Prog. Org. Coat.*, 1996, **29**, pp 55 - 60.

[83] Jha, A. and Bhowmick, A. K., *Polymer,* 1997, **38**, pp 4337 - 4344.

[84] Raboney, M., Hseih, D. T., Garner, D. T. and Peiffer, D. G., *J. Chem. Phys.*, 1992, **97**, pp 4505 - 4511.

[85] Yoon, H. and Han, C. C., *Polym. Eng. Sci.*, 1995, **35**, pp 1476 - 1480.

[86] Montaudo, G., Puglisi, C. and Samperi, F., *J. Polym. Sci., Polym. Chem. Ed.*, 1998, **36**, pp 1873 - 1884.

[87] Grassie, N., in *Weathering and Degradation of Plastic,* 1966. Columbine Press.

[88] Hoffmann, A.W., *J. Chem. Soc.*, 1861.

[89] Hurd, C.D. and Blunck, F.H., *J. Am. Chem. Soc.*, 1938, **60**, p 2419.

Blades, A. T., *Can. J. Chem.*, 1954, **32**, p 366.

DePuy, C. H. and King, R. W., *Am. Chem. Soc. Chem. Rev.*, 1960, **60**, pp 431 -

[90] Marshall, I. and Todd, A., *Trans. Faraday Soc.*, 1953, **49**, pp 67 - 78.

[91] Goodings, E. P., *Soc. Chem. Ind.*, 1961, **13**, pp 211 - 228.

[92] Ritchie, P. D., *Soc. Chem. Ind.*, 1961, **13**, pp 107 - 130.

[93] Buxbaum, L. H., *Angew. Chem. Internat. Ed.*, 1968, **7**, pp 182 - 190.

[94] Zimmerman, H., in *Developments in Polymer Degradation, Vol. 5.*, 1985, Ed. Grassie, N., Elsevier Applied Science.

[95] McNeill, I. C. and Bounekhel, M., *Polym. Deg. Stab.*, 1991, **34**, pp 187 - 204.

[96] Yoda, K., Tsuboi, A., Wada, M. and Yamadera, R., *J. Appl. Polym. Sci.*, 1970, **14**, pp 2357 - 2376.

[97] Nealy, D. L. and Adams, L. J., *J. Polym. Sci.*, 1971, **9**, pp 2063 - 2070.

[98] Spanninger, P. A., *J. Polym. Sci.*, 1974, **12**, pp 709 - 717.

[99] MacDonald, W. A., DuPont Teijin Films. Inc. Private communication.

[100] Campanelli, J. R., Cooper, D. G. and Kamal, M. R., *J. appl. Polym. Sci.*, 1994, **53**, pp 985 - 991.

Zimmerman, H. and Kim, N. T., *Polym. Eng. Sci.*, 1980, **20**, pp 680 - 683.

Weidner, S., Kuehn, G., Werthmann, B., Schroeder, H., Just, U., Borowski, R., Decker, R., Schwarz, B., Schmuecking, I. and Seiffert, I., *J. Polym. Sci., Polym. Chem. Ed.*, 1997, **35**, pp 2183 - 2192.

Seo, K. S. and Cloyd, J. D., *J. Appl. Polym. Sci.*, 1991, **42**, pp 845 - 850

[101] McMahon, W., Birdsall, H. A., Johnson, G. R. and Camilli, C. T., *J. Chem. Eng. Dat.*, 1959, **4**, pp 57 - 79.

[102] Golicke, R. C. and Lasoski, S. W. Jnr., *J. Phys. Chem.*, 1960, **64**, pp 894 - 898.

[103] Davies, T., Goldsmith, P. L., Ravens, D. A. S. and Ward, I. M., *J. Phys. Chem.*, 1962, **66**, pp 175 - 176.

[104] Ravens, D. A. S. and Ward, I. M., *Trans. Faraday Soc.*, 1961, **57**, pp 150 - 159.

[105] Carlsonn, D. J. and Wiles, D. M., in *Encyclopaedia of Polymer Science and Engineering*, 1985, pp 630 - 696.

[106] Allen, N. S., Edge, M., Mohammadian, M. and Jones, K., *Polym. Deg. Stab.*, 1994, **43**, pp 229 - 237.

Allen, N. S., Edge, M., Mohammadian, M. and Jones, K., *Polym. Deg. Stab.*, 1993, **41**, pp 191 - 196.

Allen, N. S., Edge, M., Mohammadian, M. and Jones, K., *Eur. Polym. J.*, 1994, **27**, pp 1373 - 1378.

[107] Ballara, A. and Verdu, J., *Polym. Deg. Stab.*, 1989, **26**, pp 361 - 374.

[108] Oku, A., Hu, L.-C. and Yamada, E., *J. Appl. Polym. Sci.* 1997, **63**, pp 595 - 601.

Ellison, M. S., Fisher, L. D., Alger, K. W. and Zeronian, S. H., *J. Appl. Polym. Sci.*, 1982, **27**, pp 247 -257.

Zeronian, S. H., Wang, H.-Z. and Alger, K. W., *J. Appl. Polym. Sci.*, 1990, **41**, pp 527 - 534.

[109] Solbrig, C. M. and Obendorf, S. K., *J. Appl. Polym. Sci., Appl. Poly. Symp.*, 1991, **47**, pp 437 - 444.

[110] Overton, J. R. and Haynes, S. K., *J. Polym. Sci., Polym. Symp.*, 1973, **43**, pp 9 - 17.

Farrow, G., Ravens, D. A. S. and Ward, I. M., *Polymer*, 1962, **3**, pp 17 - 25.

[111] Marchand - Brynaert, J., Deldime, M., Dupont, I., Dewez, J.-L. and Schneider, Y.-J., *J. Colloid Inter. Sci.*, 1995, **173**, pp 236 - 244.

Mougenot, P., Koch, M., Dupont, I., Schneider, Y.-J. and Marchand - Brynaert, J., *J. Colloid Inter. Sci.*, 1996, **177**, pp 162 - 170.

Bergbreiter, D. E., Srinivas, B., Xu, G.-F., Gray, H. N. and Bandella, A., *J. Plast.Film Sheet.*, 1996, **12**, pp 15 - 26.

[112] Tabankia, M. H. and Gardette, J.-L., *Polym. Deg. Stab.*, 1986, **14**, pp 351 - 365.
Scheirs, J. and Gardette, J.-L., *Polym. Deg. Stab.*, 1997, **56**, pp 339 - 350.

[113] Edge, M., Wiles, R., Allen, N. S., MacDonald, W. A., Mortlock, S. V., *Polym. Deg. Stab.*, 1996, **53**, pp 141 - 151.
Edge, M., Allen, N. S., Wiles, R., MacDonald, W., Mortlock, S. V., *Polymer*, 1995, **36**, pp 227 - 234.

[114] Grassie, N., *Chemistry of High Polymer Degradation Processes*, 1956, Butterworth, London.

[115] Inaba, A., Kashiwagi, T. and Brown, J. E., *Polym. Deg. Stab.*, 1988, **21**, pp 1 - 20.

[116] Grassie, N., McNeill, I. C. and Samson, N. R., *Polym. Deg. Stab.*, 1979, **1**, pp 17 - 35.

[117] Deng, B.-L., Hu, Y.-S., Chiu, W.-Y., chen, L.-W. and Chiu, Y.-S., *Polym. Deg. Stab.*, 1997, **57**, pp 269 - 278.

[118] Grassie, N. and Melville, H. W., *Proc. R. Soc.*, 1949, **A199**, p 1.

[119] Barlow, A., Lehrle, R. S., Robb, J. C. and Sunderland, D., *Polymer*, 1967, **8**, p 537.

[120] McNeill, I. C. and Mohammed, M. A. J., *Eur. Polym. J.*, 1972, **8**, pp 975 - 990.

[121] Russell, T. P., *Mater. Sci. Rep.*, 1990, **5**, p 171.

[122] Higgins, J. S. and Benoît, H. C., *Polymers and Neutron Scattering*, 1996, Oxford University Press, Oxford, UK.

[123] Bertin, E. P., in *Progress in Analytical Chemistry, Volume 2.*, Ed. Murt, E. M. and Guldner, W. G., 1969, Plenum Press, New York.

[124] Greef, R., in *Comprehensive Treatise on Electrochemistry, Volume 8.*, Ed. White, R. E. and Bockris, O. M., 1984, Plenum Press, New York.

[125] Paik, W.-k., in *Modern Aspects of Electrochemistry, No. 25.*, Ed. Bockris, J. O.' M., Conway, B. E. and White, R. E., 1993, Plenum Press, New York.

[126] Inoue, T. and Yukioka, S., *Polymer*, 1993, **34**, pp 1256 - 1259.
Kressler, J., Higashida, N. and Inoue, T., *Am. Chem. Soc., Div. Polym. Chem., Pre-Prints*, 1992, **33**, pp 593 - 594.
Yukioka, S., Nagato, K. and Inoue, T., *Polymer*, 1992, **33**, pp 1171 - 1176.

[127] Habicht, J., Schmidt, M., Rühe, J. and Johannsmann, D., *Langmuir,* 1999, **15**, pp 2460 - 2465.

[128] Chen, W.-L., Shull, K. R., Papatheodorou, T., Styrkas, D. and Keddie, J. L., *Macromolecules,* 1999, **32**, pp 136 - 144.

[129] Beaucage, G., Composto, R. and Stein, R. S., *J. Polym. Sci., Polym. Phys. Ed.,* 1993, **31**, pp 319 - 326.

[130] Wehrum, A., PhD thesis, 1998, St Catherines College, University of Cambridge.

[131] Styrkas, D., Doran, S. J., Gilchrist, V., Keddie, J. L., Lu, J. R., Murphy, E., Sackin, R., Su, T.-J. and Tzitzinou, A., in *Polymer surfaces and Interfaces III,* Ed. Richards, R. W. and Peace, S. K., 1999, John Wiley, New York.

[132] Lin. E. K., Wu, W.-l. and Satija, S. K., *Macromolecules,* 1997, **30**, pp 7224 - 7231.

[133] Reiter, G., Hüttenbach, S., Foster, M. and Stamm, M., *Macromolecules*, 1991, **24**, pp 1179 - 1184.

Liu, Y., Reiter, G., Kunz, K. and Stamm, M., *Macromolecules*, 1993, **26**, pp 2134 - 2136.

[134] Tronin, A., Lvov, Y. and Nicolini, C., *Colloid Polym. Sci.,* 1994, **272**, pp 1317 - 1321.

[135] Parratt, L. G., *Phys. Rev.,* 1954, **95**(2), pp 359 - 369.

[136] Born, M. and Wolf, E., *Principles of Optics,* 1970, Pergamon Press, Oxford.

[137] Heavens, O. S., *Optical Properties of Thin Solid Films,* 1955, Butterworths, London.

Penfold, J., *Prog. Colloid Polym. Sci.,*1990, **81**, pp 198 - 202.

[138] Cowley, R. A. and Ryan, T. W., *J. Phys. D., Appl. Phys.,* 1987, **20**, p 61.

[139] Fox, B., Moad, G., van Diepen, G., Willing, I. and Cook, W. D., *Polymer,* 1997, 38, pp 3035 - 3043.

[140] Kricheldorf, H. R., Makromol. Chem., 1978, **179**, pp 2133 - 2143.

Chapter 3.

Some Properties of PET / PMMA Blends.

3.1. Introduction.

In this chapter the behaviour of PET/PMMA blends will be examined. The interactions in the bulk phase between polyesters and acrylics are important because these two types of polymers may become mixed during reclaim procedures on polyester film manufacturing lines [1]. In the following chapters, the analysis of thin layers of PET and PMMA, and the interface between these two polymers, is described by the use of reflection techniques. The information will aid the comparison between bulk and thin layer behaviour of these polymers, as well as giving direct insight into the nature of the blend.

The intentions were to investigate the chemical interaction between the two polymers, and to some extent the phase behaviour of the blend, with respect to blend composition and temperature. The chemical interaction between PET and PMMA may proceed via the transesterification reactions identified by Kotliar [2]; namely alcoholysis, acidolysis and direct ester exchange (see schemes 3.1-3.3). It is well known that these reactions are commonplace in the case of two interacting main chain polyesters [3], but the extent to which transesterification occurs between acrylate based polymers and main chain polyesters has rarely been studied.

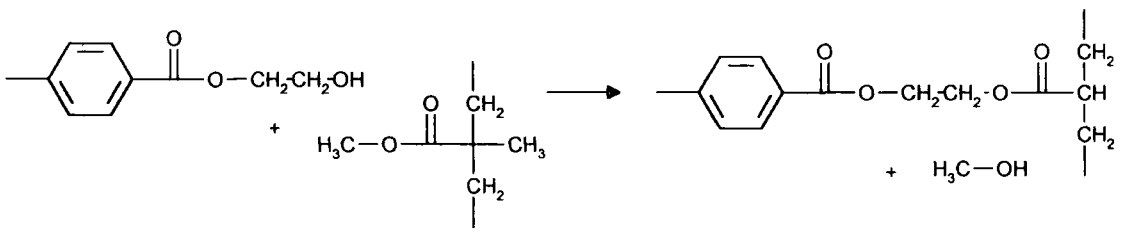

Scheme 3.1. Proposed alcoholysis between PET - OH and PMMA.

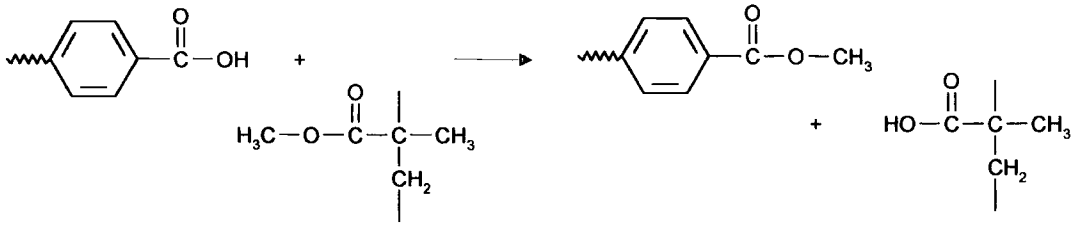

Scheme 3.2 Acidolysis between PET-COOH and PMMA

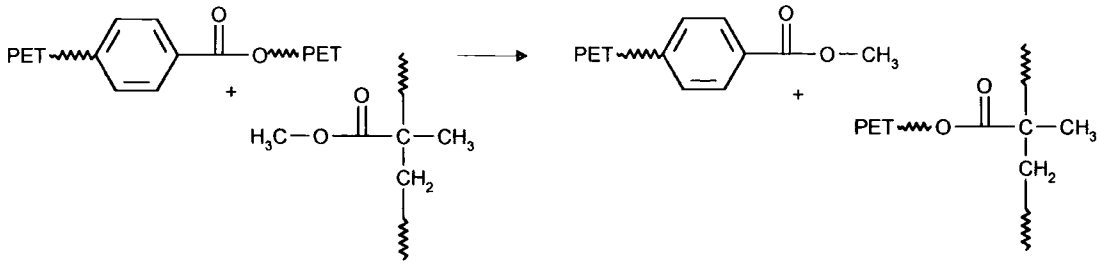

Scheme 3.3 Direct ester exchange between PET and PMMA

One specific case which is relevant to this work, is the polycarbonate (PC)/PMMA system which has spawned much literature attention over recent years. Yoon and Han [4] studied blends of the two polymers between 453 and 473K and found an interfacial thickness of ~30 Å by small angle neutron scattering (SANS). They attribute the development of an interfacial region to transesterification reactions between the two polymers. Extended reaction times at 463K led to the development spherical structures similar to those reported by Raboney *et al* [5], and they postulate that these structures could be due to the emulsifying effect of graft copolymers formed by the direct ester exchange mechanism (scheme 3.3). Kyu *et al* [6], and Ko *et al* [7], also observe the existence of transesterification reactions between PC and syndiotatic PMMA, by studying the miscibility - temperature dependence of the blend.

However, Montaudo *et al* [8] recently reported that inter chain transesterification does not occur between PC and PMMA, but occurs readily between methyl methacrylate and PC at temperatures above the PMMA degradation temperature. The thermal degradation of PC/PMMA blends has also been studied [6,7,9], but the results for the thermal stability of the mixture, are confused.

3.2. Experimental.

For the investigation of chemical interactions between PET and PMMA in the bulk phase, intimate mixtures of the two polymers were required. This was achieved by mixing homogenous solutions of the two homopolymers in a common solvent, followed by co-precipitation in a non solvent. The interaction between the polymers was assessed after annealing at fixed temperatures, in the temperature range 298 - 573K, under vacuum.

3.2.1. Material Characterisation.

PET was prepared using a small scale pilot plant facility at DuPont Teijin Polyester Films (DTF) R&T. laboratories Wilton, UK. The polymer batch code was G1063 and was produced to a nominal molecular weight, determined by the viscosity of the melt phase during polymerisation. Atatic PMMA was purchased from Aldrich Chem. Co. Ltd.

The molecular weight distribution of the two polymers was determined by GPC, using a triple detector analysis (Refractive index, solution viscometry and light scattering). The results are shown in table 3.1.

Table 3.1 Molecular weight analysis of PET and PMMA.

Sample	M_w	M_N	M_W/M_N
PET	67,500	23,200	2.9
PMMA	129,800	44,400	2.9

3.2.2. Intimate Mixtures From Co-precipitation.

Blend preparation.

PET and PMMA were purified by dissolution, filtration and Soxhlet extraction of the re-precipitated solid. Blends were prepared by weighing accurately the desired

mass of each polymer and then dissolved in ortho-chloro phenol (OCP) (approx. ~ 2g in 20 ml), followed by re-precipitation in anhydrous methanol. The re-precipitated product was Soxhlet extracted in anhydrous methanol for 48 hrs. to remove any residual solvent, and then dried under vacuum for 24 hrs at 323K.

Annealing programme.

Blends were to annealed at three temperatures, 473K, 523K and 573K. In each case the thermal treatment was carried out under continuous vacuum. (~1 mbar). For 473K and 523K, the blends were annealed in glass tubes in a dry block heater fitted with a vacuum manifold. Prior to heating, the tubes were filled with anhydrous N_2 and evacuated at least three times, in order to purge moisture from the sample environment. For heating at the highest temperature, samples were placed inside a boiling tube which was connected to a vacuum pump via an isolation tap. The tube was immersed in a high temperature solder bath maintained at 573 ± 2K.

3.2.3 Characterisation and Analysis.

Weight Loss

The rate of weight loss for the 50/50 blend and the two homopolymers was measured by difference at appropriate time intervals during the annealing programme. Sample tubes were isolated from the vacuum manifold, immediately weighed, and returned to the heating mantle or bath. The weight loss for these samples was assessed for periods up to 3 hrs. It was estimated that this method is sensitive to ~ 0.02% weight change in the 1g sample used.

For the blends of different PET / PMMA composition, the total weight loss was measured after annealing for 3 hrs. at 523K. A theoretical weight loss, assuming no interaction between PET and PMMA, can be estimated from the weight loss of the two homopolymers under the conditions of annealing, and summing these fractions for each blend composition.

Blend solubility.

The weight change of the PET and PMMA fractions were measured by removal of the PMMA phase from the blend by dissolution in acetone, in the manner described

by Kyu *et al* [6]. The acetone insoluble phase was washed in anhydrous methanol several times and dried in a vacuum oven at 343K for 48hrs. The recovered mass of solid was then compared to the original blend composition, taking into account the measured weight loss from the sample.

NMR

The 50/50 blend, and the two hompolymers were analysed by solution state H - NMR before and after annealing. The solvent used was deuterated tetrachloro ethylene (D-TCE)/$CDCl_3$ 1:1. All spectra were obtained on Jeol GSX 400 MHz, at a probe temperature of 373K.

DSC- Isothermal Crystallisation

Isothermal crystallisation of PET, PMMA and the 50/50 blend was studied by DSC, using a Perkin - Elmer DSC -7. The isothermal crystallisation temperatures were 403K, 433K and 493K. Samples were first dried at 353K for 24hrs, then placed into the DSC. The samples were heated to 553K at 200K min^{-1}, and then rapidly quenched (320K/min) to the required crystallisation temperature, where they were held until a steady state heat flow was obtained. Thermograms were analysed to ascertain the crystallisation half time and the overall rate of crystallisation was studied using the Avrami theory for polymer crystallisation.

DSC- Non isothermal Crystallisation

The thermal characteristics of the two homopolymers, the 50/50 blend and the 80/20 blend were measured using differential scanning calorimetry. The samples were dried at 353K under vacuum for 24 hrs prior to analysis. Approximately 10 mg of each sample was heated at 20K min^{-1} to 553K, held for 2 min. and then rapidly quenched at 200K min^{-1}. to 253K. The samples were then reheated at 20K min^{-1}. (reheat scan) to 553K held for 5 min. and then cooled at 20K min^{-1} to 298K (cooling scan).

3.3. Results

3.3.1. Kinetics of Blend Degradation.

Weight Loss from homopolymers and 50/50 Blend

The degradation of PET, PMMA and a 50/50 blend of the two polymers have been studied by monitoring the weight loss of the samples with time, over the temperature range 473 - 573K. The results are shown in table 3.2.

Table 3.2 % weight loss from PET, PMMA and 50/50 Blend.

	Annealing period (min)								
	0	30	60	90	120	150	180	210	240
					473K				
PET	0.00	-	-	-	0.25	0.27	0.27	0.28	0.28
50/50	0.00	-	0.55	0.65	1.20	1.30	1.55	-	-
PMMA	0.00	0.25	0.75	1.20	1.90	2.30	3.00	3.40	3.50
					523K				
PET	0.00	-	-	0.23	0.29	0.31	0.31	0.31	0.31
50/50	0.00	5.20	6.40	7.30	8.00	8.60	9.20	-	-
PMMA	0.00	10.00	18.05	27.90	32.00	41.05	48.50	49.00	51.20
					573K				
PET	0.00	-	0.20	0.31	0.38	0.38	0.40	0.44	0.44
50/50	0.00	19.20	22.60	26.90	-	-	-	-	-
PMMA	0.00	79.00	86.08	92.58	94.52	-	-	-	-

The data are displayed graphically in figure 3.1 as a first order reaction according to equation 3.1

$$\ln\left(\frac{W}{W_0}\right) = -kT \qquad (3.1)$$

where W and W_0 are the mass of sample at time $t = t$ and $t=0$ respectively and k is the first order rate constant for the reaction.

The values for k for PMMA, PET and the 50/50 blend at the various temperatures are plotted according to the logarithmic form of the Arrhenius equation;

$$\ln(k) = \ln(A) - \frac{E_a}{RT} \qquad (3.2)$$

to obtain that the activation energy E_a, for weight loss. For PMMA, PET and the 50/50 blend, this plot is shown in figure 3.1. The good linear fit shows Arrhenius compliance for these samples, and the activation energy E_a is calculated from the gradient of the straight line fit to the data. E_a for weight loss under vacuum for PET, PMMA and the 50/50 are shown in table 3.3.

Table 3.3. Kinetic data for weight loss from PET, PMMA and 50 /50 blend.

Temperature (K)	k / s^{-1}		
	Pure PET	Pure PMMA	50/50 blend
473	3.39×10^{-7}	2.61×10^{-6}	1.47×10^{-6}
523	3.99×10^{-7}	5.55×10^{-5}	1.08×10^{-5}
573	5.12×10^{-7}	5.35×10^{-4}	6.61×10^{-5}
Arrhenius (1st order)	E_a kJmol^{-1}		
	9.2	120	86

Firstly, the weight loss from PET and PMMA are considered. Figure 3.1 shows that the assumption of 1st order kinetics is correct for PMMA. It should be noted that the rate of weight loss from PET is calculated from the initial slope of the linear fit to the data. The weight loss is seen to reach a constant value after ~2.5 hrs.

The analysis has shown that PET is very stable under the conditions of annealing. Although the condensate has not been chemically identified, it is assumed that the small amount of weight loss seen at 573K is due to melt condensation of the polymer yielding small quantities of ethylene glycol and also to the removal of low molecular weight oligomer from the sample [10,11,12], or even volatalisation of residual water. The activation energy E_a, is small enough for the observed weight loss to be physical process, and as such chain degradation is not considered in this case. This result is in good agreement with published results. For instance, Jabarin and Lofgren [10] have shown that virtually no weight loss is evident from PET at temperatures < 573K under anaerobic conditions. The thermal degradation of PET under anaerobic conditions has been discussed in Chapter 2, and it is known that even in the melt state, PET will maintain its molecular weight because the polymer is able to tranesterify with itself.

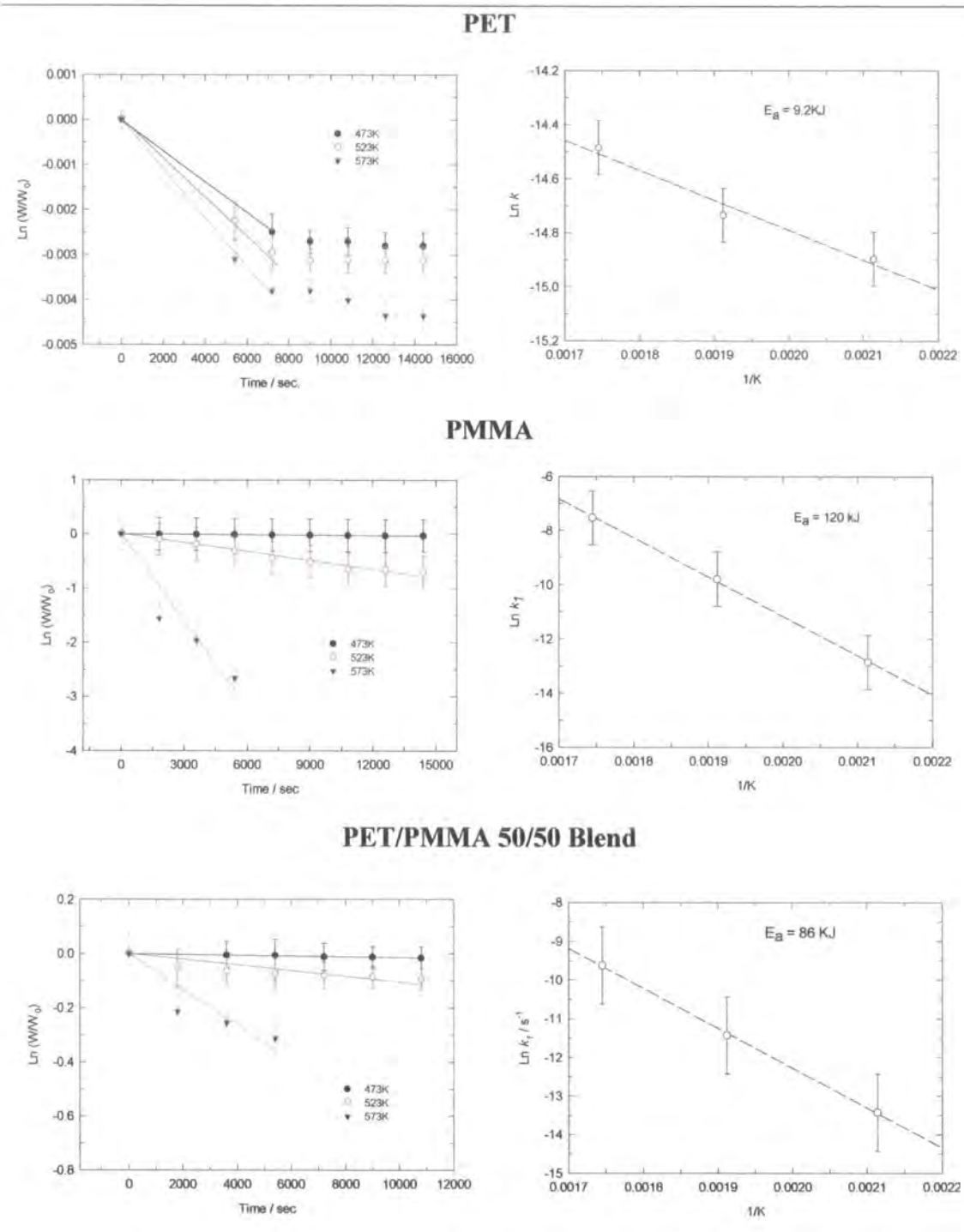

Figure 3.1 Weight loss and corresponding Arrhenius plots for PET, PMMA, and PET/PMMA 50/50 blend.

On the other hand, the weight loss of PMMA is seen at all temperatures with nearly complete reduction at 573K after 1 hr annealing. The calculated E_a for weight loss compares well with published values for PMMA thermal degradation [14],

although specific rate constants vary, presumably because of differences in experimental protocol.

These results uphold the known mechanism of weight loss for PMMA i.e. progressive depolymerisation to monomer. This is to be expected; under the conditions of this experiment the products of depolymerisation will be continuously removed.

We now turn to the weight loss from the 50/50 blend sample. As PET is known to be relatively stable under the conditions of this experiment, it is expected that the degradation of PMMA will dominate the weight loss behaviour of the blend, i.e.

$$\frac{dW_{PMMA}}{dt} >>> \frac{dW_{PET}}{dt} \tag{3.3}$$

Assuming the condition given above is correct, then the weight loss of the 50/50 blend can be attributed to PMMA entirely. A new rate constant can be calculated by normalising for the fraction of PMMA in the blend (i.e. 50%), and this result is plotted in figure 3.2 with the corresponding Arrhenius plot. As can be seen, the rate constant for weight loss of PMMA is modified in the 50/50 blend when compared to the homopolymer. The rate constants are 2.95×10^{-6} s^{-1} at 473K, 2.27×10^{-5} s^{-1} at 523K and 1.59×10^{-4} s^{-1} at 573K. E_a for PMMA depolymerisation is recalculated as 89 KJ/mol.

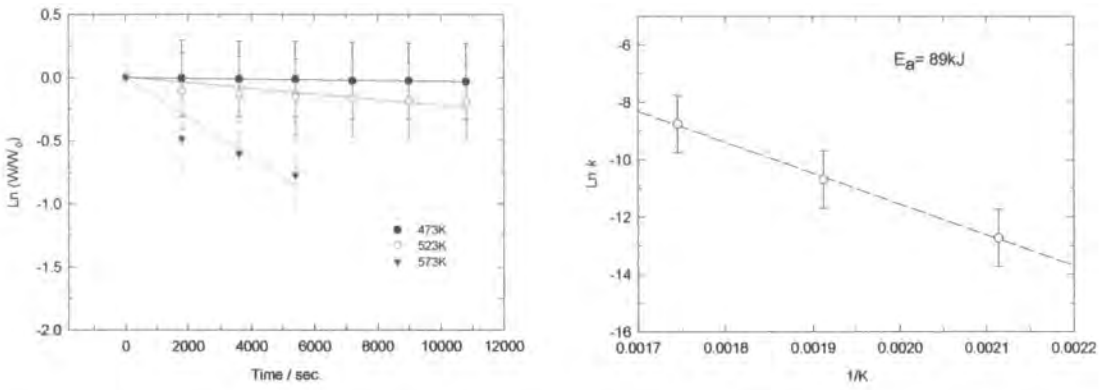

Figure 3.2 Normalised Weight loss and corresponding Arrhenius plot for PMMA in 50/50 Blend.

Dependence of Weight Loss on Initial Blend Composition

The weight loss, after 3 hrs of annealing at 523K, from the blends of differing composition are shown in table 3.4 It was assumed that the weight loss for these samples is 1st order, only the final weight loss after annealing is required to calculate a (crude) rate constant. The theoretical weight loss is calculated from the weight loss of the two homopolymers, i.e. assuming that there is no form of rate enhancement or retardation of weight loss, then the theoretical weight loss is simply the sum of the expected weight loss from each component. This value is compared to the actual weight loss and actual and theoretical rate constants are derived accordingly

Table 3.4 Weight loss from Different Blend Compositions

Blend ratio PET/PMMA (%)	Weight loss (%)		Rate constant k s^{-1}	
	Actual ± 5	Theory	Actual ± 2 × 10^{-6}	Theory
100/0	0.32	0.32	3.99×10^{-7} *	3.99×10^{-7} *
80/20	2.61	9.80	2.45×10^{-6}	9.55×10^{-6}
60/40	4.40	19.62	4.16×10^{-6}	2.02×10^{-5}
50/50	9.20	24.45	1.08×10^{-5} *	2.60×10^{-5} *
40/60	10.41	29.28	1.02×10^{-5}	3.21×10^{-5}
20/80	35.91	38.93	4.12×10^{-5}	4.57×10^{-5}
0/100	48.46	48.46	5.55×10^{-5} *	5.55×10^{-5} *

* From Table 3.3

The values shown in table 3.4 indicate that the weight loss from the blends across much of the composition range are appreciably lower than the theoretical value. The observed % weight loss for 20/80 PET/PMMA appears to be close to the theoretical value is within the estimated error of the experiment (~5%).

Figure 3.3 shows a plot of weight loss vs. PMMA blend composition (initial). The observed weight loss deviates from the theoretical line, calculated assuming that there is no interaction between the polymers. The largest difference between the observed and theoretical weight loss is at intermediate blend ratios. These results indicate that the blend composition (and presumably the blend morphology), have a profound influence upon the thermal stability of the blend.

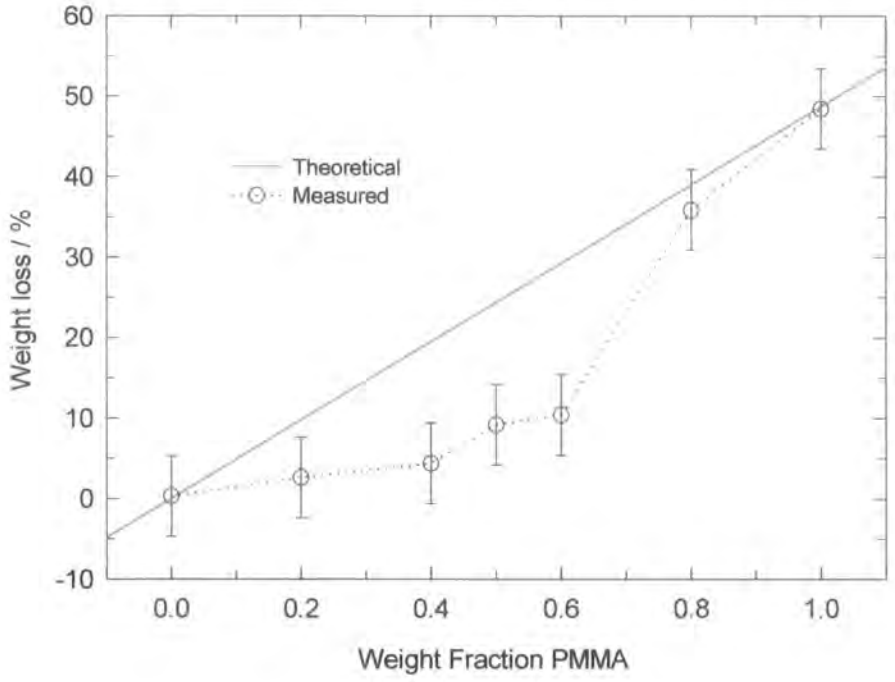

Figure 3.3. Observed and theoretical weight loss for PET/PMMA blends.

Conclusions

PET is seen to very stable under anaerobic conditions in the temperature range 473K - 573K. As expected, PMMA shows extensive weight loss under the same conditions, and the activation energy for depolymerisation is calculated as 120kJmol^{-1}, which is in good agreement with previously reported values. The rate of depolymerisation of PMMA is appreciably altered in blends with PET. The initial blend composition influences the rate of weight loss, with intermediate blend ratios showing the largest retardation in the expected weight loss. The results can be explained by considering a reaction between the two polymers. Either a chemical reaction has taken place between PET and PMMA and is therfore acting as a chain stopper, e.g.

MMA-MMA-MMA-MMA-**PET**-MMA-MMA-MMA-**PET**-MMA-MMA etc

or, the monomer produced by depolymerisation is reacting with the PET, and is subsequently unable to volatalise, e.g.

PET + MMA ——> PET-MMA.

3.3.2. PET/PMMA Blend Solubility.

The acetone soluble fraction of the homopolymers and the 50/50 blend was determined by extraction in boiling acetone for 8 hrs (see section 3.2). The recovered insoluble fraction was weighed and compared to original blend composition , taking into account the weight loss after annealing. Furthermore, in the course of preparing samples for H^1 - NMR spectroscopy, it was noticed that certain samples formed cloudy solutions in D-TCE/$CDCl_3$ solvent, indicative of insoluble material in the sample. Further investigation of this insolubility was made by dissolving blend samples in hexa- fluoro isopropanol (HFIP), (warm solution, 4 hrs.) The solubility of the blend samples is indicative of the extent of grafting reaction between the two polymers [6,7,8], and as such can be used as a quantitative representation of this reaction. The *insoluble* fractions in acetone and HFIP are given in table 3.5

Table 3.5 Solubility of Annealed Blends (% Insoluble fraction).

	PET		50/50 Blend			PMMA	
	Acetone	HFIP	Comp.*	Acetone	HFIP	Acetone	HFIP
Unannealed	100	0	50/50	50.4	0	0	0
473	100	0	52/48	53.3	7.8	2	0
523	100	0	55/45	62.3	12.1	8	2
573	100	0	68/32	79.4	9.8	12	2

* Actual blend composition calculated from weight loss data.

As expected, the PET samples were completely insoluble in acetone, (although some swelling and solvent retention was seen. Therefore, the acetone insoluble fraction of the blend samples can be considered to be consisting of the entire PET phase of the blend, plus any insoluble material formed by polymer / polymer interactions. However, PMMA also forms acetone insoluble material, hence the insoluble material in the blends could be accounted for by considering the crosslinking of PMMA alone. If we consider the HFIP insoluble fraction to be the result of extensive PET/PMMA chemical reaction, then it is apparent that this reaction is more prevalent at higher temperatures (523 and 573K). Although a small fraction of HFIP insoluble material is formed during the annealing of the pure PMMA samples, more is formed in the blend samples with respect to the overall PMMA weight fraction.

Conclusions

An appreciable amount of HFIP insoluble material is formed in PET / PMMA blends after annealing, compared to the two homopolymers. This insoluble material is seen to increase with increasing annealing temperature, and can be considered to be the product of a PET / PMMA graft reaction, or the result of a crosslinking reaction within the PMMA itself.

3.3.3. NMR of PET, PMMA and Annealed Blends.

NMR spectroscopy was used to study the chemical nature of the PET homopolymer and the 50/50 blend. The samples were analysed after completion of annealing.

Detailed investigation of the spectra revealed that the peak due to the hydroxyl end groups in PET was altered upon blending and subsequent annealing. The main feature of this peak was the change in the shape of the triplet corresponding to -OH end groups, due to the overlay of a singlet at ~3.95 ppm (see figure 3.4).

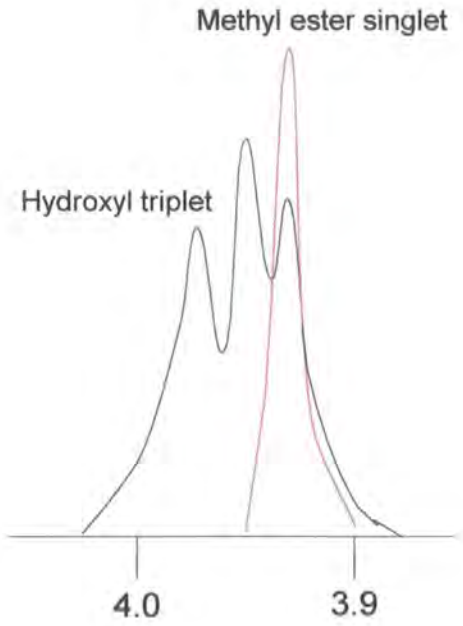

Figure 3.4. Schematic representation of the region of the H^1 - NMR spectra showing the peaks due to PET-OH (black) and PET-$COOCH_3$ (red).

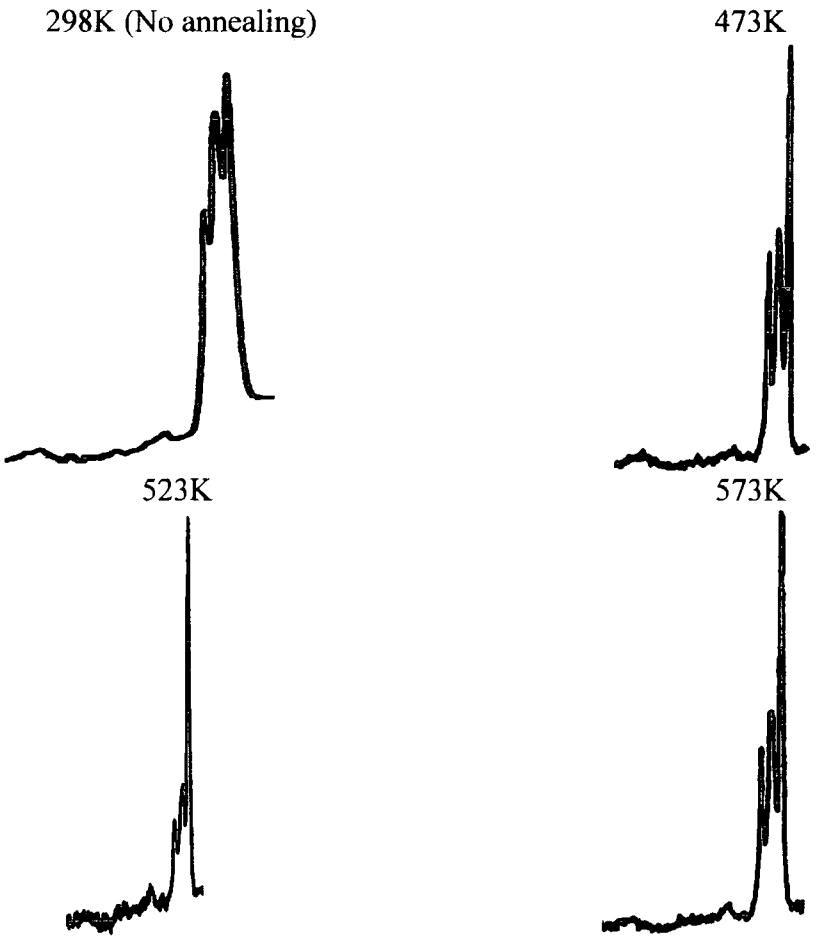

Figure 3.5. Detail of NMR spectra showing hydroxyl end group triplet and methyl ester singlet increasing for the PET / PMMA blends annealed at the indicated temperatures. The vertical scales are not the same.

This singlet has been assigned to the formation of methyl ester end groups in PET and is similar to the result obtained by Montaudo *et al* [8], who have observed a singlet at the same chemical shift in PC/PMMA blends, and assigned to a methyl ester terminal group on a PC chain.The NMR spectra for the 50/50 blend samples, unannealed and annealed at 473K, 523K, and 573K are shown in figure 3.5. Only the region of the spectrum containing peaks due the PET end groups are shown. Clearly, there are differences in the end group triplet at ~3.95ppm chemical shift. These differences will be discussed in the next section.

The hydroxyl and methyl ester end group concentration for pure PET and the 50/50 blend have been calculated per 100 repeat units of PET and these results are given in table 3.6.

Table 3.6. PET end group concentrations from H^1 - NMR Analysis.

Sample	Annealing Temp. (K)	End group conc. / 100 repeat units.	
		Hydroxyl	methyl Ester
PET	298	1.37 ±0.2	0.00
	473	1.16 ±0.2	0.00
	523	0.58 ±0.2	0.00
	573	1.31 ±0.3	0.02 ±0.001
50/50 PET/PMMA Blend	298	1.79 ±0.3	0.09 ±0.02
	473	1.51 ±0.3	0.15 ±0.02
	523	0.53 ±0.3	0.19 ±0.02
	573	1.12 ±0.3	0.19 ±0.02

These results indicate that there is no appreciable difference in hydroxyl end group concentration for PET in a blend with PMMA when compared to pure PET treated under the same regime. In fact the hydroxyl end group concentration is seen to be higher for PET in the blend; this may be the result of statistical variation as it is otherwise difficult to explain this result, particularly for the unannealed blends. The results are shown graphically in figure 3.6.

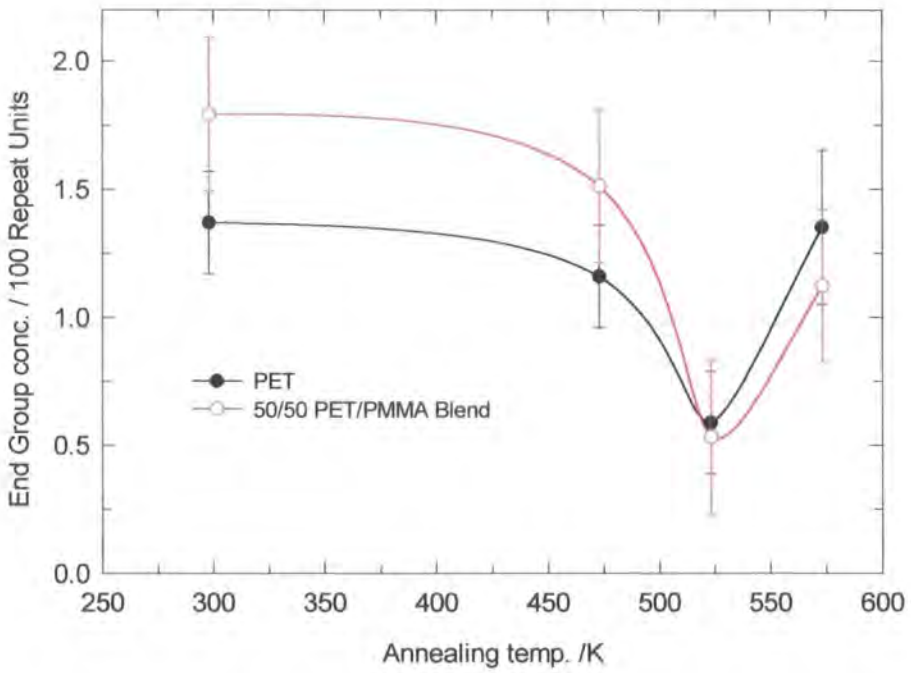

Figure 3.6. Hydroxyl end group concentration as a function of annealing temperature for pure PET and PET/PMMA blends. The line is a guide to the eye.

The concentration of methyl ester groups is seen to increase with annealing temperature in the PET/PMMA blend indicating that some form of reaction has occurred. The presence of methyl ester groups in pure PET, after annealing at 373K is consistent with the known degradation mechanisms of PET under anaerobic conditions [13]. These results will be discussed in detail in the next section.

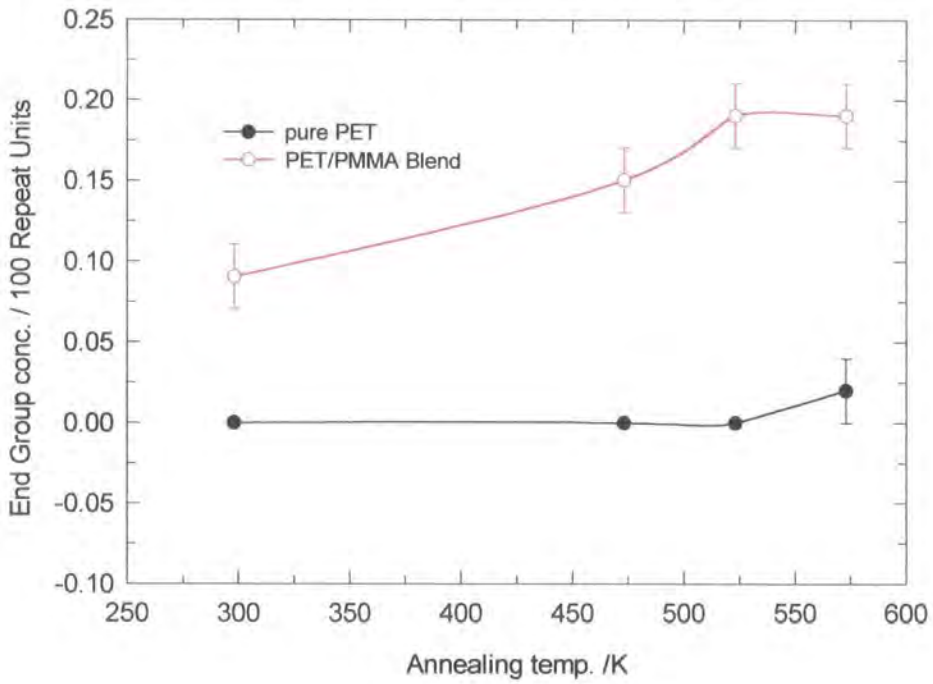

Figure 3.7 Methyl ester concentration vs. annealing temperature for pure PET and PET in PET/PMMA blend. The line is a guide to the eye.

Conclusions

Methyl ester end groups were detected at a chemical shift of 3.95 ppm in agreement with the work of *Montaudo et al* [8]. The methyl ester end group concentrations of PET in a PET/PMMA blend is appreciably higher than for the equivalent pure PET samples. There appears to be no reduction in hydroxyl end groups compared to pure PET , which is indicative of the absence of a significant alcoholysis reaction as proposed in reaction scheme 3.1.

3.3.4. Non -isothermal DSC

The heating scans after rapid quench from the melt, for PET and the 50/50 blend samples are shown in figure 3.8. It is clear that the presence of PMMA inhibits the crystallisation of PET in the blend when compared to the pure PET crystallisation; i.e. the peak crystallisation is shifted to a higher temperature. However, inspection of the cooling scans for the same samples (figure 3.9) indicate that the samples annealed at 523K and 573K show appreciably *lower* peak crystallisation temperatures compared to the equivalent pure PET. Therefore, PMMA appears to inhibit PET crystallisation on heating and cooling. It is known that the mechanisms of crystallisation of polymers are different for heating a glass above its T_g, and for cooling a melt below T_m [15,16,17]. Collier and Baer have shown that crystallisation upon heating above T_g in PET is a diffusion driven process, whereas quiescent crystallisation from the melt is known to depend upon the rate of surface nucleation [16]. In this experiment, it is evident that PMMA inhibits both these mechanisms, and therefore we must consider the inhibition effect as a function of overall blend composition.

DSC of the 80/20 blends, unannealed, and annealed for 473 and 523K are shown in figures 3.10 and 3.11. These samples were analysed to gain insight into the dependence of phase composition on the crystallisation behaviour of PET. Re-heat scans show a similar annealing temperature dependence to the 50/50 blend samples, although the extent to which the peak crystallisation temperatures are shifted upon heating and cooling less appreciable than in the 50/50 blends, indicating that this phenomena is dependent on the blend composition.

PET has been blended with other main chain polyesters, and the dependence of crystallisation on blend composition has been investigated by several workers [3,18]. The crystallisation of PET with other classes of polymers has been shown to be dependent upon the blend composition ratio and the exact nature of the second polymer in the blend. No general conclusions are apparent from these studies, although incompatible polymers are more often claimed as nucleating agents [19].

The critical temperatures derived from the non-isothermal DSC analysis are given in table 3.7. These results will be discussed in more detail in section 3.4.

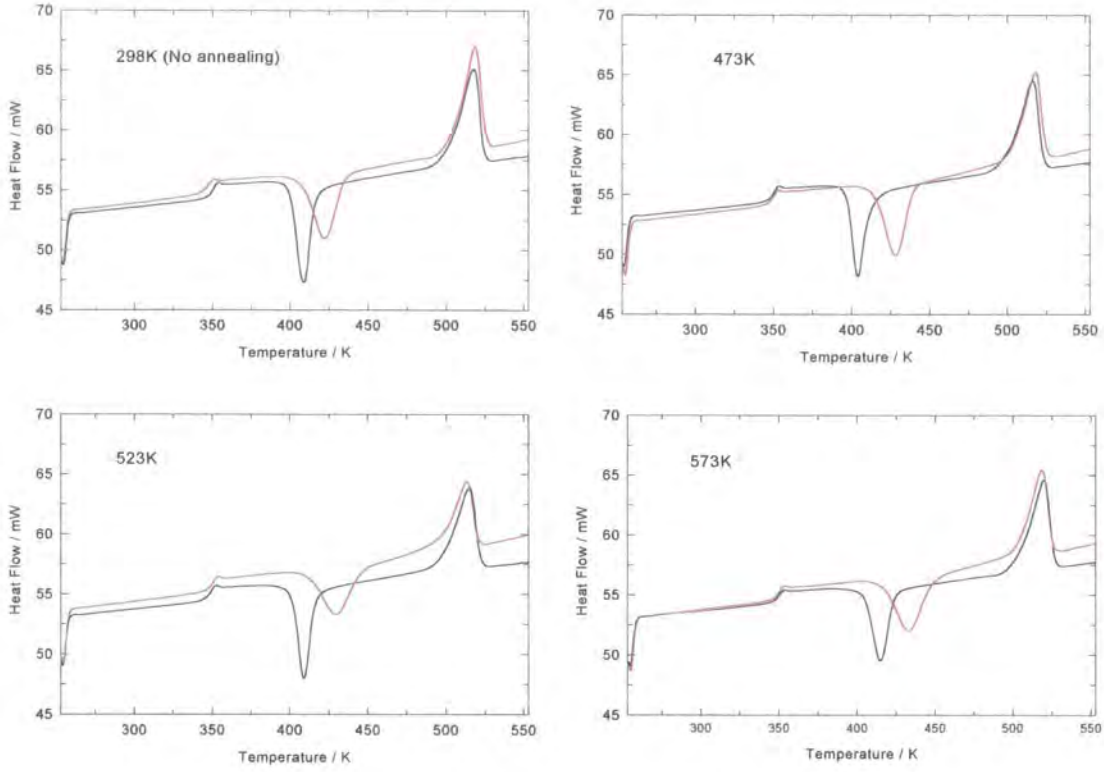

Figure 3.8. DSC heating scans for 50/50 blends. Black = PET, red = Blend

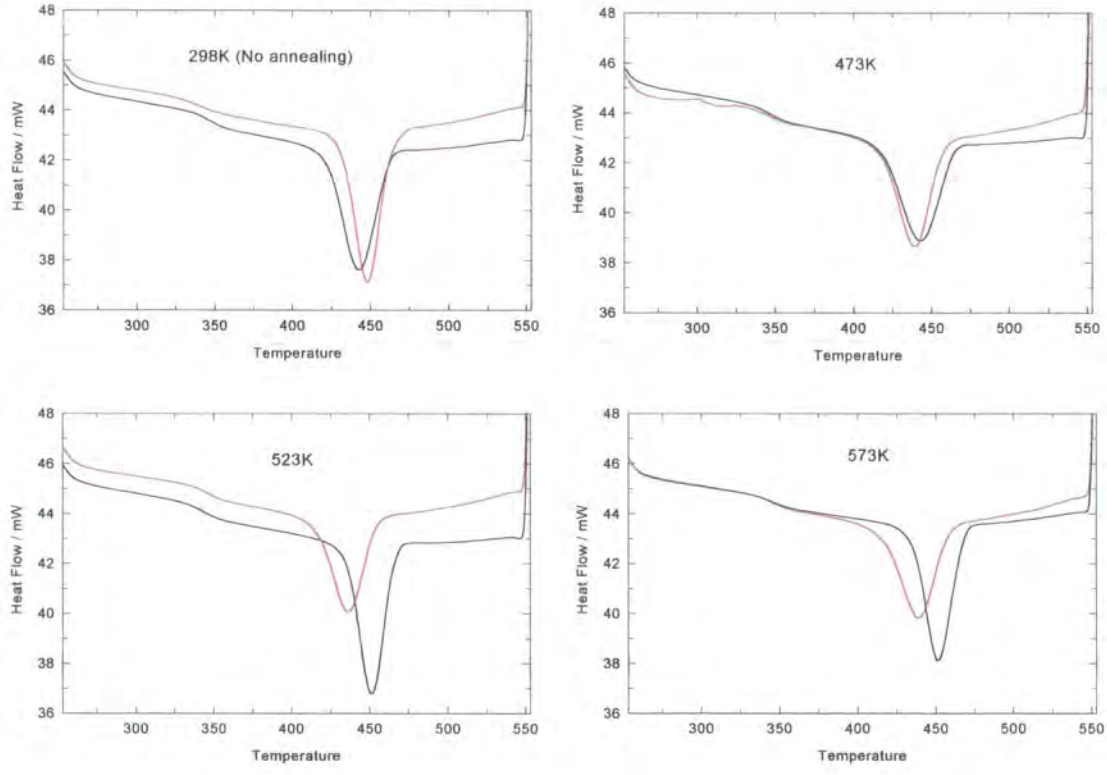

Figure 3.9. DSC cooling scans for 50/50 blend. Black = PET, red = Blend.

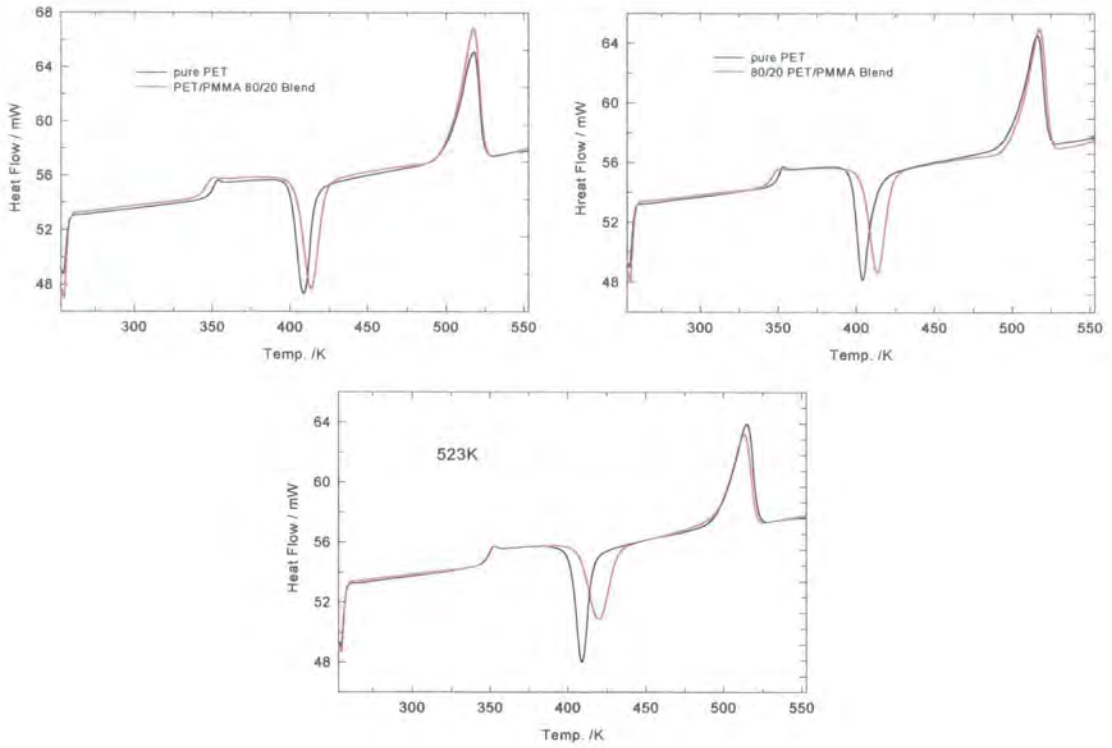

Figure 3.10 Re-heat scans for 80/20 Blends. Black = PET, red = Blend..

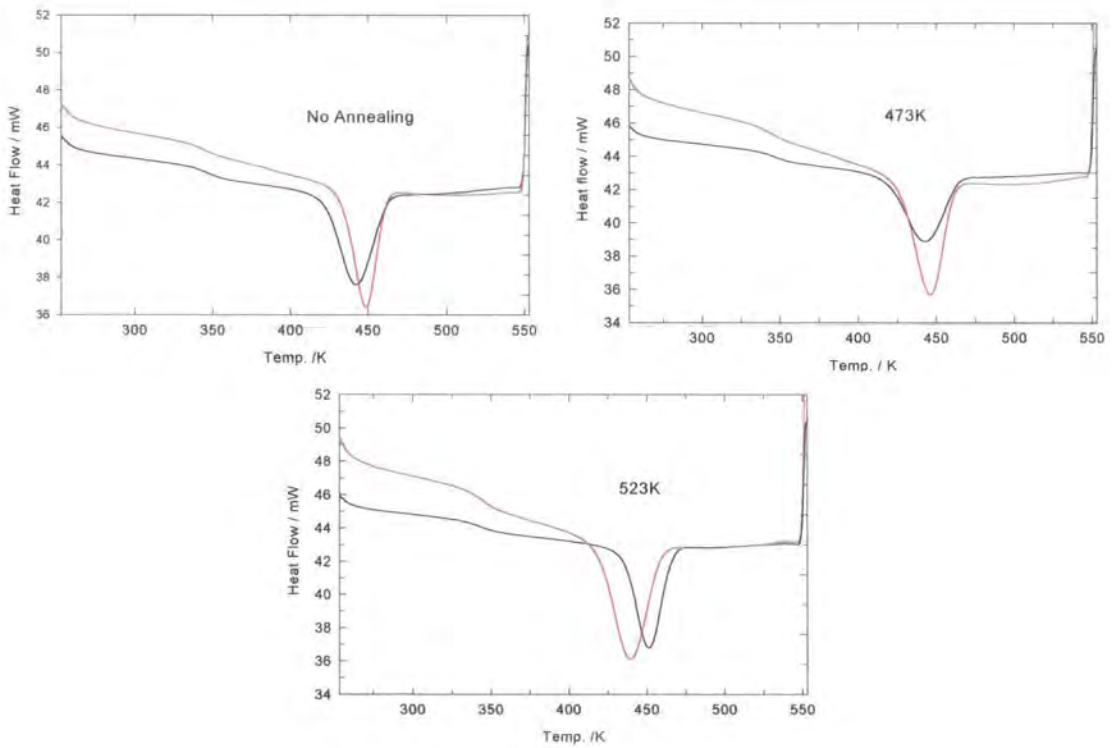

Figure 3.11. DSC cooling scans for 80/20 Blends. Black = PET, red = Blend.

Table 3.7 DSC data for re-heat and cooling scans of PET/PMMA blends.

Sample	T* (K)	T_g (K)	Re-Heat				Cooling	
			Crystallisation		Melting			
			Peak (K)	ΔH (J/g)	Peak (K)	ΔH (J/g)	Peak (K)	ΔH (J/g)
Pure PET	298	348.5	408.6	-32.6	517.5	36.1	442.1	-40.3
	473	349.3	386.9	-30.1	516.0	36.0	442.5	-39.1
	523	347.8	408.9	-28.8	514.8	33.9	451.0	-40.6
	573	349.0	414.9	-26.6	519.6	33.0	451.2	-37.8
80/20 Blend	298	344.8	413.1	25.9	517.3	30.2	448.4	-35.5
	473	347.1	417.6	28.8	517.1	30.3	445.5	-35.3
	523	348.3	419.7	28.6	512.8	28.3	439.1	-34.2
50/50 Blend	298	345.4	421.7	-32.0	518.0	36.1	447.6	-43.0
	473	348.3	427.8	-33.4	517.8	31.6	438.8	-39.6
	523	348.9	429.3	-27.9	512.8	27.0	435.8	-31.6
	573	348.6	432.7	-31.2	518.0	30.6	438.4	-35.8

* Sample annealing temperature

Conclusions

DSC has revealed that the peak crystallisation of PET in a PET / PMMA blend is inhibited compared to unblended PET. The T_g of PET in a blend appears to unaffected by the presence of PMMA. The extent to which crystallisation temperatures are shifted appears to be dependent upon both the annealing temperature and the initial blend composition ratio, (i.e. the peak crystallisation temperature are shifted to a lesser degree in 80/20 blends than in 50/50 blends.)

The fractional crystallinity, (X_c) of PET, in the blends, as indicated by the values of ΔH, is nominally independent of annealing and blend composition on re-heat, (X_c 0.22 - 0.26), but does appear to have a relationship with annealing temperature on cooling,, for the 50/50 blend samples (see table 3.7).

3.3.5. Isothermal Crystallisation

The isothermal crystallisation of the 50/50 blend and the homopolymers reveals that the crystallisation of PET in the blend is inhibited over a broad temperature range. Typically, the crystallisation of PET in the presence of PMMA is seen to be slower than

that for pure PET. The crystallisation half time, $t½$, is plotted against crystallisation temperature and is seen to be longer for the blend samples than for pure PET (figure 3.12). Only at an annealing temperature of 473K, does the subsequent crystallisation appear to be faster in the blend than for PET, and only then at the lowest crystallisation temperatures. Quite clearly, there is an effect from the annealing temperature, i.e. the thermal history of the sample has influenced the crystallisation time of the samples, despite the melt/quench cycle in the DSC, which is intended to remove any artefacts of previous thermal treatments.

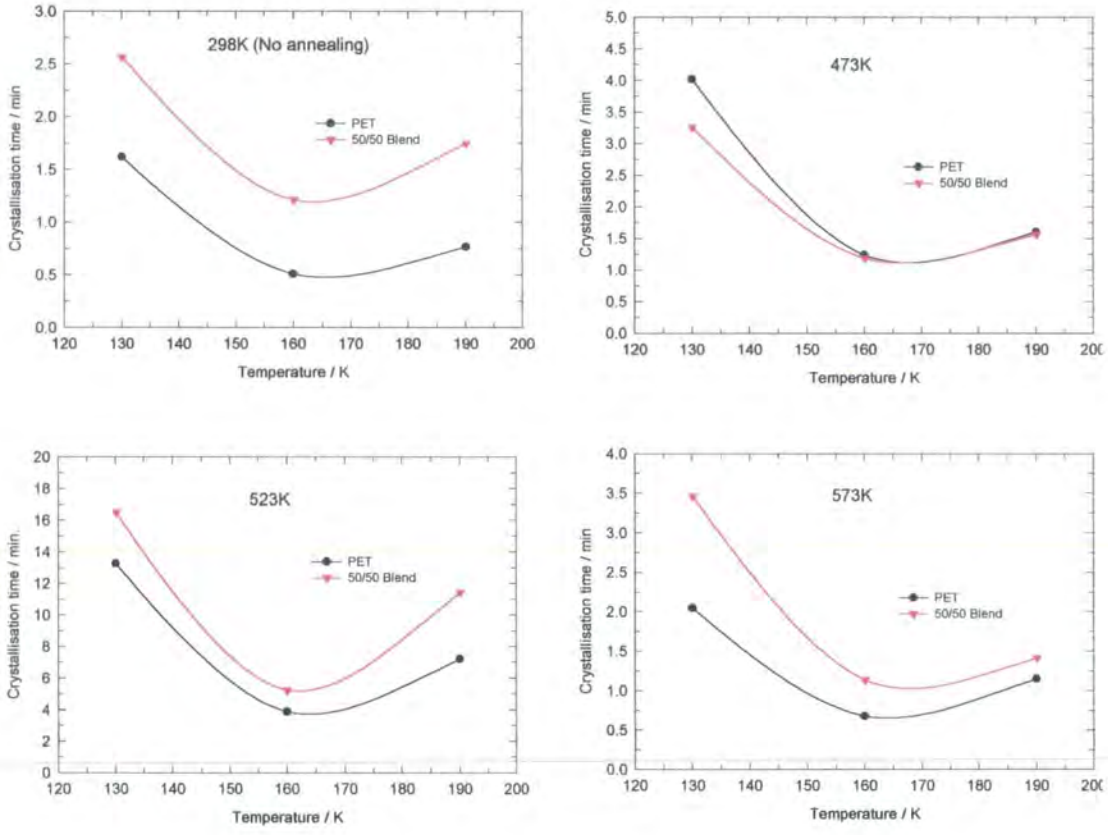

Figure 3.12. Crystallisation half times for PET and 50/50 blend. The Temperature at which the samples have been annealed is indicated on each plot. Quite clearly, the crystallisation of PET is retarded in the presence of PMMA.

The isothermal crystallisation data has been analysed following the Avrami theory of polymer crystallisation [38]. The thermograms have been analysed using the formula;

$$X_t = \frac{\int_0^t \frac{dH}{dt} dt}{\int_0^\infty \frac{dH}{dt} dt} \tag{3.4}$$

The differential *(dH/dt)* is the heat flow of the sample with time during the crystallisation process, and X_t is extent of crystallisation, which is given by v_t/v_∞, where v_t and v_∞ are the volume crystallinities at time t and ∞ respectively. The relative crystallinity is related to the rate of crystallisation by the Avrami equation;

$$\ln(1 - X_t) = -kt^n \tag{3.5}$$

where k is the rate constant for the crystallisation process and n is the Avrami exponent. k and n can be extracted graphically by plotting;

$$\ln(-\ln(1 - X_t)) = n\ln(t) + \ln(k) \tag{3.6}$$

This plot is shown for the PET/PMMA blend sample annealed at 523K in figure 3.13. Usually, only the linear (central) section of the plot is used to define the straight line fit. The Avrami exponent and the rate constants for all samples at all crystallisation temperatures are shown in table 3.8.

The value of the exponent n is indicative of the crystallisation mechanism for the polymer under investigation (see section 3.4.3), and as a qualitative assessment of the particular growth mechanism can be made. The rate constant k for crystallisation, is also a powerful tool in comparing samples annealed under different conditions and in assessing the effect of blending, as higher rates indicate that a second component is acting as a nucleating agent. The Avrami analysis of the crystallisation data will be discussed in more detail in section 3.4.

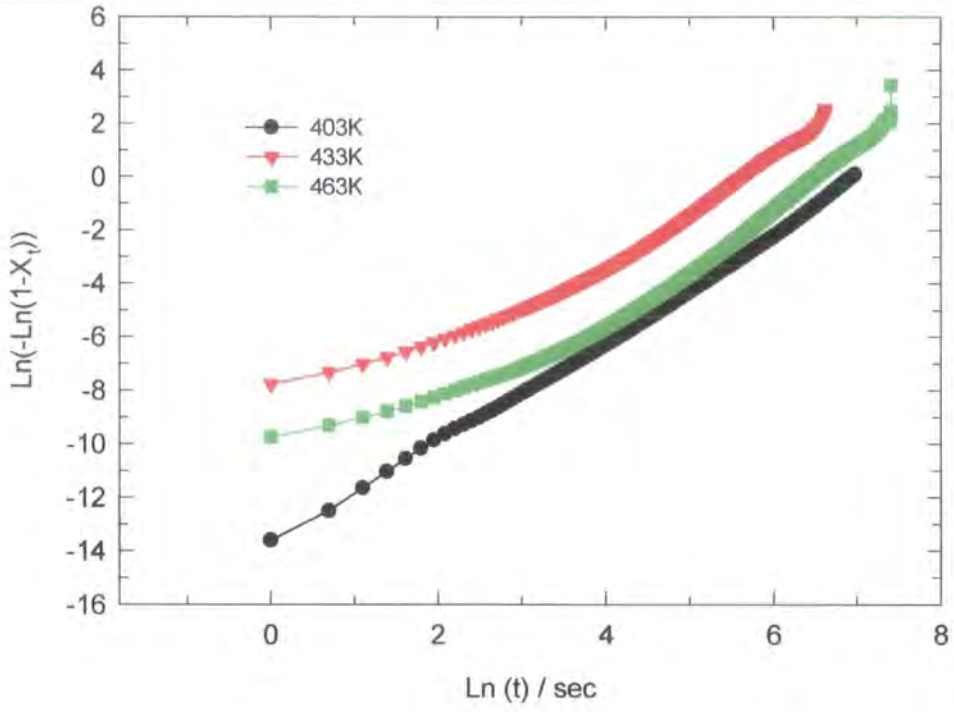

Figure 3.13 Typical Avrami plot. This one is the for PET/PMMA 50/50 Blend. Annealing temp = 523K.

Table 3.8. Avrami exponent and rate constant for isothermal crystallisation.

Sample	Anneal. Temp. (K)	Values derived from equation 3.x						Av. *n*
		$T_C = 403K$		$T_C = 433K$		$T_C = 463K$		
		n	$k\ s^{-1}$	*n*	$k\ s^{-1}$	*n*	$k\ s^{-1}$	
PET	298*	1.3	2.85×10^{-3}	0.9	7.66×10^{-2}	1.2	1.40×10^{-2}	1.1
	473	2.1	1.01×10^{-5}	2.0	3.60×10^{-4}	2	1.54×10^{-4}	2.0
	523	1.9	2.05×10^{-6}	2.4	3.72×10^{-6}	2.4	6.15×10^{-7}	2.2
	573	1.8	3.69×10^{-3}	1.9	4.11×10^{-3}	2	9.04×10^{-4}	1.9
Blend	298*	1.5	6.75×10^{-4}	1.1	2.08×10^{-2}	2.1	1.09×10^{-4}	1.5
	473	2.1	1.67×10^{-5}	1.8	1.17×10^{-3}	2.2	7.87×10^{-5}	2.0
	523	2.2	2.50×10^{-7}	2.4	1.63×10^{-6}	2.4	2.05×10^{-7}	2.3
	573	1.8	5.66×10^{-5}	1.7	1.43×10^{-3}	1.8	4.31×10^{-4}	1.8

* Ambient temperature. No effective annealing.

Conclusions

Blending and subsequent annealing has a profound effect upon the isothermal crystallisation kinetics of PET. In most cases, the crystallisation of pure PET is faster than for PET in a PET/PMMA blend. Avrami analysis can be successfully applied to the isothermal crystallisation data for PET/PMMA blends.

3.4. Discussion and Comparison with Theory.

3.4.1. Weight Loss and Degradation. Further analysis.

The rate of weight loss of PMMA appears to be significantly altered by the presence of PET. The ratio of rate constants for weight loss in pure and blended PMMA is used as a measure of the extent of retardation. This ratio, k_{BLEND}/k_{PURE}, has values of 1.13, 0.42 and 0.47 at annealing temperatures of 473K, 523K and 573K respectively.

A retarded weight loss is evident at 523 and 573K. indicating there is some interaction between the two polymers, although this analysis cannot reveal the nature of this interaction. Given the extent to which the rate is retarded at 523K, it is safe to assume that the interaction is greatest at this temperature and is significant enough to be considered a real effect (error~ ± 0.3 for k_{BLEND}/k_{PURE}). Although there is an enhancement of the rate of PMMA degradation in the PET/PMMA blend at 473K, the level of weight loss is generally very low and as such the errors in experimentation and measurement may account for this result. Consequently at this temperature it is not possible to conclude that the rate of depolymerisation is faster for the blend than for the homopolymer.

The rate of weight loss, at 523K is considered in detail. Figure 3.14 shows the weight loss at 523K for pure PMMA and the 50/50 blend. As can be seen the weight loss is relatively comparable at t ~1800 sec. The rate constant for weight loss of PMMA from the blend alone, i.e. $k_{t>30\ min.}$, is given by the gradient of the slope after 30 min. and is $1.02 \times 10^{-5}\ s^{-1}$, which is a much lower value for k than originally calculated ($= 2.27 \times 10^{-5}\ s^{-1}$, see table 3.3). This can be explained by the initial depolymerisation of 'free' PMMA in the blend, followed by a slower rate of depolymerisation because the remaining PMMA has reacted with PET. The point at which the rate of weight loss slows can be shown to be at a blend composition of ~ 53% PET/ 47% PMMA. i.e the major blend component is PET.

At 573K PET will be completely molten, and all crystallinity will be destroyed. However, at this temperature the rate of degradation of PMMA is very fast [14], and even if a chemical reaction occurred between the two polymers it is likely that the depolymerisation of PMMA will dominate the sample chemistry.

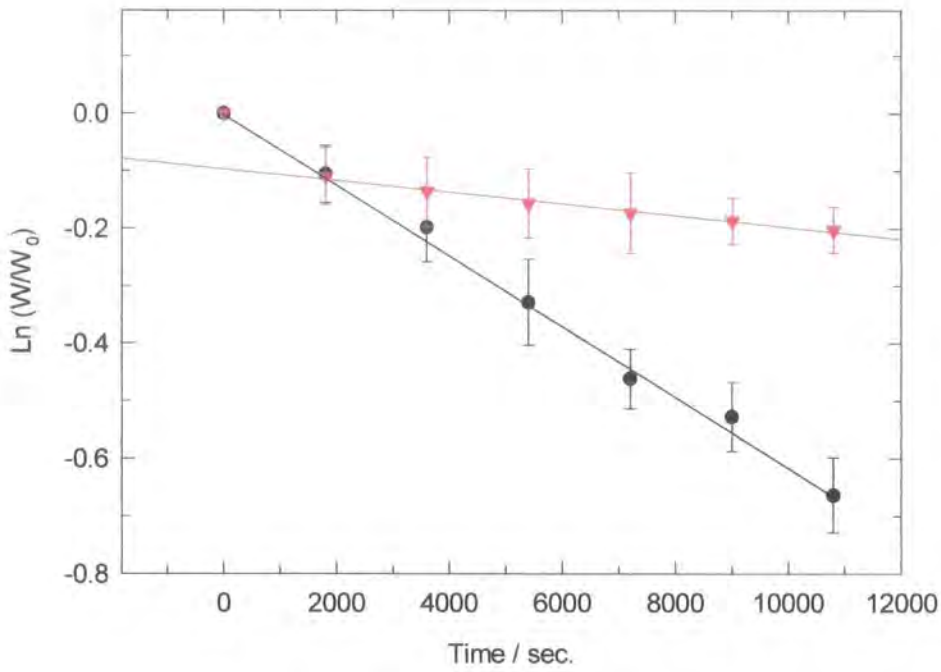

Figure 3.14. rate of weight loss for Pure PMMA (Black) and PMMA in 50/50 Blend with PET (Red).

The degradation of PMMA in the presence of other polymers has received some attention in the literature; and general conclusions are that the effect of blending on the degradation rate is a function of the particular polymer used in the blend. For example, Grassie *et al* [20,] have studied the degradation of blends of PMMA and polyacrylonitrile (PAN), and have concluded that the weight loss from PMMA is hindered in the range 473-523K by the presence of PAN at a weight ratio of 20% in the blend. Alternatively, McNeill and Neil [21] have found that blending PMMA with PVC at low temperatures destabilises the PMMA, principally because chlorine radicals, produced in the degradation of PVC, attack the PMMA backbone. Rincon and McNeill [9], have studied the thermal stability of PC/PMMA blends and concluded that although there was no change in the nature of the degradation products with respect to the pure polymers, the degradation of PC was initiated at lower temperatures in the blend because of PMMA macro radical attack upon the PC component.

Very little work has been done to investigate the effect of morphology on the rate of degradation of polymer blends. However, an analogous study to this work has

been reported by Montaudo *et al,* [8] who have shown that the thermal stability of a PC/PMMA blend is dependent upon the nature of the blend preparation and therefore the blend morphology. For instance 1:1 blend prepared by mechanical mixing exhibited a greater thermal stability than a 1:1 blend prepared by casting a clear film (i.e. one phase), from a DCB/$CHCl_3$ solution.

Other works of note are by Lizymol and Thomas [22], who studied several systems and concluded that only miscible systems displayed significantly different degradation behaviour with respect to the equivalent pure polymers. The morphology of the PET / PMMA system will now be considered in more detail.

3.4.2. A Note on Phase Morphology and Diffusion.

Previous work on PMMA/PC blends has always attributed the reduction of weight loss of PMMA when blended to the existence of transesterification reactions between the two polymers [4,5,6,7] However, it is proposed that the blend morphology will also influence the rate of degradation of the two polymers. The weight loss data presented in section 3.3 will be used to illustrate this possibility.

Figure 3.14 shows the change in rate of weight loss with annealing time for a 50/50 PET/PMMA blend. As already stated, this could be the result of a grafting reaction between the two polymers, a change in the phase structure of the blend or a combination of these two phenomena. Here we will consider the possible phase structures which lead to the observed weight loss result.

The initial weight loss is seen to be equivalent to the weight loss of the pure PMMA. Therefore it is postulated that the initial phase structure of the blend is such that there is a pure PMMA or PMMA rich component which has a rate loss unaffected by the presence of PET. It is also reasonable to assume that this phase structure has developed during the induction time required to heat the blend to the annealing temperature (see section 3.2). Above T_g, phase separation in immisible polymers has been known to occur on time scales of a few minutes; for instance Ko *et al* have shown that appreciable phase separation in PC/PMMA systems occurs over 15 minutes at 523K [7], and therefore we can assume that the majority of the observed weight loss does not occur until after gross phase separation is complete.

With this in mind, we can now construct a crude phase description of the blend system based on an a knowledge of how the blend degrades with time. This description is also based on the knowledge that in binary polymer blends, the polymer with the lowest surface energy will preferentially move to the surface of a blend; i.e. the blend is surface enriched (see chapter 2). Without referring to the the equations used to describe a phase separated structure, it is apparent that a phase portrait of the type shown in figure 3.15 would adequately explain the initial weight loss from a blend 'particle', here approximated to sphere.

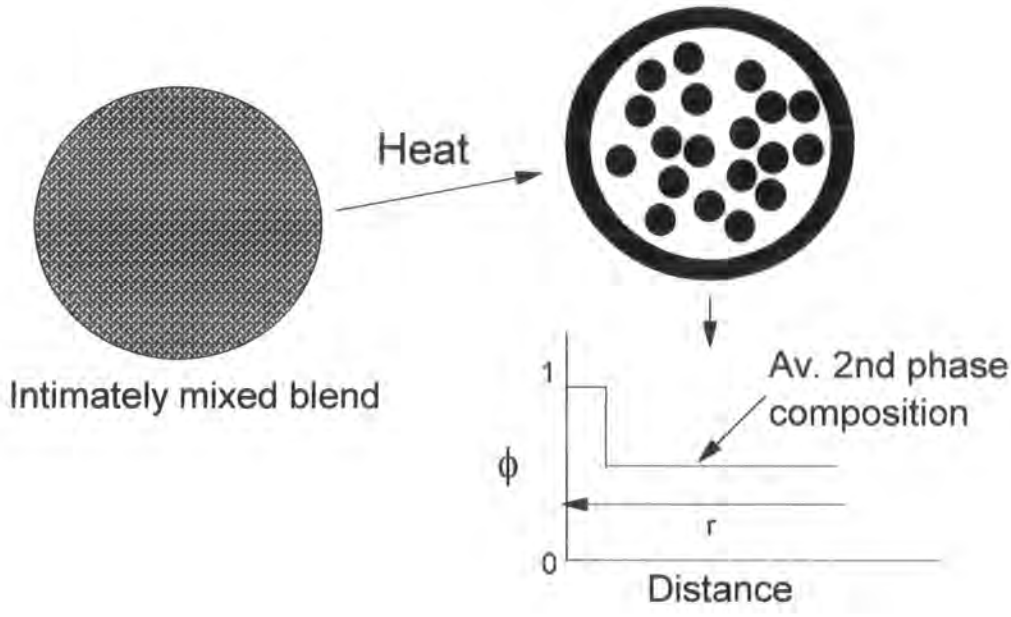

Figure 3.15 Phase separation in PET/PMMA blend 'particle'. The surface enrichment leads to a macroscopically thick wetting layer on the surface of the particle, which yields the observed bulk degradation rate.

Because the initial rate of weight loss of the PET/PMMA blend is seen to be the same within error, as that for the pure PMMA then we conclude that the surface excess must be macroscopically thick (i.e. equivalent to bulk), in order that the rate of weight loss is maintained over the time period $t < 30$ min. This qualitative assessment is in good agreement with the theory of phase separated immscible polymers [23]. From simple arithmetic, the thickness of the PMMA wetting layer in a PET/PMMA blend 'particle' is approximately 1.4% of the particle radius.

At $t >$ 30 min. we see that the bulk depolymerisation rate is no longer sustained by the blend and a lower rate of weight loss is seen . It is postulated that this is due to depletion of the wetting layer by depolymerisation such that the available PMMA at the surface is the limiting factor to observed weight loss. The rate of weight loss is now dependent upon the rate of diffusion of the PMMA depolymerisation products (monomer) through the PET rich matrix. If we make the assumption that when the monomer reaches volume fraction of 1 it is instantaneously removed from the blend surface then the rate of weight loss is equivalent is to the rate of diffusion of MMA monomer to the blend surface i.e.

$$\frac{dw}{dt} \sim \frac{dx}{dt} \tag{3.7}$$

where *dw/dt* is the rate of weight loss and *dx/dt* is the effective rate of diffusion .We now have a value for the diffusion of the MMA through a PET matrix. i.e. 1.02×10^{-5} g/sec are delivered to the surface of the blend. According to Ficks first law [24], this can be considered as the diffusion flux and we then have;

$$J = -D\left(\frac{dc}{dx}\right) \tag{3.8}$$

where D is the diffusion coefficient and *(dc/dx)* is the concentration gradient. For an immiscible bend this will be over a distance of the order of the radius of gyration of the polymer(s), R_g, which is of the order of 10 nm upto the limiting size of the bulk phase (~ 1 μm). This assumes that the effective surface area of the blend remains constant. Hence D, which we may consider as the diffusion coefficient for degraded PMMA diffusing through PET at 523K, is calculated as ~1×10^{-9} - 1×10^{-6} cm^2/sec.

Comparisons with literature values are difficult because of unknown factors such the crystalline fraction of the PET phase. Wu and Chang [25], have reported diffusion coefficients for PMMA/PVDF (polyvinylidene flouride), which like PET, is a semi-crystalline polymer, at 483K of 3.42×10^{-10} cm^2/sec, which is in relatively good agreement considering the lower temperature. However, at this temperature , it is unlikely that any contribution to the diffusion coefficient is apparent from MMA.

The diffusivity of small molecules in polymers in general is an important topic in itself, and the diffusion coefficient for liquids, and gases has often been reported in literature [26]. These values have been reported in the range 10^{-9} - 10^{-5} cm^2/sec, at the temperatures of interest.

Therefore, it has been shown that using a simple measurement such as weight loss from an immiscible polymer blend it is possible to derive information pertaining to the initial blend morphology and the diffusion of the degrading phase (PMMA) in the stable (PET) phase.

3.4.3. Evidence of an Interchange Reaction.

NMR

The presence of a methyl ester singlet in the H^1 NMR spectrum of PET/PMMA blends supports the hypothesis that an exchange reaction has occurred. As described in Chapter 2, there is some of evidence for transesterification reactions between main chain polyesters and side chain polyesters [19]. Direct evidence of changes in end groups in PET/Acrylate blends has been given by Gravalos *et al* [28]. They studied the interaction between PET and poly(ethylene - co - ethyl acrylate) at melt temperatures, and proposed the reactions shown in scheme 3.4.

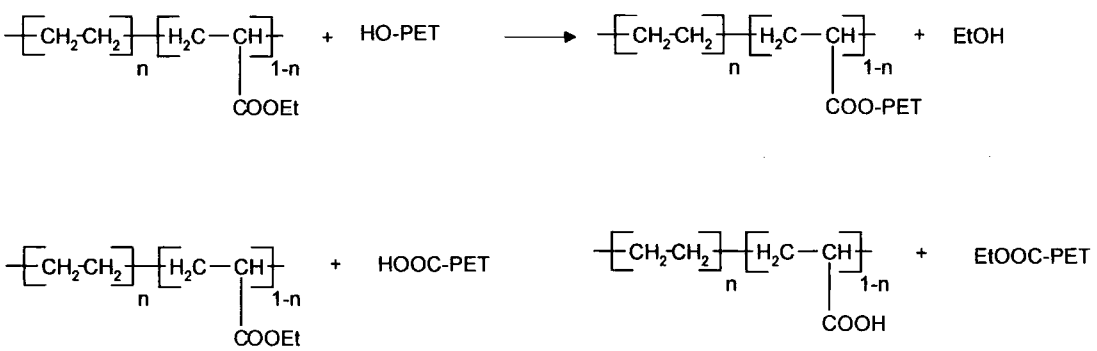

Scheme 3.4. Reaction schemes in PET/P(E - co - EA) blend. After ref. 28.

For the analogous case of PET reacting with PMMA we would expect the two equivalent reactions to produce a PET-PMMA grafted structure, and / or methyl ester terminated PET chains. Any appreciable reaction between PET-OH and PMMA methyl ester groups would result in a concurrent reduction in the PET-OH end group concentration, compared to the equivalent pure PET sample, and from figure 3.6 this is not the case. Indeed, the PET-OH concentration appears to be greater in PET/PMMA blends than in pure PET, and this cannot be adequately explained, beyond a simple statistical argument. Hence it is concluded that the proposed reaction between PET-OH and PMMA methyl ester groups does not occur under the conditions of this experiment. The changes in PET-OH concentration at different annealing temperatures are attributed to the well known transesterification reaction between PET macromolecules [2], shown in scheme 3.5

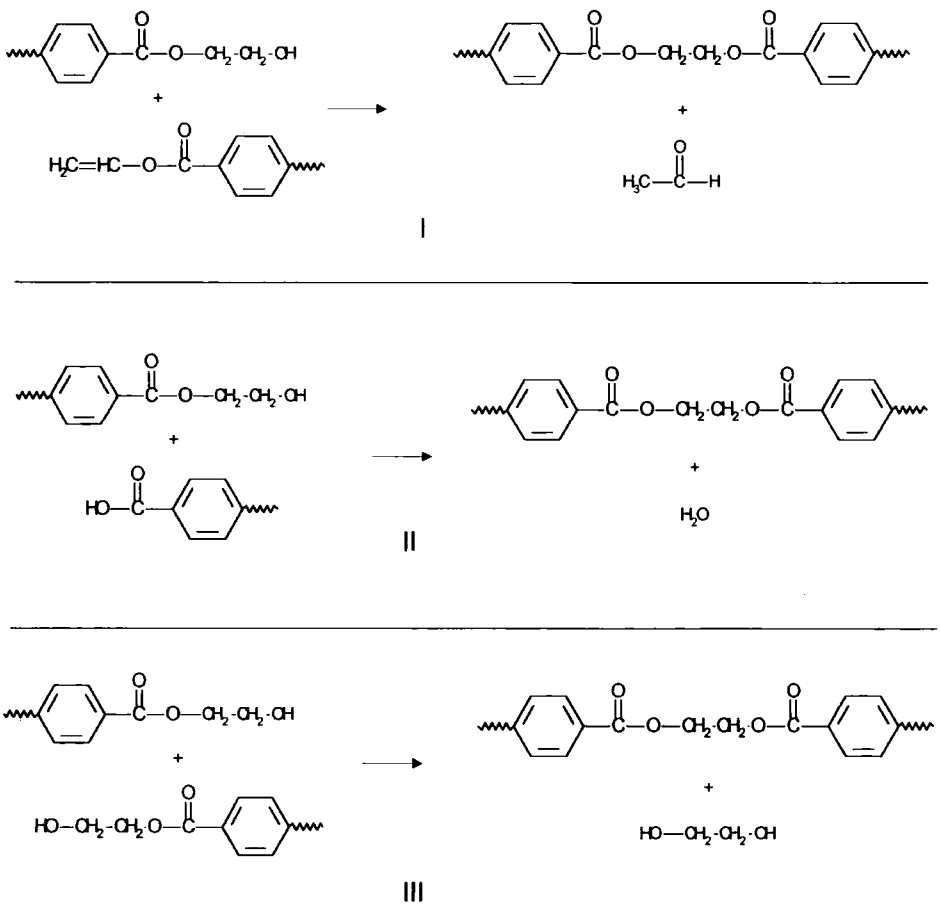

Scheme 3.5 Possible internal transesterification reactions of PET-OH groups. I) chain extension with vinyl end group, producing acetaldehyde (thermal degradation). II) Acid - hydroxyl end reaction producing water. Condensation reaction producing ethylene glycol.

Now, we turn to the formation of methyl ester groups in PET. By inspection of schemes 3.2 and 3.3 it is clear that both these reactions will yield a methyl ester terminated PET chain. Therefore, the H^1-NMR analysis suggests that the most likely chemical interactions between PET and PMMA are the direct ester exchange reaction and the acidolysis reaction. It is plausible that both these reactions are in evidence, in which case assessment of the methyl ester ends alone cannot distinguish between them.

One result of interest is the relatively high concentration of methyl ester end groups in the unannealed PET/PMMA blend. One explanation would be that the sample preparation procedure (i.e. dissolution and re-precipitation in methanol, see section 3.2), has caused methyl esterification of PET-COOH end groups. This reaction has been reported between PET and methanol, but only under specific conditions, using boron trifluoride / diazomethane catalysts [30]. Furthermore, if this reaction occurs then the pure PET sample, which had experienced the same preparation procedure, should show evidence of methyl ester end groups in an unannealed sample. From inspection of the H -NMR spectra of this sample, no methyl ester group was present, therefore, methyl esterification from a PET-COOH - methanol reaction seems unlikely.

Solubility.

Figure 3.16 shows the methyl ester end group concentration as a function of the insoluble fraction in Hexafluoro isopropanol (HFIP), of the 50/50 blends.

From the solubility tests carried out on the 50/50 PET/PMMA blend and the equivalent samples of homopolymers it is apparent that the the insoluble material formed in the blends can be accounted for by the presence of crosslinked PMMA , and/or grafted PET-PMMA copolymer. Although it is tempting to assign the increase in acetone insoluble PMMA fraction to the presence of grafted copolymer , as proposed by Kyu *et al* [6], and Ko *et al* [7], the material may in fact be crosslinked PMMA, as a PMMA insoluble fraction is also seen in the pure PMMA samples. It is postulated that the presence of HFIP insoluble material does indicate that PET-PMMA graft copolymer is present which has been formed by the direct interchange reaction shown in scheme 3.3. and this is supported by the good correlation between methyl ester end group count and the HFIP insoluble fraction.

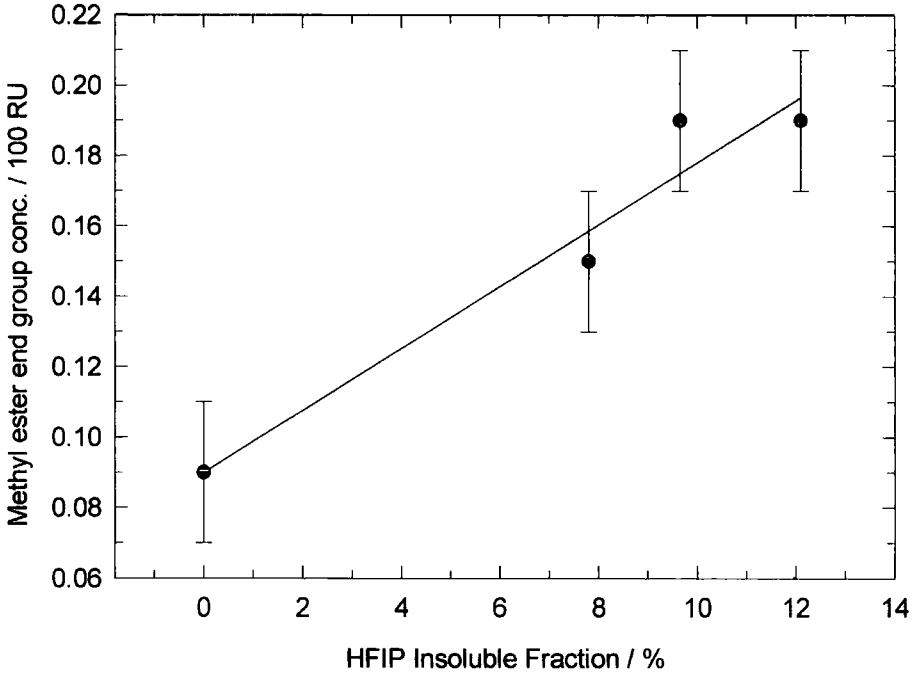

Figure 3.16. PET-COOMe as a function of HFIP insoluble fraction

3.4.4. Non-isothermal DSC.

In blends of polymers one of the indications of miscibility or interaction between the two polymers is a convergence of the separate T_g of the two polymers, to an intermediate value dependant upon the blend composition. This is evident in blends of PET/PEN [3], PET/PC [29] and , to some extent in the blends of PC and PMMA (providing a one phase system is investigated) [x]. From figures 3.8 and 3.10 it seems that only one T_g is evident. However, on closer inspection, a second transition, attributable to the PMMA phase is detectable in the blend samples. The expanded DSC scans are shown for some samples in figure 3.17. It is apparent that there is no convergence of these T_g values in the blend samples with respect to their annealing temperatures, (see figure 3.18) indicating that the majority of the sample remains unmixed. It is also apparent that the PMMA T_g in the 80/20 is much more profound than in the 50/50 blend samples, which indicates a very definable two phase morphology exists in these samples. The barely discernible PMMA T_g of the 50/50 blend samples may indicate a less well defined morphology than the 80/20 blend samples (i.e. broader

phase boundaries). Cook *et al* [31], have reported that in immiscible blends of PET and ABS (acrylonitrile-styrene-butadiene) the T_g is poorly defined compared to the PET T_g.

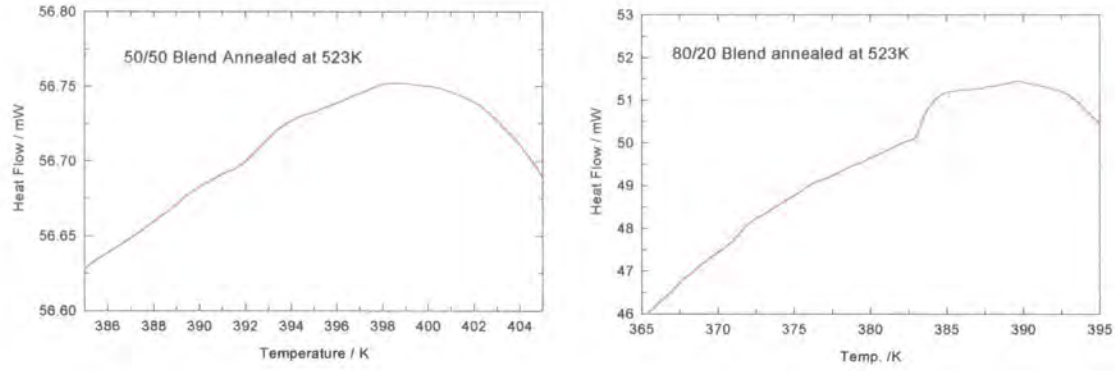

Figure 3.17. PMMA Tg determination for PET/PMMA blends

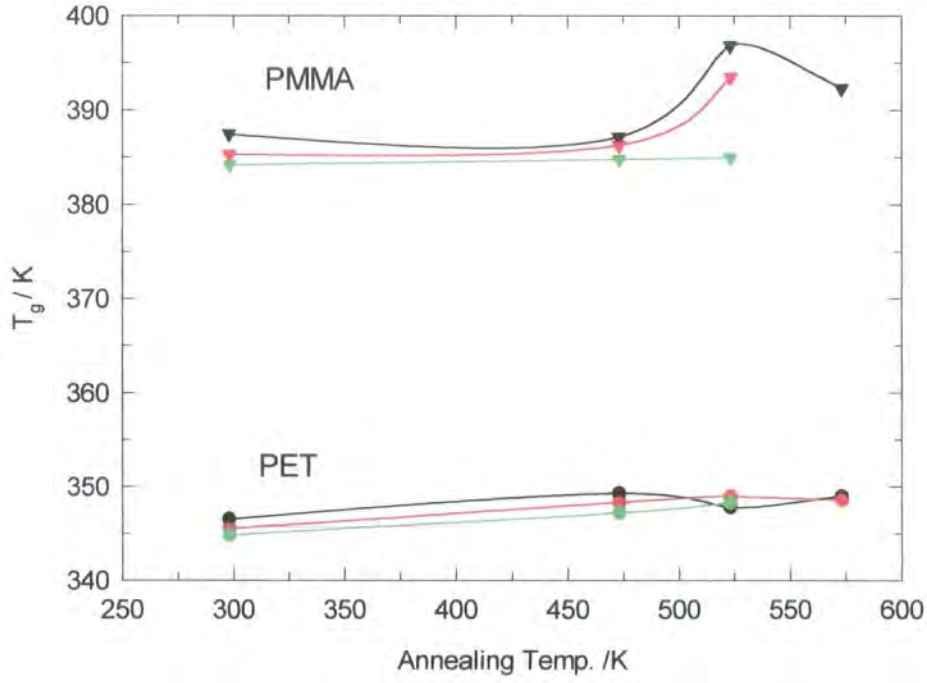

Figure 3.18 PMMA and PET Tg values. Black = pure polymers. Red = 50/50 blend. Green = 80/20 Blend.Errors bars are omitted for clarity.

The non isothermal analysis of the pure PET and blend samples has revealed that the temperatures of crystallisation are shifted on both heating and cooling. These shifts in temperature are plotted in figure 3.19, the greatest difference between pure PET and

PET in a blend with PMMA is seen at 523 and 573K. However, from table 3.7. the enthalpy of crystallisation remains relatively unaffected, indicating that the same level of crystallinity is acieved for the blend as pure PET.

The same temperature dependence is seen for the 80/20 samples although the difference is not as pronounced as with the 50/50 blends. This indicates that the mechanism of inhibition of crystallisation is the same for both blends, but the extent of inhibition is composition dependant.

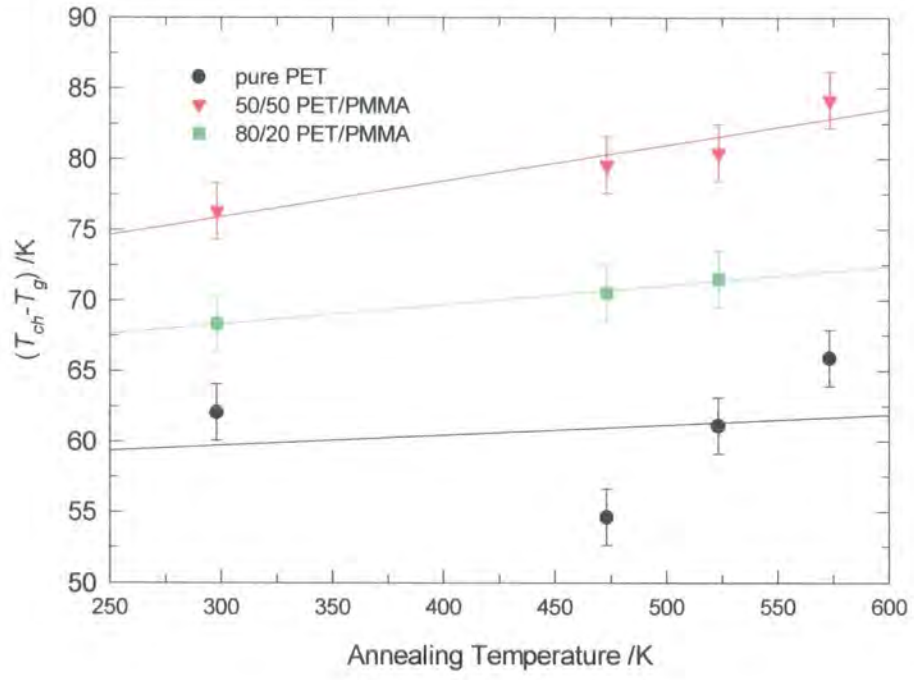

Figure 3.19 Peak crystallisation temperatures for pure PET, 50/50 PET/PMMA and 80/20 PET/PMMA blends annealed at different temperatures. The line is a guide to the eye. It appears that the difference between pure PET and the PET in the blends is dependent upon the initial blend composition.

From Figure 3.19 the increase in peak crystallisation temperature with respect to the pure PET is dependent upon the PMMA content of the blend. A temperature dependence of the increase in T_{ch} is evident for both the 50/50 and 80/20 samples, and this is attributed to the temperature dependence of crystallisation of PET itself.

The general the crystallisation temperature on cooling is shifted to a lower degree of supercooling (higher temperature) for PET (figure 3.20), but both blends show the opposite behaviour, i.e. annealing increases the degree of supercooling. Again this

points to a general inhibition of crystallisation of the PET by the presence of the PMMA phase. This is in contradiction to the results of Nadkarni *et al* [35], who have shown that the crystallisation temperature on cooling is moved to higher temperatures on blending PMMA with PET.

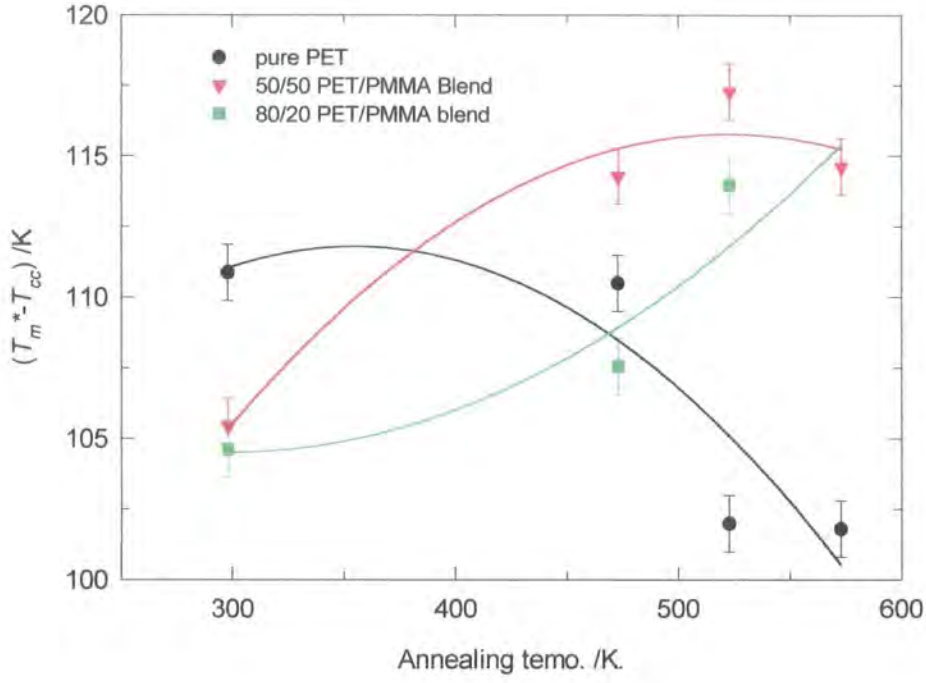

Figure 3.20. T_m- T_{cc} (degree of supercooling) vs. annealing temperature for pure PET and 50/50, 80/20 PET/PMMA Blends. The lines are a guide to eye*

These results are in better agreement with the work of Ju and Chang [36], who have shown that in an immiscible, 75/25 PET/polystyrene blend, the temperature of crystallisation on cooling is shifted to lower temperatures by ~8K. They attribute this phenomena to the retardation of PET crystallisation by the molten PS phase. Addition of a compatibilising agent further retarded the T_{cc} and this was attributed to the growth of interfacial graft copolymer between the two phases, which inhibited the PET crystallisation mechanism.

Here it is postulated that the same effect is seen in the PET/PMMA blends, i.e. that grafted interfacial structures cause an inhibition of PET crystallisation. Figure 3.21 shows a plot of the degree of supercooling for crystsllisation, $(T_m^*-T_{cc})$ vs. amount of HFIP insoluble fraction in the blend. A reasonable correlation is seen for the degree of

supercooling and the insoluble fraction. Hence, it is possible that the formation of an insoluble fraction has an influence on the thermal transitions in the sample.

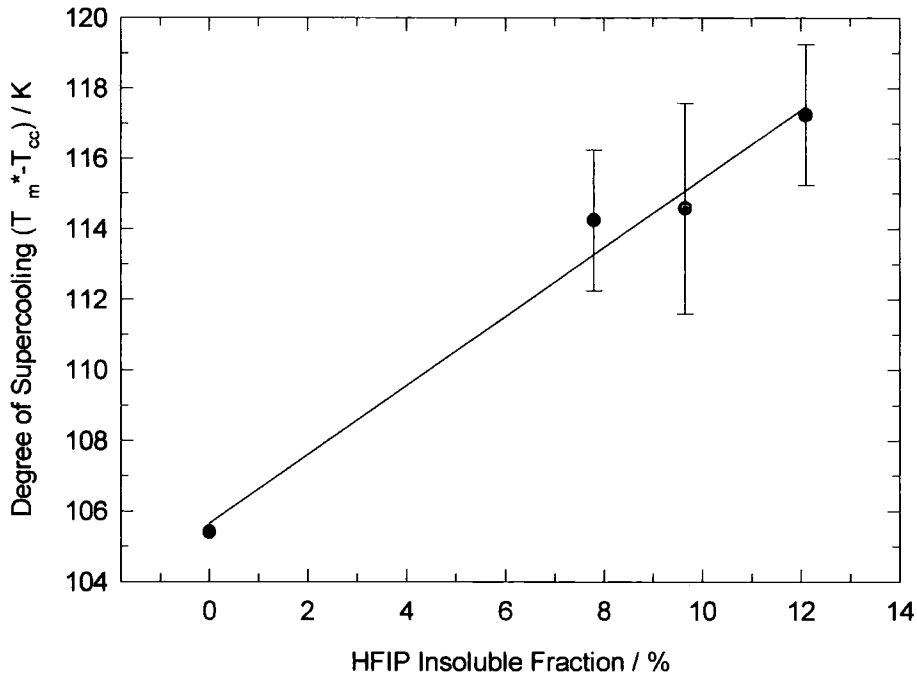

Figure 3.21 Degree of supercooling for T_{cc} as a function of % HFIP insoluble fraction in 50/50 PET/PMMA blend.

3.4.5. Isothermal DSC Studies

The isothermal crystallisation of PET and the 50/50 blend has shown that the crystallisation of PET is inhibited in the presence of PMMA. The crystallisation of PET in blends with different polymers, including PMMA, has been studied by several workers and the effect on crystallisation is dependant upon the polymer used [3,18,35,37].

In this work, it is found that PMMA retards the crystallisation of PET, and appreciably longer crystallisation times are seen in 50/50 blends compared to pure PET. This is in stark contrast to the work of Nadkarni and Jog [34], who have reported an that crystallisation of PET is accelerated by the presence of PMMA. The differences between this study and that of Nadkarni and Jog can be attributed to the differences in sample

preparation procedure, type of sample, and PMMA composition ratio. Nadkarni and Jog have used extrusion compounding to mix PET and PMMA to a maximum PMMA content of 20%. Here the much more effective technique of co-precipitation was used, (the two polymers will be mixed at a molecular level, at least initially), and the DSC technique used comparatively more sophisticated.

The Avrami analysis has also revealed that the exponent n, which in simple Avrami theory should be an integer, always has a value < 2.5. The exact values for each sample at the three crystallisation temperatures are listed in table 3.8. Theoretically the value of the Avrami exponent indicates the particular mode of crystallisation. A value of 4 indicates that nucleation and spherical growth is the predominant crystallisation mechanism. Gedde [38], has listed the type of crystal growth for each value of the Avrami exponent in terms of athermal (constant nuclei concentration), and thermal (nuclei formed at a constant rate) processes, (table 3.9).

Table 3.9. Derived Avrami exponents, n, for different nucleation and growth mechanisms.

Growth geometry	Athermal	Thermal[a]	Thermal[b]
1-Dimensional (Linear)	1	2	1
2-Dimensional (circular)	2	3	2
3-Dimensional (spherical)	3	4	5/2
3-Dimensional (Fibrillar)	1	2	
3-Dimensional (circular lamellar)	2	3	
3-Dimensional (solid sheaf)	5	6	

a = Free growth

b = Diffusion control

Many studies on PET crystallisation have produced many values for the value of the exponent, including non - integer values, and as such it is difficult to define a correct value for a given set of conditions in PET. For instance, Cobbs and Burton [39] find values of n between 2.2 and 3.1 in the temperature range 393-443K. Early work by Keller [40], showed that low temperature crystallisation had $n = 2$ and pre melt crystallisation had $n = 4$. Mitsuishi and Ikeda [41] yielded $n = 0.96$, and $n = 3.12$, for low temperature and pre melt crystallisation respectively. Fielding-Russell and Pillai have found vales of $n > 4$ for the low temperature (near T_g) crystallisation of PET [42].

The results presented here seem to be in greater agreement with , for instance, the work of Ou and Lin [43], who have studied the isothermal crystallisation of PET/copolyester blends in the temperature range 453-483K, and found an average value of n = 2.35, albeit for copolyesters which were acting as nucleating agents (i.e. increasing the rate of crystallisation). Additionally, Tan *et al* [44], have studied the isothermal crystallisation of PET as a 'meta stable melt' (their phrase), at 460K, and found a value of n = 1.2, which is in excellent agreement with the value for n at 463K found here (see table 3.8).

These results show that the exponent n varies with crystallisation temperature and with annealing temperature. According to Avrami theory, the results in table 3.8 indicate that unannealed, pure PET is nucleated via linear crystallisation across the range of temperatures under investigation. The increase in n with increasing annealing temperature (i.e. $n_{av.}$ ~2.21 at 523K), indicates that a different crystallisation mode (plate like) dominates, but this effect is seen in the blends with PMMA as well as in the pure PET samples. Therefore, it is difficult to conclude that the PMMA component has had a significant effect upon the value of n except for the unannealed blend crystallised at 463K where n has a value of 2.05 compared to 1.19 for the equivalent pure PET sample. Hence we turn to examine the rate constants for crystallisation as an indication of the effect of blending. Here we see that at annealing temperature of 523 and 573K, the rate constant has a lower value for the blend than for the pure PET sample. Hence it is concluded that blending with PMMA has no significant effect on the crystal growth mechanism in PET but does effect the rate constant for crystallisation across a broad temperature range.

3.5. Conclusions and Final Comments

In studying the behaviour of certain aspects of PET/PMMA blends, an emphasis has been placed upon defining the interactions between the two polymers with respect to the thermal treatment of the blends. Primarily the 50/50 blend has been studied, although differing blend compositions have also been used for specific purposes. The nature of the interaction has been investigated within two frameworks; firstly the presence or absence of an interchange reaction between the two polymers.

Perhaps the most compelling evidence for this is shown in figure 3.22, which is a combination of the degree of supercooling for T_{cc} for the 50/50 blend, and the observed methyl ester end groups from the NMR analysis, both plotted as a function of the HFIP insoluble fraction of the blends. This is taken as evidence that the direct ester exchange

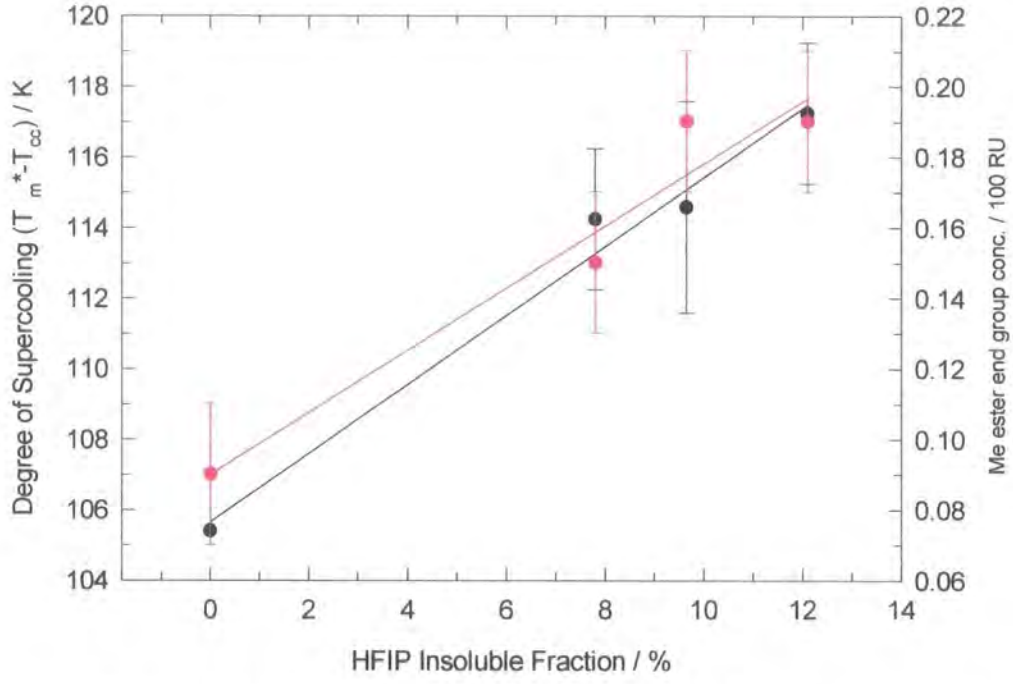

reaction (scheme 3.3) has taken place and produced a grafted copolymer structure (HFIP insoluble phase), which in turn inhibits the crystallisation of PET in the blend.

Figure 3.22. Combined plot showing relationship between degree of supercooling for T_{cc}, methyl ester end group concentration and HFIP volume fraction.

Secondly, the isothermal crystallisation of PET/PMMA blends has been studied. The experimental results have been discussed within the context of these two phenomena, and comparisons made with existing literature reports. The main conclusions from this chapter are summarised as follows.

1) The weight loss of PMMA is appreciably slowed at T > 523K when it is blended with PET. The weight loss still follows 1st order kinetics, although the value for E_a is reduced from 120 KJ/mol for unblended PMMA to 86 KJ/mol for PMMA blended with PET.

2) The decrease in weight loss of PMMA in PET/PMMA blends can be attributed to either a chemical reaction between the two polymers, or to the effects of blend morphology.

3) From weight loss data, and using a simple argument, a diffusion coefficient D, can be calculated for degraded PMMA diffusing through a PET matrix. The value of D at 523 K is ~1×10^{-9} - 1×10^{-6} cm^2/sec.

4) The NMR analysis reveals that a singlet due to methyl ester end groups in PETis present in PET in PET/PMMA blends, which increases with annealing temperature. PET-OH end groups are not seen to be diminished compared to the pure PET and as such the alcoholysis reaction (scheme 3.1) is negated.

5) The amount of HFIP insoluble material is taken as a measure of the extent of the grafting reaction between the two polymers. This result combined with the NMR result indicate that the most prevalent reaction is the direct ester exchange reaction between PET/PMMA

6) The thermal analysis of PET and PET/PMMA blends reveals that the crystallisation of PET/PMMA is inhibited on heating above T_g, and cooling from the melt.

7) The inhibition of crystallisation on cooling correlates well with the amount of HFIP insoluble fraction in the blend, and as such is taken as evidence for the aforementioned exchange reaction.

8) The crystallisation mechanism is not influenced by PMMA to any great extent, although the rate of crystallisation of PET in the presence of PMMA is generally slower.

3.6. References.

[1] J. Robinson, DuPont Teijin Films Inc. Privat Communication

[2] Kotliar, A.M., *J. Polym. Sci., Macromol. Rev.*, 1981, **16**, pp 367 - 395.

[3] Porter, R.S. and Wang, L-H., *Polymer*, 1992, **33**, pp 2019 - 2030.

Backson, S.S.E., Richards, R.W. and King, S.M., *Polymer*, 1999, **40**, pp 4205 - 4211.

Collins, S., Peace, S.K., Richards, R.W., McDonald, W.A., Mills, P.J. and King, S.M., *Macromolecules*, 2000, **33**, pp 2981 - 2988.

Collins, S., Kenwright, A.M., Pawson, C., Peace, S.K., Ricards, R.W., MacDonald, W.A. and Mills, P.J., *Macromolecules,* 2000, **33**, pp 2974 - 2980.

Okamoto, M. and Kotaka, T., *Polymer*, 1997, **38,** pp 1357 - 1361.

[4] Yoon, H. and Han, C.C., Polym. Eng. Sci., 1995, **35**, pp 1476 - 1480.

[5] Raboney, M., Hseih, D.T., Garner, D.T. and Peiffer, D.G., *J. Chem. Phys.*, 1992, **97**, pp 4505 - 4511.

[6] Kyu, T., Ko, C.-C., Lim, D.-S., Smith, S.D. and Noda, I., *J. Polym. Sci., Polym. Phys. Ed.,* 1993, **31**, pp 1641 - 1648.

[7] Ko, C.-C., Kyu, T. and Smith, S.D., J. *Polym. Sci., Polym. Phys. Ed.,* 1995, **33**, pp 517 - 525.

[8] Montaudo, G., Puglisi, C. and Samperi, F., *J. Polym. Sci., Polym. Chem. Ed.,* 1998, **36**, pp 1873 - 1884.

[9] Rincon, A. and McNeill, I.C., *Polym. Deg. Stab.*, 1987, **18**, pp 99 - 110.

[10] Jabarin, S.A. and Lofgren, E.A., *Polym. Eng. Sci.*, 1984, **24**, pp 1056 - 1063.

[11] Jabarin, S.A. and Lofgren, E.A., *J. Appl. Polym, Sci.*, 1986, **32**, pp 5315 - 5335.

[12] Goodings, E.P., *Soc, Chem. Ind.*, 1961, **13**, pp 211 - 228.

Ritchie, P.D., *Soc. Chem. Ind.*, 1961, **13**, pp 107 - 130.

Buxbaum, L.H., *Angew, Chem. Internat. Ed.*, 1968, **7**, pp 182 - 190.

[13] J. Heron, ICI plc Private communication.

[14] Grassie, N., *Chemistry of High Polymer Degradation Processes,* 1956, Butterworth, London.

[15] Ozawa, T., *Polymer,* 1971, **12**, pp 150 - 158.

Heiber, C.A., *Polymer*, 1995, **36**, pp 1455 - 1467.

Alfonso, G.C., Verdona, M.P. and Wasaik, A., *Polymer*, 1978, **19**, pp 711 - 716.

Alfonso, G.C., Pedemonte, E. and Ponzetti, L., *Polymer*, 1979, **20**, pp 104 - 112.

[16] Collier, J.R. and Baer, E., *J. Appl. Polym. Sci.*, 1966, **10**, pp 1409 - 1419.

[17] Chan, T.W. and Isayev, A.I., *J. Appl. Polym. Sci.*, 1994, **34**, pp 461 - 471.

Douillard, A., Dumazet, Ph., Chabert, B. and Guillet, J., *Polymer*, 1993, **34**, pp 1702 - 1708.

Groeninckx, G., Reynaers, H., Berghmans, H. and Smets, G., J. *Polym. Sci., Polym. Phys. Ed.*, 1980, **18**, pp 1311 - 1324.

[18] Huang, P., Zhikai, Z., zheng, S., Zhu, W. and Gou, Q., *J. Appl. Polym. Sci., 1999*, **73**, pp 639 - 647.

[19] Gedde, U.W., *Polymer Physics.*, 1995, Chapman and Hall, London.

[20] Grassie, N., McNeill, I.C. and Samson, J.N.R., *Polym. Deg. Stab.*, 1979, **1**, pp 17 - 35.

[21] McNeill, I.C. and Neil, D., *Eur. Polym. J.*, 1970, **6**, pp 569 - 583.

[22] Lizymol, P.P. and Thomas, S., *Polym. Deg. Stab.*, 1993, **41**, pp 59 - 64.

[23] Jones, R.A.L and Richards, R.W., *Polymers at Surfaces and Interfaces.*, 1999, Cambridge University Press, Cambridge.

[24] Jones, R.A.L., *Polymer*, 1994, **35**, pp 2160 - 2166.

[25] Wu, S., Chuang, H-K. and Han, C.D., *J. Polym. Sci. Polym. Phys. Ed.*, 1996, **24**, pp 143 - 159.

[26] Bharadwaj, R.K. and Boyd, R.H., *Polymer*, 1999, **40**, pp 4229 - 4236.

[27] Rueda, D.R. and Varkalis, A., *J. Polym. Sci., Polym. Phys. Ed.*, 1995, **33**, pp 2263 - 2268.

[28] Gravalos, K.G., Kallitsis, J.K. and Kalfoglou., N.K., *Polymer,* 1995, **36**, pp 1393 - 1399.

[29] Suzuki, T., Tanaka, H. and Nishi, T., *Polymer,* 1989, **30**, pp 1287 - 1297.

[30] Schmitz, F.P. and Rossbach, V., *Polym. Bulletin*, 1980, **19**, pp 491 - 496.

[31] Cook, W.D., Zhang, T., Moad., G., Van Deipen, G., Cser, F., Fox, B. and O'Shea, M., *J. Appl. Polym. Sci.*, 1996, **62**, pp 1699 - 1708.

[32] Saldanha, J.M. and Kyu, T., *Macromolecules*, 1987, **20**, pp 2840.

[33] Kyu, T. and Saldanha, J.M., *Macromolecules*, 1988, **21**, pp 1021.

[34] Nadkarni, V.M. and Jog, J.P., *Polym. Eng. Sci.*, 1987, **27**, pp 451 - 457.

[35] Nadkarni, V.M., Shingankuli, V.L. and Jog, J.P., *J. Appl. Polym. Sci.*, 1992, **46**, pp 339 - 351

[36] Ju, M.-Y. and Chang, F.C., *Polymer,* 2000, **41**, pp 1719 - 1730.

[37] Nakai, A., Shiwaku, T., Wang, W., Hasegawa, H. and Hashimoto, T., *Polymer,* 1996, **37**, pp 2259 - 2272.

Goddard, P., Dekoninck, J.M., Devlesaver, V. and Devaux, J., *J. Polym. Sci., Polym. Chem. Ed.*, 1986, **24**, pp 3301 - 3313.

Dubnikova, I.L., Kornienko, G.N., Kompaniets, L.V., Baranov, A.O., Gorenberg, A.Y., Lebedev, S.R., Turusov, R.A. and prut, E.V., *Polym. Sci. Ser. A.*, 1996, **38**, pp 621 - 627.

Kimura, M., Salee, G. and porter, R.S., *J. Appl. Polym. Sci.*, 1984, **29**, pp 1629 - 1638.

Papadopoulou, C.P. and Kalfoglou, N.K., *Polymer*, 2000, **41**, pp 2543 - 2555.

[38] Gedde, U.W., *Polymer Physics,* 1995, Chapman and Hall.

[39] Cobbs, Jr., W.H. and Burton, R.L., *J. Polym. Sci.,* 1952, **10**, pp 275 - 290.

[40] Keller, A., Lester, G.R. and Morgan, L.B., *Philos. Trans. Roy. Soc. London, Se. A.,* 1954, **247**, p 1.

[41] Mitsuishi, Y. and Ikeda, M., *J. Polym. Sci.,* A-2., 1966, **4**, p 283.

[42] Fielding-Russell, G.S. and Pillai, P.S., *Die Makromolekulare Chemie,* 1970, **135**, pp 263 - 274.

[43] Ou, C.F. and Lin, C.C., *J. Appl. Polym. Sci.,* 1994, **54**, pp 1223 - 1231.

[44] Tan, S., Su, A., Li, W. and Zhou, E., *Macromol. Rapid Commun.,* 1998, **19**, pp 11 -14.

Chapter 4.

Thin Films of PMMA and PET

4.1 Introduction.

In this chapter, the investigation of thin films of PET and PMMA is described, via the use of discrete wavelength ellipsometry. The interface between these two polymers is also investigated by neutron reflectometry. This interface is of importance when considering the adhesion and subsequent service performance of an industrially produced film article, and in the downstream reworking of the film in reclaiming procedures. The manufacture and aqueous pre-treatment of biaxially orientated films has been described previously in Chapter 1. In this study, PMMA is used as a model coating material because of its general availability, ease of manufacture and the relative low cost of the wholly deuterated form of the polymer. The compatibility and interactions between PET and PMMA in the bulk have been described in Chapter 3.

In the temperature range of interest (373K - 573K), we are primarily interested in the changes in dimensions of single polymer films. Ellipsometry offers a fast reliable and accurate method of assessing thin polymer layers on silicon substrates [1], and is used here to follow dimensional changes in PET and PMMA. As seen in Chapter 3, PMMA is expected to experience degradation at $T > 473$K. Also, PET will crystallise, at $T_g < T > T_m$ and as such this can be followed by ellipsometry because of the expected changes in layer thickness and refractive index.

In order to investigate the interfacial mixing of PET and PMMA it is necessary to consider both the physical and chemical interactions which may occur at the interface. A diffuse interface may result from the mutual diffusion (interdiffusion) of the two polymers. Transesterification between PET end groups and the pendant methyl ester groups present in PMMA will also contribute towards interfacial broadening (see Chapter 3). The contributions of each of these phenomena to the apparent mixing occurring at the interface needs to be assessed quantitatively. Attempts to decouple the diffusive and reactive broadening of the interface, by the analysis of marker movements

will be described in Chapter 5. Although this chapter deals principally with the interdiffusion of the two polymers, it is intended, that the high resolution offered by neutron reflectivity (< 1 nm) is employed to also monitor the crystallisation of PET and the degradation of PMMA, simultaneously.

Despite the intense research effort into polymer interfaces, there has been very little work undertaken on PET / acrylic interfaces, and only one reference to PET/PMMA interfacial characterisation is sited. Jones and Sivaniah [2], have measured the interfacial width between PET and deutero PMMA via neutron reflectivity and found an interfacial width of 7 nm after annealing the bilayer for 4 days at 443K. Frich *et al.* [3] used Secondary Ion Mass Spectrometry and Neutron Reflection to study inter chain transesterification between a deuterated and non-deuterated aromatic copolyester. They claim that at 553K rapid interdiffusion of the two polymers occurs accompanied by transesterification, leading to homogenous films in less than 1 hr of annealing.

Many other workers have studied incompatible interfaces. Theoretical treatments of these interfaces have been developed (see Chapter 2), and experimentation has been undertaken on many polymer systems [4], in order to align these theories with practical observation. In this study we have started from the assumption that PET and PMMA are an incompatible pair [5].

4.2 Experimental

4.2.1 Preliminary Work.

Polymer Synthesis and Characterisation

PET was prepared using a small scale pilot plant facility at DuPont-Teijin Films Inc. R&T. laboratories Wilton, UK. The polymer batch code was G1063 and was produced to a nominal molecular weight, determined by the viscosity of the melt phase during polymerisation. A-PET (40% IPA copolymer) was supplied by DuPont-Teijin Films Inc, Dumfries, UK. dPMMA was synthesised by T. Kiff at the University of Durham via an anionic addition polymerisation. The polymer was coded TK304. PMMA was purchased from Aldrich Chem. Co. Ltd, Gillingham UK.

The molecular weight distribution of the polymers was determined by GPC. The radius of gyration of the two polymers was measured by light scattering. The measurement of the radius of gyration allows an estimate to be made of the mean squared end to end distance $<R^2>$, and also allows the statistical segment length b, to be calculated according to the formula;

$$N.b^2 =< R^2 > \tag{4.1}$$

where N is the degree of polymerisation. The results of the characterisation are summarised table 4.1.

Table 4.1 Characterisation of Polymers.

Polymer	M_w	M_N	M_w/M_N	R_g	b
PET*	67,500	23,200	2.91	109.5Å	14.4Å
A-PET	72,200	25,600	2.82	115.5Å	14.7Å
PMMA	129,800	44,400	2.92	124.3Å	6.9Å
dPMMA	96,100	94,600	1.02	113.3Å	6.9Å

* The molecular weight of G1063 PET is equivalent to that specified for film grade polymer.

Spin Casting

Bilayer and monolayers of PET and dPMMA were prepared by spin coating onto silicon blocks. The conditions for spin coating flat, uniform polymer layers first needed to be defined. Previous work has shown that toluene is a good solvent for casting dPMMA, giving flat films even at high concentrations [6]. PET is, however, a relatively insoluble polymer and only dissolves in solvents which are expensive and / or toxic. The lack of literature work on preparing thin solvent cast PET films necessitated the screening of the best solvent for spin coating.

5% w/v solutions of PET were prepared in 20 ml quantities. Four solvents were selected for this screening programme, ortho-chlorophenol (OCP), hexafluoro-isopropanol (HFIP), trifluoroacetic acid (TFA) and Dichloroacetic acid (DCA). All solutions, except HFIP, required gentle warming to effect complete dissolution. These solutions were then spun onto silicon blocks at 2000 and 4000rpm

and the resultant layers qualitatively assessed by visual inspection. A selection of samples were measured by X-ray reflectometry in order to asses the surface roughness of the layers. Flat samples are essential in the interfacial analysis of bilayers. Table (4.2) summarises the results of this screening trial.

As a result of this screening trial, OCP was selected as the best solvent for spin casting PET. Spinning conditions for both polymers were selected by trial and error, with initial estimates based on the conditions reported by previous workers [7]. Target thickness' were ~ 40 nm for each layer.

Table 4.2 Spin Coating Test for PET Solutions.

Solvent	Spin Speed (rpm)	Visual assessment	Surface roughness
OCP	4,000	Flat even film produced	0.5 nm
	2,000	Flat even film produced	0.5 nm
HFIP	4,000	Grainy looking films produced.	7.7 nm
	2,000		8.9 nm
TFA	4,000	Streaky poor quality film	3.2 nm
	2,000	Grainy / uneven film	N/A
DCA	4,000	Solution did not wet out	N/A
	2,000	Improper wetting / retraction areas	2.2 nm

4.2.2. Sample Preparation

Monolayers

PET and A-PET monolayers were spun cast onto silicon substrates from solutions of OCP at 4000 rpm for 30 sec. PMMA and d-PMMA monolayers were spun cast from solutions of toluene at 4000 rpm for 30 seconds. The samples were placed in a vacuum oven at 333K for 24 hrs in order to remove residual solvent from the polymer layers.

Bilayers

PET or APET was spun from OCP at 4000rpm for 30 sec., and the resultant polyester coated silicon block was analysed by ellipsometry to establish the film thickness. These monolayers were then over coated with the PMMA or dPMMA layer via spin casting from toluene. This method of bilayer preparation was chosen over the popular 'float' method, for two reasons:

1) Floating one polymer layer onto another will require immersion in water, and PET is particularly susceptible to hydrolysis, even at low temperatures [8]

2) Intimate contact between the two polymers is established immediately. Toluene is a good solvent for PMMA but is a non-solvent for PET, and under the time regime of spin coating will not swell the PET layer to any significant degree. (This was checked by ellipsometry; no layer thickness change was observed when spin coating pure toluene onto PET). The thickness of the top PMMA layer was then measured by ellipsometry.

Annealing programme

Samples were annealed for various lengths of time under vacuum at 473K - 573K. This temperature range was chosen because as it encompasses the temperatures typically encountered in a film making, or reclaim process (see Chapter 1). As short annealing times were required, it became necessary to use a heat sink in the oven, in order that samples were brought to the required temperature as quickly as possible. On removal from the vacuum oven the silcon blocks were rapidly quenched on a mild steel block which was cooled by liquid nitrogen. The rapid quench was done in order to ensure that the physical and chemical nature of the samples at the point of removal from the oven were frozen in as quickly as possible. The shortest practical annealing period using this technique is ~ 1 min, and it is noted that there will be some uncertainty due to the time required for the sample to reach equilibrium in the oven, (this has been estimated at ~ 20 sec).

Table 4.3 Annealing regimes in PET film process.

Time	473K	573K
1 min.	Typical time regime in in-line coating process	Time needed for re-melt during reclamation of coated film
5 min	Typical stoving time in stenter/stabilisation of coated film.	Time spent in screw/static mixer section of extruder
15 min	-	Typical resonance time extrusion process
30-60 min	Maximum time in stabilisation process. Used as accelerated ageing regime.	Maximum hold up/dead time in single screw extruder

4.2.3 Characterisation of Samples.

Ellipsometry

Ellipsometry of the monolayers was performed with a Sentech SE400 auto ellipsometer, (Sentech Instruments GmbH, Germany), equipped with an automatic sample mapping stage. The measurements were taken at a fixed angle of 70°, for single films and at multiple angles between 70° and 40° for 2 layer constructs The ellipsometric parameters used for the analysis of the films are shown in table 4.4. The collected values for Ψ and Δ are used to calculate the layer thickness and apparent refractive index of the thin polymer layers.

At the temperatures encountered in the film manufacturing process, we are primarily concerned with the crystallisation of PET and the possible degradation of PMMA. Both these processes should result in dimensional changes in thin layers and hence may be studied by ellipsometry. Wehrum has used ellipsometry extensively to monitor physical processes in thin PET and PS films, by use of a specifically constructed heating cell combined with spectroscopic ellipsometry measurements, such that the expansivity of thin polymer films could be measured as a function of temperature [9]

In this study no such cell was available and hence the measurements were made ex-situ, after known periods of annealing in a vacuum oven (see above). Therefore isothermal annealing temperatures were chosen to reflect the conditions of interest for PET film manufacture.

Table 4.4 Parameters used in Ellipsometric analysis of Monolayers and Bilayers.

Material	Refractive Index RI	K (Absorption)	Density (g/cm^3)
Air	1	0	-
PMMA	1.47-1.53	~0.0	1.18
PET	1.57-1.64	~0.0	1.33 (amorphous)
Si	3.882	0.019	2.33

PMMA is wholly amorphous, and as the value of the refractive index should not change due to annealing. The Ψ, Δ values for PMMA single films on Si substrates are shown in figure 4.1. These values are determined using a constant value of n of 1.52.

The refractive index of the PMMA was determined independently using an Abbe refractometer. The value of 1.489 was established for an isotropic melt cast film of ~50μm

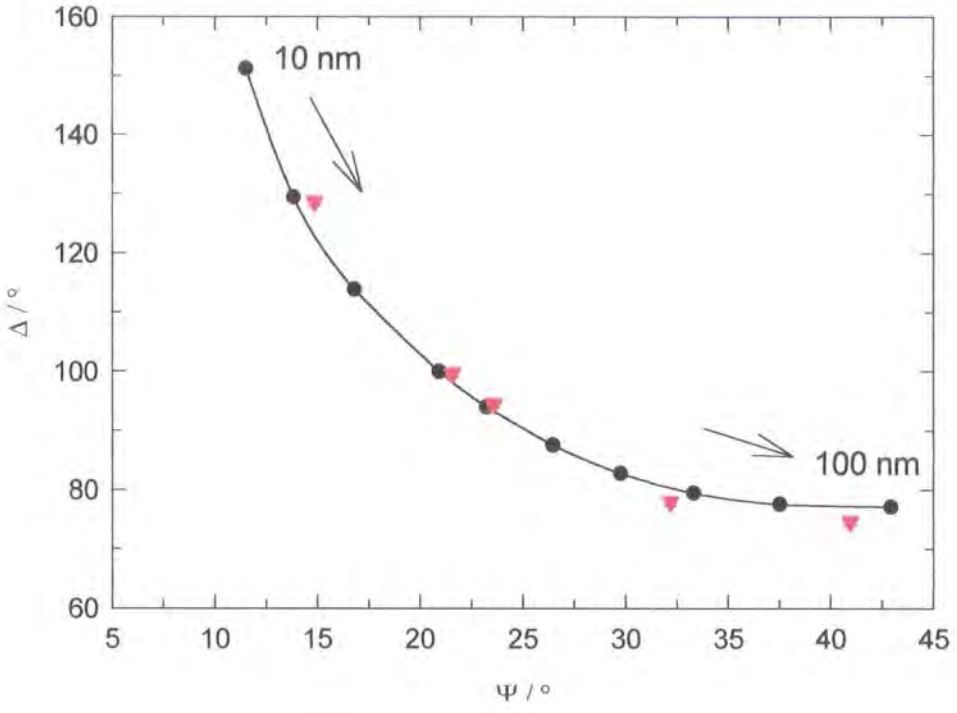

Figure 4.x Ψ,Δ plot for PMMA on silicon. The black circles represent simulated Psi/Delta pairs for thickness increments of 10 nm. The red triangles are measured films of PMMA of refractive index of 1.489

PET is expected to crystallise upon heating and a change in density is expected. Therefore consideration also needs to be given to the refractive index of PET thin films during the ellipsometric determination. Spun cast films exhibited a refractive index of ~1.58 - 1.6 (amorphous), whereas crystalline films had refractive index values of 1.63 - 1.65. Figure 4.2 shows the refractive Ψ,Δ plot for ~ 50 nm PET layers cast onto silicon. The theoretical line for increasing refractive index is shown alongside some measured values of PET layers, at various stages of densification. Deviations from the theoretical line are seen at higher refractive index values, because the layer changes dimensions. i.e. becomes thinner as crystallisation causes densification of the layer. This phenomena allows the crystallisation of thin layers of PET to be studied. (see section 4.3).

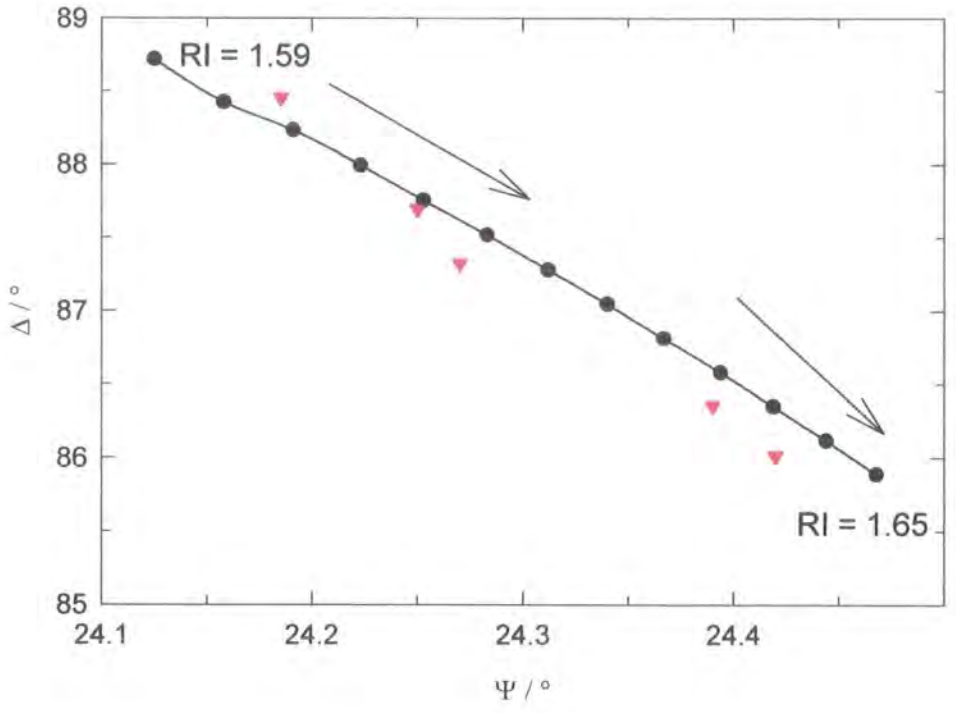

Figure 4.2 Ψ,Δ for increasing refractive index and (assumed) constant film thickness (~50 nm). The red triangle represent approximately ~50 nm films of PET at various stages of densification.

Neutron Reflectometry

Neutron reflectivity was performed on the CRISP reflectometer at the Rutherford Appleton Laboratory. The data were collected using grazing beam angles of 0.25°, 0.6° and 1.5°. These data were combined by superimposing the three data sets over a common range using a routine available in the RAL data handling software GENIE. Errors were calculated using standard Poisson counting statistics. Average acquisition time was 55 min. per sample.

Collected NR profiles were fitted using the PC MULF and Parrat software which utilise a SIMPLEX routine to fit the data. The initial values for the scattering length density of dPMMA, Si and air were taken from reference 10. The scattering length density for PET was calculated from the formula;

$$\delta = \sum_{i=1}^{n} b_i \times \frac{\rho N_A}{M} \qquad (4.2)$$

where b_i is the scattering length of atom i, n is the total number of atoms in the monomer unit, ρ is the bulk density of the polymer, M is the molecular weight of the monomer unit and N_A is Avagadro's number. It is clear that the scattering length density is dependant on the bulk density of the polymer, hence changes in the fitted parameter, with respect to annealing, are indicative of physical changes in the polymer of interest.

The thickness values derived from ellipsometry (see section 4.4.1), were used as initial values during fitting. As expected, the dominant factors in the profile analysis were the dPMMA layer thickness and roughness, and the air / sample roughness. This roughness is calculated as a Gaussian function of the Debye-Waller type [10], and as such should generate interfacial profiles with a form which can be described by an error function. Qualitatively, the fitting procedure was as follows;

1) Visually asses the reflectivity profiles relative to each other. The dominant fringes in the profiles will be due to the layer with the largest scattering length density (dPMMA), and we can therefore qualitatively asses the effect of annealing.

2) Assume an increasing Gaussian roughness between the layers. Loss of defined structure in the profiles can be generally attributed to either a lower instrument resolution, which is unlikely as instrumental resolution should remain unchanged throughout the experiment, or from increasing roughness of the interfaces present in the system. The interfaces in this system are the substrate/sample interface, which we have assumed will remain constant for all samples and will not be affected by the annealing or quenching processes; the air / sample interface, which has been included in the fitting routine for many samples, and has been shown to exert a major influence over the observed reflectivity profiles. The polymer/polymer interface is of primary interest to us in this study as the characteristics of this interface will be directly related to important interpolymer properties such as adhesion and compatibility.

3) Assume an increasing layer loss with increasing annealing time. As has been established from ellipsometry experiments, a reduction in both dPMMA and PET layer thickness is expected at the temperatures of interest.

Some attempts were made to fit the data to a three layer model; i.e. the interfacial layer is considered as a distinct layer, however, no improvement in the quality of the fits was observed, as determined by the value of the fit residual. The results reported here are for two layer models only, incorporating the roughness as described above.

4.3 Ellipsometry of Polymer Thin Films.

We now consider the case of applying thin polymer films to the substrate. Here we investigate the response of PET and dPMMA monolayers to a thermal annealing programme. A knowledge of the response of these polymer films as monolayers to the prescribed annealing programme is essential in evaluating the performance of subsequent bilayers of the two polymers. The PET layer may crystallise upon annealing (provided it is not constrained by its thin film geometry), leading to densification of the layer and possible surface roughening. The dPMMA layer, whilst atatic and therefore amorphous, may undergo depolymerisation and result in thinner layers.

4.3.1. Thin Films of PMMA.

Samples of PMMA of various thickness, were prepared by spin coating onto Si substrates. The response of these samples to annealing in the temperature range 473K-573K was monitored by ellipsometry. The results are plotted as the normalised thickness d_t/d_0, as a function of time for each temperature. The results are shown in figure 4.3

The results clearly indicate that the PMMA layer is reduced in thickness upon annealing. Firstly, densification of the PMMA layer is considered. Fernandez, *et al* [11], have observed densification of PMMA after heating 393K, of ~ 5%. Here the decrease in layer thickness would indicate an increase in density of this layer of > 45%. Hence the density of the annealed layers would be 1.7 g/cm^3 at 493K which is clearly absurd. Therefore material loss due to depolymerisation of the acrylic layer is indicated as the mechanism of layer depletion. This is not unreasonable. In Chapter 3 it has been shown that PMMA will degrade at T > 473K, and this is supported by many literature reports.

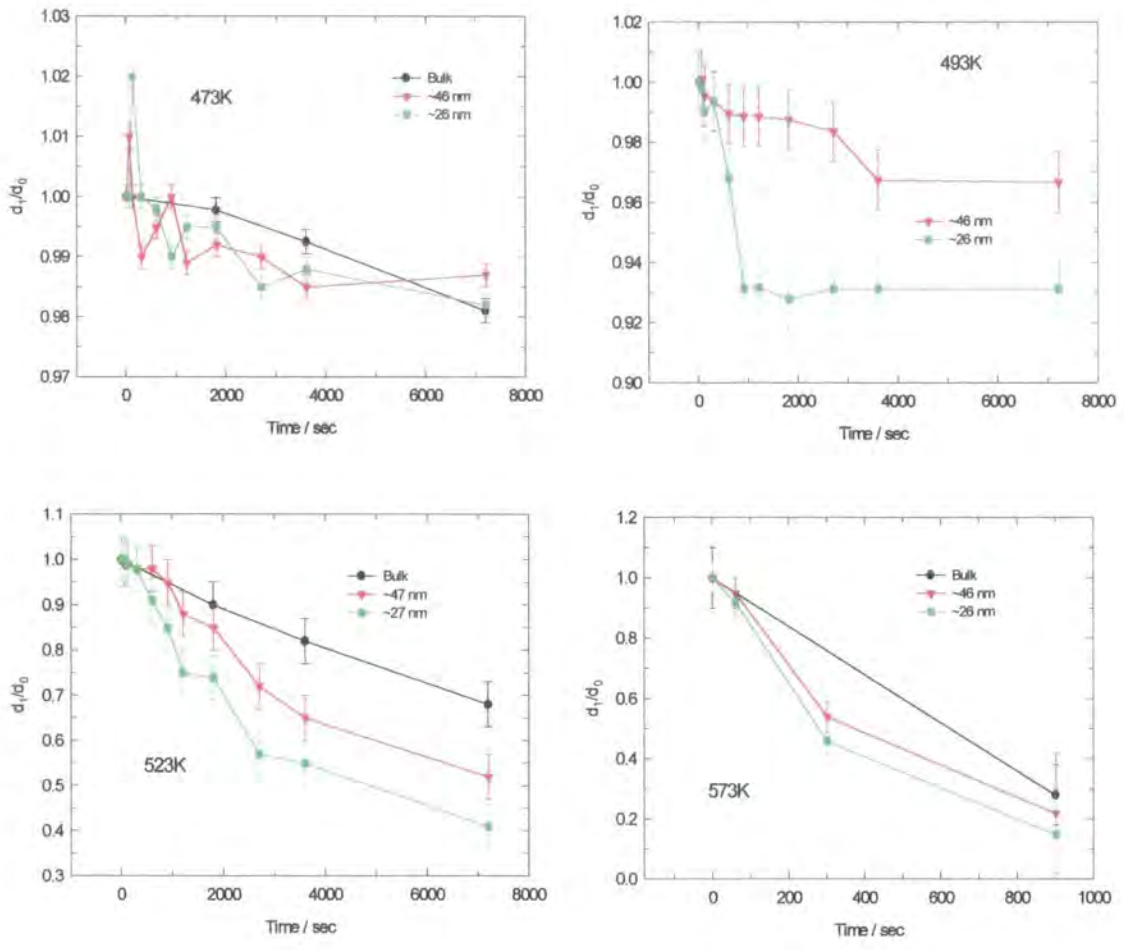

Figure 4.3. Depletion of thin layers of PMMA on Si. The depletion is compared to the bulk weight loss at 473K, 523K and 573K.

To investigate further the thickness dependence of degradation, samples of thickness' between 17 and 300 nm were prepared and annealed at 573K and the PMMA layer thickness monitored as before. The results are plotted as a first order reaction according to the equation

$$\ln\left(\frac{d_1}{d_0}\right) = -kt \tag{4.3}$$

where k is the rate constant for the reaction and is given by the straight line fit to the data. This is shown in figure 4.4.

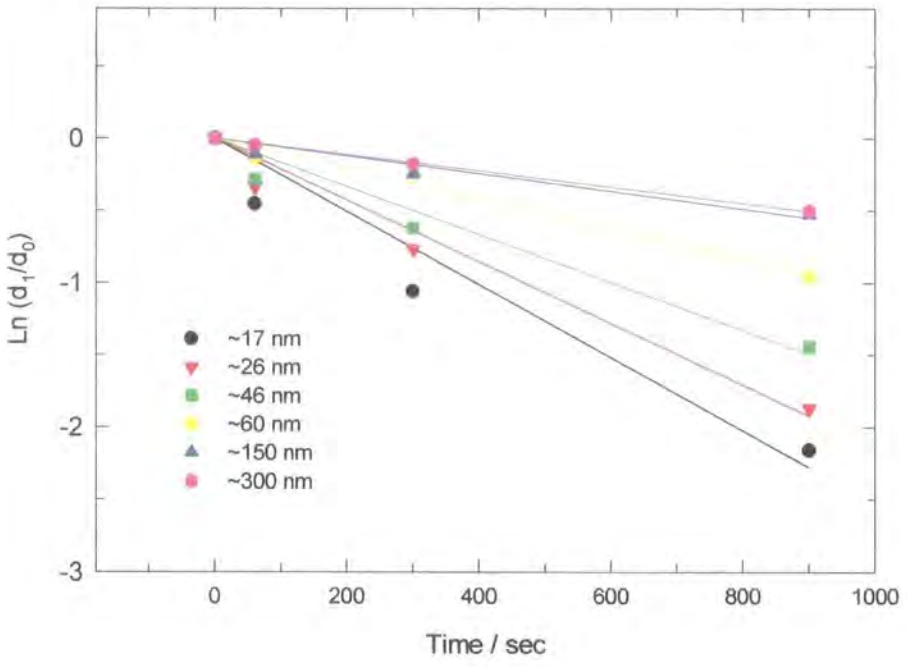

Figure 4.4 1st order layer degradation at 573K for PMMA on Si. Error bars are omitted for clarity.

The values for k are collected in table 4.5. It is clear that decreasing layer thickness increases the rate of degradation under the conditions of high vacuum at 573K. This is in agreement with the work of Lehrle *et al* [12], who have shown that the degradation of PMMA is dependant upon sample thickness, because the products of degradation have less chance to undergo secondary reactions as they diffuse through the sample matrix; i.e. the path length is shorter, (see figure 4.5)

Table 4.5. Rate constants for PMMA layer depletion at 573K.

k / s^{-1}	Bulk	~300nm	~150nm	~60nm	~46nm	~26nm	~17nm
	5.5×10^{-4}	5.6×10^{-4}	6.1×10^{-4}	1.0×10^{-3}	1.7×10^{-3}	2.1×10^{-3}	2.5×10^{-3}

The rate of layer depletion can now be plotted as a function of a fundamental polymer dimension such as R_g, the radius of gyration of the polymer. This is shown in figure 4.6. Here, it can be seen that that bulk degradation rates are recovered at a sample thickness of $\sim R_g \times 6$. Below this value an approximate linear relationship exists between sample thickness and the value of the 1st order rate constant, given by equation 4.4.

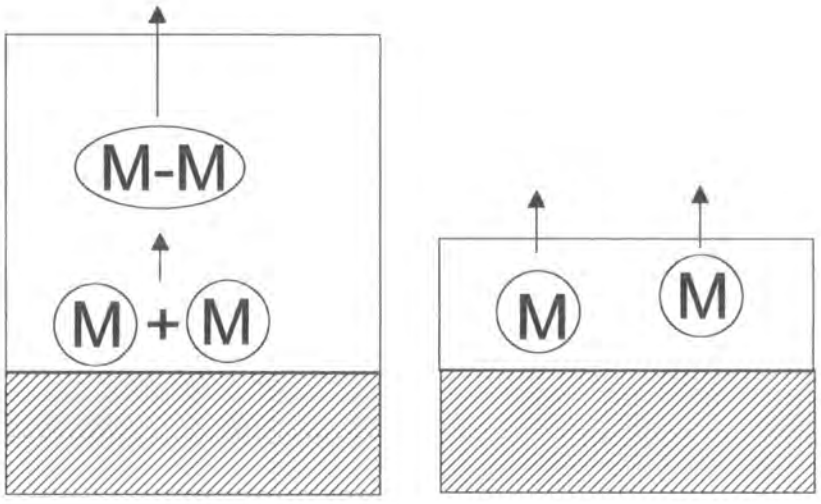

Figure 4.5. Thickness dependence of rate of degradation (weight loss) for addition polymers. The average path length for a degraded fragment or monomer, diffusing through the sample matrix is shorter, hence the probability of secondary reaction is less than in thicker samples.

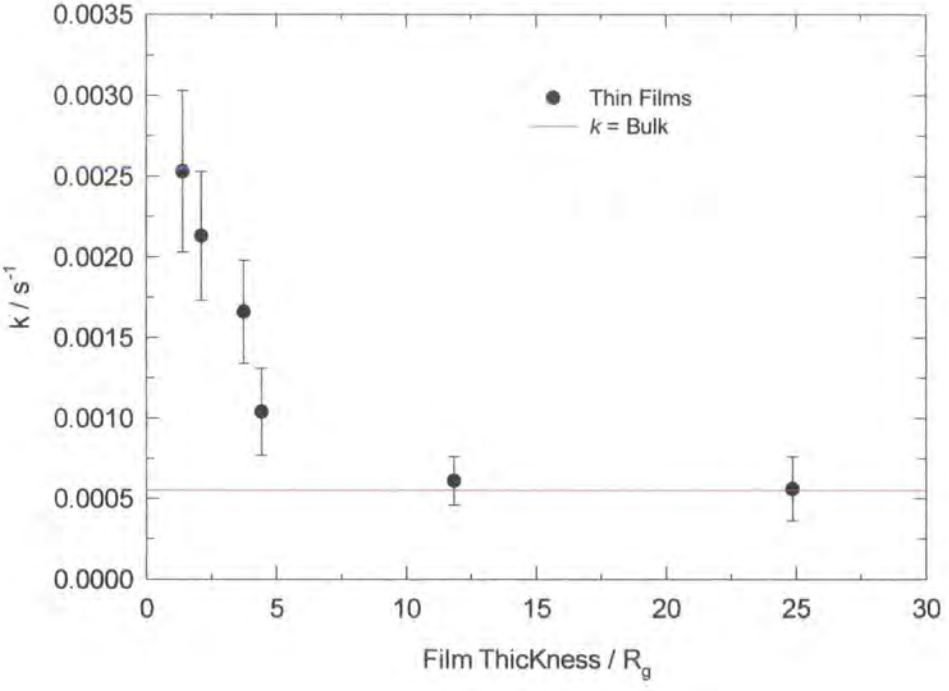

Figure 4.6 1st order rate constant, k, for degradation of PMMA thin films, as a function of Initial film thickness, normalised to R_g (12.43 nm)

$$k = -4.4 \times 10^{-4}\left(\frac{d}{R_g}\right) + 3.1 \times 10^{-3} \qquad (4.4)$$

For the PMMA used in this experiment the R_g has been measured as 12.43 nm (see section 2), and the limiting value of of the film thickness, i.e. d_{BULK} is ~74.5 nm.

An obvious consequence of this phenomena is that the rate of degradation of PMMA should increase as the sample becomes thinner, (i.e. the degradation auto-accelerates), once the limiting value for bulk degradation is reached. Inspection of figures 4.3 and 4.4 shows that, although the overall rates of degradation are faster for thinner layers, this rate does not then accelerate as is predicted by the thickness dependant hypothesis. It is postulated that this is a result of an anomaly of the ellipsometric measurement. On observing the physical appearance of PMMA layers during degradation it became immediately apparent that as the annealing period progressed the PMMA layer was seen to dewet from the Si substrate. Optical microscopy reveals that the sample surface becomes only partially covered with PMMA (figure 4.7). The discontinuity is to be expected in these samples as PMMA has been shown to de-wet from silicon substrates at temperatures above T_g [7]. It is postulated that this dewetting produces a rough surface which cannot be accurately modelled by fixed angle, discrete wavelength ellipsometry, and this accounts for the high error in measurement at longer annealing times.

The degradation of PMMA and other polymers confined to thin layers, has been studied by McNeill and Mohammed [13]. They showed that a thin layers (< 100 nm), displayed a significantly different degradation response to increasing degradation temperature compared to powdered (bulk) samples. However, this thermal analysis showed the polymer stability to be enhanced when geometrically confined, i.e. the majority of the weight loss from the sample was at higher temperatures than in the bulk. This is in contradiction to the work presented here, although the method of analysis was significantly different.

As already mentioned Lehrle *et al* [12], have proposed that thin layers of polymers display accelerated degradation (see figure 4.5) compared to bulk degradation and the results presented here agree well with this hypothesis. Lehrle, has also proposed that a layer of polymer adjacent to the filament (substrate) may display 'diffusion restriction of termination' of degraded fragments or monomer, and this layer is of the

order 20 -50 nm thick, i.e. the of the order of the dimensions of a polymer chain in the melt. Here we have seen increased rates of degradation for thin film samples ~ 75 nm thick which, given the uncertain nature of the experiment is in relatively good agreement. A cautionary note is that the work reported here has been carried out at temperatures higher than the temperatures usually reported in literature.

Although the thickness dependence of the PMMA film degradation is an interesting observation, the principle reason for investigating PMMA thin films is to ascertain the expected degradation behaviour when compared to PET/PMMA bilayers, and further detailed study, lies beyond the scope of this thesis.

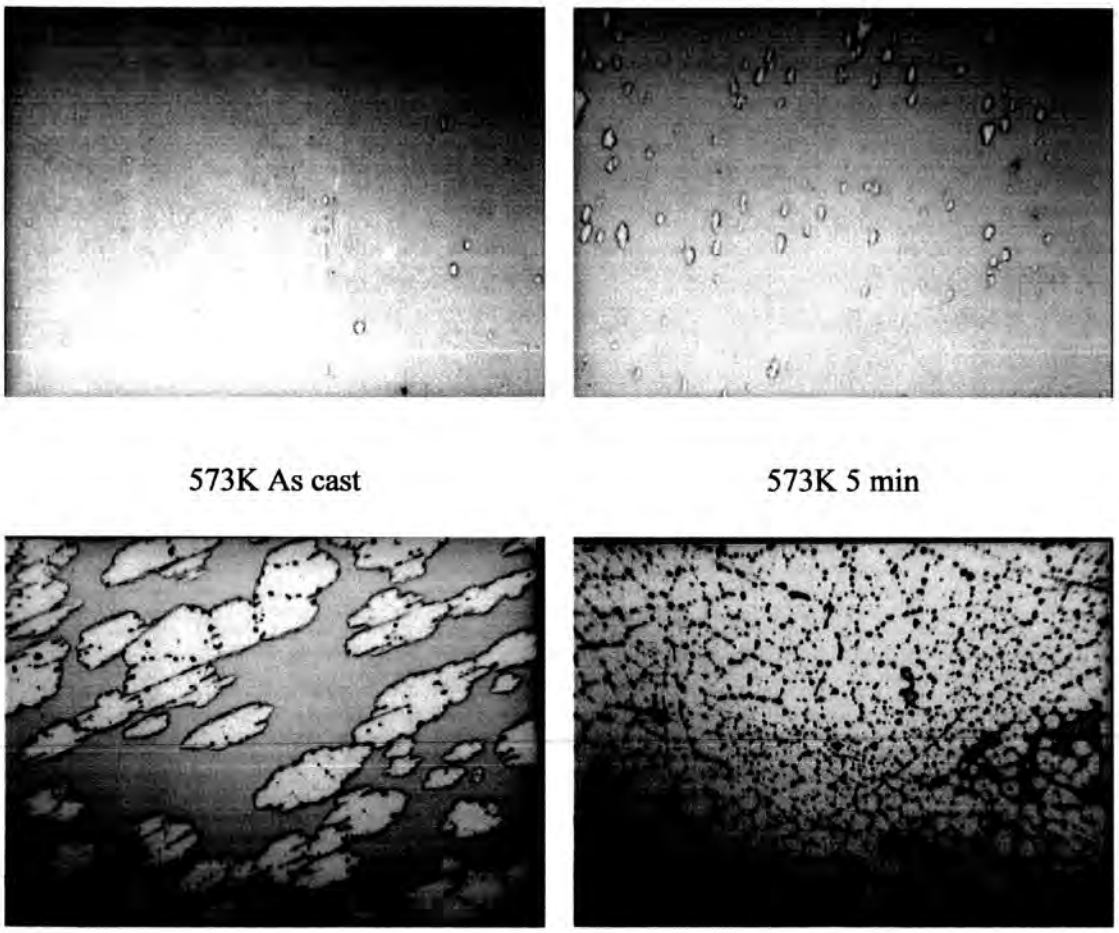

Figure 4.7 Optical microscopy of PMMA thin films dewetting from Si substrate at 573K. Magnification = × 80

4.3.2. Thin Films of PET.

Layer depletion in PET has been studied at 573K and 493K, in the manner described for PMMA layers. At 573K the thickness of single layers on Si substrates was seen to reduce by only ~0.2%. This slight reduction in thickness on annealing is attributed to the relaxation of the spun cast layer to the melt state. No significant change is then seen over ~2 hr annealing, indicating the molten layer is stable to degradation over this period.

Annealing thin PET at 493K does produce significant changes in the layer thickness. Several films of various initial thickness were prepared and the subsequent influence of annealing monitored as before. The normalised thickness is plotted against the annealing time and the results shown in figure 4.8

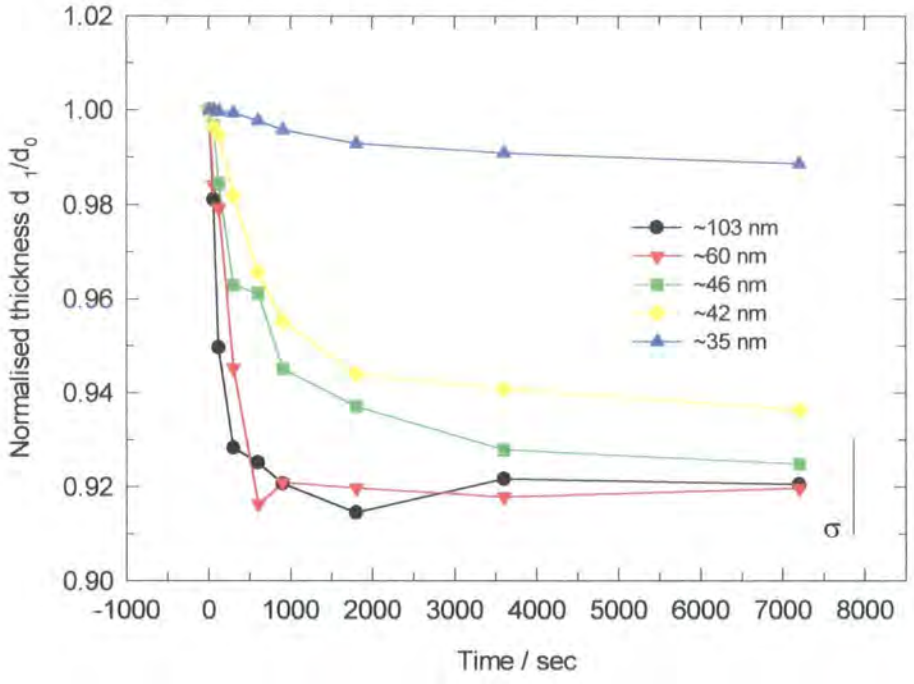

Figure 4.8 Normalised thickness as a function of time for PET layers annealed at 573K. The maximum error is indicated by the bar at the bottom right of the plot.

This reduction in film thickness is attributed to densification due to crystallisation. This explanation is favoured over any possible degradation or weight

loss mechanisms because we have already seen that PET thin films are stable at 573K. i.e. ~50K above the melt temperature. In order to achieve accurate thickness measurements the refractive index *n*, of PET was allowed to vary during the fitting of thickness values to the observed Ψ,Δ pairs. the fitted value of n was found to increase with increasing annealing time. This is shown graphically for the ~60 nm sample (figure 4.9). This increase in *n* is further evidence that densification, and therefore crystallisation, is taking place in these thin films.

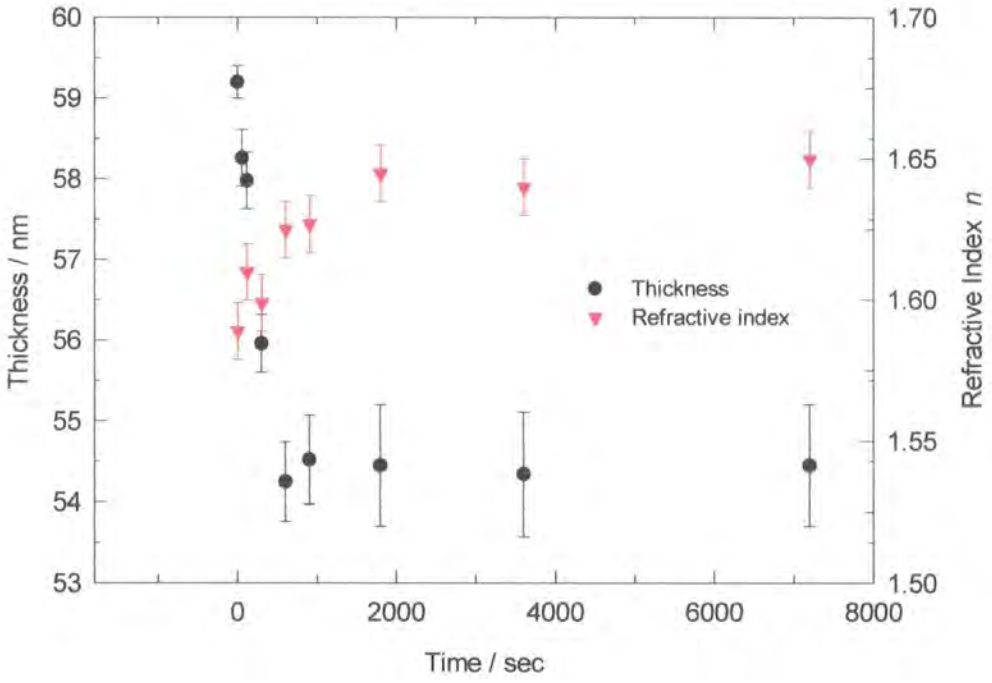

Figure 4.9 Thickness and refractive index variation of ~60 nm PET film during isothermal annealing at 493K.

The thickness depletion can now be treated with the Avrami theory for polymer crystallisation. The Avrami theory was used in Chapter 3 to analyse the differences in PET crystallisation between blended and unblended samples. Equation 4.5 is used to extract a linear plot;

$$\ln(-\ln(1-X_t) = n\ln(t) + \ln(k) \qquad (4.5)$$

where X_t is the relative crystallinity, t = time, n is the Avrami exponent, and k is the rate constant for crystallisation. Assuming an amorphous density of 1.333 g/cm^3 [x], the density of the annealed films can be calculated from the equation;

$$\rho_0 d_0 = \rho_1 d_1 \tag{4.6}$$

where ρ_0 and ρ_1 are the densities of the unannealed and annealed films respectively and d_0 and d_1 are the film dimensions before and after annealing, respectively. The total crystallinity of the film can now be calculated by using a simple two phase density model, assuming the crystalline phase has a density of 1.515 g/cm^3 [14], and employing the equation,

$$X_c = \frac{\rho_m}{\rho_c - \rho_a} \tag{4.7}$$

where ρ_c and ρ_a have the values given above and ρ_m is the measured or calculated density of the PET film. The crystallinity of can now be extracted and used to study the isothermal crystallisation of the PET layers, (see figure 4.10).

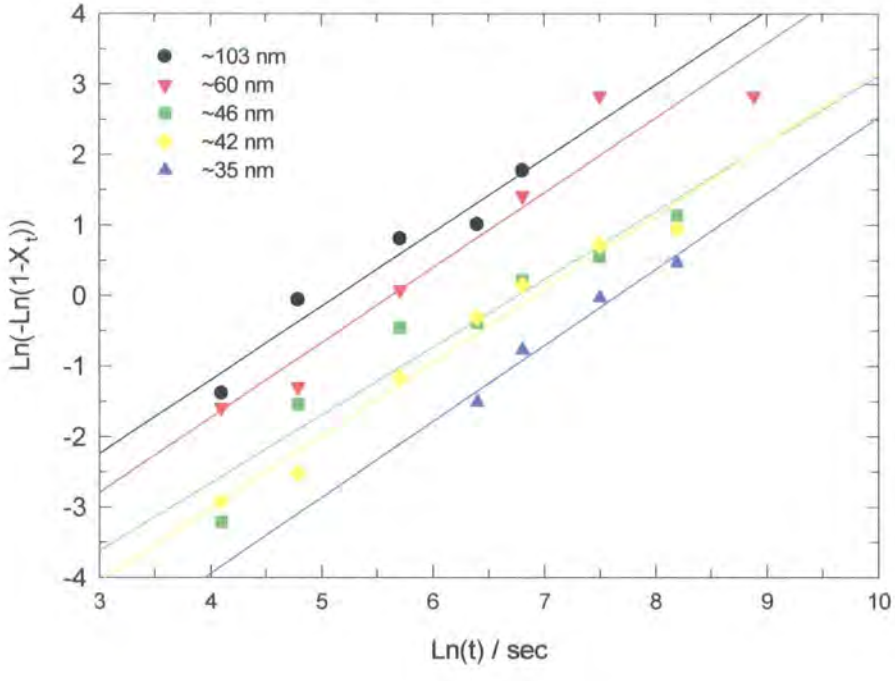

Figure 4.10 Avrami plots for PET layers crystallised at 493K.

The critical parameters derived from the Avrami analysis are shown in table 4.6. Here we see that the value of the exponent n, which indicates the mechanism of crystallisation, is comparable for all sample thicknesses. However, the rate of crystallisation is affected by film thickness, as is the extent of crystallinity achieved in the sample. When the initial layer thickness is ~ 35 nm only 8% crystallinity is induced over a 2 hr annealing period, whereas 8% crystallinity is achieved in a few minutes in the sample with initial film thickness ~ 103 nm.

Table 4.6. Avrami analysis of thin layer crystallisation of PET at 493K.

d_0 / nm	n	k / s^{-1}	X_c
103	1.0	$(4.7\pm1.4) \times 10^{-3}$	0.63
60	1.0	$(2.5\pm1.1) \times 10^{-3}$	0.64
46	1.1	$(1.5\pm0.7) \times 10^{-3}$	0.56
42	1.0	$(7.7\pm3.1) \times 10^{-4}$	0.46
35	0.9	$(2.6\pm0.9) \times 10^{-4}$	0.08

A note on surface roughness

A further complication of crystallisation in PET is the apparent increase in surface roughness of the annealed films. This phenomena was detected during the collection of multiple data points for thickness measurement. The statistical variation of annealed samples was seen to be far greater than the variation of as cast samples. In order to quantify this, data was collected from a series of points along a straight line on an as cast sample and measurements taken every 100 μm. The sample was annealed and the line scan repeated to asses the changes in the statistical variations due to annealing. From figure 4.11 it is clear that the thickness variation across the sample has increased markedly after annealing. The sample variance for the as cast layer and the annealed layer are ~0.02 and 2.3 respectively, indicating that a large increase in apparent surface roughness has occurred. Although no further analysis has been made, it is not unreasonable to assume that this apparent roughness is due to the increase in crystallinity of the layer. The lateral resolution, (100 μm) is too poor to derive a value for the surface roughness of the layer, although it is imagined that under careful experimental conditions, a value approximating surface roughness could be obtained.

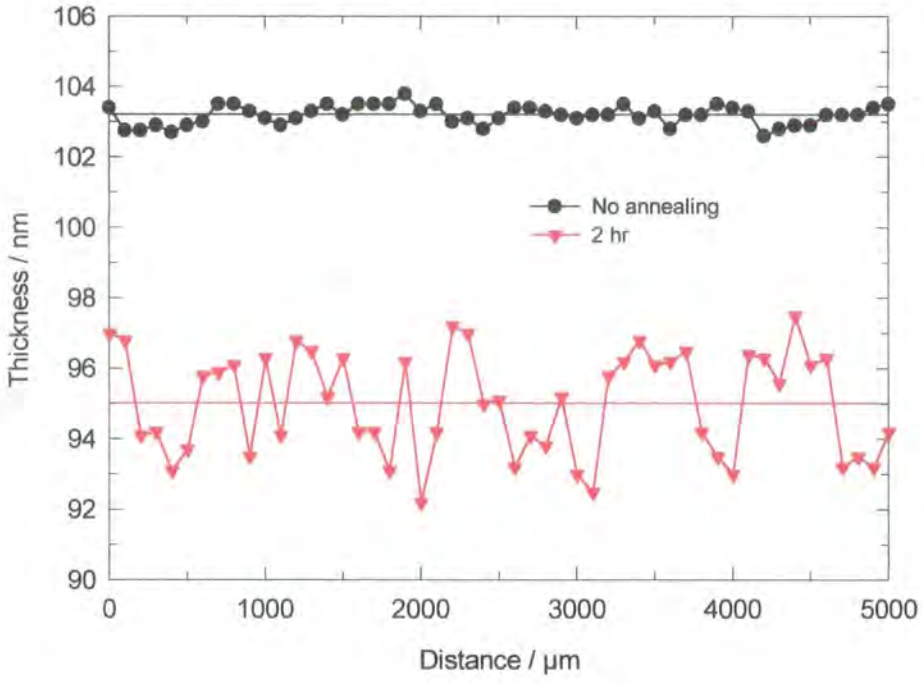

Figure 4.11 Statistical variation of ~100 nm PET layer before and after annealing at 493K.

The crystallisation of PET has been studied on many occasions, but the study of the crystallisation of PET confined as very thin films is very rare. Groeninckx *et al* [15], have studied 50 nm films of PET by electron microscopy and shown a certain degree of crystallisation inhibition at lower temperatures. A much more detailed investigation was carried out by Wehrum [9], who used spectroscopic ellipsometry to monitor the crystallisation of very thin films of PET in situ. Here it was shown that samples as thin as 7.5 nm were seen to crystallise, although the rate of crystallisation was significantly reduced, compared to films of 170 nm thickness. This is in good agreement with the results obtained here, where it has been shown that, under isothermal conditions, the rate of crystallisation shows a marked dependence on the thickness of the PET film. Despite this apparent agreement, contradictions to other works exist, particularly Hayes *et al* [16], who have shown that the crystallisation of PET at the surfaces of thicker films is enhanced. Also, the reduction in the rate of crystallisation of thin PET films implies a reduction in chain mobility, which is in contradiction to the work of Keddie *et al* [17], who have shown that the T_g of thin layers of polystyrene are reduced compared to bulk

samples indicating enhanced chain mobility. Despite these results, the good agreement with the work of Wehrum, is taken as validation of the observed restriction of crystallisation in thin PET films.

4.3.3. Ellipsometry of PET/PMMA Bilayers.

Samples of PMMA cast onto A-PET were prepared, and examined by multiple angle ellipsometry (MAE). A-PET was used in order to avoid interference from crystalline roughness which is believed to develop in PET (see above), during subsequent annealing. The analysis of PET based bilayers by MAE will be discussed in the context of neutron reflectivity results (see section 4.3.4). The sample was annealed for ~ 4hrs. and measured at appropriate intervals within this period. The Ψ, Δ signature for an as cast and an annealed sample are shown in figure 4.12. Here the sample was annealed at 493K for ~60 min. under constant vacuum, and the sample immediately quenched after removal from the oven. The Ψ, Δ pairs were collected at incidence angles of 40,45,50,55,60,65 and 70°.

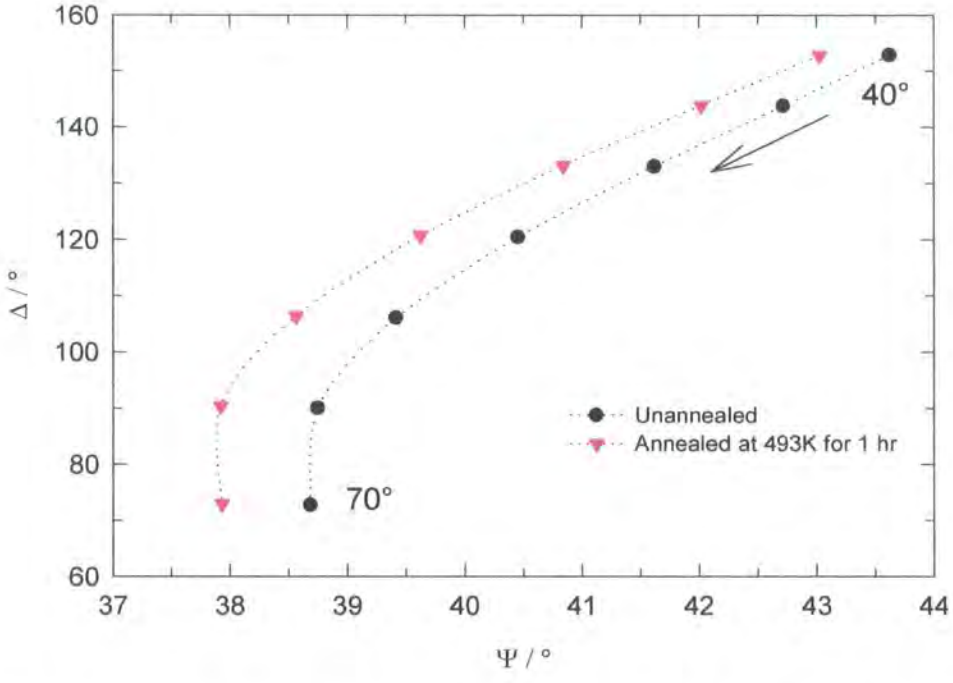

Figure 4.12 Ψ,Δ signature curves for A-PET/PMMA bilayers on Si, before and After annealing. The lines are a guide to the eye.

The ellipsometric parameters were fitted against values for the thickness of the layers. Fitting routines for both two and three layer (interfacial layer) models were run. In the latter case, constrained fits were performed, whereby initial thickness of the polymer layers was chosen to be slightly lower than the measured values, and the thickness of these layers and the interfacial layer were allowed to vary, only so a limiting value for total thickness was not exceeded. These models are illustrated in figure 4.13. It is evident that depletion of the PMMA layer can occur by depolymerisation or interdiffusion, hence an accurate measurement of the width of an interface is necessary to establish the exact extent of PMMA degradation when applied as a thin film on a PET or APET surface. The relaxation of PMMA chains across the interface will lead to the thinning of this layer as the interfacial width develops. Alternatively, thinning by depolymerisation may yield bilayers with similar total thickness.

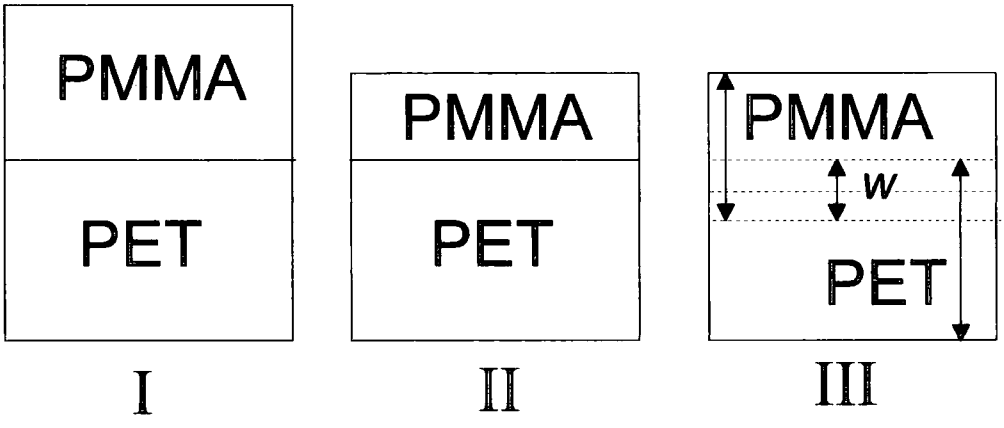

Figure 4.13 Thickness changes in A-PET / PMMA bilayers. I). As prepared. II) PMMA layer thins due to depolymerisation. III) Total Thickness change due to interdiffusion, creating a characteristic interfacial width, w.

The interfacial profiles used to fit the ellipsometry data are shown in figure 4.14. In case I the system is considered to be a two layer construct with an infinitely sharp interface. In case II the refractive index of the interface is assumed to vary in a linear manner across the interface, (APET n = 1.59, PMMA n = 1.49), hence the interface is constructed according to the matrix method of Born and Wolf [18], (see Chapter 2).

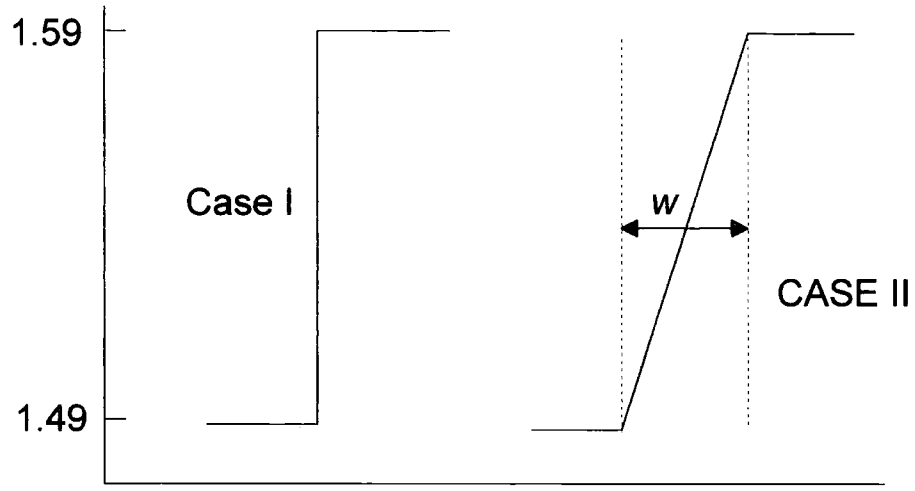

Figure 4.14. Interfacial profiles used to fit interfacial layer thickness for MAE measurements. I) Simple step profile. II) Linear Interfacial gradient.

For the APET / PMMA system annealed at 493K, the values of the fitted layer thickness are shown in table 4.6. for both the two layer and three layer models. The analysis shows that the PMMA layer did reduce in thickness in accordance with the depolymerisation of thin layers already discussed. The rate of degradation of this layer was also seen to accelerate as the layer became thinner, which is in accordance with the hypothesis discussed earlier (see figure 4.5), indicating that the proposed hypothesis for the absence of this phenomena in single layers of PMMA, (i.e. ellipsometric variations due to film de-wetting from Si substrate) is perhaps, not unreasonable.

Table 4.6. Fitted values for layer thickness of APET/PMMA bilayers.

Time	2 layer model / nm		R^2	3 layer model / nm			R^2
(sec)	PMMA	A-PET		PMMA	*w*	A-PET	
0	42.5	48.3	0.52	42.5	0.0	48.3	0.51
300	42.3	48.1	0.53	42.5	0.0	48.2	0.53
900	42.4	48.1	0.48	42.3	0.0	48.1	0.48
1,800	41.5	48.2	0.41	42.2	0.0	48.1	0.42
3,600	41.3	48.2	0.62	40.6	2.0	47.1	0.61
7,200	40.2	48.0	0.68	39.8	2.5	46.9	0.55
10,800	39.5	48.2	0.67	38.6	5.3	46.1	0.51
14,400	35.7	48.1	0.69	34.5	4.8	46.2	0.62

The thickness of the PMMA layer is plotted as a function of time for both models (figure 4.15). As can be seen the depolymerisation of PMMA is evident from both models, even accounting for an interfacial layer, in the three layer model analysis. However, as can be seen, the improvement in the fit is only marginal for the three layer models after 4 hrs annealing.

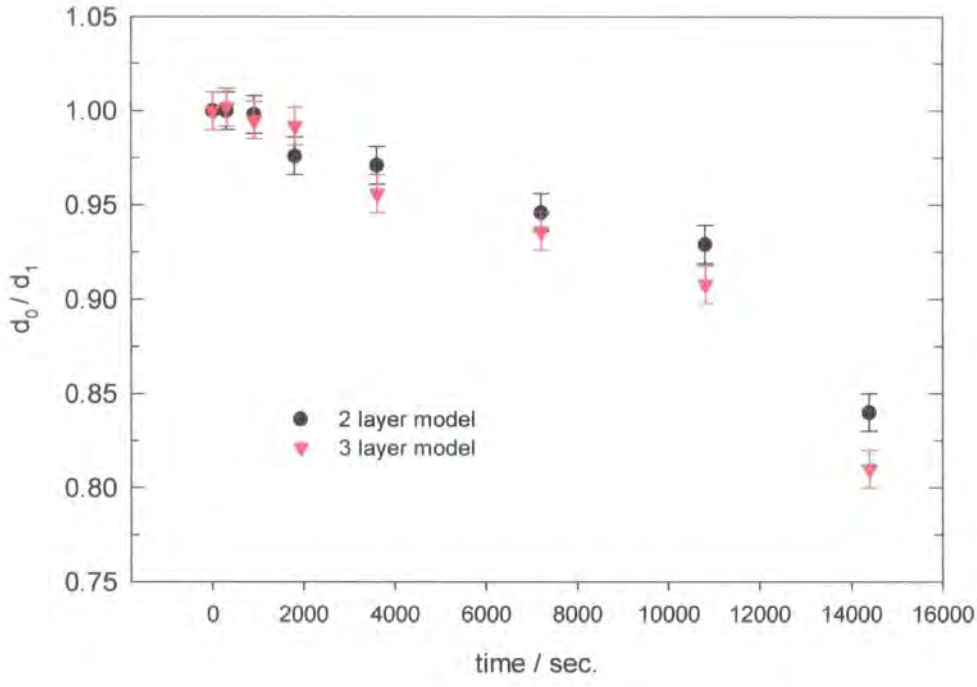

Figure 4.15. Normalised thickness for PMMA layer in APET/PMMA bilayers annealed at 493K.

The interfacial layer described in figures 4.13 and 4.14 is seen to grow with time, as expected for a polymer / polymer diffusion process. The fitted value for the interfacial width , *w*, is plotted against time (figure 4.16). However, these results must be treated with caution as, the returned value for the interfacial layer in the three layer model has a large estimated error, i.e. of the same order as the layer thickness itself. This is partly due to the relatively small difference in the fit residual for 2 and 3 layer models. This is further illustrated by the use of simulations of APET-PMMA models. For comparative purposes, simulations of the models incorporating different interfacial widths but maintaining similar overall bilayer dimensions, were run via the ESIM software and compared to the measured and best fits for the APET/PMMA system

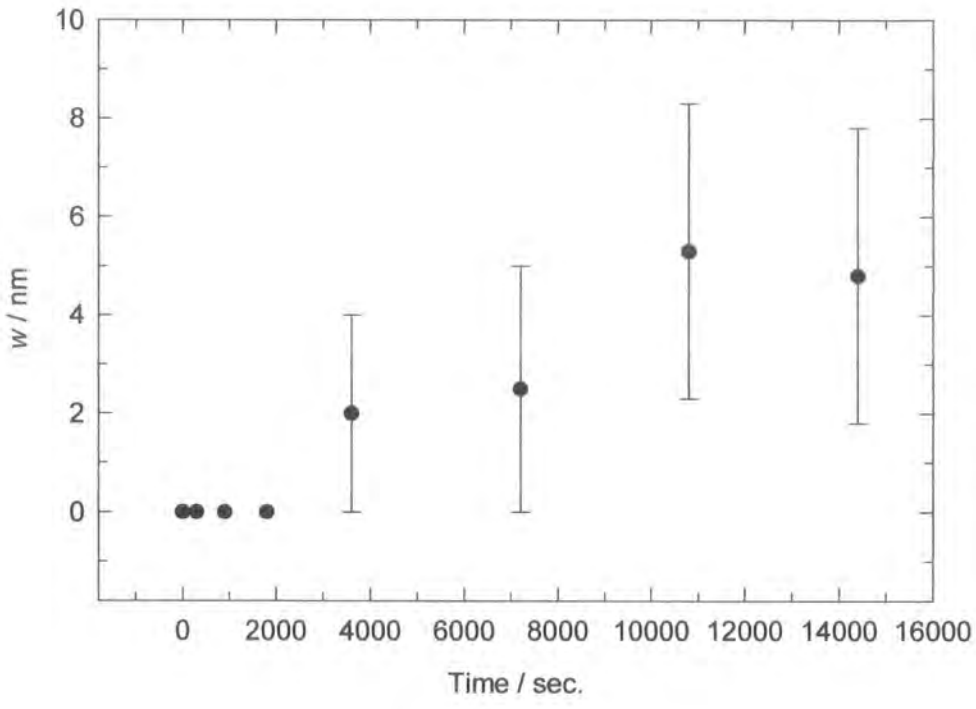

Figure 4.16. Interfacial width as a function of annealing period. elucidated from 3 layer model, for APET/PMMA bilayers annealed at 493K.

These simulation are shown in figure 4.17. The width of the interface is only seen to show a significant effect upon the resultant Ψ,Δ signature at values > 5nm. This result indicates that the value for w, obtained by this method should be considered with caution, and under ideal circumstances, these values need to be independently determined by a more sensitive technique.

Previously, several workers have attempted to elucidate an interfacial width from asymmetric polymer bilayers. Sauer and Walsh [19], have used spectroscopic ellipsometry to measure an interfacial width of 5.3 ± 3.0 nm from the polystyrene / poly(vinyl metylether) and compared this to NR measurements made on the same sample which gave a value for the interfacial width of 4.8 ± 0.5 nm. Inoue *et al* [20], have used fixed angle (70°) discrete wavelength ellipsometry to ascertain the interfacial width between styrene - acrylonitrile (SAN) / PMMA bilayers, and used this to extract a value for the Flory - Huggins interaction parameter.

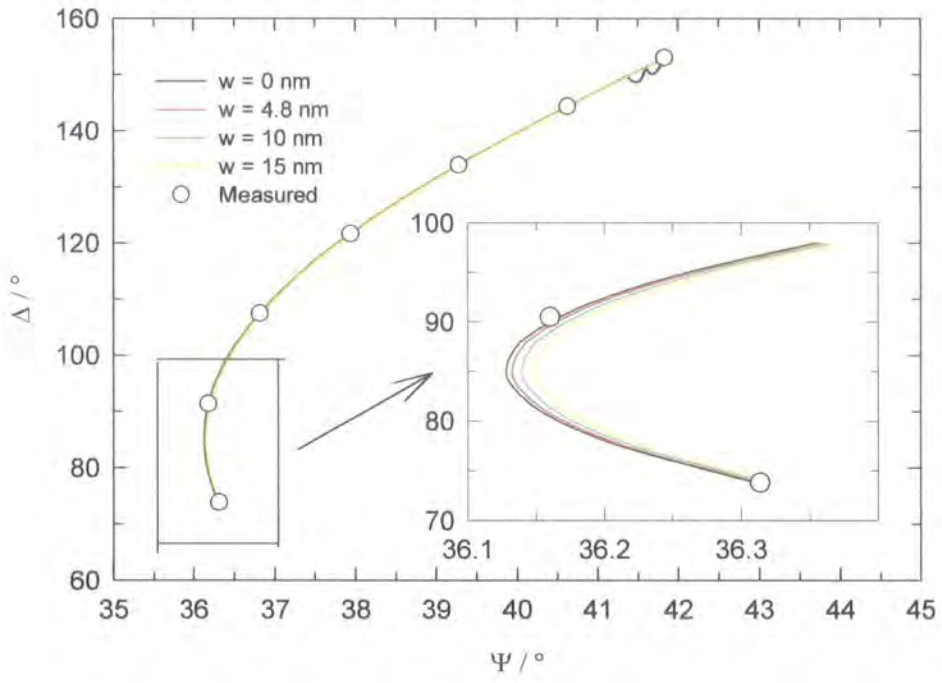

Figure 4.17. Measured data for APET/PMMA bilayers annealed for 4 hrs at 493K (open circles). The simulations are for interfacial widths, w of 0, 4.8 (best fit value), 10 and 15 nm. The total thickness of the bilayer is kept constant (~85 nm). As can be seen the simulations give very similar results; resolving the simulations is only possible around the Ψ,Δ inflection (Ψ = 85°), which highlights the disadvantage of MAE compared to variable angle ellipsometry.

Kim *et al* [21] have reported that polymer concentration profiles at a liquid - solid interface can be successfully measured using variable angle ellipsometry and Habicht *et al* [22], have shown that variable angle ellipsometry is sensitive to a refractive index profile of 1.46 - 1.42, and as such were able to observe (broad ~ 200 nm), interfacial widths during the swelling of polystyrene with cyclohexane at different temperatures. A distinction does need to be made here, variable angle ellipsometry does utilise a more sensitive angle - of - incidence method , than MAE. i.e. the angle of incidence can be varied continuously around the Brewster angle for the sample under investigation which yields higher quality ellipsometric information. [23], (see figure 4.17). Because of the unreliability of the values elucidated for *w*, further interpretation, such as extraction of a mutual diffusion coefficient, has not been attempted in this case, and is reserved for the analysis of neutron reflectivity data (see section 4.4.3).

4.4. Neutron Reflectivity of PET/dPMMA Bilayers

4.4.1. Determination of Layer Dimensions.

Neutron reflectivity was performed on PET/dPPMA bilayers. Initially, the bilayers were characterised by ellipsometry at a fixed angle of incidence (70°), as described in section 4.2.3. The PET layer was characterised before the dPMMA layer was applied. After spin casting the dPMMA layer, the bilayer was characterised assuming a two layer model with an infinitely sharp interface. The thickness values derived by this method are used as starting values in the fitting procedure for analysing NR data. The ellipsometry results are shown in table 4.7

Table 4.7 PET/dPMMA Bilayers prior to annealing

Sample	PET layer (nm)	dPMMA layer (nm)
1	41.9±0.2	36.1±0.1
2	41.2±0.1	36.4±0.1
3	42.0±0.2	35.8±0.2
4	42.5±0.2	35.2±0.3
5	41.5±0.3	35.7±0.3
6	41.1±0.1	35.9±0.2
7	41.7±0.1	35.3±0.3
8	40.1±0.2	36.4±0.1
9	41.1±0.1	36.3±0.3

These samples were annealed at either 493K or 573K, temperatures of interest for the manufacture of biaxially orientated PET film, in the manner described in section 4.2.2. After annealing the samples were again measured by ellipsometry to establish the extent of dimensional changes in the film. Using fixed angle discrete wavelength ellipsometry for two layer systems, results in thickness values which are ambiguous; i.e. the collected values of Ψ and Δ are not unique to a particular sample geometry, hence absolute values for the layers cannot be obtained. Despite this, estimates of the changes in the layers can be used to aid the fitting of neutron reflectivity profiles.

The profiles and the best fits for neutron reflectivity from samples 1-9 (table 4.8) are shown in figure 4.18. The values for layer thickness, roughness and scattering length density are given in table 4.8.

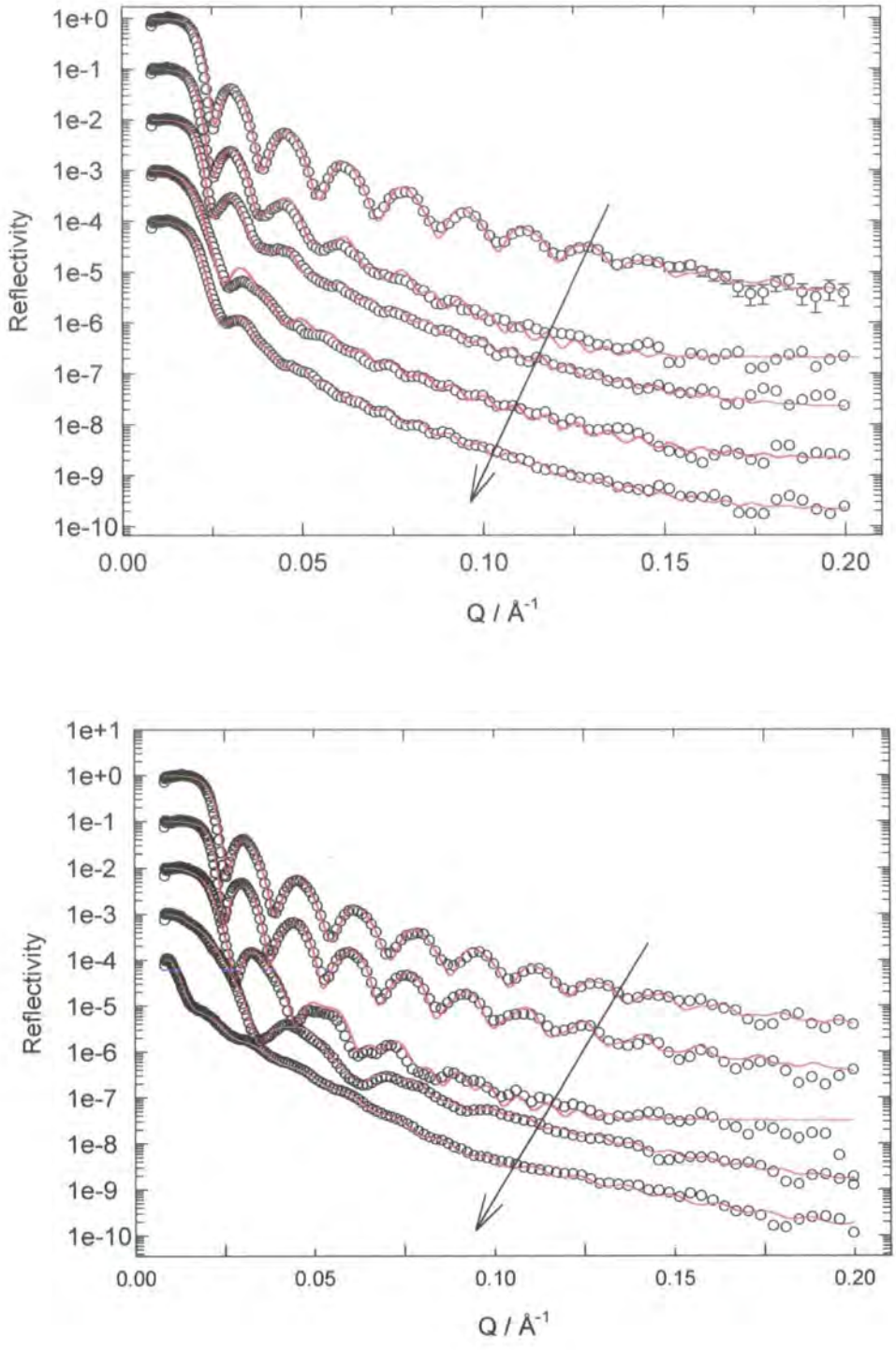

Figure 4.18 Neutron reflectivity profiles and best fits (red lines) for PET/dPMMA bilayers on Si annealed at 493K (top) and 573K (bottom) For the sake of clarity the profiles have been shifted verically, and the error bars have been omitted. The arrows indicate increasing annealing time (see table 4.8)

Table 4.8 Fitted parameters from NR data.

i) Samples annealed at 493K

Time (min)	PET layer			dPMMA layer			
	d (nm) ± 2	SLD($Å^{-2}$) × 10^6	σ (nm) ±0.25	d (nm) ±0.25	SLD($Å^{-2}$) × 10^6	σ (nm) ±0.25	R^2
0	41.90	2.60	1.00	37.00	7.20	0.80	1.05
1	41.20	2.60	2.70	37.00	6.70	1.40	1.23
5	41.00	2.60	3.60	37.50	7.00	0.90	2.01
30	42.00	2.60	4.00	30.70	6.40	0.95	1.25
60	42.20	2.60	4.70	32.00	6.70	0.95	1.36

ii) Samples annealed at 573K

Time (min)	PET layer			dPMMA			
	d (nm) ± 2	SLD($Å^{-2}$) × 10^6	σ (nm) ±0.25	d (nm) ±0.25	SLD($Å^{-2}$) × 10^6	σ (nm) ±0.25	R^2
0	41.90	2.60	1.00	37.00	7.20	0.80	1.05
1	41.10	2.60	1.20	38.30	7.20	0.50	2.36
5	41.00	2.70	2.40	31.00	6.70	1.50	2.36
15	40.00	2.50	2.20	21.50	6.70	0.70	2.52
30	42.50	2.50	2.00	6.00	7.00	0.70	2.10

These values are used to determine the physical and chemical processes occurring in the PET/dPMMA bilayers. Each of these processes is now considered, and the extent of each quantified.

.

4.4.2. Degradation of dPMMA.

The values for the thickness of the dPMMA layer are used to study the degradation of PMMA. Once again the normalised thickness is used, and the result plotted as a first order reaction. This is shown in figure 4.19, and compared with the results obtained by ellipsometry for single layers. The first order rate constants k, elucidated from the NR measurement are given in table 4.9. The value of k at 573K is in good agreement with the values derived from ellipsometry, although at 493K the overall layer depletion is significantly faster than the results obtained from single PMMA layers.

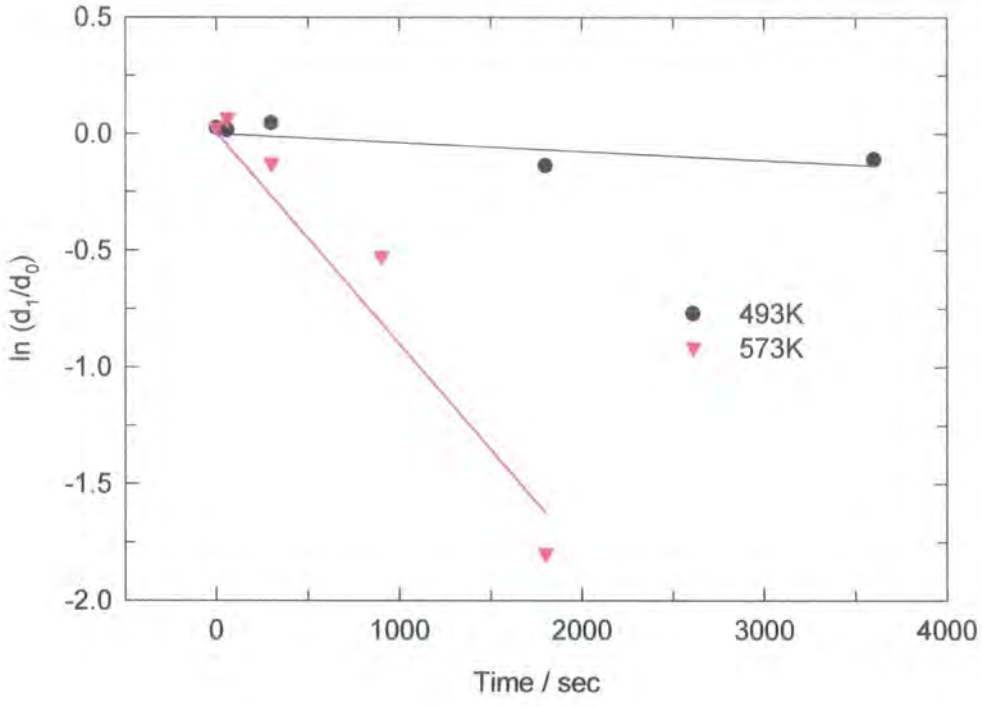

Figure 4.19 1st order layer depletion of dPMMA on PET as measured by neutron reflectometry. The errors are too small to be significant.

Table 4.9 1st order rate constants, *k*, for dPMMA layer depletion by NR.

Temp (K)	NR data (s^{-1})	Ellipsometry (single layer) (s^{-1})	Bulk (s^{-1})
493K	$(5.4 \pm 2.9) \times 10^{-5}$	$(7.9 \pm 3.5) \times 10^{-5}$	-
573K	$(9.3 \pm 5.3) \times 10^{-4}$	$(1.7 \pm 1.0) \times 10^{-3}$	$(5.5 \pm 2.2) \times 10^{-4}$

Again, this shows that thin PMMA layers display higher rates of degradation than do bulk samples, although further investigation is necessary to determine any apparent layer depletion due to interdiffsuion of the two polymers. It is interesting to note that the dewetting observed for single layers on Si did not appear to occur for dPMMA cast onto PET. The visual appearance of sample 9 after annealing indicated that the remaining layer(s) had a flat, uniform surface. Further ellipsometry performed on the sample produced a very low error for both Ψ and Δ values over an area 5 mm^2, indicating that the film / air interface was relatively sharp and consistent.

This residual dPMMA layer is of great interest as it reveals that even after prolonged heating at PET melt temperatures, a significant amount of PMMA is left in contact with the PET. This has obvious ramifications to the reclaim procedures in the

polyester films manufacturing industry. Large amounts of contamination can cause serious process disruptions, which lead to lost production.

4.4.3. Crystallisation of PET at 493K

Although the NR technique is extremely sensitive to the thickness and roughness of the dPMMA layer, (deuteration dramatically alters the scattering length density), there is a relatively large error in the fitted value of the PET layers, principally because of the PMMA SLD dominates the reflection profile. This is illustrated graphically in figure 4.20, in which simulations of dPMMA on PET are run. As can be seen very similar profiles are obtained for the same thickness and roughness of dPMMA on PET, when PET d ~ 50 nm and 50 μm respectively. Hence, the layer depletion of dPMMA and the interfacial broadening can be monitored with a high degree of confidence, but the crystallisation of PET cannot be, from thickness evaluation alone. Additionally, one would expect a corresponding increase in the SLD of PET as the polymer crystallises, but best best fits were obtained for all samples with very similar values for the SLD (± 5%). The reasons for this are unclear.

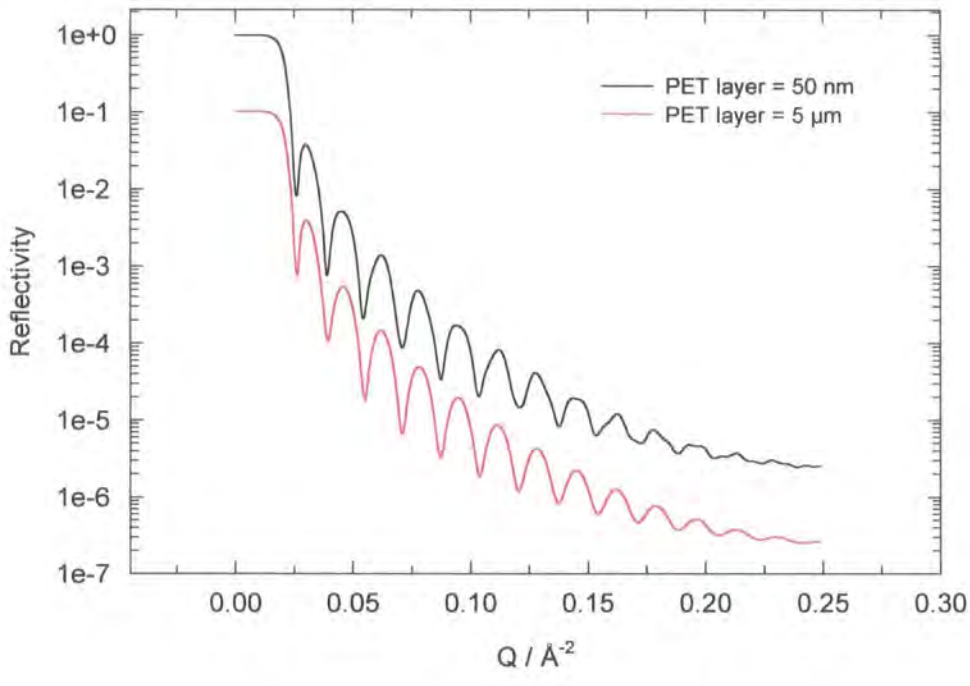

Figure 4.20. Neutron Reflectivity simulations of dPMMA (50 nm) on PET/Si. where the PET /dPMMA roughness is 1 nm.

The values in tables 4.7, derived from ellipsometry measurements before annealing, are compared to those in table 4.8, the fitted parameters from neutron reflectivity experiments. The values appear to be the same within error, indicating that either no layer densification has occurred or that NR has not detected the change in layer thickness. With reference to the experiments described in section 4.3.2, it is apparent that a ~ 42 nm PET layer will crystallise, hence it appears that in this case neutron reflectivity cannot detect densification due to crystallisation in PET. Again, the reasons for this are unknown.

4.4.4. Mutual Diffusion Between PET and dPMMA

The roughness between the PET and dPMMA layers is a critical factor as this is a direct measure of the extent of the interfacial broadening between the two polymers, and hence estimates of the compatibility of the two polymers can be made. Furthermore, the equilibrium interfacial width can be used to qualitatively assess the adhesion between the two polymers, and quantify the interfacial tension [24,25], factors which are very important in the manufacture of in-line coated polyester films. The interfacial width is obtained from inspection of the interfacial volume fraction profile.

The volume fraction profiles of the interfacial regions of PET/dPMMA bilayers are shown in figure 4.21. These volume fraction profiles provide the basis for establishing the characteristic interfacial width of a sample, and have been calculated using an error function of the type described by equation 4.8

$$\Phi_{dPMMA} = \frac{1}{2}\left\{\mathrm{erf}\frac{h+x}{a} + \mathrm{erf}\frac{h-x}{a}\right\} \qquad (4.8)$$

where, h = layer thickness (tracer layer), x = profile co-ordinate, a = is the interfacial roughness, (not interfacial width). This is the classical solution to Ficks second law and has been used to describe polymer interfaces in many circumstances [26].

The interfacial roughness is numerically related to the characteristic interfacial width, w by a factor of $\sqrt{\pi}$. Table 4.10 shows the interfacial dimensions calculated from the model fitting of the neutron reflectivity data.; w is plotted in figure 4.21.

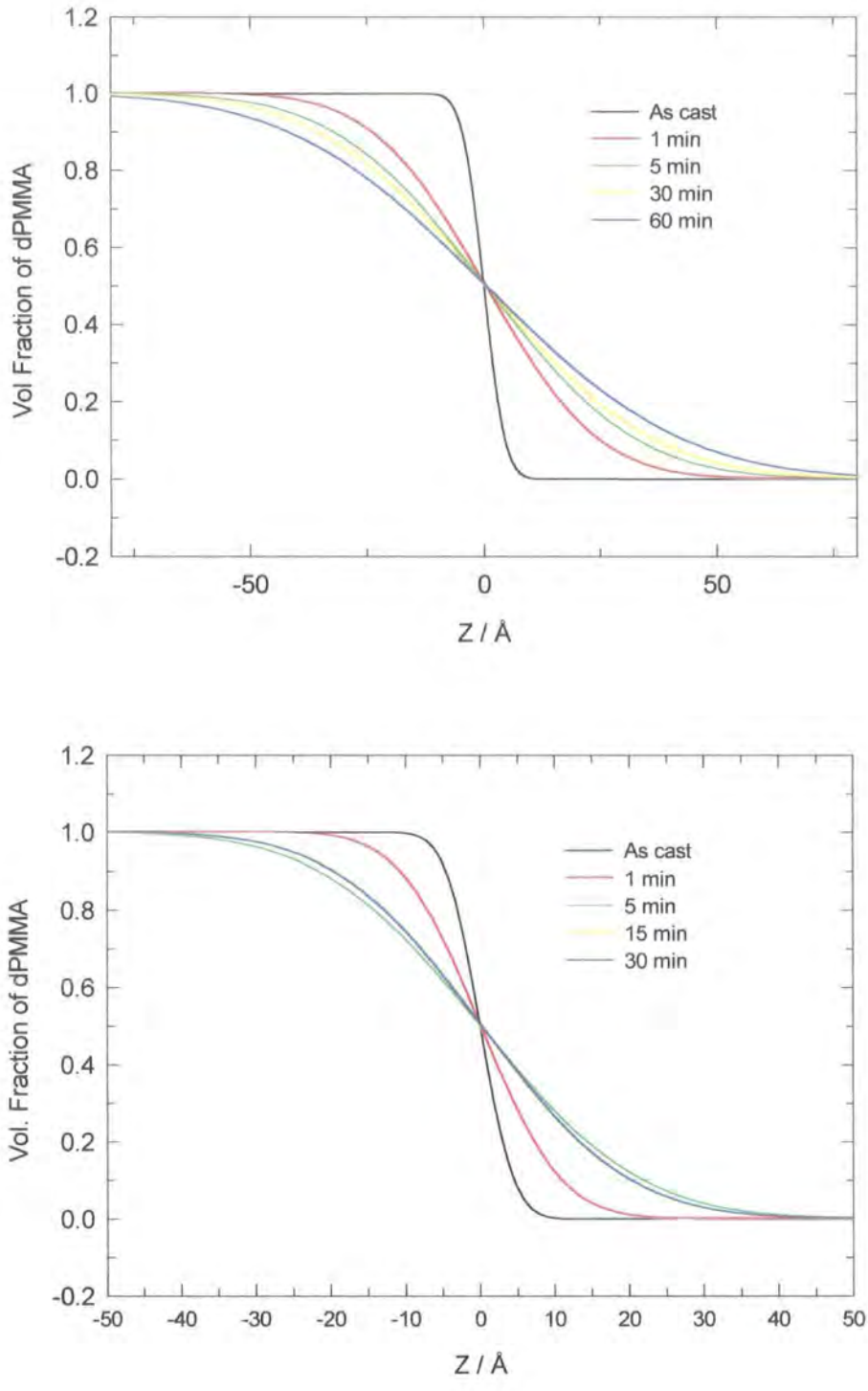

Figure 4.21. Volume fraction profiles of PET/dPMMA interfaces. the profiles are calculated from the error function of equation 4.8. Top = samples annealed at 493K, bottom = samples annealed at 573K. Note the difference in lateral scales for the two plots.

Table 4.10 Interfacial distances for PET/dPMMA bilayers.

Temp (K)	Time (min)	Roughness a (nm)	Interfacial width w (nm)	Interfacial overlap w_L (nm)
As cast		1	1.8	1.25
493	1	2.7	4.8	6.8
	5	3.6	6.4	9.0
	30	4.0	7.7	10.0
	60	4.7	8.3	11.8
573	1	1.2	2.1	3.0
	5	2.4	4.3	6.0
	15	2.8	5.0	5.5
	30	2.8	5.0	5.5

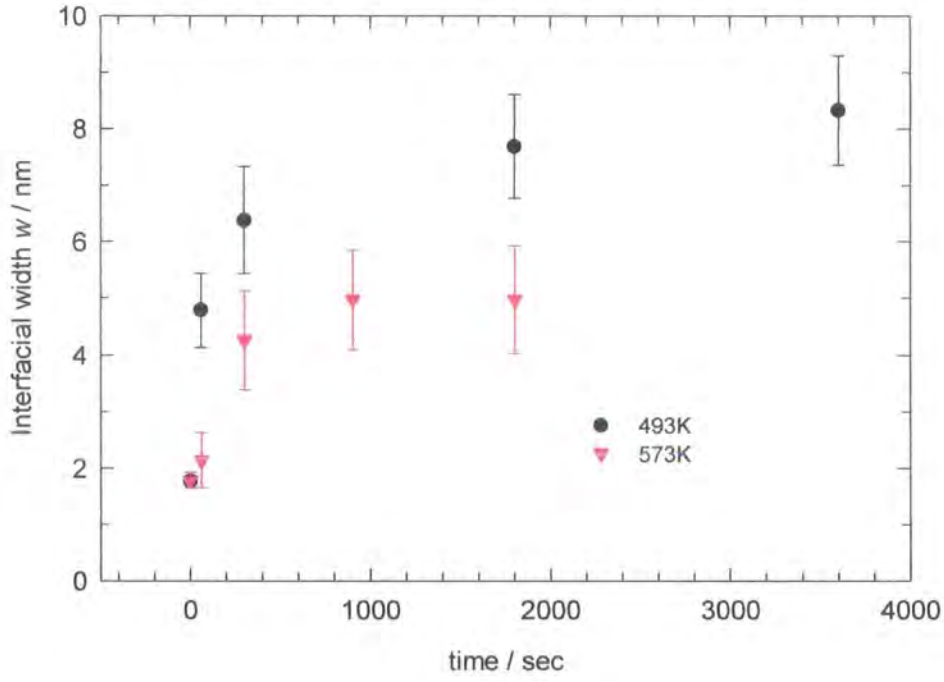

Figure 4.21. Interfacial width as a function of time for the PET/dPMMA system.

The interfacial width due to interdiffusion can be determined by subtraction of the value for w for the as cast film. Here, the procedure used by Genzer and Composto [27] is adopted;

$$w_i = \sqrt{w_t^2 - w_0^2} \tag{4.9}$$

where w_i is the intrinsic interfacial width, w_t is the observed interfacial width at time t and w_0 is the initial interfacial width of the as cast sample. The time dependence of the development of w_i is shown in figure 4.22. At both temperatures there is an initial rapid increase in the interfacial width followed by a slower growth, which is indicative that an equilibrium is being approached, as is expected for an incompatible polymer pair. Using a classical diffusion treatment, w_i is related to the mutual diffusion coefficient D_m, by;

$$w_i = \sqrt{\pi 4 D_m t} \tag{4.10}$$

Hence, a plot of w_i vs. $t^{1/2}$ should yield a value for D_m. This is shown in figure 4.23. The values of D_m derived by this method are 4.9×10^{-21} cm^2/sec, and 3.0×10^{21} cm^2/sec. at 493 and 573K respectively. Thus it is concluded that the PET / PMMA system is highly incompatible. For comparison, Fernandez et al [11], have estimated D_m for the PS/ PMMA system, which is also known to be incompatible, as $\sim 3.6 \times 10^{-21}$ cm^2/sec. at 393K. However, these results must be treated with caution because the data sets are limited and a qualitative assessment shows that at both temperatures the interfacial width is tending toward an equilibrium value. This equilibrium value is seen to be higher for the samples annealed at 493K compared to the samples annealed at 573K. On first consideration this would suggest that the polymers are more compatible at the lower temperature, indicating the blend would exhibit an lower critical solution temperature (LCST). An equilibrium interfacial width is expected for an incompatible polymer pair, as one would expect the Flory -Huggins interaction parameter, χ, to be +ve and relatively large. Hence, the interfacial width is determined by the statistics of chain conformations (entropy) [28]. The equilibrium values for the interfacial widths are estimated as ~7.7 nm at 493K and 4.0 nm at 573K (see figure 4.22).

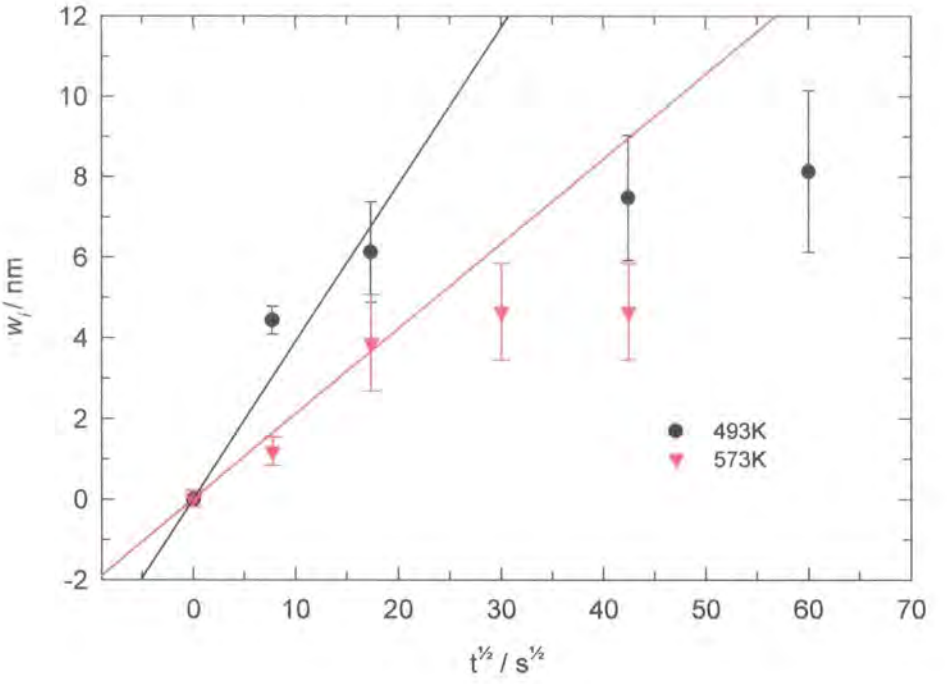

Figure 4.23. Interfacial width w_i vs. $t^{1/2}$ for PET/dPMMA bilayers. The slope of the straight line fit ~ D_m and is taken for (initial) rate of interdiffusion only

4.4.5. Interfacial Widths and Crystallinity.

Although layer densification due to crystallisation was not observed in these samples, it is envisaged that crystallisation is in evidence in another more subtle way.

Referring to the ellipsometry results obtained for thin layers of PET in section 4.3.2., it has been postulated that thin PET films will develop a measurable roughness due to crystallisation of the layer. This has been observed by Wehrum [9], a phenomena which inhibited the interfacial analysis in that particular case. Therefore it is postulated that there is a contribution from crystalline roughness to interfacial broadening at 493K. To estimate the extent of this, a simple comparison with the data at 573K can be made. At this temperature PET can be considered to be amorphous as the layer will be molten and all crystallinity will be destroyed. To extract the contribution to interfacial broadening, the following expression is used,

$$w_{obs}^2 = w_c^2 + w_a^2 \tag{4.11}$$

where w_c is the width due to crystalline roughness and w_a is the width of a wholly amorphous interface. This gives a value for w_c of 6.5 nm. However, this crude analysis fails to take into account the difference in temperature, and so we also compare the data at 493K to ellipsometry data obtained on the APET/PMMA system at the same temperature (see section 4.3.3). Here we see a maximum interfacial width of ~ 5nm, (notwithstanding the large associated errors in this method). Hence, a value for crystalline roughness, w_c of 5.8 nm is obtained.

Therefore, by a simple comparison we can see that the crystalinity of the PET layer imparts ~5.8 - 6.5nm to the interfacial width as measured by NR. This is an important result, as this knowledge is required to extract a realistic value for the Flory Huggins interaction parameter, χ, which is used as an indication of the polymer - polymer compatibility.

4.4.6. Capillary Wave Broadening and Extraction of χ

We must also consider a contribution from capillary wave broadening [29,30] to the amorphous interfacial width. This phenomena is invoked to explain experimentally measured interfacial widths which are much broader than those predicted by theory. This can be written as

$$w_{obs}^2 = w_0^2 + w_{cap}^2 \tag{4.12}$$

where w_0 is the interfacial width without capillary wave broadening and is given by the familiar term derived by Helfand and Tagami [31], i.e.

$$w_0 = \frac{2b}{\sqrt{6\chi}} \tag{4.13}$$

where b is the statistical segment length and χ is the Flory - Huggins interaction parameter. w_{cap} is the contribution to the interfacial width from capillary wave broadening and is defined by equation 4.14;

$$w_{cap}^2 = \frac{kT}{2\pi\gamma}\ln\left(\frac{\lambda_{max}}{\lambda_{min}}\right) \quad (4.14)$$

where γ is the interfacial tension, λ_{max} is taken as the coherence length for the neutron beam (~ 1 μm), and λ_{min} can be assumed to be the minimum interfacial width i.e. ~ w_0 As there is no independent value for the interfacial tension between PET and PMMA the expression developed by Helfand [31], is used;

$$\gamma = b\rho_0 kT(6/\chi)^{1/2} \quad (4.15)$$

where ρ_0 is the number average monomer density. Substitution of values for b and ρ_0 reported by Wehrum [9], Imai [32], and van Krevelen [33], yield a value for χ of ~0.03. at 573K, by finding the numerical solution to w = 25 nm.

Table 4.11 Parameters used to determine extent of Capillary wave broadening.

	b Å	ρ Å^{-3}
PET	14.4	237
dPMMA	6.9	174

This solution gives a value for w_{cap} of ~ 1nm which is not unreasonable, although smaller than other reported values [34,35]. This may be a consequence of the lack of experimentally verified interfacial tension data for PET/PMMA. It is noted that the interfacial tension at 573K predicted by the harmonic mean equation (see Chapter 2), is ~1.2 dynes/cm^2, with a corresponding interfacial width of ~8.6 nm. The equilibrium interfacial width at 573K is measured as ~5 nm which gives an interfacial tension of ~ 2 dynes/ cm^2 (equation 2.6).

Hayashi *et al* [34], have recently observed that the value for w_{cap} will increase for increasing values of γ, for a given $w_{obs.}$ This dependence could have a significant effect upon the results obtained here; w_0 at higher values for the interfacial tension will dominated by w_{cap} and w_0 is therefore reduced even further. Interfacial tensions as high as 10 dynes/cm^2 have been reported for PET/PE at 543K (melt phase) [36], and it is envisaged that γ for PET/PMMA could be much higher than the values estimated here. γ

= 10 dynes/cm^2 would yield a value for w_{cap} ~4.9 nm and w_{obs} of ~1 nm. Figure 4.24. shows the calculated contributions of w_0 and w_{caps} for a fixed w_{obs} of 5 nm.

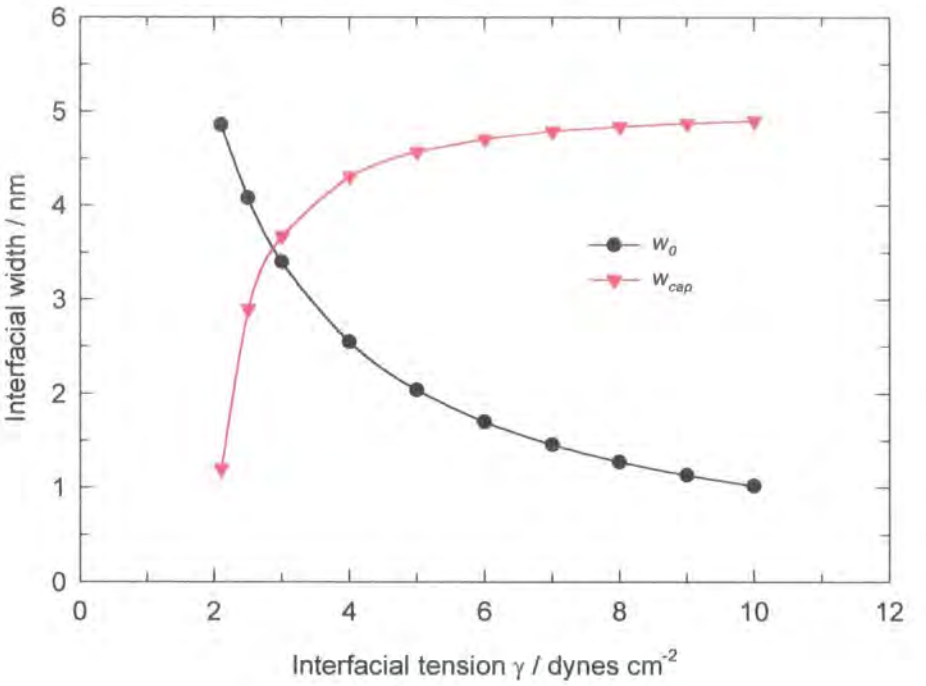

Figure 4.24 Dependence of w_{cap} and w_0 on surface tension for an observed interfacial width of 25 nm. There is a crossover in dependence at $\gamma \sim 3$ dynes/cm^2

The bare interfacial width at equilibrium, for PET/dPMMA at 573K is therefore estimated to be <5 nm. The lack of an independent value for either the interfacial tension or the Flory-Huggins interaction parameter renders the estimation of the contribution from capillary wave broadening somewhat arbitrary, although it is recognised that there will be a contribution.

Asymmetric Interfaces.

The above approach does not account for the asymmetry between polymers, i.e. different monomer lengths and monomer densities. The symmetric restriction was removed by Helfand and Sapse [37], who extended the mean field theory to take account of the differences in statistical step length and bulk densities of the two polymers at an interface. The characteristic interfacial width is given by:

$$w_0 = 2\left(\frac{\beta_1^2+\beta_2^2}{2a}\right)^{\frac{1}{2}} \tag{4.16}$$

here $\beta^2 = \rho b^2/6$ (ρ is the bulk density of pure polymer i, and b is the statistical step length), and $a = \rho\chi$,(ρ is taken as the geometric mean of the densities of the two polymers). Again this allows extraction of the Flory-Huggins interaction parameter. This form of the mean field theory is substituted in equation 4.14 and yields a higher value for χ, ~ 0.04

Both the above treatments were developed in the limit of infinite molecular weight and monodispersity. A further extension to the mean field theory has been developed by Brosetta [38] which utilises an expression for incompatibility, χN where N is the degree of polymerisation of the polymer.

$$w_0 = D_\infty\left(1 + \ln 2\left(\frac{1}{\chi N_1} + \frac{1}{\chi N_2}\right)\right) \tag{4.17}$$

where $D_\infty = 2b/\sqrt{6\chi}$. For the system under investigation, the dPMMA is virtually monodisperse, (M_w/M_N = 1.02) and N is taken as ~1000. For PET N ~ 116. This treatment wields a value of χ of ~0.02

The obvious discrepancy in this approach is that the value of D_∞, is based on the symmetric interface, and a geometric mean for the value of the statistical step length has to be taken. Broseta did not extend the theory to the asymmetrical case of Helfand and Sapse, however it seems a facile procedure to do so. Replacing D_∞ in equation 6 with a_i from equation 5 yields an expression incorporating asymmetry for both the statistical segment length and the degree of polymerisation in an incompatible polymer pair;

$$w_0 = 2\left[\frac{(\beta_1^2+\beta_2^2)}{2a}\right]^{\frac{1}{2}}\left[1 + \ln 2\left(\frac{1}{u_1} + \frac{1}{u_2}\right)\right] \tag{4.18}$$

This expression is gives χ ~0.017 As can be seen, the inclusion of asymmetry in the calculation increases the interfacial mixing. Other expressions for w_0, such as those derived by Tang and freed [39], yield similar values for the value of χ.

As a comparison, Wehrum [9], has found a value for χ of ~ 0.025 at T = 423K, for PET/dPMMA which considering the difference in temperature is in remarkable agreement, with the estimates made here. Jones and Sivaniah [2] have measured an interfacial width of ~ 7 nm at a temperature of 443K, which is in excellent agreement with the interfacial width found here (493K).

4.5. Conclusions and Final Comments.

In this chapter, the thin film behaviour of PET and PMMA has been studied. The single films of PMMA and PET have been studied using ellipsometry to follow dimensional changes of the films in response to annealing at different temperatures.

The degradation of PMMA has been observed to have a thickness dependence below a limiting value, which has been estimated as 74.5 nm (×6 R_g). This phenomena is in good agreement with the theory proposed by Lehrle *et al* [12].

The rate of crystallisation of thin PET films was also seen to have a thickness dependence, when analysed by the Avrami theory, and the results obtained agree qualitatively with those of Wehrum [9]. The dimensionality of the crystallisation process was not seen to change when the thickness of the PET layer was reduced to ~ 35 nm. At this thickness the PET layer was only seen to develop 8% crystallinity over 2 hr annealing. At a thickness of ~ 60 nm the crystallisation behaviour of thin PET films was similar to that of bulk polymer (~100 nm).

Ellipsometric (MAE) investigations of A-PET/PMMA bilayers have revealed that, although the depolymerisation of PMMA can be successfully monitored, the interdiffusion of the two polymers cannot be elucidated with an acceptable degree of confidence. It is proposed that MAE does not have the sensitivity to the small changes in Ψ and Δ at the Brewster angle, and that variable angle ellipsometry or spectroscopic ellipsometry is more suitable for the elucidation of interfacial widths.

Neutron reflectometry of PET/dPMMA bilayers has revealed that the depolymerisation of dPMMA and the interdiffusion of PET and dPMMA can be monitored simultaneously. The rate constants for the degradation of dPMMA as a 1st order reaction are 5.4×10^{-5} s^{-1} at 493K and 9.3×10^{-4} s^{-1} at 573K, which are in good agreement with the results obtained for PMMA monolayers. By inference, the

crystallisation of PET can also be monitored, by considering crystalline roughness at the interface. For reasons unknown, densification of the PET layer was not in evidence in this experiment. The NR analysis of PET/dPMMA bilayers has also revealed the following;

1) The mutual diffusion coefficients D_M are measured as 4.9×10^{-21} cm^2/sec. and 3.0×10^{-21} cm^2/sec. at 493K and 573K respectively. The validity of the value at 493K is questionable because of the aforementioned crystalline roughness at the interface.

2) At 493K, the interfacial broadening due to crystalline roughness has been estimated as 6.5 nm. The amorphous interface at 573K is measured as ~ 5 nm although a contribution from capillary wave broadening is expected.

3) Further analysis of the interface has revealed that the value for γ, the interfacial tension is in excess of 2 dynes/cm^2 at 573K, which is much higher than predicted by the harmonic mean approximation.

4) The relatively small interfacial distances achieved, indicate that PET and PMMA will not form a strong interface, particularly in a commercial coating process. The adherence of PMMA to PET will require the use of cross-linking agents or compatibilising agents.

5) At 573K, an appreciable amount of dPMMA remains at the PET - dPMMA interface. Therefore in typical reclaimation procedures, residual PMMA maybe present, leading to a non-homogenous polymer matrix, which can disrupt the film making process.

4.6 References

[1] Styrkas, D., Doran, S.J., Gilchrist, V., Keddie, J.L., Lu, J.R., Murphy, E., Sackin, R., Su, T.-J. and Tzitzinou, A., in *Polymer Surfaces and interfaces III*, 1999, John Wiley & Sons, Ed. Richards, R.W. and Peace, S.K.

[2] R.A.L. Jones. Private Communication.

[3] Frich, D., Hall, A. and Economy, J., *Macromol. Chem. Phys.* 1998, **199**, pp 913 - 921.

[4] Anastasiadis, S.P., Russell, T.P., Satija, S.K. and Majkrzak, C.F., *J. Chem. Phys.* 1990, **92**, pp 5677 - 5691.
Shearmur, T.E., PhD Thesis, University of Surrey, 1997.
Jordan, E.A., Ball, R.C., Donald, A.M., Fetters, L.J., Jones, R.A.L. and Klein, J., *Macromolecules*, 1988, **21**, p235
Jabbari, E. and Peppas; E.A., *Polymer*, 1995, **36**, pp575 - 586.
Tomba, P., Carella, J.M., Pastor, J.M. and Fernandez, M.R., *Macromol. Rapid Commun.* 1998, **19**, p413,.
R.J. Composto, E.J. Kramer, D.M. White; *Macromolecules.*, 21, p2580, (1988)

[5] P.J. Mills, Private Communication.

[6] Shearmur,T.E., Clough, A.S., Drew, D.W., van der Grinten, M.G.D., and Jones, R.A.L., *Polymer,* 1988, **39**, pp 2155 - 2159.

[7] Extrand, C.W., *Polym. Eng. & Sci.,* 1994, **34**, No. 5, pp 390 - 394.

[8] Buxbaum, L.H., *Angew. Chem. Internat. Edit.*, 1968, **7**, p182

[9] Wehrum, A., PhD Thesis, University of Cambridge, 1999.

[10] Russell, T.P., *Mater. Sci. Reports*, 1990, **5**, pp 171 - 271.
Higgins, J.S. and Benoît, H.C; 'Polymers and Neutron Scattering' 1996, Oxford Science Publications.

[11] Fernandez, M.L., Higgins, J.S., Penfold, J., Ward,R.C., Shackleton, C., and Walsh, D.J., *Polymer*. 1988, **29**, pp1923. - 1928

[12] Lehrle, R., Atkinson, D., Cook, S., Gardner, p., Groves, S., Hancox, R. and Lamb, G., *Polym. Deg. Stab.*, 1993, **42**, pp 281 - 291.

[13] McNeill , I.C. and Mohammed, M.A.J., *Eur. Polym. J.*, 1972, **8**, pp 975 - 990.

[14] Gedde, U.W. *Polymer Physics*, 1995, Chapman & Hall.

[15] Groeninckx, G., Reynaers, H., Berghmans, H. and Smets, G., *J. Polym. Sci., Polym. Phys. Ed.*, 1980, **18**, pp 1311 - 1324.

Groeninckx, G. and Reynaers, H., *J. Polym. Sci., Polym. Phys. Ed.*, 1980, **18**, pp 1325 - 1341.

[16] Hayes, N.W., Beamson, G., Clark, D.T., Law, D. S.-L and Raval, R., Surf. *Int. Anal.*, 1996, **24**, pp 723 - 728.

[17] Keddie, J.L., Jones, R.A.L. and Cory, R.A., *Europhys. Lett.* 1994, **27**, p 59.

Keddie, J.L., Jones, R.A.L. and Cory, R.A., *Faraday Duscussions*, 1994, **98**, p 219.

[18] Born, M. and Wolf, E., *Principles of Optics*, 1975, Oxford, Pergammon Press.

Lekner, J., *Theory of Reflection*, 1987, Martinus Nijhoff.

[19] Sauer, B.B. and Walsh, D.J., *Macromolecules*, 1994, **27**, pp 432 - 440.

[20] Yukioka, S., Nagato, K. and InoueT., *Polymer,* 1992, **33**, pp 1171 - 1176.

Yukioka, S. and Inoue, T., *Polymer,* 1993, **34**, pp 1256 - 1259.

[21] Kim, M.W., Peiffer, D.G., Hsiung, W.C., Rasing, Th. and Shen, Y.R., *Macromolecules*, 1989, **22**, pp 2682 - 2685.

[22] Habicht, J., Schmidt, M., Rühe, J. and Johannsmann, D., *Langmuir,* 1999, **15**, pp 2460 - 2465.

[23] J.L. Keddie, Private Communication

[24] Wu, S., Polymer Interface and Adhesion,

[25] Cho, K., Brown, H.R. and Miller, D.C., *J. Polym. Sci., Polym. Phys. Ed.*, 1990, **28**, pp 1699 - 1718.

[26] Composto, R.J., Kramer, E.J. and White, D.M., *Macromolecules.*, 1988, **21**, pp 2580 - 2588.

Brown, H.R., Yang, A.C.M., Russell, T.P., volksen, W. and Kramer, E.J., *Polymer*, 1988, **29**, pp 1807 -1811.

Stoffel, N.C., Kramer, E.J., Volksen, W. and Russell, T.P., *J. Polym. Sci. Polym. Phys. Ed.*, 1998, **36**, pp 2247 - 2258.

Mills, P.J., Green, P.F., Palmstrøm, C.J., Mayer, J.W. and Kramer, E.J., *Appl. Phys. Lett.*, 1984, **45**, pp 957 - 959.

[27] Genzer, J. and Composto, R.J., *Polymer*, 1999, **40**, pp 4223 - 4228.

[28] Wool, R.P., *Polymer interfaces, Structure and Strength.* 1995, Hanser Publishers.

[29] Jones, R.A.L. and Richards, R.W., *Polymers at Surfaces and Interfaces*, 1999, Cambridge University Press.

[30] Sferazza, M., Xiao, C., Jones, R.A.L., Bucknall, D.G., Webster, J. and Penfold, J., *Phys. Rev. Lett.*, 1997, **78**, p 3693.

Lacasse, M.-D., Grest, G.S. and Levine, A.J., *Phys. Rev. Lett.*, 1998, **80**, pp 309 - 312.

[31] Helfand, E. and Tagami Y., *J. Chem. Phys.* 1972, **56**, p3592

Helfand, E. and Tagami, Y., *Polym. Lett.*, 1971, **9**, pp 741 - 746.

[32] Imai, M., Kaji, K. and Kanaya, T., *Phys. Rev. Lett.*, 1993, **71** p 4162.

[33] Van Krevelen, D.W., *Properties of Polymers*, 1972, Elsevier Publishing.

[34] Hayashi, M., Grüll, H., Esker, A.R., Weber, M., Sung, L., Satija, S.K., Han, C.C. and Hashimoto, T., *Macromolecules*, 2000, **33**, pp 6485 - 6494.

[35] Sferazza, M., Jones, R.A.L., Penfold, J., Bucknall, D.B. and Webster, J.R.P., *J. Mater. Chem.*, 2000, **10**, pp 127 - 132.

[36] Ihm. D.J. and White, J.L., *J. Appl. Polym. Sci.*, 1996, **60**, pp 1 - 7.

[37] Helfand, E. and Sapse, A.M., *J. Chem Phys.*, 1975, **62**, pp 1327 - 1331.

[38] Brosseta, D., Fredrickson, G.H., Helfand, E. and Leibler, L., *Macromolecules.*, 1990, **23**, pp132

[39] Tang, H. and Freed, K.F., *J. Chem. Phys.*, 1991, **94**, pp 6307 - 6302.

Chapter 5

Marker Movements

5.1 Introduction

In the previous chapter, the interdiffusion of PET and PMMA was characterised by ellipsometry and neutron reflectometry. In this chapter the interface between PET and PMMA is further investigated by the use of inert interfacial markers, which are used to observe the movement of an interface with respect to time and temperature. This approach is complimentary, in that only the position of the interface is monitored, as opposed to the width of the interface. This technique was originally developed to investigate the thermodynamics of mutual diffusion between high and low molecular weight polystyrene [1,2] using FRES (forward recoil spectroscopy). The technique has also been used to investigate the time regimes involved in the reptation model of polymer dynamics [3], and the interface between amorphous and semicrystalline polymers [5]. The intention of our experiment is to use marker movements to decouple the interfacial broadening of the PET and PMMA system by comparison with interfacial profiles from the previous experiments. The equilibrium position of the average marker distribution will determine the position of the interface for this system and this can be compared with the symmetrical approach adopted in the previous chapters.

In order to monitor interfacial movement the exact interface needs to be defined with respect to both polymers and physically marked. Definitions of interfacial position can be made in terms of the gradients the functional form of the interface, or by other methods such as the Boltzmann - Matano treatment, which assumes geometrical equality in asymmetric interfaces [10]. One of the most successful methods of interfacial marking has been achieved by the utilisation of colloidal gold rafts, formed from particulate gold, which have been set into the sample by vacuum deposition. This method has been successfully used by Green *et al* [1], and by Reiter *et al* [3], for the analysis of diffusion couples.

In this study we use gold as an interfacial marker and follow the method and sample geometry of Reiter *et al*, to measure PET/PMMA couples by X-ray reflectivity. These experiments have been carried out at the same time and temperature regimes as the diffusion couples discussed in Chapter 4. X-rays provide an excellent probe for gold markers in an organic polymer matrix because a large differential in electron density exists, (see figure 5.1).

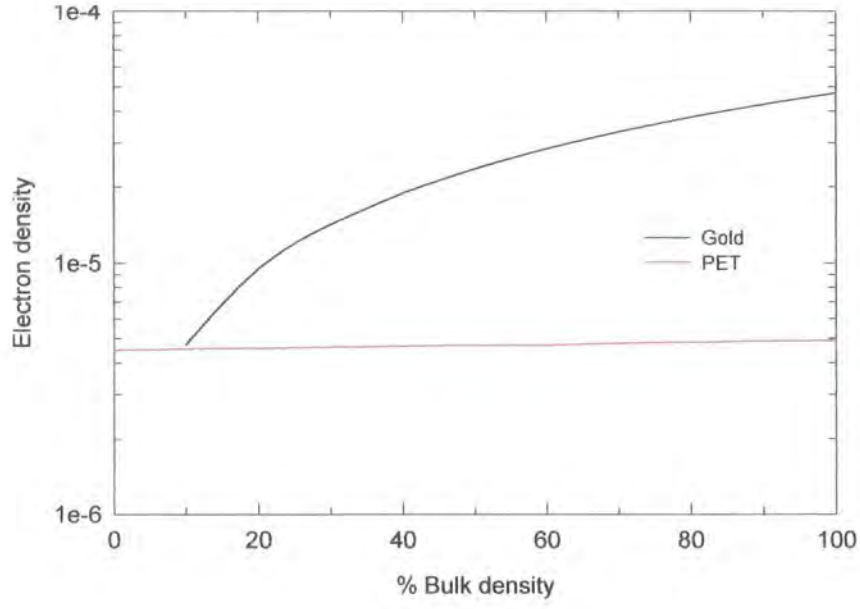

Figure 5.1. Electron density differential between Gold and PET as a function of the % of bulk density. ρ_{max} is taken as 19.3 g/cm^3 for Gold, and the PET values are calculated in the range of 1.333 g/cm^3 (amorphous) to 1.515 g/cm^3 (100% crystalline). The ρ_{max} for PMMA (not shown) is typically 1.15 g/cm^3. All values are calculated for an X - ray wavelength of 1.54Å

Because most commercial organic polymers exhibit very similar densities, and are comprised of the same elements, (C, O, H), X-ray investigations of interfaces rely upon chemical manipulation of the polymer backbone, usually by replacement of protons with an electron rich species such as Cl or I. Utilisation of gold markers overcomes this problem, but as will be discussed later in this chapter, presents a different set of issues. Figure 5.2 shows X-ray reflectivity simulations of a 100 nm PET monolayer, a 100 nm PET / PMMA bilayer (50 nm each with 1 nm interfacial

roughness), and a PET / PMMA bilayer with a gold marker layer (5 nm width, ρ = ~7 g/cm^3), resident at the interface between the two. Quite clearly, the reflectivity profile of the PET monolayer and the PET / PMMA bilayer are virtually identical and would be impossible to resolve with any degree of confidence. This graphically shows how the change in profile due to the addition of a gold layer can aid the analysis of the interface. The theory of X-ray reflection has been discussed in Chapter 2, and a detailed description of the use of this technique in polymer science is given in ref. [8].

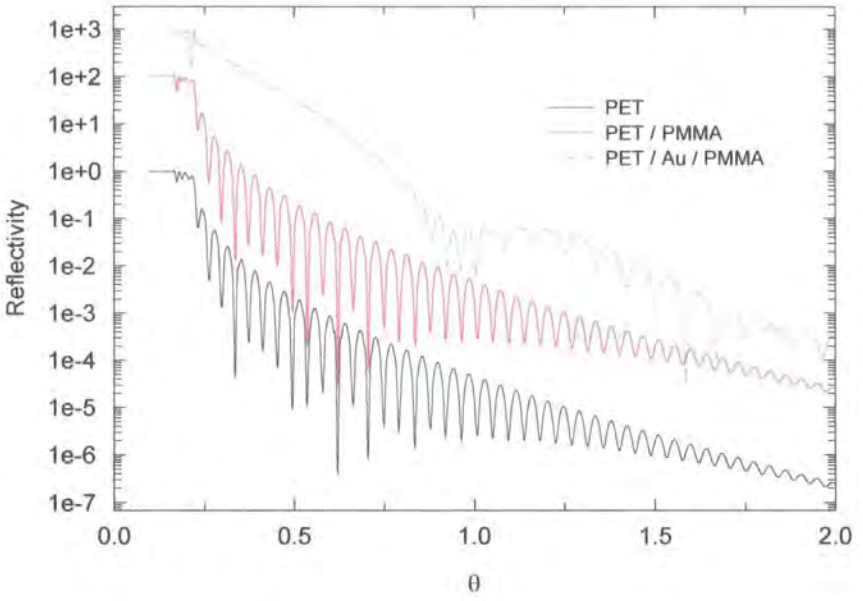

Figure 5.2 Simulated X-ray reflection profiles for PET and PET / PMMA bilayers, with and without interfacial gold markers. The curves have been shifted by 2 (PET / PMMA), and 3 (PET / Au / PMMA), decades, to aid visualisation.

The movement of the interface in a PET/PMMA system can be the result of one or a combination of factors. In Chapter 3, the reaction between PET and PMMA has been studied and a grafted structure has been proposed to form at the interface between the two polymer phases. It is postulated that this phenomena could lead to a change in the position of the interface as the structure swells upon subsequent growth

In Chapter 4, an attempt was made to monitor interdiffusion, PMMA degradation and PET crystallisation simultaneously. Although interfacial roughening due to crystallisation was observed, ellipsometry and neutron reflectivity could not

unambiguously detect densification of the PET layer. The use of marker movements will allow the elucidation of the thickness of the PET layer in conjunction with any interfacial movement.

The translational behaviour of the interfacial markers can indicate the thermodynamic principles underlying the interdiffusion of PET and PMMA; i.e. is the system best described by 'slow' diffusion [6] or 'fast diffusion [1,2], or a hybrid diffusion equation [7]. In slow theory the rate of inter-diffusion is dominated by the slowest moving component, whereas in fast theory the fastest component controls interfacial development, which is accompanied by the relaxation of the slowest component by bulk flow, moving the interface towards the 'fast' side of the couple. Hence monitoring the interfacial position with respect to time and temperature should allow the qualitative elucidation of the particular mode of diffusion which applies to this system, provided that the time regime under which the system is analysed is long enough to have encompassed the disengagement or reptation time, τ_d. The theory underlying this principle is discussed in the Appendix to this Chapter.

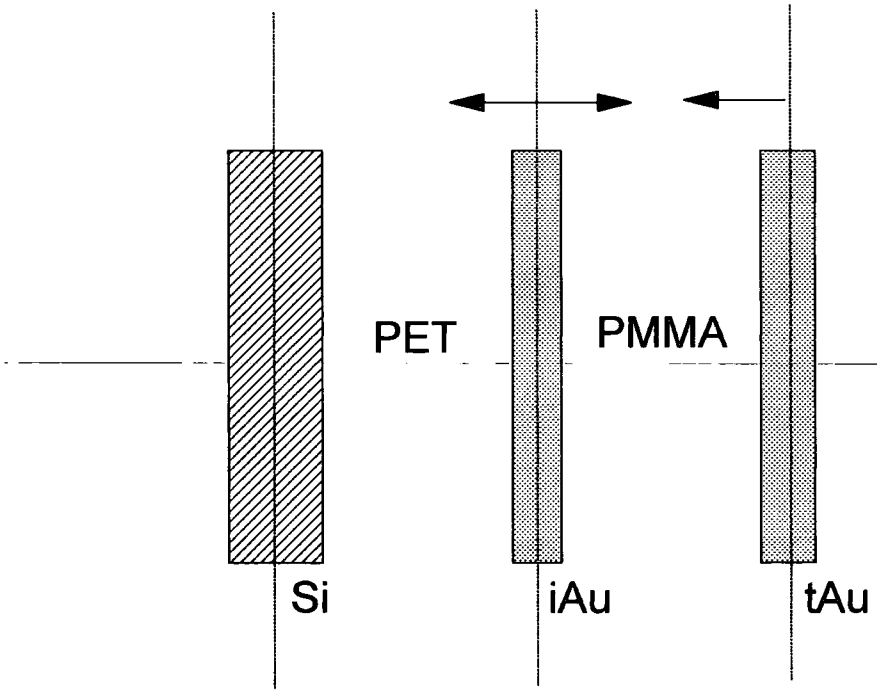

Figure 5.3 The Marker movement system as defined by the three planes of reference, the substrate Si, the interfacial gold layer, iAu, and the top gold layer tAu.

5.2. Experimental

5.2.1. Experimental Considerations

For the purposes of this experiment it is necessary to measure the movement of an interfacial gold layer. To do this we must have a detailed knowledge of all the layer dimensions in the system. The experiments described in Chapter 4 show that extensive depletion of thin PMMA layers will occur, at the temperatures of interest. At 493K the decrease in layer thickness of a PET/dPMMA bilayer can be attributed to the interdiffusion of the two layers, coupled with dimensional changes associated with the crystallisation of the PET layer and degradation of the dPMMA. At 573K the most significant process which leads to layer depletion is the depolymerisation and volatilisation of the acrylic layer. Hence, it is important to monitor all the variables within a layer stack if meaningful insight is to be gained.

The construction of the samples needed for this study was not a trivial process. Figure 5.4. illustrates the stages involved in the preparation of a sample. Extreme care is required for each of the construction stages to ensure no defects are present, prior to measurement. Uniform polymer layers are needed, and the interfacial marker layers need to be porous to the surrounding polymer matrix. Therefore, the markers must be discontinuous, (a continuous solid coating will prevent any movement of polymers across the interface), small enough not to disrupt the interfacial profile seriously, but posses the correct characteristics to be detected by the chosen analysis technique. The preparation of colloidal gold particles at an interface is achieved via annealing the deposited layer to coarsen the particulate texture. The deposition of the thin gold layers is affected by thermal evaporation under high vacuum, and successful results can only be achieved by careful investigation of the evaporation parameters prior to sample preparation.

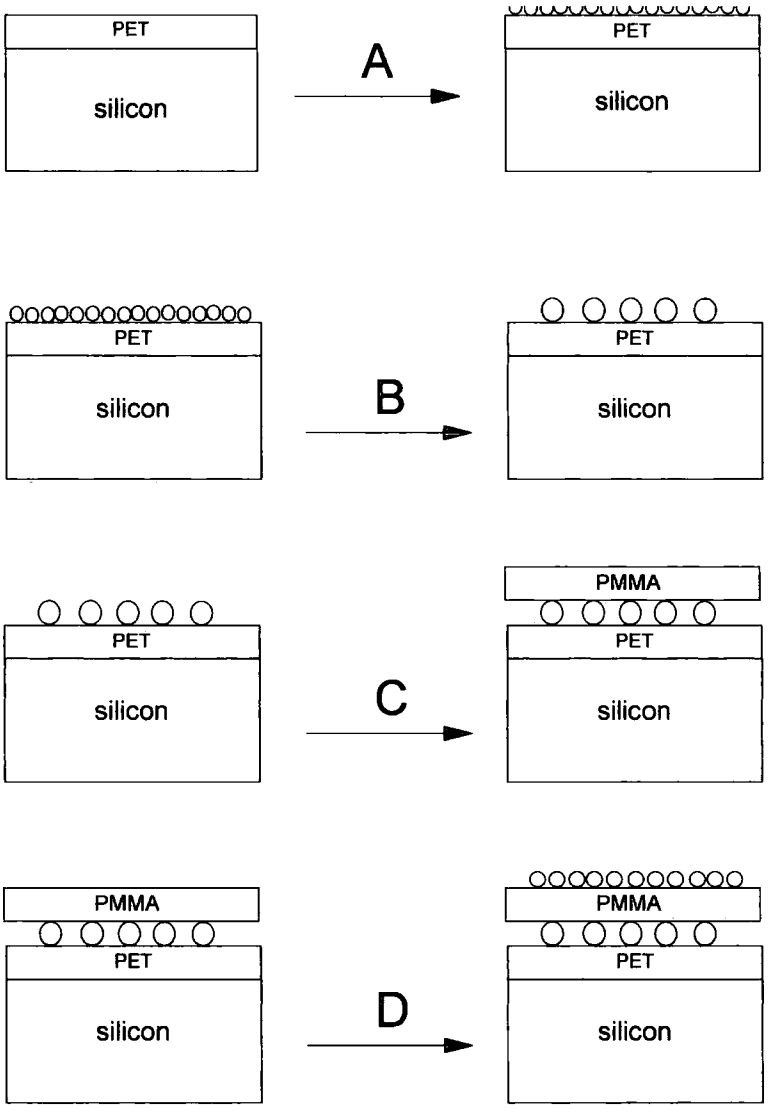

Figure 5.4 Sample preparation stages of 4 layer stacks for X-ray reflectivity experiments. 1.PET is cast from ortho-chloro phenol solution onto a clean silicon surface. 2. Gold is thermally evaporated onto the PET monolayer, and then annealed in order to coarsen the particulate structure of the layer. 3. PMMA is cast from toluene onto the gold / PET bilayer. 4. Top layer of gold is thermally evaporated onto the PMMA surface to provide contrast for this layer.

5.2.2. Establishing Conditions for Gold Evaporation

In order to control the construction of interfacial gold markers it was first necessary to establish the parameters by which thermal evaporation produces uniform layers. This was achieved by evaporating a known weight of gold onto a silicon surface, and measuring the thickness of the deposited layer by X-ray reflectometry. By varying the distance of the sample from the evaporation source, the layer thickness can be controlled. A theoretical coating thickness can be calculated by assuming that the gold evaporates from a point source at the centre of a perfect sphere. The total area of coverage is then $4\pi r^2$.

The vacuum deposition of gold was achieved using an Edwards 306a coating machine, equipped with an adjustable sample mounting assembly. A known weight of gold wire was wrapped around the central portion of the tungsten element. Silicon discs were placed onto a large diameter sample plate and held securely with double sided adhesive tape. This plate was then secured in position so that the silicon discs were inverted above the electrode at a known distance. The vacuum chamber was then sealed in position and the pressure in the chamber reduced to $\sim 10^{-8}$ torr.

Once the required vacuum was reached, gold was evaporated from the element by application of a high voltage current for approx. 20 sec. Three samples were prepared, each at a different element to sample distance. These samples were prepared on silicon substrates and the thickness' assessed by X-ray reflectometry. The X-ray reflection profiles for the single gold layers are shown in figure 5.5. These profiles were fitted against a single layer model and the thickness and layer density allowed to vary. The best fit results are taken as accurate values of the actual layer parameters. The results for these fits are shown in table 5.3.

Table 5.1. Theoretical and Measured values for single Gold layers

Sample	Weight of Gold used (g)	Evaporation distance (mm)	Theoretical Coat thickness (nm)	Measured Coat Thickness (nm)	Model layer Density (g/cm^3)
a	0.056	70	47.12	51.86	17.67
b	0.051	120	14.6	18.87	16.92
c	0.051	170	7.28	9.18	16.85

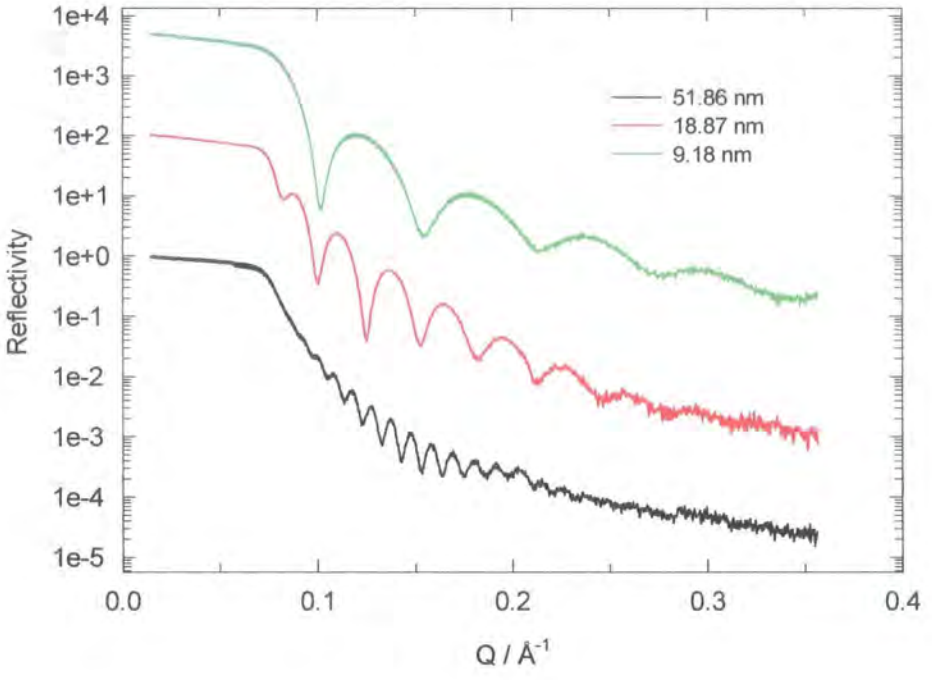

Figure 5.5 X-ray reflection profiles for gold monolayers on silicon.

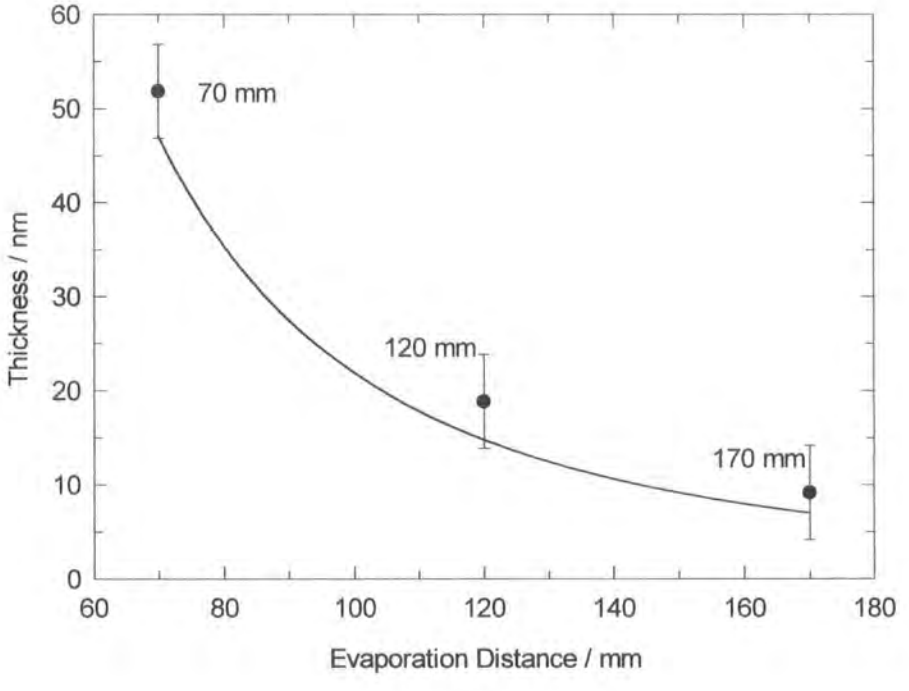

Figure 5.6. Theoretical and measured values for gold layers on silicon: Solid line = theoretical response of coat thickness with respect to evaporation distance for a weight of gold of ~0.05g.

As can be seen from the results of the model fitting, the layers are deposited in a particulate manner. This is evident from the density of the gold layer, which is less than the bulk density of gold (19.3g/cm^3). This is to be expected as it is known that the thermal evaporation procedure produces layers comprised of micro crystals [16]

The theoretical gold coating thickness is compared to the actual measured thickness, a standard calibration curve is used to calculate the necessary weight of gold needed to produce a desired film thickness.

Once the conditions for gold evaporation were established the sample preparation could proceed.

5.2.3. Materials.

PMMA, purchased from Aldrich Chem. Co. (M_w ~100,000g/mol.) was re - precipitated from toluene in anhydrous methanol.. PET, (M_w 67,500 g/mol. - G1063), supplied by DuPontTeijin Films inc. was used as manufactured. The characterisation of these polymers was described in Chapter 4. Gold wire, purchased from Aldrich Chem. Co. was used as supplied.

5.2.4. Sample Construction.

A PET layer was deposited onto bare silicon block by spin coating from ortho-chlorophenol solution. This layer was allowed to dry under vacuum for 24hrs at 333K. A thin gold layer was then vacuum deposited using the Edwards 306a vacuum coater by the method described earlier. This sample was annealed for 24 hrs at 333K in order to coarsen the gold layer. A PMMA layer was then spin coated from toluene onto this PET / Au sample, and the sample dried. The final gold layer was vacuum deposited onto the sample by the method described previously.

The changes in the X-ray reflectivity profile for each stage of preparation are shown in figure 5.7. These profiles were fitted against models for a sample geometry based on a four layer structure (substrate -(PET / Au / PMMA / Au)- Air), and assuming Gaussian roughness between the layers. Again, note that the density of both gold layers in this structure is below the value for the bulk density of gold.

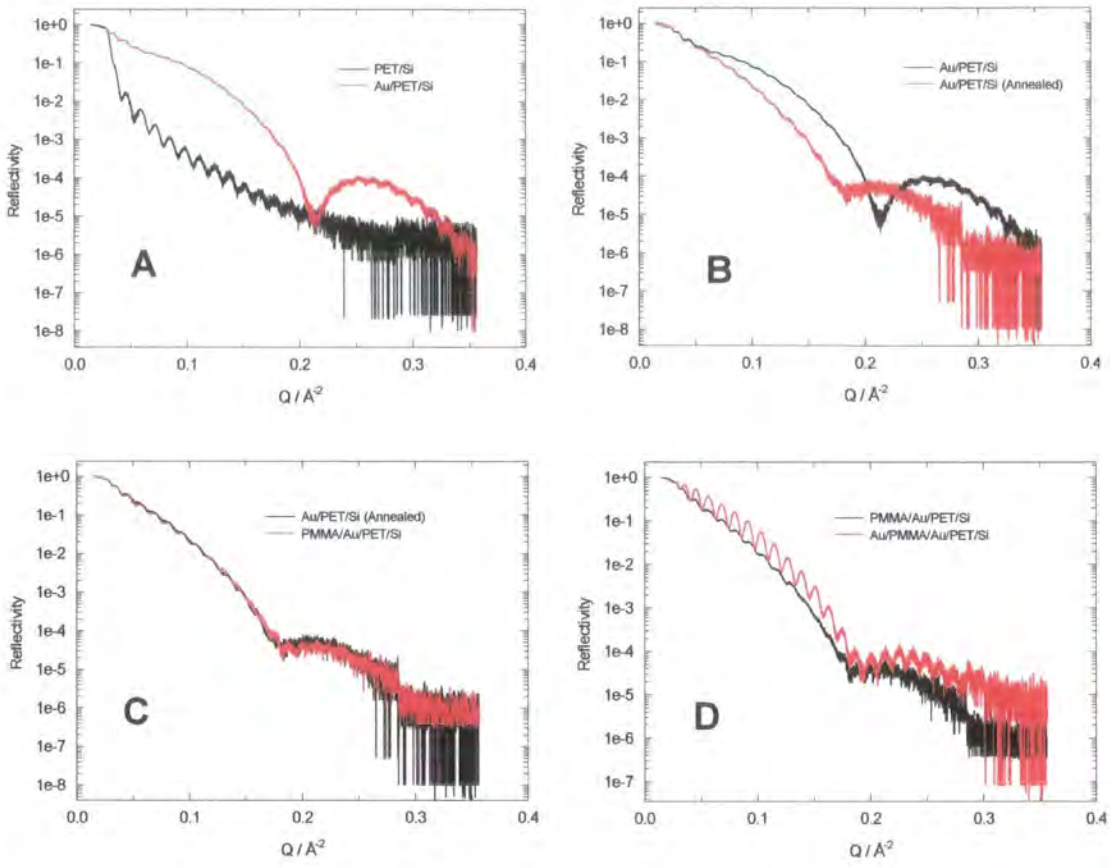

Figure 5.7 X-ray reflectivity profiles for the stages of sample construction. The designations A,B,C and D refer to the stages described diagramatically in figure 5.4.

5.2.5. Annealing Programme.

Samples were prepared, and designated by number. These samples were annealed under vacuum at 473, or 573K, for a specific time before rapid quenching on a liquid N_2 cooled steel block. The annealing procedure was identical to that described in Chapter. 4

5.2.6. X-ray Reflectometry.

For all samples, X-ray reflection profiles were collected using a Siemens D5000 X-ray diffractometer, fitted with a reflection stage. Sample alignment was performed using the proprietary software interfaced to the diffractometer, which allowed for a

rocking curve and a detector scan to define the zero point for the goniometer setting. Once aligned a 2θ scan was collected for each sample between 0.2 and 5 degrees (2θ). The X-ray source was CuKα, which produced X-rays with a wavelength of 1.54Å

5.2.7. Fitting Procedure.

The collected profiles were analysed using Refsim or Parrat software, both of which allow for the fitting of multiple layer stacks in a defined Q (or θ) range. Because there are many variables to consider, the fitting procedure requires as much knowledge as possible about the sample and the way the layers will respond to the annealing procedure. The considerations were as follows:

Substrate.

It was assumed the density, and hence the electron density and complex absorption coefficient for the silicon substrate would not be significantly altered by the annealing procedure. The mean squared roughness of the substrate / stack interface was selected as a variable during the fitting procedure, but it was found to reduce the detail of the profiles at higher values (>1nm), and these fits deviated grossly from the measured profiles.

PET layer

The PET layer thickness was used as a variable because this parameter is critical in determining the interfacial movement of the gold markers. It was assumed that an increase in roughness would occur between this layer and the marker layer, due to the Brownian motion of particulate gold in the interfacial marker layer. These parameters were used as variables for fitting the profiles to particular models. Reiter *et al* [3] state that information about the bottom layer thickness is unavailable. However, the fitted profiles in these experiments were very sensitive to both the thickness and roughness of this layer. The reasons for the discrepancy between this experiment and that of Reiter *et al*, can be attributed to the differences in equipment resolution, experimental set up and the nature of the samples. The fitted values for PET were compared to models for interfacial movement and crystallisation.

Interfacial gold marker layer

It was expected that this layer would move with the PET / PMMA interface. This layer would become broader due to colloidal roughening and Brownian motion of particulates in the respective polymer matrices, and hence a decrease in density was expected. The reflections from this layer greatly influence the appearance of the reflectivity curve, and so it was assumed that the roughness of the layer was an important parameter during the fitting procedure. The combined parameters of thickness, density and roughness are of great interest as this information can indicate the characteristics of the interfacial properties of the PET/PMMA system. Green *et al* [2] have stated that the gold layer profile remains symmetrical during their experiment, despite differences in the diffusion coefficients of the two polymer layers. However, here the layer was found to develop a high degree of asymmetry in response to increasing annealing time (see section 5.4).

Further consideration was given to the density of this layer, as this parameter directly influences the interdiffusion of the two polymers. High values for the density of this layer, approaching the bulk density of gold (19.3g/cm^3), are indicative of a layer which has not undergone colloidal roughening, and hence will not be porous to the polymers on either side of it. Therefore, one assumption which needs to be made is that lower layer densities indicate a greater degree of colloidal roughening, (i.e. increased particulate size, increased layer thickness), but an increased porosity of the layer. A simple model for the colloidal nature of the gold layer is to assume a spherical packing for the individual particles., as shown in figure 5.8.

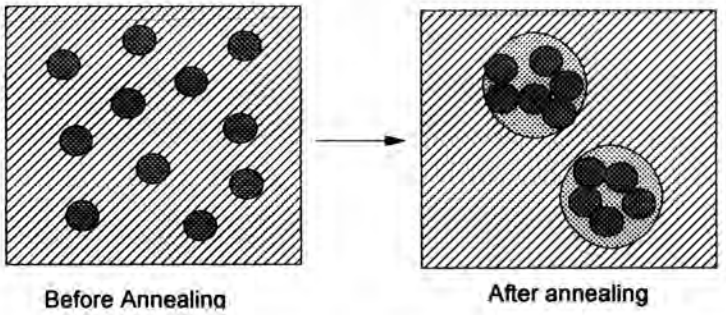

Figure 5.8. Model for colloidal roughening of gold layers, planar view. Density is decreased, coverage is decreased, thickness is increased.

PMMA layer

At 493K it was assumed that this layer would become thinner during annealing due to interdiffusion and, depolymerisation. The roughness of this layer was also expected to increase due to the Brownian motion of the particulates diffusing from the gold layers on either side. At 573K, it was expected that the layer thickness would change appreciably, so this not used as indicative of any interfacial movement, but was an important parameter in producing accurate fits, because this thickness determines the period of the profile produced by the interference of the reflections from the two gold layers. This parameter showed most sensitivity at low Q (low θ).

Layer density was also used as a fitting variable, principally to take account of the depolymerisation, densification and encapsulation of particulate gold.

Top gold layer

This layer coarsened at the sample / air interface and some diffusion into the PMMA layer was expected, again due to Brownian motion. The layer thickness and profile were again important in producing accurate fits to the measured reflectivity. Shull and Kellock [24] report that a gold layer deposited at an air / polymer interface should roughen in an asymmetric manner, with little or no broadening of the gold / polymer interface. This model was incorporated into the analysis of these data, and was found to be useful in describing features of this layer.

Sample Symmetry

Initial trials showed that information pertaining to the change in dimensions of the sample stack was more accessible by deliberately mismatching the initial thickness of the polymer layers. For this reason, ~42 nm PET layers were used, and ~52 nm PMMA layers.

5.2.8. Rheological Measurements.

The bulk viscosity of the two polymers was measured using a Rheometrics mechanical spectrometer Series IV. Both polymers were dried under vacuum prior to measurement (PET ~ 443K, PMMA ~ 363K) 40 mm parallel plates were used at a

separation distance of 1-2 mm. Frequency sweeps were run at both temperatures for both polymers.

The viscosity measurement for PET at 493K was done by heating the sample to 553K, holding at this temperature for 5 min. before a rapid quench to 493K. The sample was held at this temperature for a further 5 min., and then the frequency sweep was performed.In this way the viscosity of PET in the *crystalline* state could be determined. The zero frequency viscosity was deduced by extrapolation of the response in the Newtonian (plateau) region.

5.3. Results.

5.3.1. X-ray Reflectometry.

The collected profiles, and best fits for the samples annealed at 493 and 573K are shown in figure 5.9. The fitted parameters for the sample structures of these samples are shown in table 5.2. The values for the thickness of the layers after annealing are compared to the initial layer structure and the movement of the interface is then calculated with respect to the reference planes of the sample defined in figure 5.3. Not only the thickness of the layers is important; the density of the gold interfacial layer in particular, plays an important role in the interdiffsuion mechanism between the two polymers. Particular attention was paid to this parameter during the fitting procedure for these samples.

Inspection of figure 5.9, shows that the profiles for 120 and 360 min annealing are very similar and all detail due to the interference of the two layers has been destroyed. Fitting these profiles was subject to large error as only the top gold layer was seen to exert a major influence over the appearance of the profile. The PET - Au - PMMA system was shown to be a diffuse layer in which the iAu layer had diffused into the polymer matrix on either side of it, hence the electron density profile showed a broad Au layer of relatively low density. The values for these fits given in table 5.2, are therefore more subjective than for other fits. Reasonable estimations of the layer structure of these samples could still be made, however.

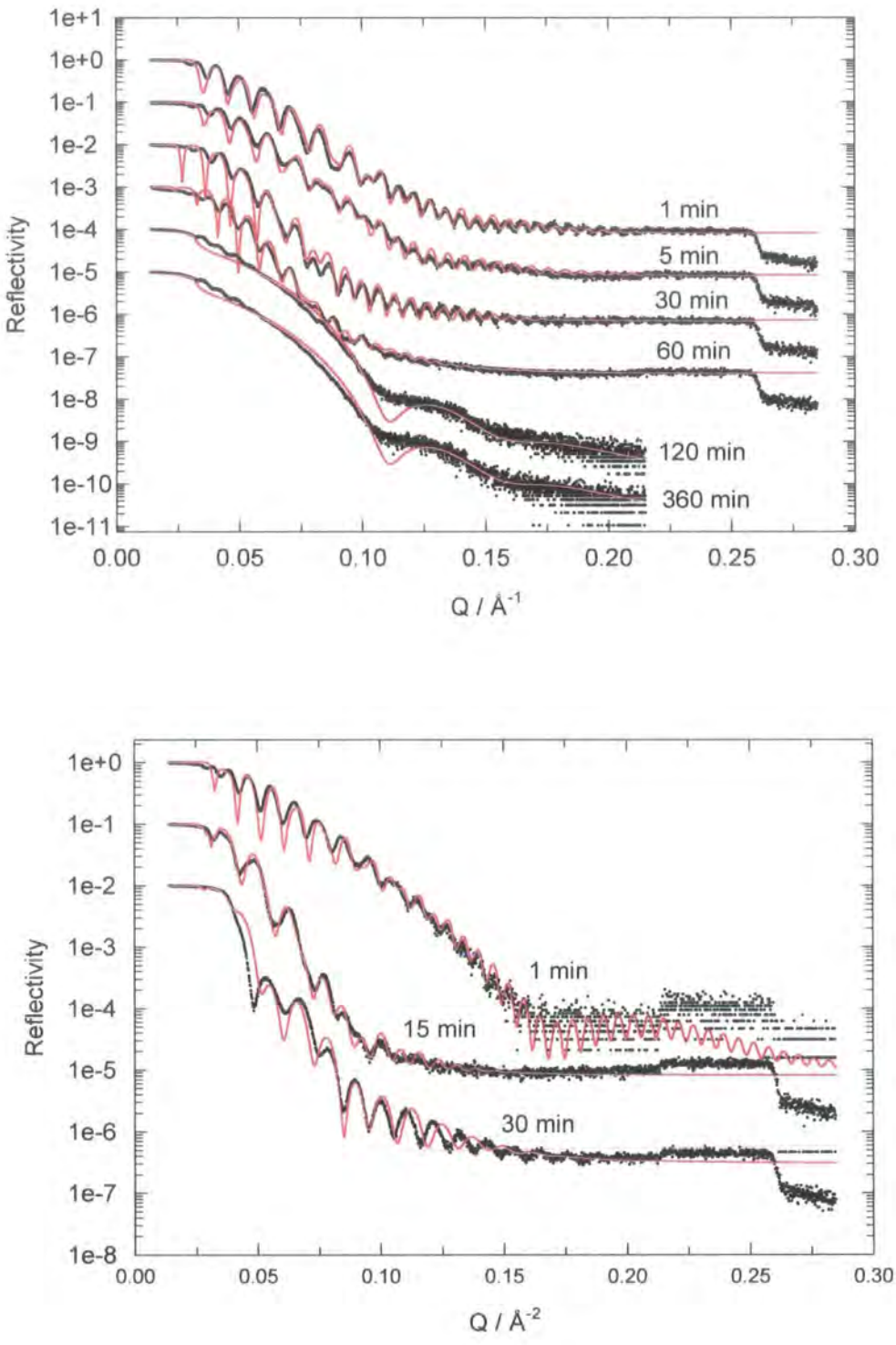

Figure 5.9. X-ray reflectivity profiles for samples annealed at 493K (top) and 573K (bottom). In each case, the black line is the measured reflectivity profile, and the red line is the best fit. The profiles have been shifted vertically to aid visualisation The time of annealing is indicated on the graph. The profiles collected at 120 and 360 min (493K) are from the same sample, sequentially annealed.

Table 5.2 Layer structures for Marker movement experiment.
Samples annealed at 493K

	Before annealing			After annealing		
	thickness (nm)	roughness (nm)	Density (g/cm³)	thickness (nm)	roughnes s (nm)	Density (g/cm³)
Sample 1 (Annealed at for 1 min.)						
Gold	3.58	0.92	12.02	4.80	1.70	7.00
PMMA	50.70	0.42	0.73	50.00	1.00	0.72
Gold	3.60	1.85	9.41	4.00	2.50	8.80
PET	42.05	1.90	1.33	43.20	1.80	1.40
Substrate		0.35	2.32		0.50	2.32
Sample 2 (Annealed for 5 min.)						
Gold	3.62	0.89	11.80	5.10	1.70	7.00
PMMA	50.60	0.41	0.77	49.20	1.10	0.80
Gold	3.65	1.82	9.40	4.40	2.70	8.40
PET	42.17	2.02	1.34	38.20	2.30	1.40
Substrate		0.40	2.32		0.51	2.32
Sample 3 (Annealed for 30 min.)						
Gold	3.59	0.88	12.30	6.80	2.50	5.80
PMMA	50.50	0.44	0.75	47.00	1.50	1.00
Gold	3.64	1.77	9.20	7.90	3.00	6.90
PET	41.19	1.79	1.35	37.50	2.50	1.40
Substrate		0.40	2.32		0.75	2.32
Sample 4 (Annealed for 60 min.)						
Gold	3.61	0.86	12.10	7.50	2.60	6.60
PMMA	50.50	0.39	0.77		1.70	1.40
Gold	3.64	1.85	9.20	9.80	3.50	5.40
PET	42.10	1.85	1.34	36.70	2.50	1.45
Substrate		0.38	2.32		0.50	2.32
Sample 5 (Annealed for 120 min.)						
Gold	2.82	0.90	13.30	6.20	2.70	5.20
PMMA	52.40	0.60	0.80	44.00	5.00	1.40
Gold	3.41	1.90	9.40	13.00	5.00	3.80
PET	37.20	1.90	1.35	33.50	6.00	1.45
Substrate		0.42	2.32		0.50	2.32
Sample 5 (Annealed for 360 min.)						
Gold				6.00	2.70	5.20
PMMA				43.20	5.50	1.40
Gold		As above		12.80	5.00	3.70
PET				33.20	5.80	1.44
Substrate					0.50	2.32

Table 5.2 (cont.)
Samples annealed at 573K

	Before annealing			After annealing		
	thickness (nm)	roughness (nm)	Density (g/cm³)	thickness (nm)	roughnes s (nm)	Density (g/cm³)
Sample 6 (Annealed for 1 min.)						
Gold	3.62	0.91	12.20	3.90	0.90	9.50
PMMA	50.40	0.42	0.78	50.75	0.70	1.50
Gold	3.64	1.81	9.30	3.50	2.50	9.00
PET	44.86	1.84	1.33	41.50	2.00	1.35
Substrate		0.42	2.32		0.50	2.32
Sample 7 (Annealed for 15 min.)						
Gold	3.61	0.92	11.90	7.50	2.50	5.30
PMMA	50.50	0.41	0.74	35.00	1.80	1.20
Gold	3.63	1.81	8.90	7.50	2.50	5.20
PET	44.75	1.91	1.34	37.50	3.50	1.40
Substrate		0.39	2.32		0.50	2.32
Sample 8 (Annealed for 30 min.)						
Gold	3.62	0.90	12.10	7.35	1.80	4.89
PMMA	50.50	0.47	0.76	1.00	2.20	1.93
Gold	3.62	1.82	9.10	7.50	3.20	4.75
PET	44.37	1.89	1.34	36.20	3.00	1.37
Substrate		0.40	2.32		0.50	2.32

5.3.2. Determining the Extent of Marker Movement

The movement of the markers is monitored with respect to one of the reference planes in the sample. These are defined within the electron density profile, calculated from the fitted parameters for each sample (see figure 5.10). Layer definitions are as follows, The substrate is labelled Si, the interfacial gold layer iAu and the top gold layer tAu. The polymer layers after diffusion are labelled as the Si - iAu (layer original PET layer), and the tAu - iAu layer (original PMMA layer). In the original theory of marker movements, the markers were observed to move as $t^{1/2}$, hence here the same graphical representation is adopted (see figures 5.11 and 5.12.). In the notation adopted here the direction of the markers is always to the main plane of reference, i.e. for the Si - iAu layer +ve movement is towards the substrate (Si plane). For the tAu - iAu layer +ve movement is towards the top gold layer (tAu plane).

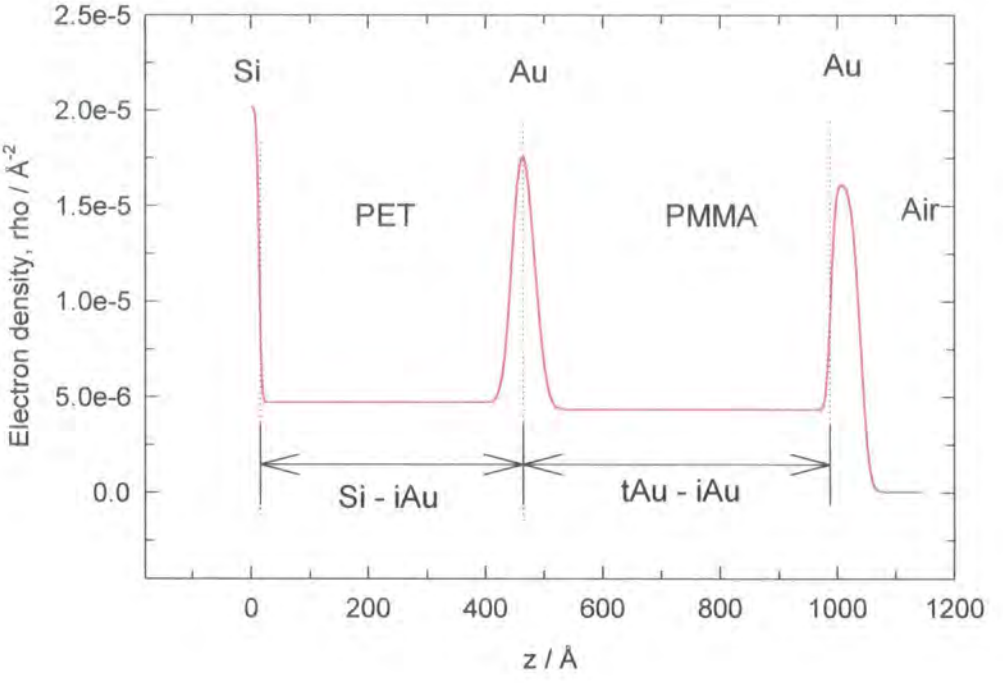

Figure 5.10 Definition of the reference planes and the movement of the interfacial markers, with respect to the electron density profile for unannealed sample.

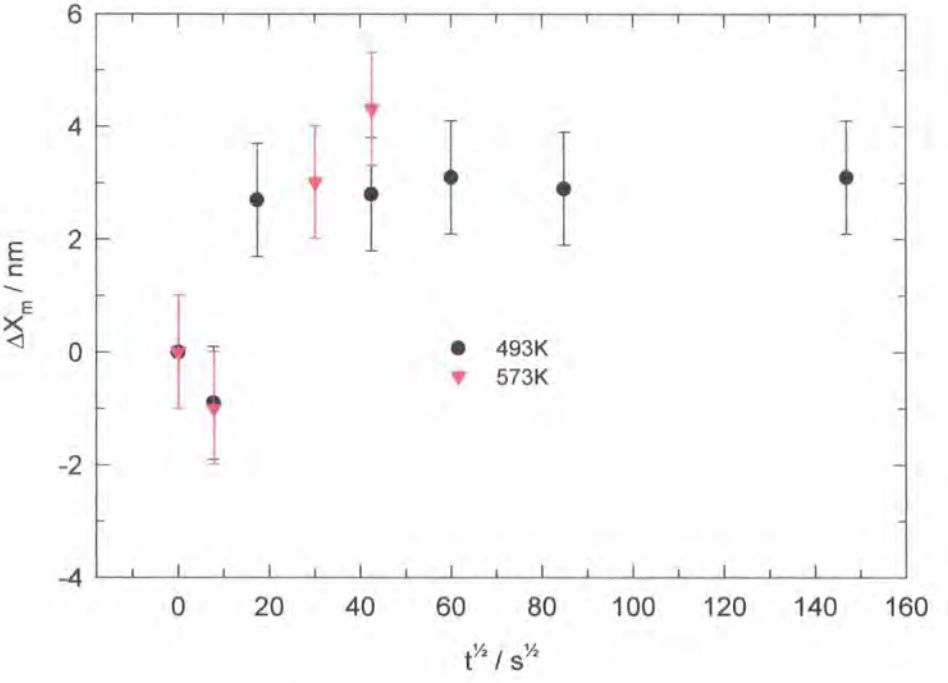

Figure 5.11 Marker displacement with respect to the Si plane of reference, i.e. depletion of the original PET layer.

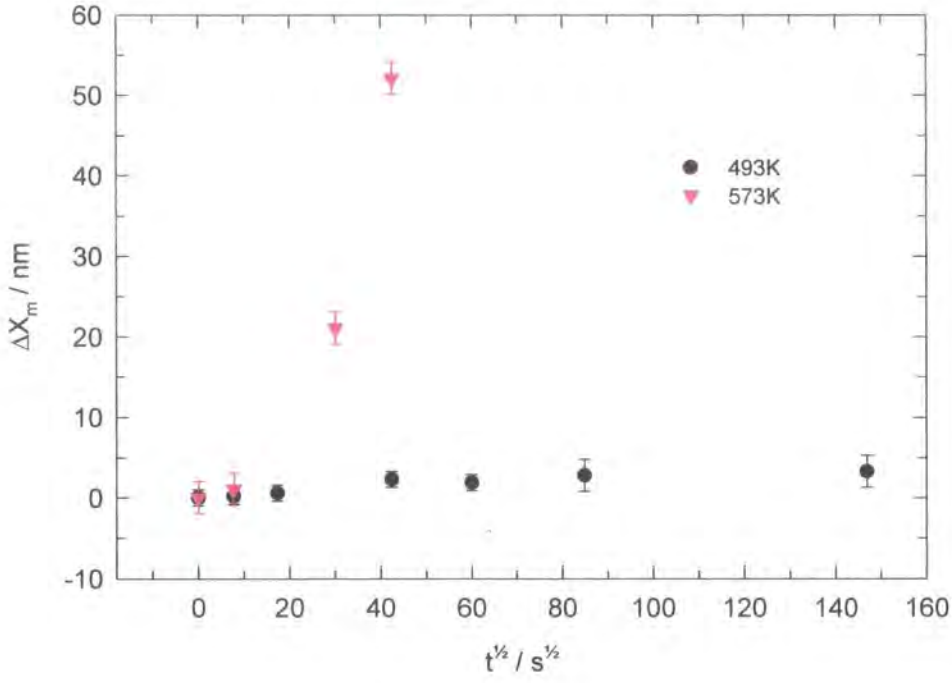

Figure 5.12 Marker displacement with respect to the tAu plane. i.e. depletion of the original PMMA layer.

Within the framework of the 'fast' theory of mutual diffusion [1,2], figures 5.11 and 5.12 should allow the extraction of the self diffusion coefficient for the fast moving species, by utilisation of equation 5.1.

$$\Delta x_m = C\sqrt{D_0 t} \tag{5.1}$$

where Δx_m is the marker displacement, C is the marker displacement factor, D_0 is the self diffusion coefficient for the fast species, and t is the diffusion time. The derivation of this equation is described in the Appendix.

It is immediately apparent that there is a contradiction with these results. At 493K and 573K, there is apparent movement towards both the tAu plane and the Si plane, which is clearly not possible if fast diffusion only is considered. A resolution of this contradiction will be discussed in the section 5.4. For the sake of completeness the self diffusion coefficients extracted from these plots are given in table 5.3 Independent verification of self diffusion coefficients is made via melt viscosity measurements.

Table 5.3. Self Diffusion Coefficients D_0 from Marker Displacements.

Temp.	D_0 cm^2/sec *	
	PET	PMMA
493K	$(3.6 \pm 2.9) \times 10^{-17}$	$(2.9 \pm 1.9) \times 10^{-17}$
573K	$(3.2 \pm 2.5) \times 10^{-16}$	$(4.2 \pm 2.3) \times 10^{-14}$

* The marker displacment factor is taken as ~0.45 ($N_{PET}/N_{PMMA} \sim 0.1$)

5.3.3 Rheological Measurements

The bulk viscosity of the two polymers is shown as a function of frequency in figure 5.13 The zero frequency viscosity was deduced by extrapolation of the response in the Newtonian (plateau) region, and these data are shown in table 5.4.

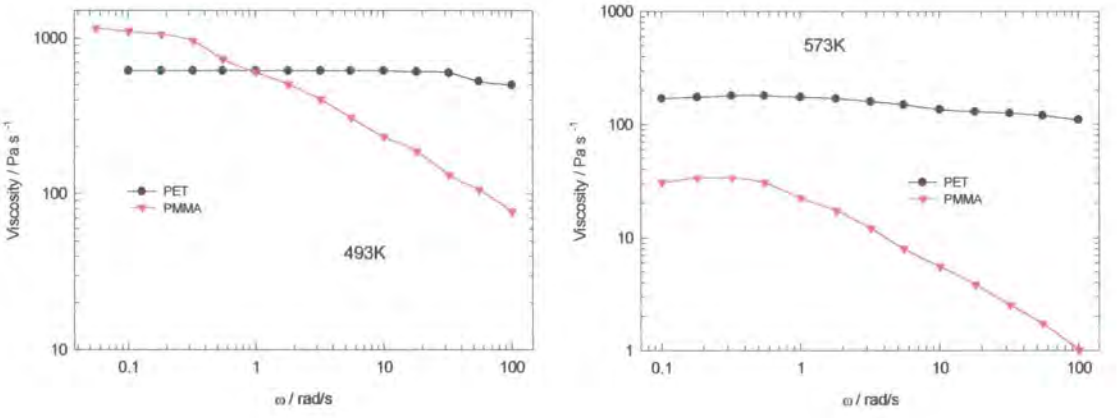

Figure 5.13. Viscosity vs. frequency for PET and PMMA at 493 and 573K.

These data show that PET maintains a higher viscosity at 573K, but at 493K the zero - shear viscosity of PMMA is higher. This result will be used in the analysis of the shape of the interfacial gold layer profile and in the estimation of D_0 using equations 5.2 - 5.4 A knowledge of the zero shear viscosity allows is also important for understanding the shape of the interfacial gold layer profiles; it is anticipated that a difference in viscosity will lead to asymmetric profiles as described by Shull and Kellock [24].

Table 5.4 Zero - Frequency viscosity for PET and PMMA.

	Viscosity (Pa)	
	493K	573K
PET	620	160
PMMA	1,150	30

Using these values the self diffusion coefficients for a polymer can be calculated using the expression developed by Graessley;

$$D^* = \frac{G_0}{135}\left(\frac{\rho RT}{G_0}\right)^2\left(\frac{R_e^2}{M}\right)\left(\frac{M_c}{M^2\eta_0(M_c)}\right) \tag{5.2}$$

where G_0 is the plateau modulus, ρ is the density of the polymer, R is the universal gas constant, T is temperature (Kelvin), R^2_e, is the mean squared end to end distance of the polymer, (the radius of gyration, R_g can also be used), M is the molecular weight, M_c is the critical molecular weight, and $\eta_0(M_c)$ is the zero-shear vicosity for the critical molecular weight. G_0 needs to be determined via interpretation of rheological measurements, or alternatively can be derived from the simple expression;

$$G_0 = \frac{\rho RT}{M_e} \tag{5.3}$$

where M_e is the entanglement molecular weight for the polymer, (there exists an approximate equality, $M_c = 2M_e$) (36).

The zero shear (low frequency) viscosity is also embodied in the expression

$$\eta_0 = \frac{15}{4}\left(\frac{G_0}{\rho RT}\right)^2\left(\frac{M^3\eta_0(M_c)}{M_c}\right) \tag{5.4}$$

with notation as before. Utilisation of these equations requires a knowledge of the molecular parameters, Table 5.5 lists the parameters and their sources, used to predict D_0, and hence estimate the extent of any marker movement. The D_0 values calculated from these equations are given in table 5.7.

Table 5.5. Parameters required for utilisation of equations 5.2 - 5.4.

Parameter	PET		PMMA	
	Value	Ref.	Value	Ref.
M_e	1,450	23	9,200	23
			13,600	19
M_c	3,500	23	29,500	19
ρ	0.99	23	1.11	23
	1.22	34	1.09	19
R_e^2/M_{mon}	1.08 (Å²)	this work	0.425 (Å²)	19
			0.449 (Å²)	this work

5.3.4. Values of D_0 from Literature.

Previous workers have also derived values for self diffusion coefficients of PET and PMMA. These values and their sources are given in table 5.6.

Table 5.6. Self diffusion data for PET and PMMA.

Polymer	D_0 (cm²/sec.) (typical)	Reference	Comment
PET	$\sim 10^{-14}$	12	Measured from crystallisation data above T_g. Max. temp. use 387K
PMMA	$\sim 10^{-15}$ - $\sim 10^{-18}$	13	Measured using Rutherford backscattering Spectroscopy. Temp range ~423 - 453K
PMMA	$\sim 10^{-22}$	15	From fracture toughness measurements. Temp. ~390K.
PMMA	$\sim 10^{-16}$	4	Measured using marker movements at 418K

In order to use the values in table 5.6, it is necessary to scale in temperature to the conditions used in this experiment. This can be achieved by utilising the well known WLF (Williams - Landel - Ferry) equation [17], which takes the general form;

$$\log a = \frac{C_1(T-T_r)}{C_2+T-T_r} \qquad (5.5)$$

where T = temperature, T_r= reference temperature, C_1 and C_2 are constants and the factor a is the ratio for the quantities of interest, e.g. diffusion coefficients, relaxation times etc.

The data of Collier and Baer for PET [12], and Shearmur *et al* for PMMA [13], has been scaled to 493K and 573K using the appropriate WLF factor, and these results are shown graphically in figure 5.14.

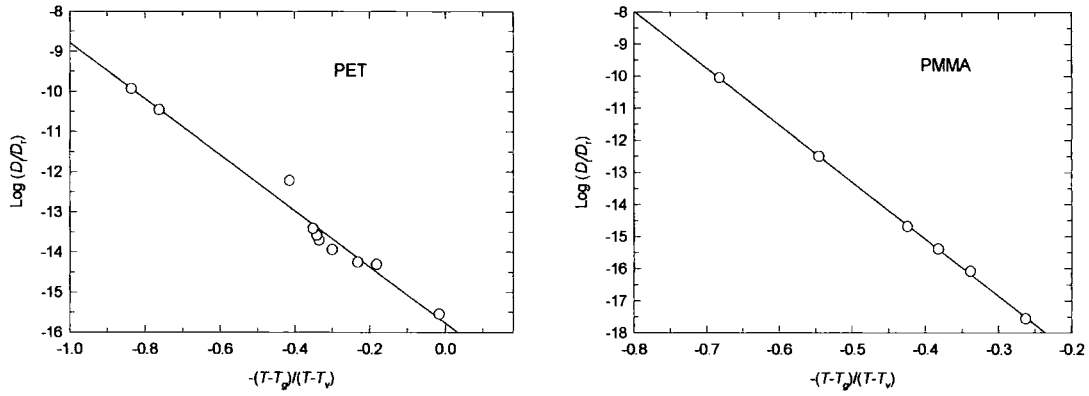

Figure 5.14. WLF shifts for PET and PMMA.

The WLF shifts shown in figure 5.14 are scaled up to T = 493 and 573K in order that comparisons can be made with this study. The WLF scaling of literature data for PMMA is considered acceptable for 493K, as the temperature increase is relatively small.

The larger temperature scaling does render the result somewhat dubious; for instance at 573K PMMA will undergo degradation and as such the relative molecular weight will be lower. Even more significant is the effect of scaling the PET data of Collier and Baer. This data was derived from a primary crystallisation study at temperatures < 387K, (see table 5.6), and as such its use is questionable; the maximum crystallisation rate for PET is usually observed between 530 and 550K after which crystallisation slows down appreciably, (in fact a different crystallisation mechanism is in operation). Therefore the WLF scaling of PET diffusion data across a crystalline transition is thought to be unreliable in this case

The values for D_0 derived by WLF scaling procedure and those derived from the measurement of zero - shear viscosity are given in table 5.7.

Table 5.7 Values for D_0 by viscosity and WLF treatment.

	D_0 (cm²/sec.)			
	WLF shift		Viscosity measurement	
	PET	PMMA	PET	PMMA
493K	3.2×11^{-11}	4.1×10^{-13}	4.0×10^{-13}	6.7×10^{-15}
573K	1.1×10^{-10}	1.3×10^{-11}	1.2×10^{-12}	7.8×10^{-13}

This data will be used in the analysis of marker movements (see section 5.4). As can be seen the WLF data is 1 ~ 2 orders of magnitude higher than the viscosity based data. This highlights the large discrepancies which can arise when attempting to elucidate diffusion mechanisms in polymers. A reveiw of the literature reveals that a broad range of D_0 values exits, covering several orders of magnitude; even for chemically identical polymers of similar molecular weight, treated at similar temperatures. [1 - 4, 13, 15, 20, 37,38]

5.4 Discussion.

5.4.1. Interfacial Movement at 493K

tAu - iAu layer.

Figure 5.12 shows that an equilibrium value of ~3nm is reached for the depletion of the inter-gold distance (PMMA layer). This observation is compared to the thin layer behaviour reported in Chapter 4. Figure 5.15 shows a plot of the thickness loss of the PMMA layer, compared to the data from the neutron reflectometry experiment described in Chapter 4.

The apparent layer depletion in the marker movement experiment is seen to be less than for the NR and ellipsometry experiments. Certainly at longer annealing times the marker movement and ellipsometry experiments both show a tendency towards an equilibrium layer thickness. One explanation of this phenomena would be the restrictive nature of the top gold layer which maintains a relatively high value even after 6 hrs annealing (see table 5.2)

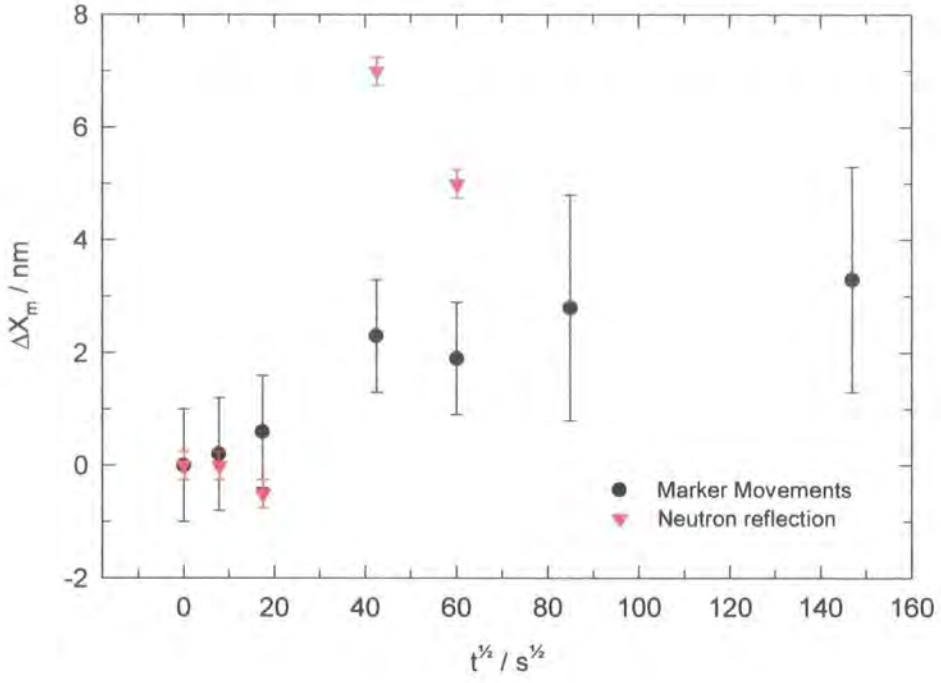

Figure 5.15. tAu - iAu layer depletion compared to neutron reflectivity experiment

Si - iAu layer

At $t < 5$ min., a remarkable difference between the initial and final PET layer thickness is seen. This could be construed as a rapid movement of the gold markers in response to an interfacial shift as a result of interdiffusion. On further consideration, some of this movement at least, must be attributable to crystallisation of PET. At 493K it is known that PET will crystallise rapidly [25,26,27]. Indeed, 493K was one of the temperatures chosen for this experiment as this is a typical annealing temperature used in PET film manufacture for crystallisation [28]. Therefore, the possibility of layer densification as a result of crystallisation must also be considered.

Figure 5.16 shows the marker displacement of the iAu layer and is compared to the thin layer depletion of PET as measured by ellipsometry. It is quite apparent that the similarity between the marker movement and ellipsometry experiments implies that the marker movement is a result of densification of the Si - iAu layer due to crystallisation of the PET .

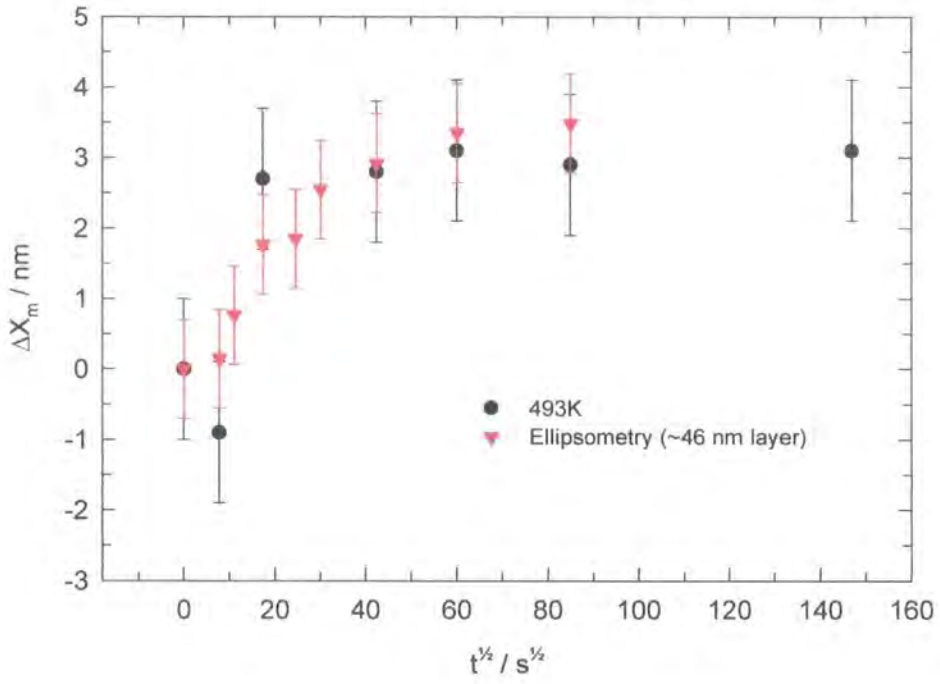

Figure 5.16 Marker displacement at 493K with respect to Si plane, compared to layer depeltion of PET as measured by ellipsometry.

The layer depletion due to crystallisation in the PET layer is controversial when compared to the neutron reflection results. In Chapter 4 it was shown that the neutron reflectivity of PET / dPMMA bilayers is relatively insensitive to the thickness of the PET layer, principally because of the large scattering length density contrast between PET and dPMMA. However, here it appears the marker movement is sensitive to this decrease in Si - iAu layer thickness.

Therefore it is concluded, that the marker displacement at this temperature can be attributed to crystallisation of the PET. The application of the fast theory of interdiffusion under these circumstances, is not valid.

5.4.2. Interfacial Movement at 573K

tAu - iAu layer

Once again the layer depletion of the inter - gold distance is plotted as a 1st order degradation reaction and compared with NR and ellipsometry results, (figure 5.17). It is apparent that at this temperature the layer depletion can be adequately accounted for by PMMA degradation. The rate constants for these results are given in table 5.8. Inspection of these results shows that the values for k are in good agreement indicating that this is the predominant process in the inter - gold layer, and elucidation of smaller distance changes due to interdiffusion would be impossible given the extent of the degradation and the errors in the experiment.

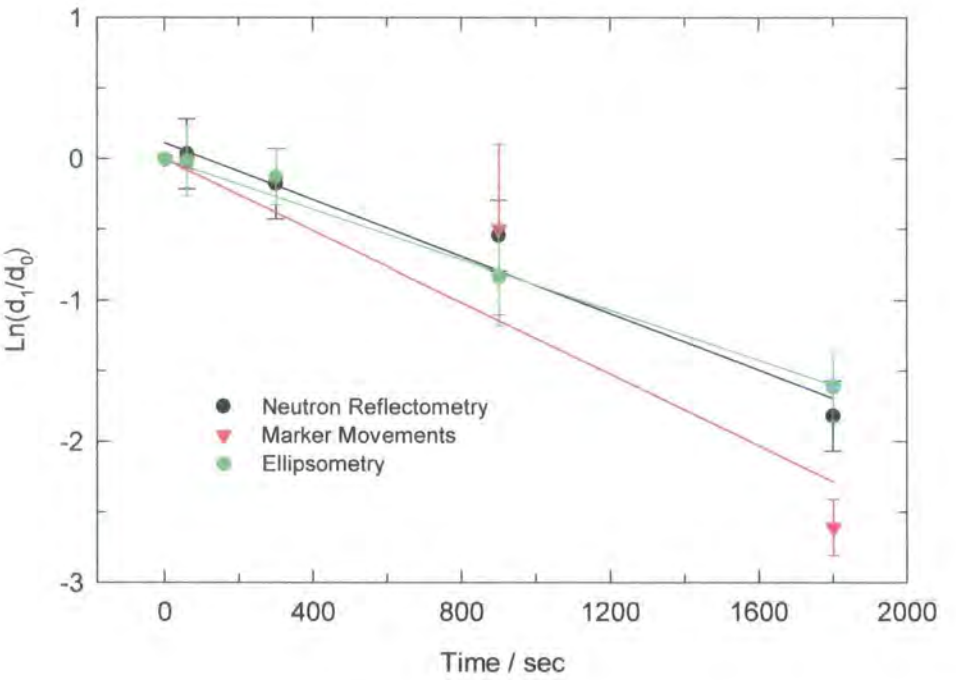

Figure 5.17. 1st order degradation of PMMA from marker movement, ellipsometry and neutron reflectometry experiments.

Table 5.8. 1st order rate constant, k, for PMMA degradation from different thin layer techniques

Marker Movement	Neutron Reflectometry	Ellipsometry
$(1.3 \pm 1.0) \times 10^{-3}$ s^{-1}	$(1.0 \pm 1.0) \times 10^{-3}$ s^{-1}	$(8.9 \pm 4.0) \times 10^{-4}$ s^{-1}

Si - iAu layer

At 573K the most interesting results are obtained. As can be seen from figure 5.15 the marker displacement appears to respond in the expected manner. The melt viscometry data described in section 5.3 indicates that at this temperature PMMA is the slow species, and any interfacial movement should be towards this PET side of the sample. Initially it appears that there is some movement towards the tAu plane of reference, however, this behaviour is sharply reversed at $t \sim 15$ min. This cannot be explained adequately by invoking one particular phenomena, which result in dimensional changes in the PET layer. At 573K PET will be in the melt state, and as such can be considered as wholly amorphous. Therefore any degree of crystallinity which is formed in the sample, will be due to the efficiency of the rapid quench process of the samples. By inspection of the values used to fit the the X-ray reflectivity data we can see that the PET layers are somewhat less dense than at 493K, and by inference less crystalline. Therefore the interfacial movement at 573K is not attributed to crystallisation of the PET.

However, qualitatively another discrepancy comes to the fore. As, the annealing period continues, one expects the depolymerisation of PMMA to produce material with an increasing self diffusion coefficient, due to depolymerisation. It appears that although the marker displacement agrees qualitatively with independent values for D_0, further explanation is necessary in this case

Presumably, there is some chemical reaction taking place, such as gelation of the PMMA, producing an immobile, crosslinked polymer network, in which the definition of individual polymer chains becomes irrelevant. This gel type structure is swollen by the PET as the 'faster' species and the interface is seen to move towards the PET side of the couple. Alternatively, an interfacial reaction has occurred between the PET and PMMA, again producing a network type structure, which becomes increasingly immobile. The network structure is swollen in the same way as described previously. In Chapter 3, a grafting reaction was proposed between PET and PMMA to account for the observed results, (i.e. inhibition of crystallisation, increase in HFIP insoluble fraction etc.), and the results here appear to support these findings.

Resorting to the classical fast diffusion theory, the self diffusion coefficient of PET can be extracted from a straight line fit to the data presented in figure 5.15. If a crosslinked structure is present at the interface then one presumes the molecular weight

to be very high and therefore the classical definition of C, the marker displacement factor can be made i.e.

$$\frac{N_{PET}}{N_{PMMA}} \rightarrow 0, C \rightarrow 0.5 \tag{5.6}$$

As the molecular weight on the PMMA side of the interface becomes very large, the factor C tends towards a limiting value, (0.48, Green *et al*, 0.51 Reiter *et al*). As there is no indication as to the nature of C for different polymer diffusion couples, an approximate value of 0.5 is used. This yields a value for D_0 for PET of 3.2×10^{-14} cm^2/sec. which given the approximations used is in relatively good agreement with the value derived from viscosity measurements (see table 5.7)

Alternatively, if D_0 from melt viscometry for PET is used, (1.2×10^{-12} cm^2/sec), then a value for C of ~0.08 is obtained. Using the simple relationship given by Green *et al* [x], the molecular weight (M_N) of the slow species (PMMA) ~ 1×10^6 g/mol. for PET with M_N 25,000 g/mol, which indicates a chain building reaction at the interface.

This hypothesis is supported by the asymmetric shape of the interfacial gold layer, iAu, profile (see figure 5.18). This is in disagreement with the observations of Green *et al* [2], who maintain that marker layer profiles remain symmetrical throughout their experiment. The results of this experiment are in accordance with the observations of Shull and Kellock [24] who claim that interfacial gold will diffuse into both polymers, to an extent which is determined by the viscosity of the polymers. It appears that at longer annealing times the profile has a longer tail towards the PET side of the couple, indicating that this is the lower viscosity material.

Further support for an interfacial reaction is given when considering the movement of the individual gold markers. Reiter *et al* [3], have postulated that the mobility of the gold particulates is governed by the size of the characteristic entanglement distance, i.e. the gold rafts cannot move when their size is comparable to , or greater than this distance. The mean squared end to end distance is calculated using literature values for M_e [23], and the values for $<R^2_e>$, are 16 .6 nm^2 for PET and 41.3 nm^2 for PMMA. This indicates that PMMA should be more porous to colloidal gold than PET, which, from figure 5.18 is not the case. Hence a reduction in the entanglement length by crosslinking at the interface is implied.

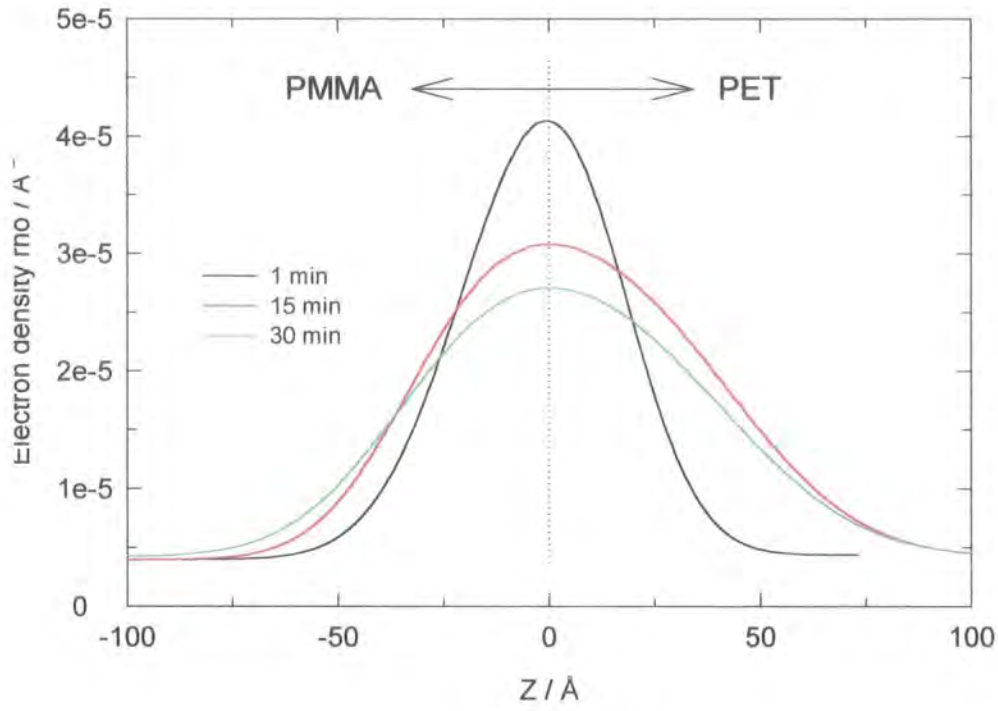

Figure 5.18 electron density profile of the iAu marker layer. The asymmetric tail is seen growing in the PET side of the couple as the annealing time increases.

5.5. Conclusions

This Chapter has attempted to monitor the movement of the PET and PMMA layers simultaneously, with particular attention to the interfacial position. The Marker movement experiment is sensitive to movements of ~ 1nm, hence small dimensional changes can were able to be monitored. With reference to the NR experiment, only small changes (if any) were expected due to interdiffusion, however, it was shown that crystallisation, degradation and an interfacial reaction could be monitored.

1) At 493K the movement of the interface towards the 'fast' side of the couple (PET) is attributed to crystallisation of the PET, and 'fast' diffusion is negated.
2) At 493K the depletion of the tAu - iAu distance is attributed to degradation of PMMA. However, the rate of degradation is less than is seen for the equivalent samples

in the neutron reflectometry experiment, and restriction of volatile products by the top gold layer is postulated.

3) At 573K there is no contribution to interfacial roughness from crystallisation.

4) After 30 min. annealing at 573K the interface is seen to move towards the PET side of the couple by ~4nm, indicating this to be the fast species in the system. By analysing the iAu electron density profiles, an increase in viscosity on the PMMA side of the couple evident. This is attributed to a chemical reaction occurring at the interface between PET and PMMA.

5) Using $C \sim 0.5$, gives D_0 (PET) as 3.2×10^{-14} cm^2/sec. Using D_0 (PET_{visco}) $\sim 1.2 \times 10^{-12}$ cm^2/sec, yields a value for C of 0.08, which implies a large increase in molecular weight on the PMMA side of the couple, (i.e. crosslinking).

6) The interfacial analysis has successfully decoupled the interfacial broadening observed by NR. layer densification due to crystallisation has also been observed, whereas in NR, for reasons unknown, this phenomena was not apparent

5.6. Appendix. Theory of Marker Movements.

The theory underlying the phenomenon of marker movements was originally developed by Kramer *et al*, [1] who used marker movements to confirm the so called 'fast' theory of polymer / polymer interdiffusion.

Consider a diffusion couple consisting of polymer A and polymer B. The initial interface between these two polymers, i.e. prior to any interdiffusion, is decorated with an inert marker. The experiment is designed such that the polymers have very different self diffusion coefficients, and during interdiffusion there will be a net flux of matter across the interface towards the side of the couple containing the 'slow' species. In order that unacceptable density gradients are not created, the slower species must relax, and does so by bulk flow, and hence the markers placed at the interface will move with this bulk flow and the interface will be seen to move towards the side of the couple containing the fast species. The velocity of the markers for two chemically different polymers with different molecular weights, is given by equation 5.7,

$$v = k_B T\left(\frac{B_A(Ne)_A}{N_A} - \frac{B_B(Ne)_B}{N_B}\right)\times\left(\frac{1-\phi}{N_A} + \frac{\phi}{N_B} + 2\phi(1-\phi)|\chi|\right)\nabla\phi \quad (5.7)$$

where k_B is Boltzmann's constant, B_i is the polymer mobility, Ne_i is the number of segments per entanglement length, N_i is the number of segments per chain (degree of polymerisation), ϕ is the volume fraction of polymer B, χ is the Flory - Huggins interaction parameter and ∇ represents the gradient operator. In its simplest form equation 5.7 can be written as,

$$v = (D_A - D_B)\nabla\phi \quad (5.8)$$

where D_A and D_B are the intrinsic diffusion coefficients of polymer A and polymer B respectively, and $\nabla\phi$, is the gradient in chemical potential of the system. The intrinsic diffusion coefficients are given by

$$D_A = N_A D_A^*\left[\frac{(1-\phi)}{N_A} + \frac{\phi}{N_B}\right] \quad (5.9)$$

$$D_B = N_B D_B^*\left[\frac{(1-\phi)}{N_A} + \frac{\phi}{N_B}\right] \quad (5.10)$$

where D_i^* is the self diffusion coefficient which are given by the well known reptation equation

$$D^* = \frac{N_e B_0 k_B T}{N^2} \quad (5.11)$$

By integrating equation 5.11, the following expression for the displacement of markers is obtained

$$\Delta x_m = C\left(D_A^* t\right)^{\frac{1}{2}} \quad (5.12)$$

where C is a constant, the marker displacement factor, and is a function of N_A/N_B. The limiting value for this constant (i.e. when $N_A/N_B \rightarrow 0$) has been computed by Green *et al* as 0.48 [2] and by Reiter *et al* as 0.51 [3], both of whom investigated polystyrene interfaces. Note that the movement of the markers is predicted to move with $t^{1/2}$, in accordance with reptation theory.

In the marker / polymer construct it is necessary to define a co-ordinate system, the origin of which is fixed at one end of the diffusion couple. In this system the markers are located at x_m. If a second co-ordinate system is defined, with the markers at the origin, such that

$$x = x_0 + x_m \tag{5.13}$$

The markers are now always at x_0. Since this second co-ordinate system allows the following equivalence to be made;

$$\frac{\partial}{\partial x_0} = \frac{\partial}{\partial x} \tag{5.14}$$

Fick's second law can now be written as,

$$\frac{\partial \phi}{\partial t} = \frac{\partial}{\partial x_0}\left(D'(\phi)\frac{\partial \phi}{\partial x_m}\right) \tag{5.15}$$

For the infinite diffusion couple it is useful to make the Boltzmann transformation [11] and define the variable;

$$u = \frac{x_0}{\sqrt{t}} \tag{5.16}$$

In terms of this variable, the diffusion equation may be written as :

$$-\frac{1}{2}u\frac{d\phi}{du} = \frac{d}{du}\left[D'(\phi)\frac{d\phi}{du}\right] \tag{5.17}$$

The concentration $\phi = \Phi(u)$ is now the solution to an ordinary differential equation. Moreover, as the particle is always at $x_0 = 0, u = 0,$ it always stays at a constant composition $\phi_0 = \Phi(0)$, as time increases. In reality the diffusion coefficient is strongly dependant on concentration and as such no analytical solution exists. One must rely on numerical analysis to derive values for the interfacial profile. Large differences between D_A and D_B will lead to a strong asymmetric ϕ dependance of the mutual diffusion coefficient.

5.7 References

[1] Kramer, E. J., Green, P. F. and Palmstrøm, C. J. *Polymer*, 1984, **25**, pp 473 - 480.

[2] Green, P. F., Palmstrøm, C. J., Mayer, J. W. and Kramer, E. J. *Macromolecules*, 1985, **18**, pp 501 - 507.

[3] Reiter, G., Hüttenbach, S., Foster, M. and Stamm, M., *Macromolecules*, 1991, **24**, pp 1179 - 1184.

[4] Liu, Y., Reiter, G., Kunz, K. and Stamm, M., *Macromolecules*, 1993, **26**, pp 2134 - 2136.

[5] Wu, S., Chuang, H-K. and Han, C. D., *J. Polym. Sci., Polym. Phys. Ed.*, 1996, **24**, pp 143 - 159.

[6] Brochard, F., Jouffroy, J. and Levinson, P., *Macromolecules*, 1983, **16**, pp 1638 -1641.

[7] Jabbari, E. and Peppas, N. A., *Polymer*, 1995, **36**, pp 575 - 586.

[8] Russell, T. P., *Mater. Sci. Rep.* 1990, **5**, pp 171 - 271.

[9] Doi, M. and Edwards, S., *The Theory of Polymer Dynamics*, Clarendon Press, Oxford, 1986

[10] Composto, R. J. and Kramer, E. J., *J. Mater. Sci.*, 1991, **26**, pp 2815 - 2822.

[11] Boltzmann, L. *Ann. Phys.*, 1894, **53**, pp 953.

[12] Collier, J. R. and Baer, E. *J. Appl. Polym. Sci.*, 1966, **10**, pp 1409 - 1419.

[13] Shearmur, T. E., Clough, A. S., Drew, D. W., van der Grinten, M. G. D. and Jones, R. A. L. *Polymer*, 1998, **39**, pp 2155 - 2159.

[14] Montserrat, S. and Cortres, P., *J. Mater. Sci.*, 1995, **30**, pp 1790 - 1793.

[15] Jud, K., Kausch, H. H. and Williams, J. G., *J. Mater. Sci.*, 1981, **16**, pp 204 - 210.

[16] Heavens, O.S. *Thin Film Physics*, Methuen & Co Ltd, London, 1970.

[17] Ferry, J. D., *Viscoelastic Properties of Polymers*, 3rd Edn., Wiley, New York, 1980.

[18] Le Bourvellec, G. Thesis Doct. Ing., Universite Pierre et Marie Curie, Paris, 1984.

[19] Fetter, L. J., Lohse, D. J., Milner, S. T. and Graessley, W. W., *Macromolecules*, 1999, **32**, pp 6847 - 6851.

[20] Van Alsten, J. G. and Lustig, S. R. *Macromolecules*, 1992, **25**, pp 5069 - 5073

[21] Graessley, W. W., *J.Polym. Sci.*, 1980, **18,** pp 27 - 34.

[22] Blundell, D. J., Oldman, R. J., Fuller, W., Mahendrasingam, A., Martin, C., MacKerron, D. H., Harvie, J. L. and Rickel, C., *Polym. Bulletin*, 1999, **42**, pp 357 - 363.

[23] Wu, S., *J. Polym. Sci.*, 1989, **27**, pp 723 - 741.

[24] Shull, K. R. and Kellock, A. J., *J. Polym. Sci.*, 1995, **33**, pp 1417 - 1422.

[25] Yu, T., Bu, H., Chen, J., Mei, J. and Hu, J., *Makromol. Chem.*, 1986, **187**, pp 2697 - 2709.

[26] Ou, C.- F. and Lin, C.- C., *J. Appl. Polym. Sci.*, 1994, **54**, pp 1223 - 1231.

[27] Jackson, J. B. and Longman, G. W., Presented at the SPE 27th Annual Technical conference, held in Chicago, May 1969, pp 873 - 884.

[28] Werner, E., Janocha, S., Hopper, M.J. and Mackenzie, K. J. in *Encyclopaedia of Polymer Science and Technology*, **12**, 1984.

[29] Fischer, E. W. and Fakirov, S., *J. Mater. Sci.*, 1976, **11**, pp 1041 - 1065.

[30] Struik, L. C. E., *Polymer*, 1987, **28**, pp 1521 - 1533.

[31] Fakirov, S., Fsicher, E. W. and Schmidt, G. F. *Makromol. Chem.*, 1975, **176**, pp 2459.

[32] Hayes, N. W., Beamson, G., Clark, D. T., Law, D. S.-L. and Ravel, R., *Surf. Int. Anal.*, 1996, **24**, pp 723-728.

[33] Wehrum, A. PhD Thesis, St Catherines College, Cambridge, 1999.

[34] Ingermells, H. and Bandrup, M., *Polymer Handbook*, 2nd edn., 1975

[35] Madorsky, S. L. *Thermal Degradation of Organic Polymers*, Wiley Interscience, 1964.

[36] Lacasse, M. D., Grest, G. S. and Levine, A. J. *Phys. Rev. Lett.*, 1998, **80**, pp 309 - 312.

[37] Seggern, J. V., Klotz, S. and Cantow, H. J., *Macromolecules*, 1989, **22**, pp 3328 - 3332.

[38] Green, P. F. and Doyle, B. L., *Macromolecules*, 1987, **20**, pp 2471-2474.

Chapter 6.

Degradation of Acrylic coated PET Films

6.1. Introduction.

Polymer feed stocks for PET film lines consists of two main types. The majority, (~70%), is virgin material, i.e. polymer which has not seen any previous melt processing, other than the final stages of polycondensation. A smaller proportion of feed stock, (~30%), is recovered material, i.e. polymer derived from a reclaim procedure, and hence can be considered to be second generation, and as such will generally exhibit a lower molecular weight, a higher degree of colour formation and have a higher level of contamination [1].

If this reclaim polymer is derived from film which was wholly or partially coated, (from, for instance, a sample which had failed quality control inspection), the apparent level of degradation is increased further [2]. Therefore, an important aspect of the recovery of PET film is the effect of coatings on their reclaimability [3].

A plethora of literature concerning the degradation of PET exists, in all its aspects, and a review of the degradation of PET was given in chapter 2. However, very little of this work pertains to the effect of inclusions and contamination, which a surface coating is considered to be during a reclaim cycle. The extent of this inclusion is easily illustrated with a simple calculation.

Consider a sheet of finished PET film 100μm thick, and coated on one side with a typical acrylic / melamine coating of 400Å thickness. Given a PET film density of 1.395 g/cm^3, and a coating density of 1.15 g/cm^3 then the weight of coating included during recycle can be calculated.

For a 1cm^2 sheet of film the weight of PET is given by $(1\times1\times100\times10^{-4}) \times 1.395 = 0.01395$g, and the weight of acrylic is given by $(1\times1\times40\times10^{-8}) \times 1.15 = 4.6 \times 10^{-6}$ g.

The weight ratio is therefore $4.6\times10^{-6} / 1.395\times10^{-2} = 3.29\times10^{-4}$, or 329 ppm.

On first consideration this would seem to be too small an amount of material to cause any adverse effects. However, similar amounts of 'contamination', in the form of catalyst residues and polymer additives, have been shown to exert a large influence on the stability and chemistry of PET [4,5] Obviously, such a small concentration could not be detected during the gross degradation of PET, normally measured by weight loss or end group concentration. In this study the inclusion of such contamination is investigated in terms of its effect on the degradation of PET. For instance, the coating may cause an increase in the rate of chain scission of PET, by some catalytic effect, or may cause an increase in the formation of crosslinked or gel structures. The purpose of these experiments is to determine the extent to which the presence of an acrylic based coating increases the apparent degradation of PET during a simulated reclaim cycle. To this effect, three approaches were adopted. Firstly, model coating formulations, of increasing complexity were coated and degraded, and compared to uncoated and real coatings, prepared and treated in the same way. Secondly, the concentration of the components used in coating formulations was investigated to ascertain the extent to which coating formulation differences influenced the recycle of such coated products. Finally, in order to test the validity of this approach, the results of the laboratory experiment were compared to an industrial reclaim procedure.

In order to investigate the degradation of PET film in the laboratory, small scale simulations of the coating and reclaim operations were developed. The coating simulation used a model coating formulation based on a PMMA latex. These model coating formulations were compared to real coating formulations with respect to their 'reclaimability'.

It is not intended to elucidate the exact mechanisms by which a coating interacts with PET during a degradation procedure. However, it will be necessary to refer to certain mechanisms and theories, and it is hoped that the results obtained here will indicate which of the many diverse theories apply under the conditions of these experiments.

6.2 Experimental

6.2.1. Experimental Protocol

In order to test the effect that the presence of a coating has upon the melt degradation of PET films, three experiments were considered. Firstly, the identification of the coating components responsible for the apparent increase in degradation was considered. To do this, coatings of increasing complexity would need to applied to PET films and the subsequent degradation behaviour measured. Secondly, the effect of varying the concentration of selected coating components would be determined, by judicious choice of coat weight and sample formulation variation. Thirdly, these tests would need to be validated against an industrial scale experiment in order to confirm their applicability. Therefore, the three experiments attempted here can be summarised as follows;

(I) Identification of coating component responsible for the apparent increase in PET degradation

(II) Determination of the effect of varying the concentration of coating components.

(III) Compare laboratory and Industrial scale procedures

6.2.2. Materials and Sample Preparation

Base Film

Biaxially drawn film was prepared on the DuPontTeijin Films Ltd. Semi -Tech facility Wilton, UK. This film was used as the base film for all the experimentation subsequently described. The film was produced from standard, unfilled polymer (grade E47). Details of the polymer and film properties are given in table 6.1. The process of film manufacture by sequential biaxial stretching has been described in chapter 1.

Table 6.1. Polymer and film properties for standard base film manufacture.

Polymer		Film	
Property	Value	Property	Value
Batch code	E47	Batch code	MH/34
IV	0.65	IV	0.6
Av. chip weight	50 mg	Density	1.396 g/cm^3
Density	1.334 g/cm^3	Thickness	101μm
colour	clear	Draw ratios	MD 3.3, TD 3.5
DEG conc. w/w%	1.85	Haze	~0.5%
Caltalyst	330 ppm Sb	Tensile strength	23 Kgf/mm^2
T_g, T_m	350K, 525K	T_m	534k

Coating Materials

A PMMA latex was prepared via a free radical emulsion polymerisation in aqueous media. Sodium dodecyl sulphate was used as the emulsifying agent and potassium per sulphate was used as the free radical initiator. 50ml of methyl methacrylate monomer (99.995% ICI Acrylics), was used in a total volume of 1000ml. The solids content of this latex was 21.45% (w/w). Water used for the polymerisation and for further formulation was demineralised and degassed. This PMMA latex was used as a model for the lattices commonly used for industrial treatments.

Other coating materials were used as supplied. These additives are listed in table 6.2, indicating their function and nominal level.

Coating Formulations

Several coating formulations were prepared, with a view to investigating the parameters of interest. These were all made to 100ml volume. The formulations are listed in table 6.3. All formulations were based upon a PMMA solids content of 5% (w/w). Other components were added as concentrated aqueous solutions, prepared accurately prior to formulation. The required mass of additive for each solution is indicated in the appropriate column. Errors are based upon the experimental errors in weighing the additives and pipetting the subsequent solutions.

Table 6.2. Coating formulation additives.

Name	Structure	Type	Typical concentration
Tri - methylated methyl melamine resin TMMM 'Cymel 350' Cytec INC.	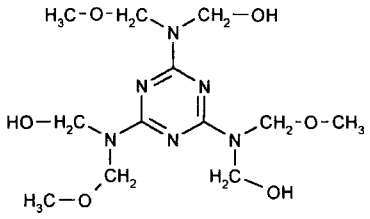	Acid catalysed crosslinker	10-15% of overall solids content (0.015M)
Ammonium *p* Toluene sulfonic acid APTSA Aldrich Cem. Co.	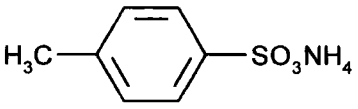	crosslinker catalyst	10% of crosslinker level (0.003M)
Nonyl Phenol ethoxylate 'Synperonic NP10' ICI Plc.	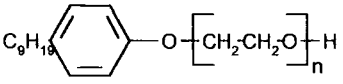	surfactant / wetting agent	2g / litre (0.0035M)

Table 6.3. Coating formulation details

Formulation No.	Conc. Coating component			
	Synp. NP10	PMMA	TMMM	APTSA
1	2g / litre			
2	2g / litre	23.36g		
3	2g / litre	23.36g	0.5g	
4	2g / litre	23.36g	0.5g	0.05g
5	2g / litre	AC201*		0.05g
6	2g / litre	23.36g	0.05g	
7	2g / litre	23.36g	0.25g	
8	2g / litre	23.36g	2.5g	
9	2g / litre	23.36g	5.0g	
10	2g / litre	23.36g	0.5g	0.01g
11	2g / litre	23.36g	0.5g	0.025g
12	2g / litre	23.36g	0.5g	0.25g
13	2g / litre	23.36g	0.5g	0.5g
Error	0.01g	0.01g	0.001g	0.001g

* AC201 is an acrylic based terpolymer in latex form, and is commonly used in many coatings in DuPont Teijin Films Inc. The formulation of AC201 includes ~ 12% TMMM.

Coated film samples

A4 sized samples were coated using the standard draw down technique [6]. A No. 1. Meyer bar was used which deposits approx. ~6μm wet coat thickness. The A4 sheets were clamped in a frame and immediately transferred to an oven, in which the samples were dried for 90 sec. at 453K. Table 6.4. shows the characteristics of the coated samples prepared. 20-30 A4 sheets of each coating were prepared. An uncoated set of samples was also prepared by the method described above.

Table 6.4 Coated samples prepared by hand draw coating.

	Formulation	No.	Coat thickness *	sample designation
Increasing Formulation complexity	None	S0		Uncoated
	1	S1	~5 nm	Wash coated
	2	S2	100 nm	PMMA coated
	3	S3		PMMA + TMMM
	4	S4		Full model
	5	S5	90 nm	Real Coating

	Formulation	No.	Coat Thickness	Sample designation
Variations in crosslinker conc.	6	S6	99 nm	TMMM 1
	7	S7		TMMM 2
	3	S3	101 nm	TMMM 3
	8	S8		TMMM 4
	9	S9	117 nm	TMMM 5
Variations in crosslinker catalyst level	10	S10		APTSA 1
	11	S11	105 nm	APTSA 2
	4	S4		APTSA 3
	12	S12	109 nm	APTSA 4
	13	S13		APTSA 5

* Measured by ellipsometry

6.2.3. Controlled Degradation

Samples were degraded in air, (thermoxidative degradation), using a specifically built apparatus hereafter referred to as the 'Hot block'. The design of this apparatus is shown in figure 6.2.

Film samples were cut into squares approx. 5 mm^2 and placed into aluminium dishes, ready for placement on the hot block. The samples were then dried for 4 hrs at

393K under constant vacuum, to ensure no influence on degradation came from hydrolysis, or low temperature thermoxidative degradation [7]. The samples were weighed and placed onto the hot block, ensuring the aluminium sample pans made intimate contact with the hot block surface. The samples were degraded for a specified time, removed from the hot block and immediately quenched in liquid N_2. The samples were removed from the aluminium dishes and homogenised by cryogenic grinding.

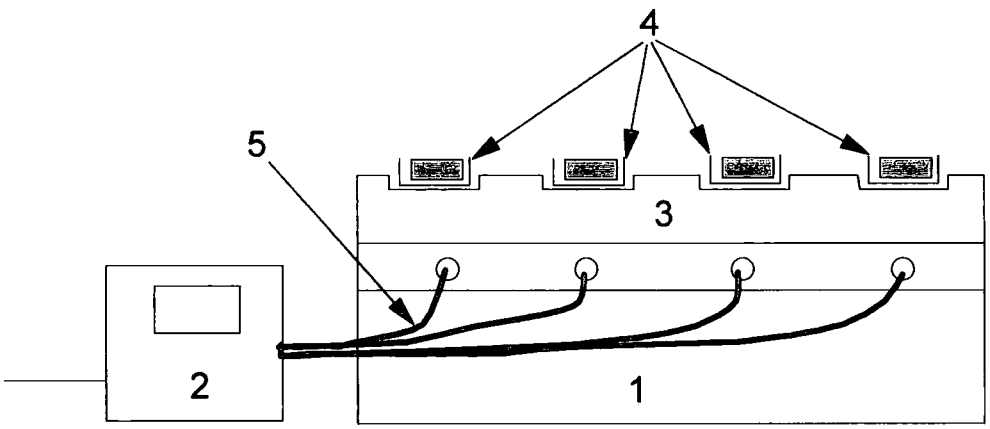

Figure 6.2. Hot block degradation apparatus. 1) Ceramic insulating base. 2) Control unit. 3) Aluminium heating plate. 4) Aluminium sample dishes. 5) Thermocouple leads.

6.2.4. Large Scale Experiments

The laboratory scale experiment described above was validated by comparison with an industrial scale procedure, in which film was recycled on an industrial scale. To do this coated and uncoated films were manufactured on the DuPont Teijin Films Inc. Semi-Tech facility, Wilton, UK.

200 Kg of uncoated and coated film were manufactured. The uncoated film was the same as the base film used in the laboratory scale experimentation, and its characteristics are described in table 6.1. The coated film was produced by interdraw coating MH/34 film (interdraw coating is described in detail in chapter 1). The relevant characteristics of the coated film are shown in table 6.5

Table 6.5. Interdraw coating characteristics

Coating Formulation	S5 (AC201 based)
Applicator speed	100 % Line speed
Av. wet coat thickness	6 μ
measured coat thickness	51 nm

The two films were cut into flake using a Masson cutter [8], equipped with a 6mm filter grid and operating at 4000 rpm. The flake produced by this procedure had a bulk density of 0.75 g/cm^3, and was segregated by a conventional air mover. This flake was dried for 4 hrs at 453K in an air circulating oven, and then re-extruded in a single screw extruder. The resultant melt was cast and quenched in the standard manner, using a water filled casting trough, and was cut into chip using an automated pellitiser. This chip produced by this 'reclaim' operation was then dried and re-extruded in the same manner. This cycle was repeated three times . The configuration and standard conditions for the extruder are shown in table 6.6. A schematic representation of the reclaim procedure is given in figure 6.3. Samples of polymer chip were taken for characterisation, after each cycle of this experiment.

It must be noted that there are important difference between the laboratory and industrial scale reclaim procedures. The coating applied in the laboratory simulation was twice as thick as the coating applied by interdraw coating, which has obvious consequences in the light of the calculation described in section 6.1. It is assumed that vacuum drying is very much more efficient than air drying. Jabarin and Lofgren have shown that drying PET in air increases the molecular weight degradation during subsequent extrusion, and this has been attributed to the occurrence of low temperature thermo-oxidation and hydrolysis [9]. Another significant difference between the two experiments, is the manner in which melt degradation was achieved. During extrusion, polymers are subjected to phenomena such as mechanical shear and increased pressure, and are additionally heated by frictional forces within the extrusion equipment [10]. In the laboratory, the samples remained unmixed and hence the polymer did not experience any shear during melt degradation.

Table 6.6. Extruder configuration and extrusion condition.

Screw Diameter	53 mm
Barrel length	1050 mm
Screw Speed	60 rpm
Barrel temperature	558K
Av. residence time	6 min.
Output	12 Kg / hr
Av. chip size	~50 mg

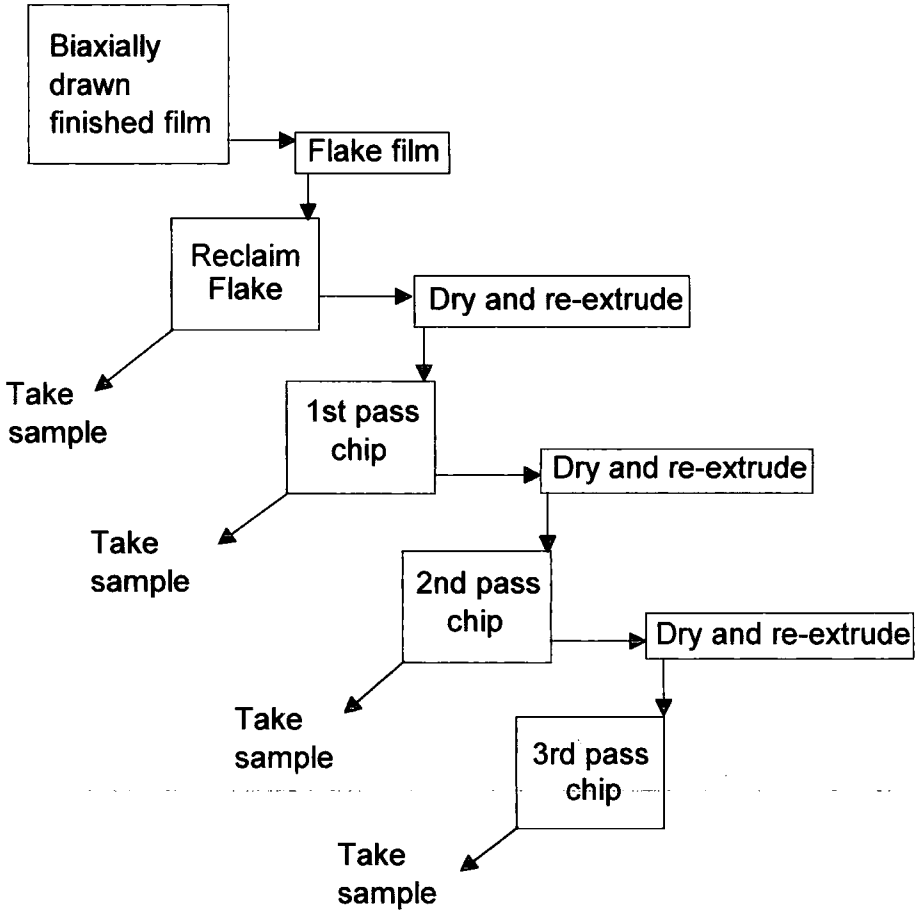

Figure 6.3. Schematic representation of reclaim experiment.

6.2.5. Characterisation and Analysis.

Weight loss

Weight loss was calculated by gross difference between initial and final mass of samples. This has been a popular, informative yet simple method of following degradation [9, 11 - 15]. This test was only used for the laboratory experiment, as mass reduction cannot be assessed by extrusion.

GPC

Change in molecular weight and molecular weight distribution was measured using gel permeation chromatography. Molecular weights were established against a polystyrene standard, and hence values quoted for these experiments are for polystyrene equivalent molecular weights. A typical chromatogram for PET is shown in figure 6.4. The column packing was crosslinked polystyrene (Shodex AT 80 M/S), and the column oven was set to 393K throughout the analysis. Samples were dissolved in distilled OCP (Aldrich Chem. Co. Ltd UK.) at a concentration of approx. ~0.25 % (w/v). Refractive index detection was used.

UV / visible spectrophotometry

The colour change due to thermoxidative degradation was monitored by inspection of the UV - visible spectrum of the degraded samples. 0.25 g of sample was dissolved in 1,1,1,3,3,3 - Hexafluoroisopropanol (HFIP), This solution was filtered in order to determine the mass of insoluble material (see later). 1 ml of this solution was then made up to 25 ml with chloroform (99.95% Aldrich chem. Co. Ltd UK), and this solution shaken for 30 min. The UV / visible spectrum was recorded on a Shimadzu 160A double beam spectrophotometer, using a base line correction for 4% HFIP in chloroform. The UV / visible absorption spectra for the degraded uncoated samples are shown in figure 6.5. As can be seen, the major differences in spectra are seen at 200 - 400nm. This is typical for discolouration of polyesters. The absorption at 335 nm was used as the wavelength most sensitive to discolouration. This region of the visible spectrum has proven to be the most sensitive to discolouration in aromatic polyesters [16,17,18]. Values for the absorption at 330 nm, normalised to the concentration of PET, are shown in table 6.7.

Gel formation

The propensity for gel formation was estimated by measuring the mass of insoluble material in each sample. This was done by filtering the solutions used for UV / visible spectroscopy, (see above). The mass of insoluble material is taken as gel for the purposes of this experiment, and this method has been used for PET by several other workers [19,20].

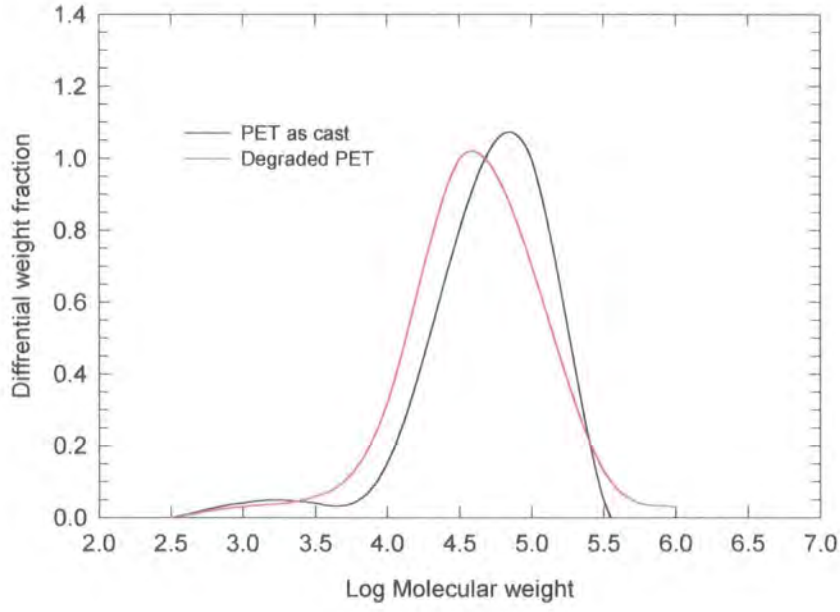

Figure 6.4. GPC chromatagram of PET as cast and degraded

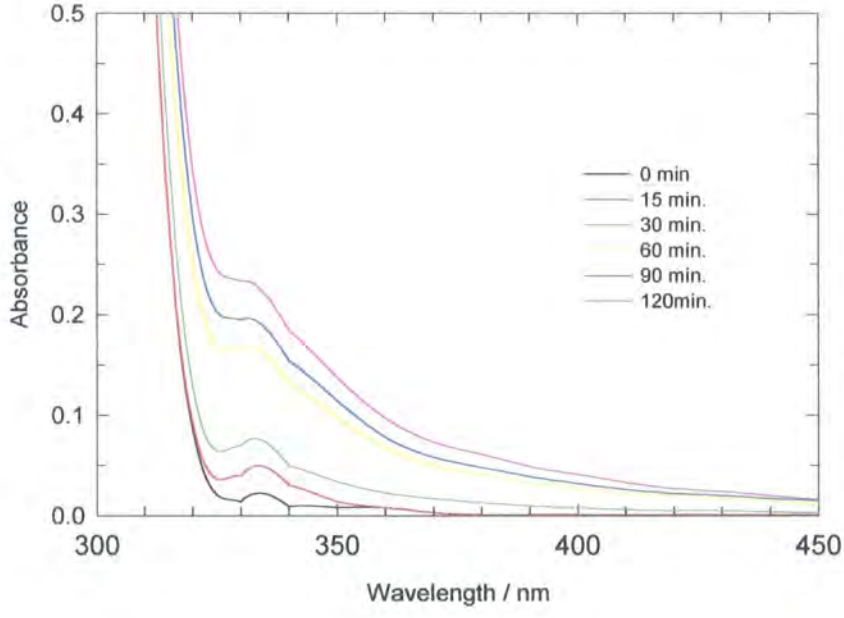

Figure 6.5. UV / visible spectra for degraded uncoated samples .

6.3. Results and Discussion.

6.3.1 Identification of Components Responsible for the Apparent Increase in Degradation.

Weight loss

The weight loss for samples S0 - S5 is shown in figures 6.6 and 6.7. In figure 6.6, the % mass reduction is plotted against degradation time; in figure 6.7 the weight loss is plotted according to the 1st order expression described by Zimmermann and Schanf [21];

$$\ln\left(\frac{w_t}{w_{t0}}\right) = -kt \qquad (6.1)$$

where w_0 is the initial weight of the sample, w_t is the weight of sample at time t, and k is the rate constant for the reaction.

From figure 6.6 and 6.7 we see that the data is equally well described by either a zero order or a 1st order rate law for all samples. The thermo-oxidative degradation of PET is thought to be a first order process, although the exact kinetics of degradation are dependant upon the parameter used to follow degradation [22,23]. For example, Halek has shown that the generation of acetaldehyde, which leads to weight loss is a zero order process [24], whereas several other workers have shown that weight loss from PET is a 1st order process [22,23,25]. The rate constants for samples S0 - S5 are calculated from the slopes of the linear regression fits, and are identical within experimental error of $(3.1\pm0.1) \times 10^{-6}$ s^{-1}.

Table 6.8. Rate constants for weight loss of samples S0 - S5 for a 1st order reaction.

Sample	Rate constant / s^{-1}
Uncoated (S0)	3.1×10^{-6}
Wash coated (S1)	3.2×10^{-6}
PMMA coated (S2)	3.1×10^{-6}
PMMA + TMMM (S3)	3.0×10^{-6}
Full model (S4)	3.1×10^{-6}
Real coating (S5)	3.0×10^{-6}

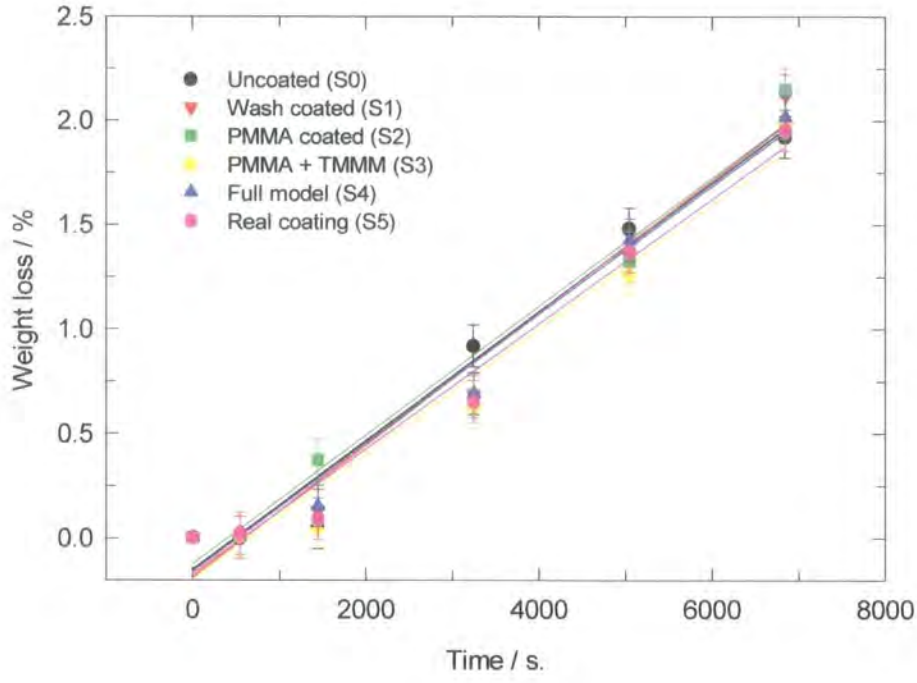

Figure 6.6. Weight loss plotted as a 0 order reaction for S0-S5

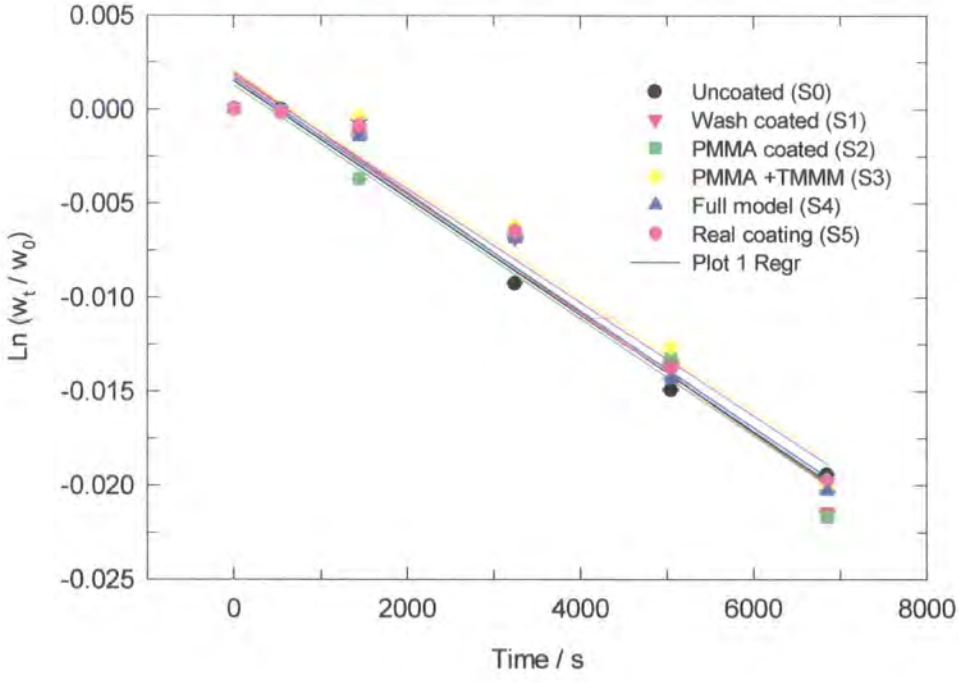

Figure 6.7. Weight loss plotted as a 1st order reaction for S0 - S5

By inspection of the data published by Jabarin and Lofgren [9], a comparison of degradation isotherms can be made. Their studies yield an approximate rate constant for thermo-oxidative weight loss of 2.8×10^{-5} s^{-1} at 553K and 1.2×10^{-4} s^{-1} at 573K, which are, respectively, one and two orders of magnitude faster than the results obtained here. However, Jabarin and Lofgren also show that the rate of weight loss is significantly reduced for samples which have been dried under vacuum prior to thermo-oxidative degradation, as is the case here. For this case they found a rate constant of 4.3×10^{-5} s^{-1} at 563K, which is still an order of magnitude greater than the rate constants for samples S0 - S5. The lower rate of weight loss in this study is attributed to the much higher experimental sample mass (~3g), and to the nature and form of the sample. Jabarin and Lofgren used commercial PET chip and as such it will have seen no previous melt processing history. The samples used in this study are biaxially finished films which have seen a drying process (453K, 4 hrs), an extrusion process (~558K, 20 min.), and several heating and stretching stages throughout the film making process. It is envisioned that the low molecular weight materials which account for the majority of weight loss upon degradation [11-15], are no longer present in the film, having being evolved in the drying, extrusion and filming process stages.

To test this assumption, a weight loss test of 'virgin' polymer chip and uncoated film was undertaken at 563K. The results are shown in figure 6.8. As can be seen PET chip displays a higher rate of weight loss than film , and this is attributed to the arguments given above. The initial slope ($t < 3600\ s$), yields a rate constant of 3.5×10^{-5} s^{-1}, which is in good agreement with the results of Jabarin and Lofgren.

For comparative purposes the data shows that there exists no difference between the weight loss of the samples in this study, hence a broad conclusion is that the mechanisms leading to weight loss have not been significantly effected by the presence of coatings. This is not surprising; the mechanisms which lead to weight loss in PET are thought to be chain end dependant [11,13,15], and as the PET is in great excess to the coating, chain end concentrations should be the same for all the samples in this experiment.

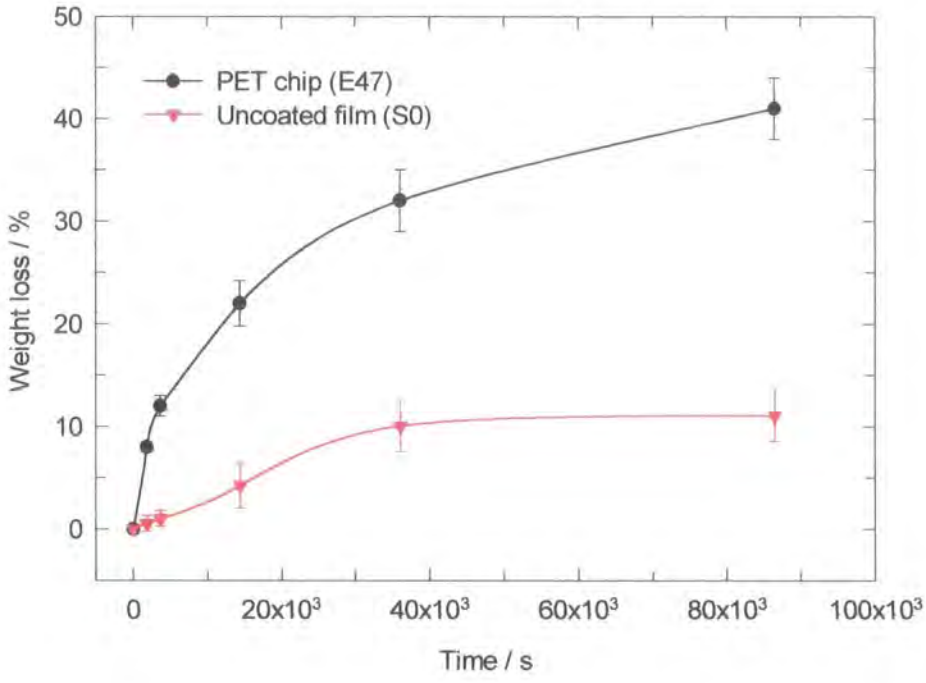

Figure 6.8. Comparisons of thermo-oxidative weight loss of PET chip (E47) and film at 563K

Molecular weight loss

The degradation of PET films with respects to the change in molecular weight and molecular weight distribution, is now considered. The molecular weight degradation has been shown to follow the following rate law for a random scission process [26];

$$\frac{1}{N_t} - \frac{1}{N_0} = k_1 t \qquad (6.2)$$

where N_t is the number average degree of polymerisation at time t, N_0 is the initial number average degree of polymerisation, and k_1 is the rate constant for the reaction. Hence the rate constant k_1 can be extracted from a plot of $1/N_t$ - $1/N_0$ vs t (see figure 6.9)

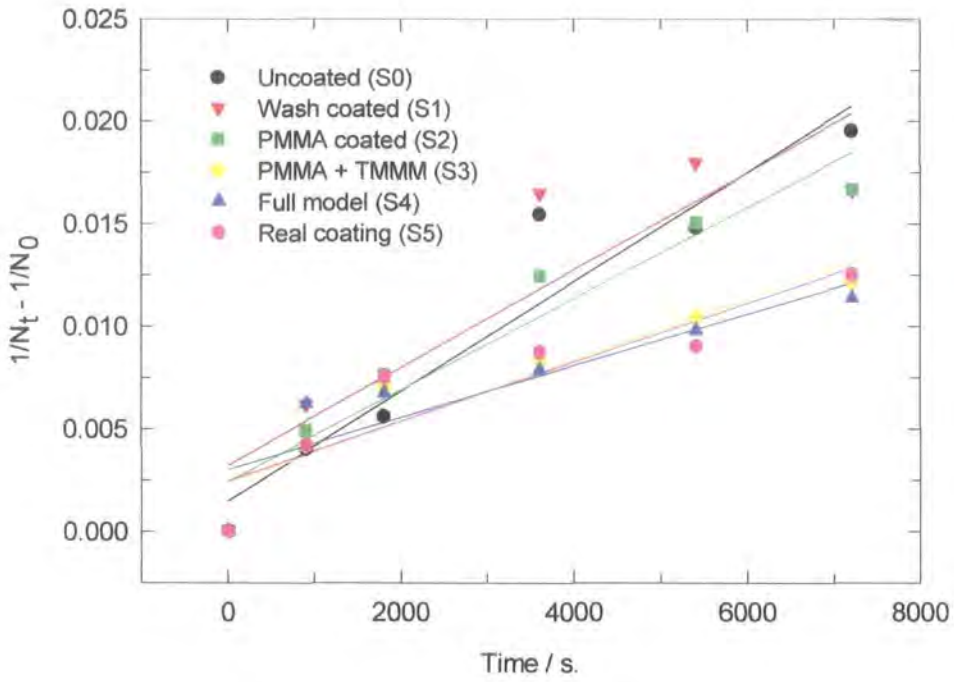

Figure 6.9. Rate of M_N degradation for samples S0 - S5 for $t < 7200$ s Note the demarcation between samples with and without TMMM.

The rates of chain scission is calculated from the slope of the linear regression fit to the data for each sample and these are shown in table 6.9. The rate of chain scission for melt degradation under a N_2 has been studied by Jabarin and Lofgren and is approximately one order of magnitude lower than the results obtained in this study. They state that equation 6.2 cannot be used in the case of melt degradation in air as the chain scission will not be random. However, other workers have used the relationship successfully.

Peiyuan and Rongrui [23], have studied the molecular weight degradation by following iv. (intrinsic viscosity) through a controlled regime of thermal degradation, at 558K. For a system incorporating a butyl titanate polycondensation catalyst they obtained values of k of ~2-3×10^{-6} s^{-1}, depending on the concentration of phosphoric acid stabiliser added after esterification. This is in good agreement with the results obtained here for samples S0, S1 and S3, despite the difference in degradation temperature.

Table 6.9. Rate constants for random scission approximation.

Sample	k / s^{-1}
Uncoated (S0)	2.5×10^{-6}
Wash coated (S1)	2.5×10^{-6}
PMMA coated (S2)	2.3×10^{-6}
PMMA + TMMM (S3)	1.4×10^{-6}
Full model (S4)	1.2×10^{-6}
Real coating (S5)	1.4×10^{-6}

However, it is also apparent from figure 6.9 that a linear regression does not yield an adequate kinetic description of this data. This is further compounded by inclusion of the data for longer degradation times. By analysing the molecular weights of samples degraded for 4 and 18 hours we are able to refine the model for the kinetics of degradation. The simple analysis adopted for degradation times < 2 hours is now inadequate, and the rate of degradation is significantly altered during this degradation regime (see figure 6.10). The analysis of degradation kinetics over longer periods will be discussed later.

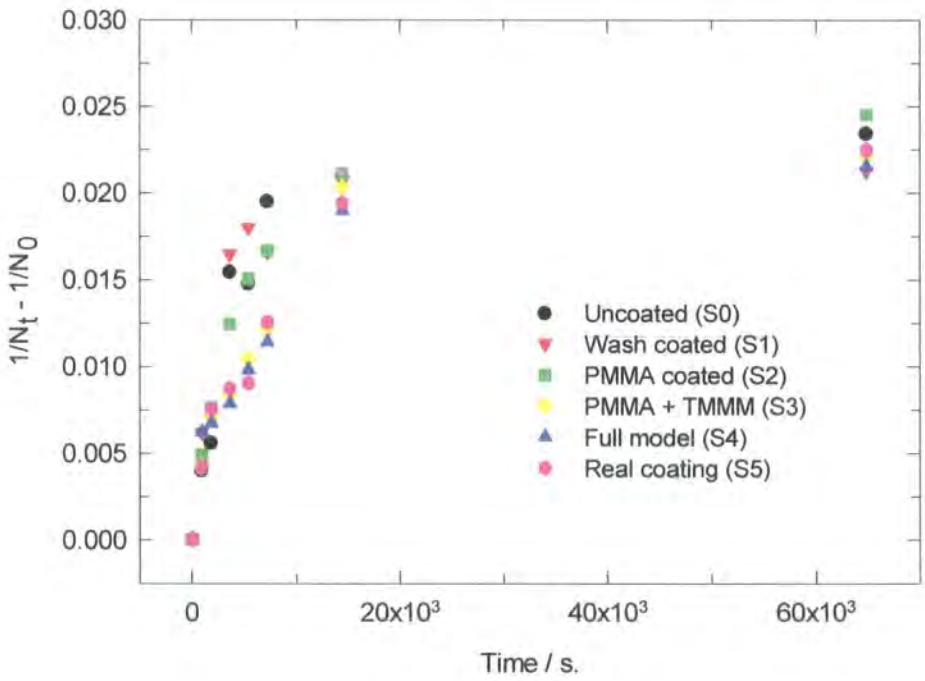

Figure 6.10. Rate of chain scission for longer term degradation. Error bars have been omitted from the plot to aid visualisation.

It is quite clear that the addition of crosslinking agents to the coating formulation (samples S3-S5) has had a profound effect on the degradation rate of PET films., and this will be discussed later, with reference to the possible mechanisms of interaction.

UV / visible spectroscopy

The spectra show a characteristic peak at ~295-305 nm due to the absorption of the terephthalate ring in the PET backbone. During the degradation of these samples, the spectra were seen to change in a predictable fashion. The absorption attributed to the aromatic component of PET was seen to broaden at both shorter and longer wavelengths. However, the most significant difference were observed between 320 and 350 nm (i.e. red shifted). This phenomena has been observed by several workers studying the degradation of polyesters. The spectra shown here displayed remarkable similarity to those of Tabankia and Gardette [16] who have studied the discolouration of PBT by photo-oxidation. The sensitivity of this region of the visible spectrum to changes in colour of PET has also been shown by other workers, and is now believed to be due to the formation of mono and disubstituted hydroxy terephthalate moieties [17,18,27,28]. Here we have seen a typical increase in the absorption at 330 nm for samples S0-S5., and the absorbance is plotted against the degradation time (figure 6.11). It is evident from this plot that no appreciable differences are seen between the samples. The lower absorption of the S2 cannot be adequately explained by any physical phenomena apparent in the sample, and as such this result is considered to be erroneous.

The lack of sensitivity of the analysis to the colour changes between samples S0-S5 is on first reflection surprising. A visual inspection of the samples showed that the samples with more complex coating formulations (particularly S4 and S5) were more intensely coloured, and it was hoped that this would become apparent from the spectral characterisation. Apparently some of the discoloured polymer is not dissolved, presumably because it is crosslinked, in samples S4 and S5, and thus the spectrometry records apparently little difference.

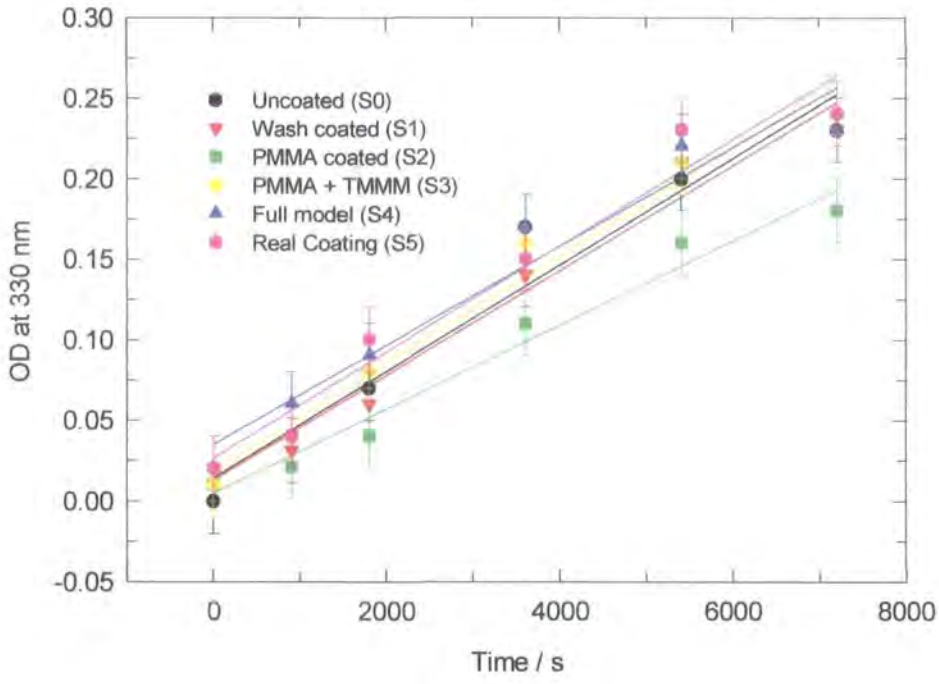

Figure 6.11 Increase in absorbance at 330 nm with increasing degradation time for samples S0-S5

Gel formation

The extent to which insoluble material is examined in samples S0-S5. Gel formation in PET is known to be the result of free radical interactions on the polymer backbone [19,20,25,29]. The gel formation as a result of irradiation of the polymer has been studied many times and electron spin resonance studies have identified specific radicals [18]. The rate of gel formation of samples S0-S5 is shown in figure 6.12. It has been assumed that this is a 1st order reaction, and follows the rate law,

$$\ln\left(\frac{a}{a-x}\right) = kt \qquad (6.3)$$

It can be seen from figure 6.12 that there is a greater propensity for gel formation in the samples S3-S5, again indicating that the presence of a formulated coating including TMMM, influences the degradation chemistry of PET in a discernible and observable way. This result has quite obvious implications for film manufacture. Table 6.10. lists the values of k for gel formation

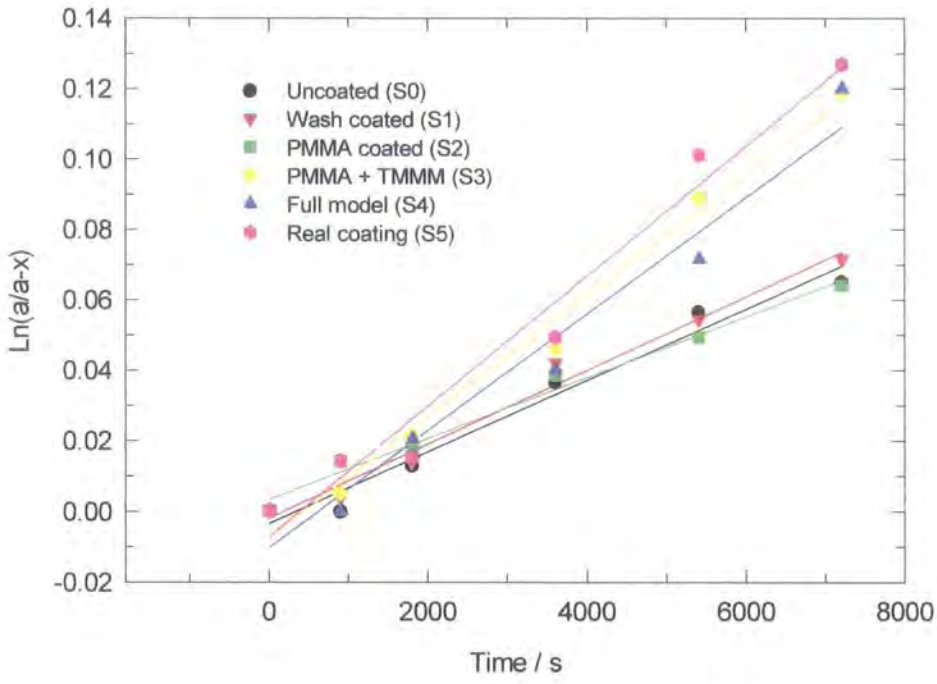

Figure 6.12. Rate of increase of gel formation for samples S0-S5 plotted as a first order reaction

Table 6.10. Rate constants, k for gel formation in samples S0-S5 (1st order reaction)

Sample	k / s^{-1}
S0	1.01×10^{-5}
S1	1.05×10^{-5}
S2	8.64×10^{-6}
S3	1.72×10^{-5}
S4	1.65×10^{-5}
S5	1.85×10^{-5}

It must be noted that the data for gel formation fits equally well to a second order rate law, yielding rate constants almost identical in magnitude. It is assumed that the simplest case applies, and the gel formation is a 1st, or pseudo 1st order reaction. A kinetic treatment of gel formation in PET has not been found in the literature, hence comparison with previous work is impossible in this respect. However, Yoda *et al* [19], have reported on the time dependency of gel formation at 573K as a function of polymerisation catalyst used. A treatment of these results comparable to that of Yoda *et al* will be made in section 6.4

Conclusions

The rate constants for degradation over a 2 hr. period have been found to be within the range covered by previous studies. Weight loss from film has been shown to be significantly reduced compared to 'virgin' chip.

The inclusion of a simple PMMA coating does not significantly alter the chain scission rate constant, and does not appear to alter the physical characteristics of the degraded product (gel content or colour), to any measurable degree. This implies very little interaction between the PET and PMMA during the degradation cycle. Previous chapters in this thesis have shown that the major chemical change in PMMA at PET process temperatures is depolymerisation and subsequent volatilisation of the low molecular weight product.

We have seen that the inclusion of TMMM, the standard crosslinking agent used in coating formulations, has a profound effect upon the rate of thermo-oxidative chain scission of the subsequent coated film, with respect to an equivalent uncoated film. This effect is only apparent after 30 minutes degradation at 563K and is not due to an alteration of the mechanisms which lead to weight loss.

Differences in the rate of colour formation have not been detected by UV / visible spectroscopy, although visually there was a more intense discolouration of those samples which included APTSA, (S4 and S5). However, the gel formation over 2 hours degradation does highlight a difference between samples, again showing that the inclusion of TMMM influences the measured rate with respect to uncoated and non-TMMM containing samples.

6.3.2. Variations in Concentrations of Additives

Inspection of the previous results shows that the most significant changes in degradation are due to the addition of TMMM and APTSA to the relevant coating formulation. Variations in the concentration of these additive in the coating formulations are now considered with respect to the kinetics of molecular weight degradation, gel formation and discolouration.

Effect of TMMM concentration in coating formulation on chain scission during degradation

As can be seen from figure 6.13. there appears to be a gradual increase in the observed molecular weights which is particularly apparent for the weight average value, for increasing concentrations of TMMM in the coating formulations. The concentrations of TMMM used in the respective coating formulations for each sample are within the range commonly used for industrial coating processes [30], so the result is particularly relevant in that aspect. However, the nature of the interaction of the TMMM / coating / PET system is not evident from this analysis. Again it can be postulated that certain mechanisms, such as chain extension or radical entrapment, are in evidence, but without more detailed characterisation, an area beyond the scope of this thesis, only speculation based on circumstantial evidence can be made. Some of the possible mechanisms will be discussed in the next section.

Effect of APTSA concentration in coating formulation on Chain scission during degradation

Figure 6.14. shows the observed molecular weights for samples S10-S13. degraded for 30 minutes at 563K. The concentrations of APTSA used in the relevant coating formulations are within the range commonly used in industry, and show that there a variation in concentration of this species does not affect the molecular weight upon degradation. The observed values are therefore considered to be the result of a statistical distribution, of samples with the same molecular weights within the error of the measurement technique, (GPC). Note that the concentration of APTSA in the coating formulation is typically an order of magnitude lower than the concentration of TMMM.

Although there appears to be little effect on the rate of chain scission after 30 min. at 563K, the effect on the discolouration of these samples was also investigated in the manner described for samples S0-S5. The results of this are shown in figure 6.15.

In this case, the absorption at 400 nm was used to differentiate between the samples. Although the absorption at 330 nm was seen to increase with APTSA concentration, the differences were much more pronounced at the longer wavelength. Figure 6.15. shows this difference adequately, although the linear fit to the absorption data is perhaps an oversimplification of the response.

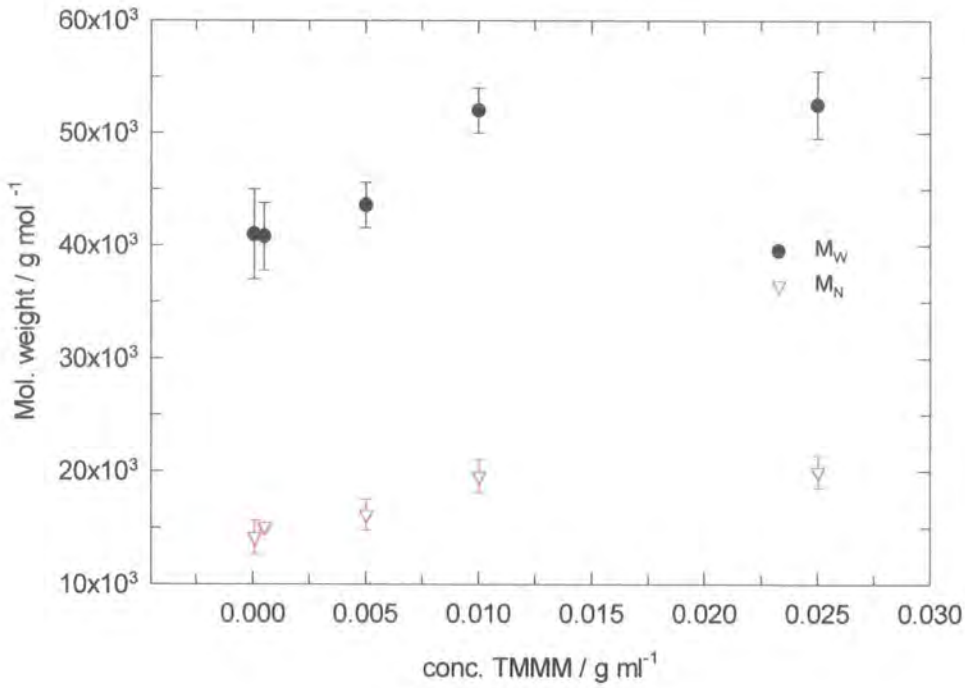

Figure 6.13 Molecular weight vs. concentration of TMMM in coating solution for 30 minutes degradation at 563K.

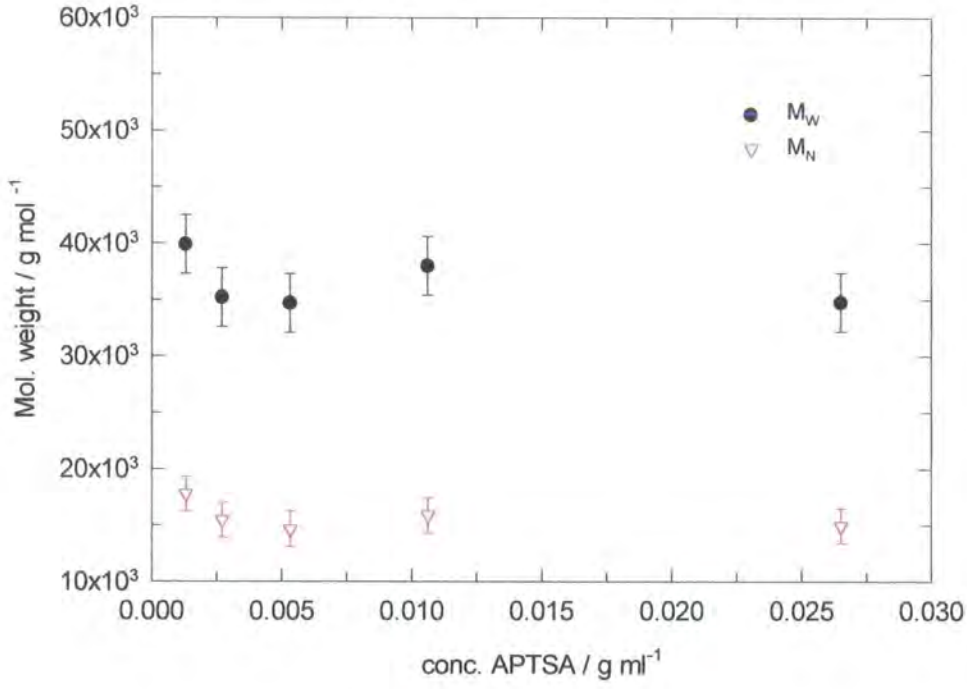

Figure 6.14 Molecular weight vs. concentration of of APTSA in coating solution for 30 minutes degradation at 563K.

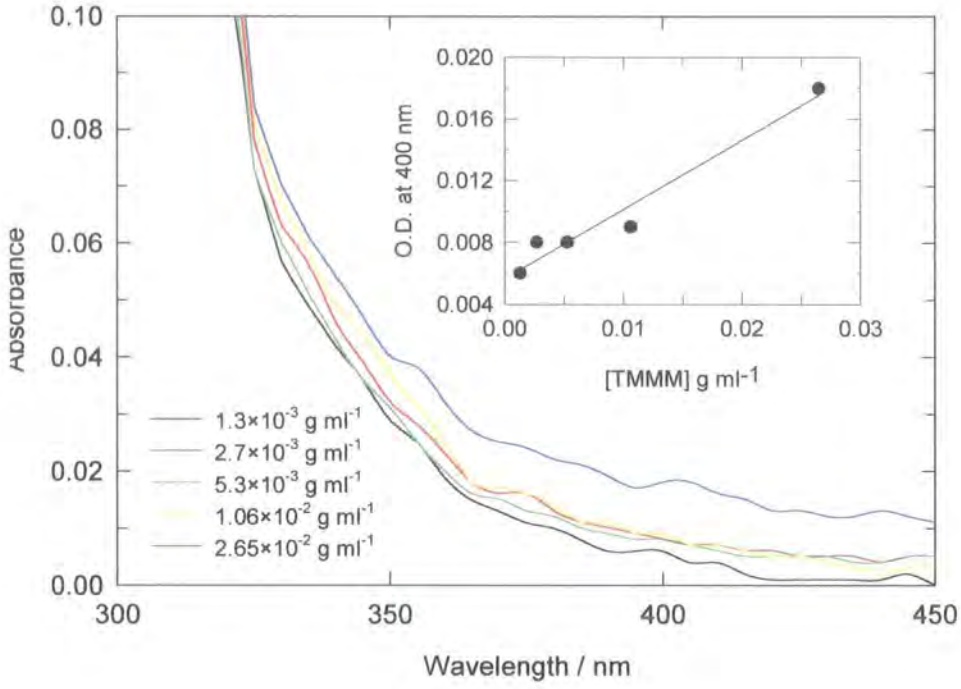

Figure 6.15. UV / visible spectra for samples S10-S13 (APTSA variants) showing increase in optical density at ~400 nm for highest conc. of APTSA

Gel content as a function of additive concentration.

Figure 6.16. shows the measured insoluble content of the two sets of samples S6-S9 (TMMM variants) and S10-S13 (APTSA variants). There appears to be an appreciable increase in gel content at the extremes of concentration for the TMMM additive only. An increase in the gel content at the highest APTSA level cannot be defined within error. The errors in measurement render the observed relationship between TMMM concentration and gel content somewhat uncertain, and hence it would be futile to try to elucidate a quantitative formula which expresses this relationship.

These results are limited in that only short term degradation (< 30 min.) has been investigated. With comparison to the results seen for samples S0-S5, it is assumed that much larger increases in gel formation would be seen, particularly for samples containing the highest levels of additives (S9 and S13).

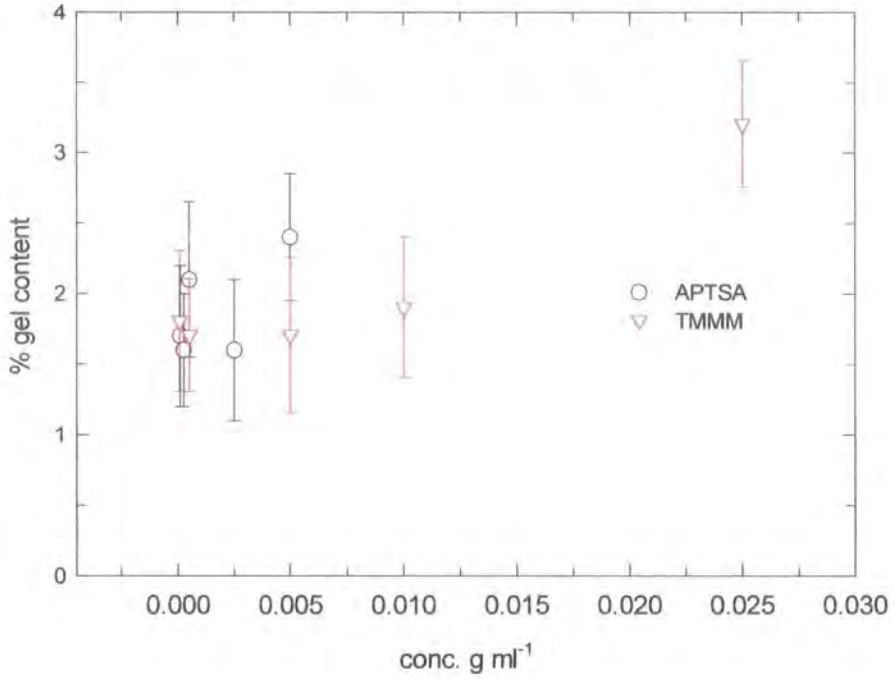

Figure 6.16. gel content of degraded PET films as a function of concentration of additive.

Conclusions

An increase in the concentration of TMMM in the coating formulation causes a decrease in the observed rate of chain scission after 30 min. degradation at 563K. Appropriate variations in the concentration of crosslinker catalyst, APTSA, have no significant effect on the rate of chain scission after this time. However, an increase APTSA concentration causes an increase in absorption at 400 nm indicating an increase in yellow colouration of the degraded film. This increase in discolouration is only significant at the highest concentration of APTSA investigated, although this level is within the range used for industrial formulations.

Variations in TMMM and APTSA concentration cause an increase in the propensity for gel formation, only at the highest concentrations used in this experiment.

6.3.3. Larger Scale Experiments.

The results of the comparative experiments described in section 6.2 are now discussed. the validation of the laboratory procedure is made by comparison with less well controlled experiments using typical reclamation equipment used for industrial recycle procedures.

The chain scission expression used to determine the rate constants for molecular weight degradation is applied here with respect to the number of process cycles experienced by the polymer. This result is shown in figure 6.17.

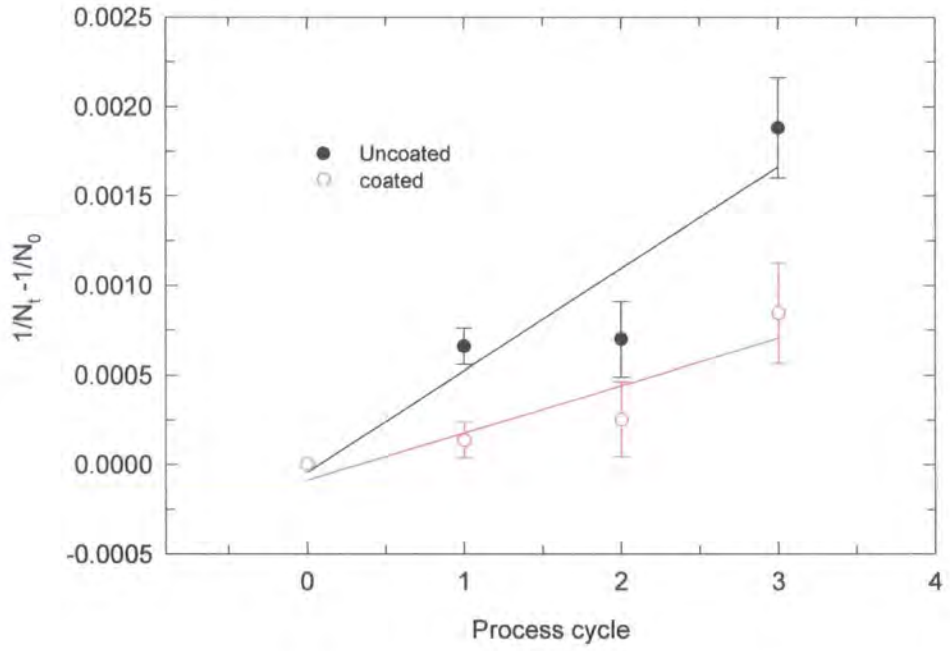

Figure 6.17. Rate of chain scission foe each process cycle for coated and uncoated samples.

Figure 6.17. clearly shows that the coated film displays the same characteristic reduction in rate of chain scission as the formulated films used in the laboratory. This goes some way towards validating the laboratory procedure, but also highlights some of the differences between the two approaches. The estimated time under melt conditions is very much shorter than the melt time of the laboratory experiment, indicating the effect of the coating to be starting much earlier during the degradation. It is possible that

this due to the much higher degree of mixing occurring during extrusion, compared to the static situation using the hotblock.

The rate of colour formation has also been investigated at each cycle and this result is shown in figure 6.18 Here it can be seen that a significant difference does appear between the coated and uncoated films, as opposed to the laboratory experiment where no differentiation between samples could be made with any certainty.

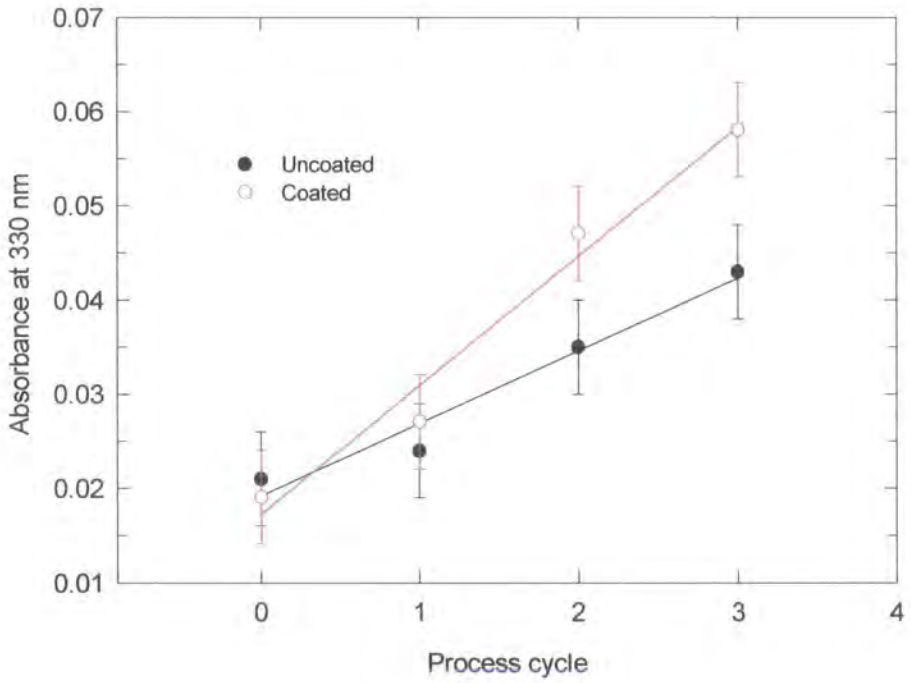

Figure 6.18 Absorption at 330 in coated and uncoated samples

Gel formation in these samples was studied but little gel was detected at any stage of reprocessing, and certainly no difference could be detected between the coated sample and the uncoated sample (see table 6.7). Again, this is attributed to the difference in melt residence time.

Conclusions

The rate of chain scission of re-extruded films is lower for coated material than for uncoated material. This supports the observations seen in the laboratory experiment. The difference between coated and uncoated samples is, however, much greater in this

experiment, and this has been attributed to the differences in sample preparation and the melt regime experienced during degradation.

Unlike the laboratory experiment, a significant difference in the rate of colour formation was seen between coated and uncoated samples, as measured by UV / visible spectroscopy. Again, it is possible that this has arisen because of the fundamental differences in experimental procedures.

experiment, and this has been attributed to the differences in sample preparation and the melt regime experienced during degradation.

Unlike the laboratory experiment, a significant difference in the rate of colour formation was seen between coated and uncoated samples, as measured by UV / visible spectroscopy. Again, it is possible that this has arisen because of the fundamental differences in experimental procedures.

6.4. Further Commentary.

6.4.1 Degradation Kinetics.

The degradation of samples S0-S5 as followed by mass reduction indicates that there is little difference between them, and by implication, the presence of a coating does not interfere with this process. However, examination of the results of the molecular weight degradation show that the addition of TMMM to the coating formulation has a profound effect on the rate of thermo-oxidative degradation. The results presented in table 6.7 show that, for the random scission approximation, those samples including TMMM have a significantly lower rate constant, k, than the samples which do not include TMMM. This analysis appears inadequate in light of the longer term degradation of samples S0-S5, and so an attempt to develop a single kinetic expression has been made. This has been attempted following the principles of Seo and Cloyd [31], and an expression incorporating two different modes of degradation is derived.

By examining the plot of $1/N_t$-$1/N_0$ vs. t (figure 6.9) two distinct regions are apparent. At longer times, the rate of degradation appears to be reduced, and the rate of degradation can be approximated to;

$$\frac{1}{N_t} - \frac{1}{N_0} = A + k_2 t \qquad (6.4)$$

where A is the intercept on the $1/N_t$-$1/N_0$ axis, and k_2 is the rate constant for the slow (predominantly thermal), degradation. At shorter times the degradation can be approximated to the expression already used, (equation 6.2),

$$\frac{1}{N_t} - \frac{1}{N_0} = k_1 t \tag{6.2}$$

where k_1 is the rate constant for the fast (predominantly thermo-oxidative), degradation. To combine both approximations into a single useful expression, the equation developed by Seo and Cloyd has been adapted to this experiment. An equation of the general form,

$$y = A + Ae^{bt} + k_2 t \tag{6.5}$$

where y is $1/N_t$-$1/N_0$, $b = k_1\alpha$, and α is a factor dependant upon the particular nature and concentration of the agents responsible for chain scission. For the hydrolysis of PET, Seo and Cloyd have used $\alpha = k_H(\theta - x)$, where k_H is the rate constant for hydrolysis, and θ and x, are the molar concentrations of ester groups and water respectively. Here, because of the intractable nature of the thermo-oxidative mechanism, no such definition is made. Therefore, α, is defined as a factor by which the rate constant for thermo-oxidative degradation is multiplied in order that the observed rates of degradation are realised. Hence fitting equation 6.5 to the data for sample S0 yields values for k_2 (thermal degradation), and the product $k_1\alpha$. If we assume that k_1 (thermo-oxidative degradation) is approximated by a linear fit to the data at $t < 3600$ s, we can use these values as parameters in the constrained curve fitting for all samples in this set. The results of this are shown in table 6.11. and figure 6.19 shows the non-linear regression fit of equation 6.5 to the data for S0 (uncoated) and S5 (real coating). Given the simplistic form of the model and the constraints of the fitting procedure, acceptable compliance is observed for both these samples.

The values derived for k_1 by the random scission approximation at $t < 3600$ s are similar to, but generally higher than those derived earlier for $t < 7200$ s, see table 6.9. It is noteworthy also, that the rate constant k_2 found by fitting the long time degradation data to equation 6.5 is generally an order of magnitude lower than literature values for

the thermal degradation of PET. For instance, Zimmerman [22] has found values for k_2 of ~3×10^{-7} s^{-1} compared to ~2×10^{-8} s^{-1} here.

We can also use the term b to gain a measure of the extent to which thermo-oxidative degradation is either retarded or accelerated with respect to S0 (i.e. uncontaminated PET). To do this the simple ratio, b_{SX}/b_{S0} is used, and this value is characteristic for each sample, see table 6.11.

At this point it is impossible to determine the nature of the retardation of thermo-oxidative degradation for samples S3-S5. Although it appears that TMMM has caused a change in degradation rate, TMMM may also react with PMMA, or other polymeric components of the coating formulations [32,33], thus producing high molecular weight species, which themselves may interact with PET. It is also possible that such high molecular weight species may account for the decrease in the degradation rate seen in samples S3-S5, without interaction with the PET matrix; if the species remains soluble then it is possible that these fragments are detected by GPC analysis and so skew the relative molecular weight distribution to a higher values. However, given the ratio of coating to PET, this possibility remains somewhat remote.

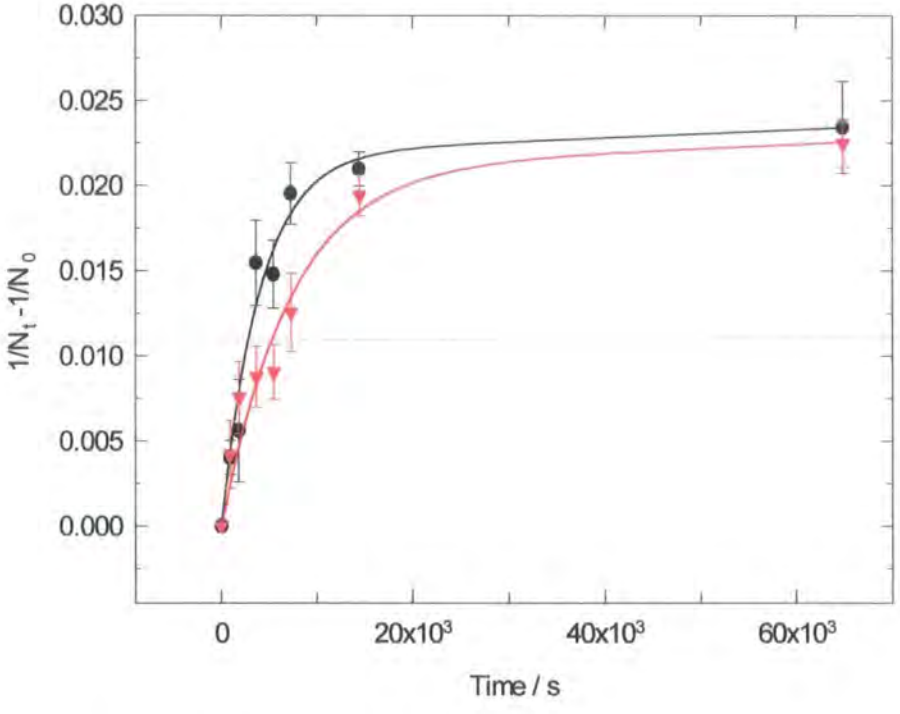

Figure 6.19. Non-linear regression fits of equation 6.5 to data for S0 (black) and S5 (red).

Table 6.11. Coefficients of equation 6.5 for fitted data of samples S0-S5

Sample	Fitted parameters				Residual
	A	b	α	b_{SX} / b_{S0}	R^2
S0	2.2×10^{-2}	2.5×10^{-4}	0.01	1	0.97
S1	2.0×10^{-2}	3.6×10^{-4}	0.007	~1.44	0.97
S2	2.2×10^{-2}	2.1×10^{-4}	0.011	~0.84	0.99
S3	2.1×10^{-2}	1.5×10^{-4}	0.01	~0.6	0.96
S4	2.0×10^{-2}	1.4×10^{-4}	0.01	~0.56	0.93
S5	2.1×10^{-2}	1.4×10^{-4}	0.01	~0.56	0.96

6.4.2. Limiting Molecular Weight.

An interesting feature of the GPC analysis of samples S0-S5 is that there appears to be a limiting minimum molecular weight, which is similar for all samples in the set. It has already been established that the initial reaction is approximately 100 × faster than the reaction rate at longer times, i.e. > 2 hrs. It has been postulated that this phenomena is due to the difference between thermo-oxidative and thermal degradation. Why does thermo-oxidation seem to slow and give way to thermal degradation at ~ 2hrs degradation ? The answer to this seems to lie in the mechanism of chain scission during thermo-oxiadative degradation (schemes 6.1 and 6.2). It is well established that oxidation of PET occurs by abstraction of methylene protons [27-30], and that DEG protons are approximately ~1000 × more reactive than protons of an ethylene glycol unit [29,34]. Hence it is reasonable to assume that chain scission will occur preferentially at a DEG unit. If this were the case it should be possible to calculate the minimum M_N given a knowledge of the initial DEG content.

The initial DEG content of this polymer is 1.7 % by weight, which is equivalent to 3.0 mol % of glycol as DEG. If we consider that the time period of the reaction is long enough to exhaust all the DEG units it is a facile matter to calculate the limiting M_N, based on the initial M_N for each sample. The theoretical minimum M_N is shown in table 6.12.

Table 6.12 Theoretical minimum M_N for samples S0-S5.

Sample	M_N (theoretical)	M_N (measured)
S0	6,410	6,170
S1	6,820	6,720
S2	6,050	6,051
S3	6,410	7,250
S4	6,250	7,500
S5	6,150	7,400

The values in table 6.12 compare well with the M_N values obtained by GPC for degradation times in excess of 2 hrs, and qualitatively supports the hypothesis given above. At this juncture, any further inferences concerning the rates of DEG scission compared to the scission of normal glycol units is impossible because of the influence of other degradative mechanisms (thermal, cross linking etc.).

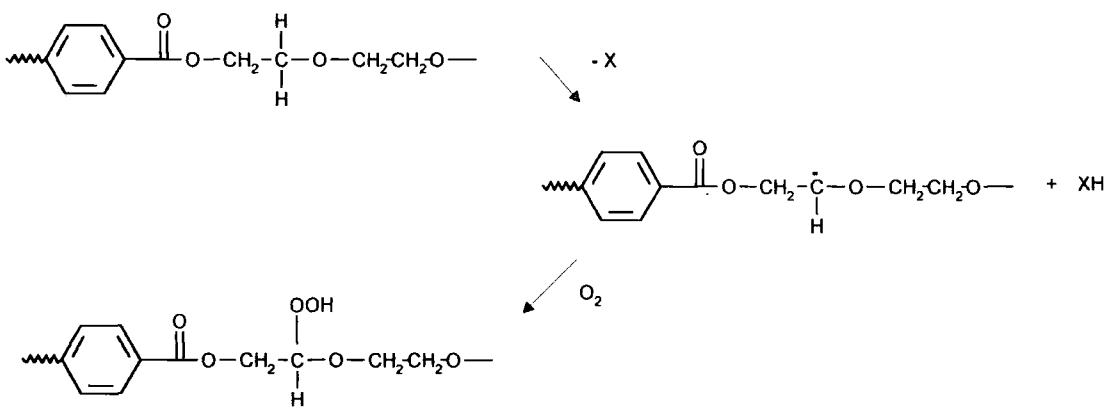

Scheme 6.1. Oxidation of PET glycol protons.

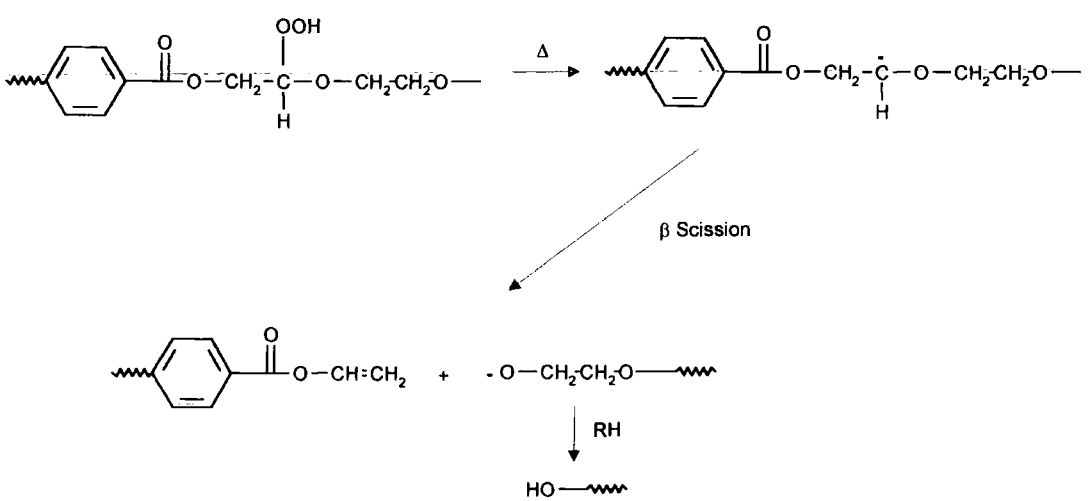

Scheme 6.2 Breakdown of peroxy radical on DEG unit and subsequent chain scission.

6.4.3. Effect of Coatings additives on Chain Scission

It has now been established that the presence of TMMM or the reaction product of TMMM and other coating components, has a retarding effect upon the rate of chain scission during thermo-oxidative degradation. The effect of varying the concentration of TMMM and the catalyst associated with this crosslinking agent, APTSA, will now be discussed.

From figure 6.13. it is apparent that an increase in the concentration of TMMM in the coating formulation has an influence on the resultant molecular weight after 30 minutes thermo-oxidative degradation at 563K. Over this timescale, it is assumed that the degradation can be approximated by a random scission process, and therefore the data for samples S6-S10 can be replotted in the form of rate vs. $[TMMM]^x$, where x is the order of the reaction. The rate of reaction vs. [TMMM] for different values of x (order of reaction) are shown in figure 6.20, and it is clear that the reaction is ~½ order with respect to [TMMM].

The rate of degradation of coated PET with respect to the concentration of TMMM can now be expressed as;

$$1/N_t - 1/N_0 \approx a[TMMM]^{½} + c \qquad (6.6)$$

where a is the gradient of the straight line and c is the rate of degradation when [TMMM] = 0. It must be emphasised that this expression is only applicable in the approximation of a random scission degradation process, and as such is only valid for shorter degradation times, (~ 30 minutes).

It is noted that the inclusion of TMMM within a coating solution has a greater effect upon the value for M_W than for M_N. This is to be expected as the second moment of the distribution of molecular size is weighted towards the higher molecular weight chains, (see Chapter 2).

In the case of APTSA, the effect of concentration upon rate of molecular weight degradation is less well defined. From figure 6.14 it is clear that there is no recognisable trend in the plot of molecular weight vs. concentration of APTSA added to the coating formulation for samples S11-S15. In this experiment, the errors in molecular weight

measurement are large enough to negate any reduction in molecular weight being due to increasing APTSA concentration, (see figure 6.14), and it is concluded that this component has no real influence upon the rate of chain scission.

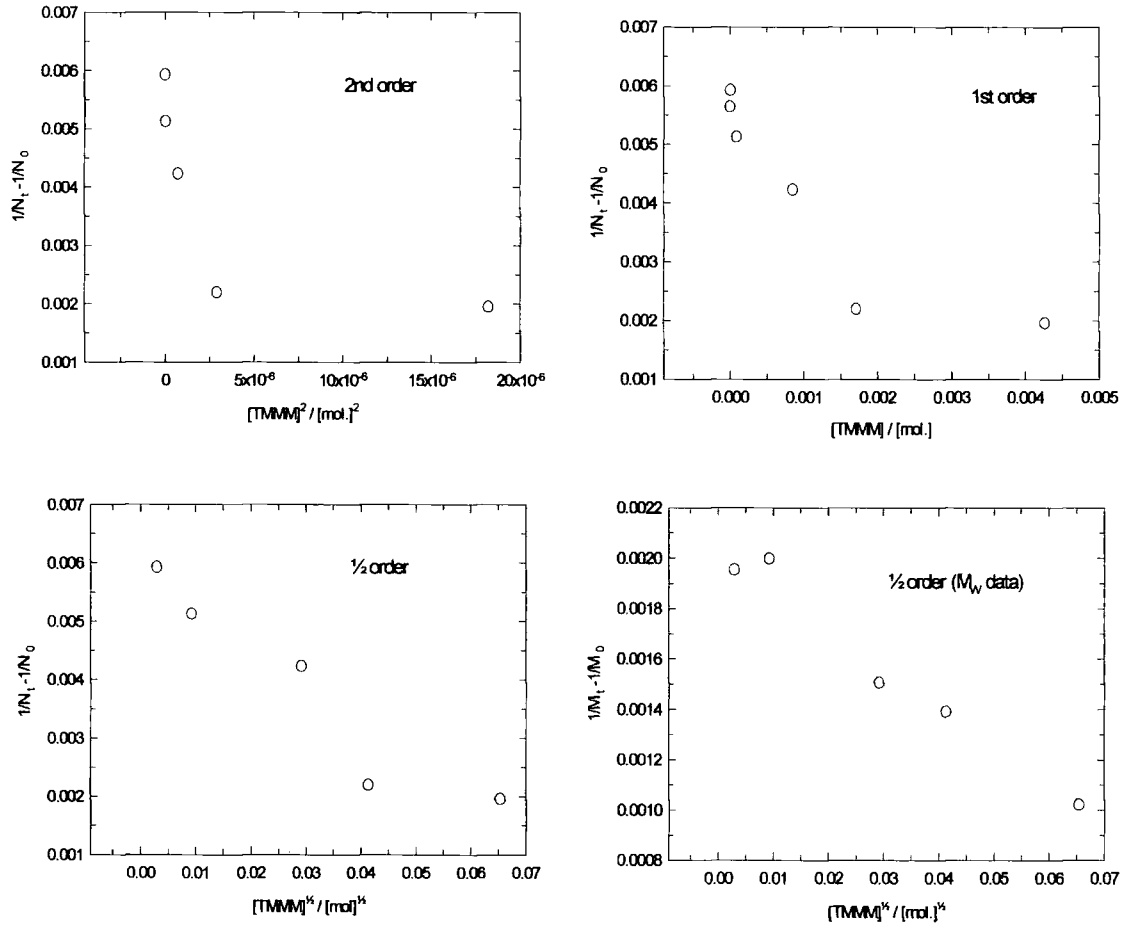

Figure 6.20. Rate of chain scission vs. [TMMM]

6.4.4. Relationship Between Chain scission and Gel formation

The results described in section 6.3 have shown that samples S3-S5 show a marked reduction in chain scission, compared to samples S0-S2, but have a greater propensity for gel formation (see figures 6.9 and 6.12). In order to establish if a relationship exists between these two phenomena the chain scission data are plotted against the gel content for each sample in figure 6.21. Not surprisingly, the samples

S3-S5 occupy distinct and separate area of the plot. This was expected given the nature of the previous results for gelation and chain scission. However, the gel formation in all samples seems to accelerate as chain scission progresses beyond ~ 30 min. Indicating dependency of gel formation with chain length.

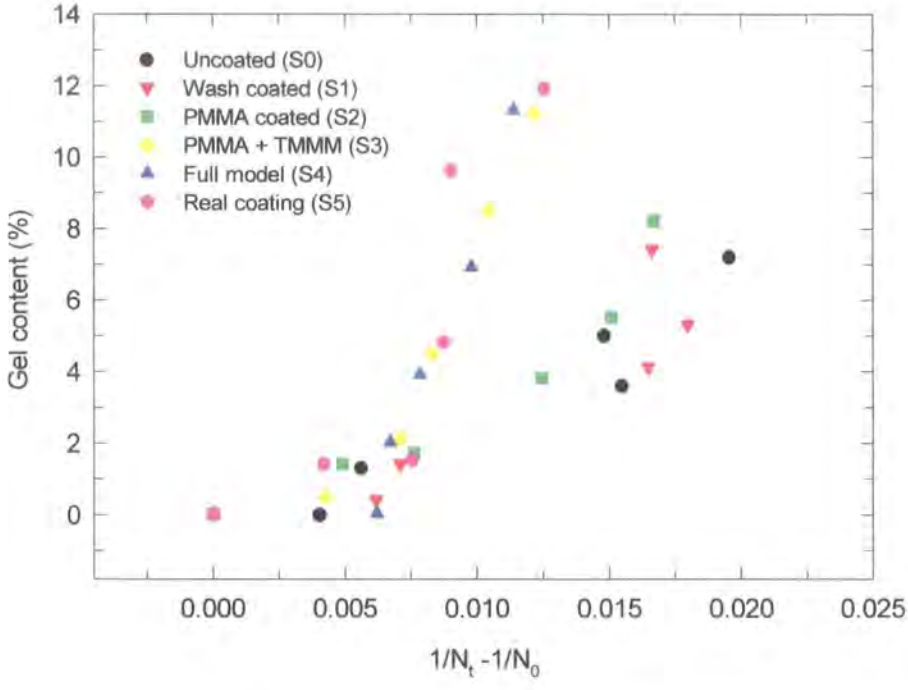

Figure 6.21. gel content vs. $1/N_t - 1/N_0$ for samples S0-S5.

To further this analysis, the theoretical treatment adopted by Yoda *et al* [19], was followed. Here, an expression developed by Charlesby and Pinner [35], was used;

$$S + S^{\frac{1}{2}} = pq^{-1} + (qut)^{-1} \tag{6.7}$$

where S is the soluble fraction of the polymer sample, p and q are the probabilities that a repeating unit is fractured and crosslinked respectively, in unit time, and u is the average number of repeating units in a polymer chain at time $t=0$. Hence, information pertaining to the probabilities of scission and crosslinking are obtained from a plot of $S+S^{½}$ vs. $(ut)^{-1}$. Such a plot is shown in figure 6.22. Values for u, are derived from M_N values (GPC) shown in table 6.7. As can be seen, all samples display a similar behaviour at $t <$ 1 hr, indicating a similar rate of crosslinking, whereas after 1 hr. samples with TMMM

develop a larger gel fraction at an accelerated rate. Figure 6.22 shows a change in behaviour at $(u.t)^{-1} \sim 2 \times 10^{-6}$ (i.e. approximately 1 hr degradation), whereas Yoda *et al,* observed this change at approximately 2 hrs at 573K.

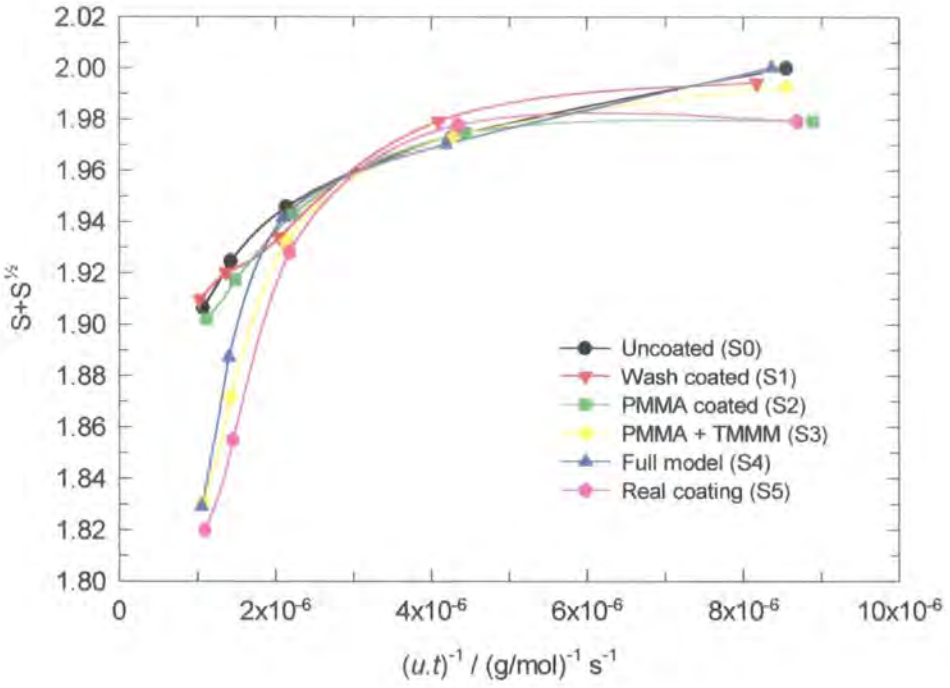

Figure 6.22. $S+S^{1/2}$ vs. $(u.t)^{-1}$ after Charlesby and Pinner [35] and Yoda et al [19].

This difference could be the result of experimental differences and sample geometry, i.e. the thickness of the melt layer will play an important role as the oxidation of PET is known to be diffusion controlled [19,20,36].

It is quite clear from figures 6.21. and 6.22. that samples S3-S5 behave in a significantly different way to samples S0-S2. The inclusion of TMMM in the coating formulation has not only altered the chain scission mechanism, but has also increased the propensity for gel formation. This at first would seem to be a discrepancy in the analysis. Yoda *et al* [19] have postulated that the gelation of PET is time dependant, in that gel product is only formed when a significant degree of chain scission has occurred. this would lead to the conclusion that a lower rate of chain scission, or higher retained molecular weight, would yield a product with a lower gel content. In the case of samples S3-S5, the lower rate of chain scission has *increased* the rate of gel formation. Although no conclusions as to the nature of this discrepancy can be made, it is

postulated that the mechanism by which the TMMM / coating product interacts with PET has produced structures with a low enough crosslink density to still be soluble, and therefore detectable by GPC, and so these contribute towards the molecular weight distribution. Other structures of higher crosslink density are also formed, which are non-soluble and these contribute towards the high gel content. This would imply some chain extension mechanism by the TMMM, which is not unreasonable assumption. Chain extension of PET by multi valent species has been shown to be an effective way of maintaining molecular weight during melt processing [37,38]. (see figure 6.23)

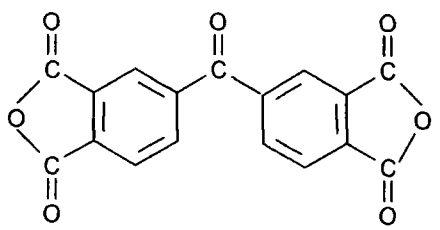

Benzophenonetetracarboxylic dianhydride.
(BDTA)

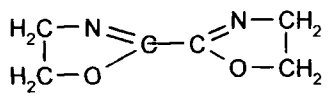

2,2'-bis(2-oxazoline)
(2,2BO)

Figure 6.23. Chain extenders used in PET. BDTA ref 37, 2,2BO ref 38.

Other possible interactions may alter the mechanisms of the free radical reactions which lead to chain scission and gel formation in PET. Hong has shown that HMMM (hexa methoxy methylmelamine) has a profound effect upon the rates of peroxidation and crosslinking of polyglycols. [39] If a similar reaction can be inferred for TMMM then this could also explain the increase the gel formation in samples S3-S5 see schemes 6.3 and 6.4.

The mechanism of gel formation in pure PET is shown in scheme 6.5. If the gel product formed in the coated samples was shown to contain no traces of TMMM or other coated products then, this would support the hypothesis of increased gelation by a catalytic effect. If gel product was formed as a result of the reaction of TMMM with the coating and with PET then these species should be detectable within the insoluble gel. An attempt to detect coating species within gel products from S4 and S5 was attempted by NMR, but little progress was made because no solvent could be found in which the gel was adequately soluble. Hence, we can only speculate as to the nature of this gel.

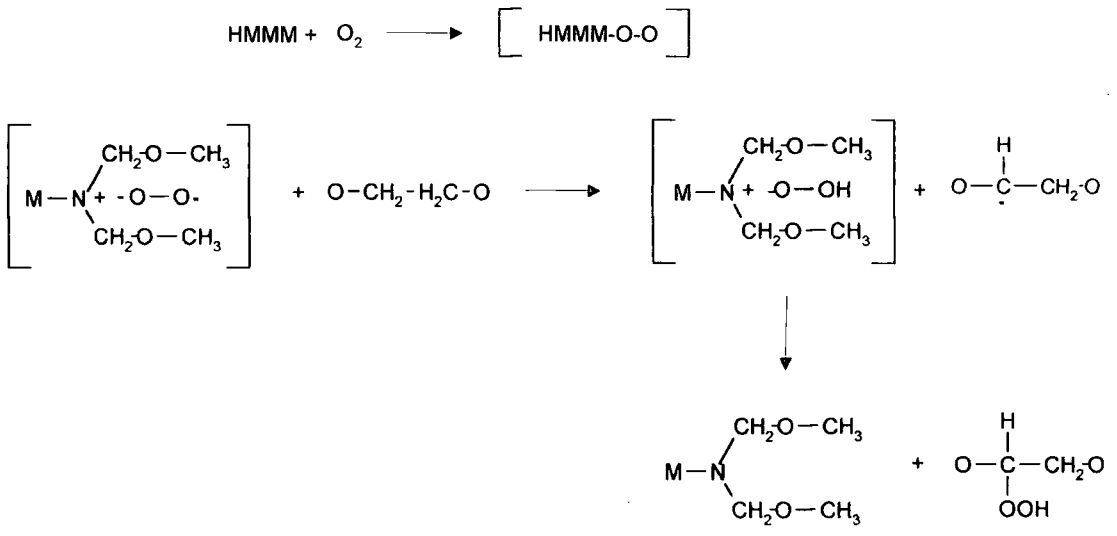

Scheme 6.3 Hong's mechanism for the HMMM catalysed peroxidation of glycols

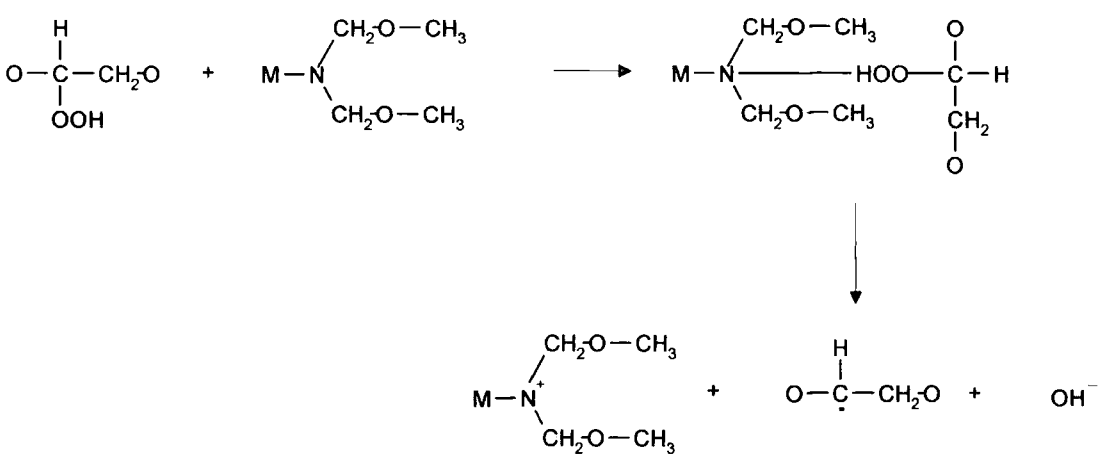

Scheme 6.4 HMMM catalysed decomposition of peroxy glycol . In this scheme and scheme 6.3. M represents the rest of the methyl melamine structure.

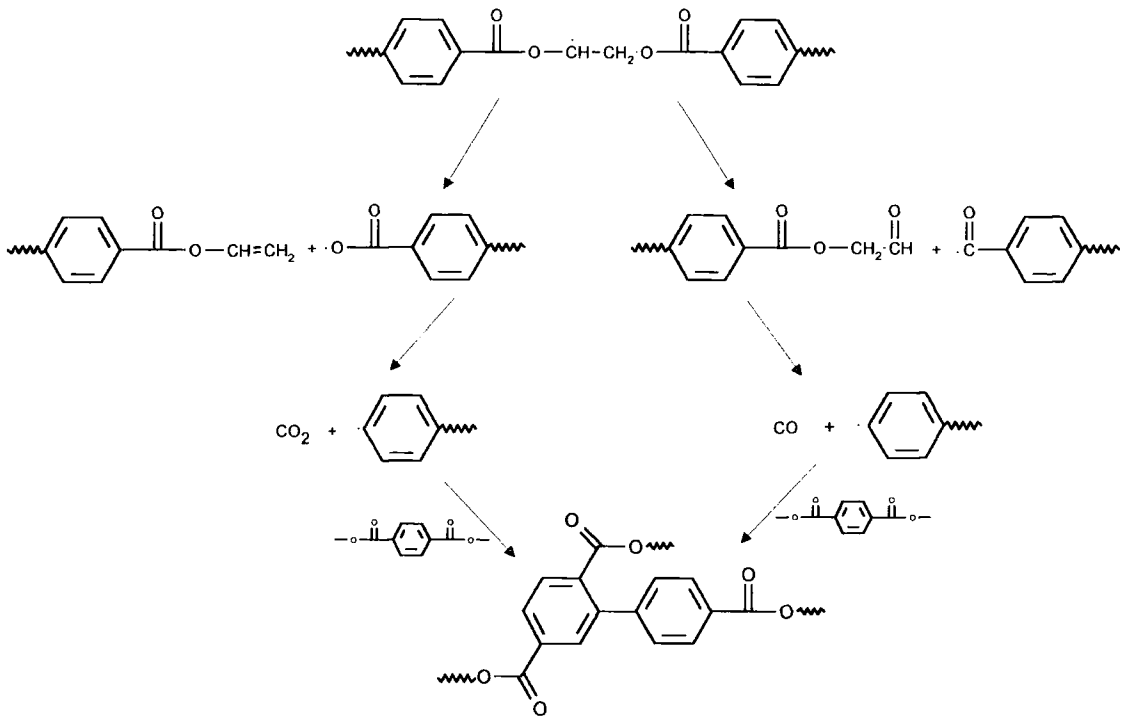

Scheme 6.5. Formation of gel in pure PET, after Nealy and Adams [20]

6.4.5. Industrial Scale Experiments.

As already described the large scale reprocessing of PET is of commercial importance to producers of finished polyester articles. The recycle of PET in film processing is generally of an uncontrolled nature, and it is rare that feedstocks are separated or differentiated with respect to their source or properties. Many reclaim streams may even include significant proportions of other polymers (i.e. > 1%) [40].

With respect to the manufacture of PET film, reclaimed material has been generated and characterised by the techniques previously described. The complexity and financial constraints which would burden a thorough and exact reclaim experiment, mean that industrial scale recycling experiments are themselves usually curtailed, and results extrapolated into time scales and processes normally used during film manufacture. To this end, the reclaim procedure used in this study has taken the form of

a several re-extrusions, accompanied by the associated drying and handling procedures, of specifically tailored films of known composition. The films described in the previous section are discussed thoroughly here.

Firstly we consider the molecular weight characterisation of polymer taken from each stage of the experiment.

From figure 6.17 it is obvious that the rate of chain scission for the coated film is lower than that of the uncoated film, supporting the laboratory scale observations for continuous melt degradation. The data is plotted for each pass through the extruder, but as the equilibrium residence time is known for the extruder operating under the condition discussed in section 6.2, then an estimate of the time in the melt can be made. This result is plotted in figure 6.24.

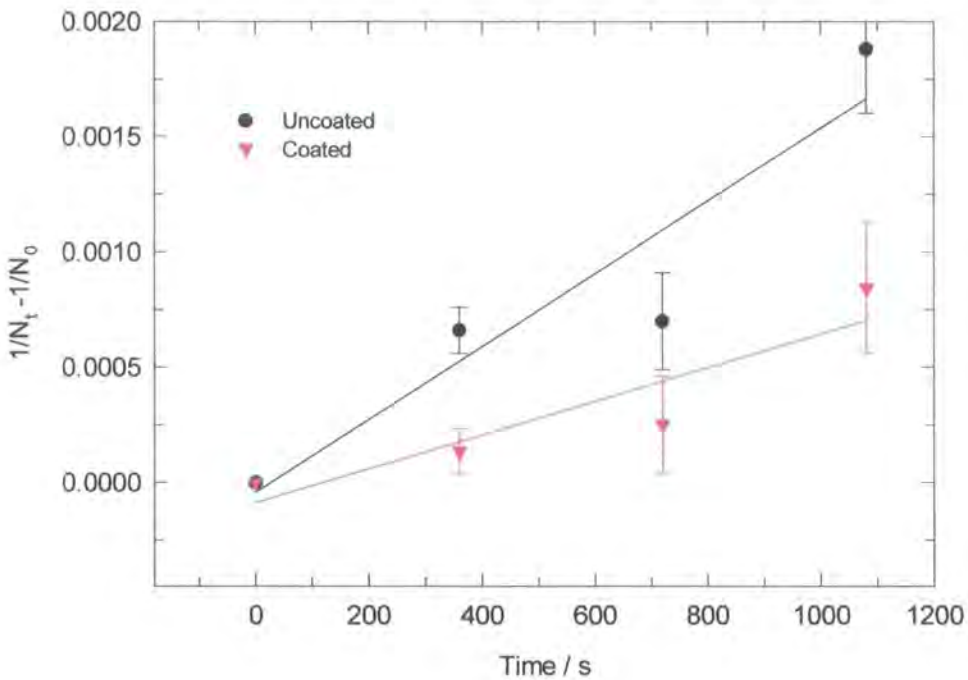

Figure 6.24. Chain scission for extrusion experiment replotted with as a function of time in melt.

This graphical representation of the data allows an estimation of the rate of degradation to be made in the limit of the random scission approximation. The rate constants for chain scission are given in table 6.13. These results are in good agreement with the results obtained earlier for the laboratory experiment, despite the radical

differences in the experimentation. However, it is immediately apparent that the difference between uncoated and coated is evident from the first re-extrusion process, (the extrusion process during film making has been ignored as the difference between the two films was generated *after* this process).

Table 6.13. Rate constant k for M_N degradation of re-extruded samples

Sample	k / s^{-1}
Uncoated	1.5×10^{-6}
Coated	7.3×10^{-7}

Thiese rate constants must be treated with caution; the estimate of melt time is by no means a definitive time of degradation. The time between each extrusion must also be considered, as the samples were subjected to an air drying regime, and Jabarin and Lofgren have shown that drying is a critical parameter in the thermo-oxidative stability of PET [9].

6.5. Conclusions.

1) The presence of a coating, of varying degrees of complexity was found to have no influence on the weight loss stability of PET films.

2) The rate constants found for the degradatiion of PET are in good agreement with previously published results. The thermo-oxidative stability of PET films has been shown to be influenced by the presence of formulated coatings, and the presence of these coatings reduces the measured rate costant by a factor of ~1.6 - 2.

3) A single kinetic term for thermo-oxidative degradation has been established in which a rate constant for thermal degradation has been estimated as $\sim 2 \times 10^{-8}$ s^{-1}. The equation is of the general form;

$$y = A + Ae^{bt} + k_2 t$$

4) Variations in the concentrations of coatings components have been shown to exhibit an influence upon the thermo-oxidative degradation rate. The commonly used

crosslinking agent TMMM (tri-methoxy methymelamine) was found to influence the rate of chain scission according to the following relation;

$$1/N_t - 1/N_0 \approx a[TMMM]^{½} + c$$

where [TMMM] is the initial concentration.

5) Variations in APTSA, the acid catalyst for TMMM, were shown to have no discernable effect on rate of chain scission within the random scission approximation. However, high concentrations of APTSA were shown to give a greater discolouration upon degradation after 30 min.

6) The presence of a fully formulated coating also has a pronounced effect on the propensity for gel formation. The rate constant for gel formation has been shown to be 1st order or pseudo 1st ordr, and is approximately ~ 1.6-1.8 times faster for samples with coatings containing TMMM.

7) Variations in concentration of TMMM and APTSA only influenced the gel formation at the highest levels investigated.

8) An industrial scale experiment has shown that the degradation of coated PET is similarly reduced when measured via repeated re-extrusion, yielding a rate constant approximately one - half of that for the uncoated product.

9) The industrial scale experiment has also shown that coated PET discolours to a greater extent than the uncoated equivalent, during repeated re-extrusion. A colour difference between laboratory samples was not detected by UV / visible spectroscopy.

6.6. References.

[1] Davies, C., Naoush, H. F. and Rees, G. J., *Polym. Int.*, 1996, **41**, pp 215 - 225.

[2] Subramanian, P. M., Mehra, V., *Antec '93*, 1993, pp 3206 - 3207.

[3] Janocha, E., Janocha, S., Hopper, M.J. and Mackenzie, K.J. in '*Encyclopeadia of Polymer Science and Technology*' **12** , 1984.

[4] Kamatani, H. and Kuze, K., *Polym J.*, 1979, **11**, pp 787 - 793.

[5] Karayannidis, G., Sideridou, I., Zamboulis, D., Stalidis, G., Bikiaris, D. and Wilmes, A., *Angwandte Makromol. Chem.*, 1993, **208**, pp 117 - 124.

[6] Booth, G. L. "Coating equipment and processes".1970, Lockwood Pub. Co. Inc.

[7] Buxbaum, L. H., *Chem. Int. Edit.*, 1968, **3**, pp 182 - 190.

[8] Briston, J.H., '*Plastic Films*' 1974, Iliffe Books.

[9] Jabarin, S. A. and Lofgran, E. A., *Polym. Eng. & Sci.*, 1984, **24**, pp 1056 - 1063.

[10] Butler, T. I., *J. Plastic Film & Sheeting*, 1990, **6**, pp 247 - 259.

[11] Goodings, E. P., *Soc. Chem. Ind.*, 1961, **13**, pp 211 - 228.

[12] Marshall, I. and Todd, A., *Trans. Faraday Soc.*, 1953, **49**, pp 67 - 78.

13) Montaudo, G., Puglisi, C. and Samperi, F., *Polym. Deg. Stab.*, 1993, **42**, pp 13 - 28.

[14] Allan, R. J. P., Iengar, H. V. R. and Ritchie, P. D., *J. Chem. Soc.*, 1957, pp 2107 - 2113.

[15] Villain, F., Coudane, J. and Vert, M., *Polym. Deg. Stab.*, 1994, **43**, pp 431 - 440.

[16] Tabankia, M. H. and Gardette, J. -L., *Polym. Deg. Stab.*, 1986, **14**, pp 351 - 365.

[17] Scheirs, J. and Gardette, J. -L., *Polym. Deg. Stab.*, 1997, **56**, pp 339 - 350.

[18] Day, M. and Wiles, D. M., *J. Appl. Polym. Sci.*,1972, **16**, pp 191 - 202.

[19] Yoda, K., Tsuboi, A., Wada, M. and Yamadera, R., *J. Appl. Polym. Sci.*, 1970, **14**, pp 2357 - 2376.

[20] Spanninger, P. A., *J. Polym. Sci.*, 1974, **12**, pp 709 - 717.

[21] Zimmermann, H. and Schanf, E., *Therm. Anal.*, 1974, **2**, p 137.

[22] Zimmermann, H., "Developments in Polmer Degradation", 1984, **5**, pp 79 - 119.

[23] Peiyuan, L. and Rongrui, W., *Acta. Polym. Sinica*, 1988, **5**, pp 331 - 336.

[24] Halek, G. W., *J. Polym. Sci.*, 1986, Polym. Symposium **74**, pp 83 - 92.

[25] Fredrikssen, E., *D. Phil. Thesis*, 1999, Univ. Sussex.

[26] Jellineck, H. H., *J. Polym. Sci.*, 1950, **5**, p 264.

[27] Edge, M., Allen, N. S., Wiles, R., McDonald, W. and Mortlock, S. V., *Polym.*, 1995, **36**, pp 227 - 234.

[28] Edge, M., Wiles, R., Allen, N. S., McDonald, W. A. and Mortlock, S. V., *Polym. Deg. Stab.*, 1996, **53,** pp 141 - 151.

[29] Gächter, R., Muller, H., " Plastics Additives Handbook 3rd Edition.", 1990, Hanser Pub.

[30] Robinson, J., Dupont Teijin Films Ltd., Private Communication.

[31] Seo, K. S. and Cloyd, J. D., *J. Appl. Polym. Sci.*, 1991, **42**, pp 845 - 850.

[32] Haacke, G., Brinen, J. S. and Larkin, P. J., *J. Coatings Technol.*, 1995, **67**, pp 29 - 34.

[33] Blank, W. J., *J Coatings, Technol.*, 1979, **51**, pp 61 - 70.

[34] Looney, K., Dupont Teijin Films Ltd., Private Communication.

[35] Charlesby, A. and Pinner, S. H., *Proc. Roy. Soc.*, 1959, **249**, p 367.

[36] Nealy, D. L. and Adams, L. J., *J. Polym. Sci.*, 1971, **9**, pp 2063 - 2070.

[37] Ibeh, C., Graham, G. W. and Doone, R. G., *Antec '93,* pp 3198 - 3205.

[38] Cardi, N., Po, R., Giannotta, G., Occhiello, E., Garbessi, F. and Messina, G., *J. Appl. Polm. Sci.*, 1993, **50,** pp 1501 - 1509.

[39] Hong, X. -Y., *Prog. Org. Coatings*, 1995, **26**, pp 121 - 129.

[40] La Mantia, F.P., *Polym. Deg. Stab.* 1993, **42**, pp 213 - 218.

Chapter 7

Conclusions and Further Work

7.1 Thesis Conclusions

This thesis has attempted to investigate the interactions between poly(ethylene terephthalate) and poly(methyl methacrylate), in the bulk state as intimately mixed blends, as thin films, and as a an industrially produced finished film. An emphasis has been placed upon the physical changes in these two polymers as a result of thermal treatments, in order that the degradation of the two polymers can be followed. The thermal treatments employed have generally been within the PET processing window (i.e. ~ 573K), a temperature at which PMMA rapidly degrades, hence we are concerned with the degradation of the PMMA and the interaction of degradation products with PET, and with each other.

As intimately mixed blends, the increase in methyl end groups of PET in the blend was seen at all temperatures of reaction, whereas the pure homopolymer only showed an increase at the highest annealing temperature (573K). This was taken as evidence of the direct interchange reaction between PET and PMMA as shown in figure 3.3. Further evidence for this reaction was seen an inhibition in crystallisation of the blends compared to pure PET, by as much as 8K (at 523K) which is consistent with a grafted gel structure forming at the interface between the two polymer phases. This grafted structure could be separated by its non soluble nature. Further more the degradation of PMMA was seen to be inhibited in the presence of PET and this could be rationalised as the result of an interpolymer reaction.

Throughout this thesis the degradation of PMMA has been assumed to be a 1st order reaction and this was seen to be consistent with literature reports concerning the degradation of PMMA at temperature > 473K. The weight loss from PET is consistent with a physical process such as volatilisation of the low molecular weight products, etc., and under anaerobic conditions PET is seen to be very stable.

Using ellipsometry, thin films of PET were seen to reduce in thickness upon annealing at 493K, and this has been attributed to the crystallisation of the polymer. Avrami analysis has shown that the rate of crystallisation reduces as the film thickness is reduced, and the extent of crystallinity in the film was also much reduced by decreasing the film thickness

Thin films of PMMA were also seen to reduce in thickness an this was attributed to the normal depolymerisation of PMMA under thermal conditions. At 573K the layer depletion was seen to be dependent upon the film thickness and thinner films degraded quicker than bulk samples in accordance with the shorter diffusion path hypothesis.

Neutron reflectivity has revealed that the interdiffusion of PET and PMMA occurs at 493 and 573K, although comparatively narrow interfaces are formed ($< R_g$). The equilibrium interfacial width at 493K is seen to be 7.7 nm, and 5 nm at 573K. Mutual diffusion coefficients have been calculated as 3-5 $x10^{-21}$ cm^2/sec, much lower than self diffusion coefficients for these polymers indicating that the polymers are immiscible. The increased distance at 493K is attributed to crystalline roughness developing in the PET, a phenomena also seen at the surface of single PET films. The Flory -Huggins interaction parameter for the PET -PMMA system is calculated as 0.03 using the symmetrical approach of Helfand and Tagami, and 0.04 using the asymmetrical approach of Helfand and Sapse. A contribution from Capillary wave broadening, and is estimated from a numerical solution as between 1 and 4.9 nm. The interfacial tension calculated from these interfacial widths is > 2 dynes/cm^2 at 573K. Depolymerisation of the PMMA layer was seen at 493K and 573K. as expected under these conditions However, at 573K only a thin layer of PMMA was seen to still in evidence (~ 6 nm). Most interestingly, this layer was completely wetted across the PET surface. This indicated that, in an industrial process, a significant amount of PMMA will remain even during high temperature reclaim procedures, which could then interact with the PET to form non-processable structures.

Marker movement analysis has shown that crystallisation and interfacial movement can be monitored simultaneously provided accurate comparisons are made with independent measurements for single layers. The interfacial movement at both 493K and 573K is seen to be 1-2 nm. i.e. the distance of a few statistical segment lengths. At 493K this phenomena has been attributed to the densification of the PET layer by crystallisation. At 573K, formation of a grafted structure at the interface as seen

in the thermally reacted blend system, is postulated. This is supported by observing the asymmetric nature of the marker distribution across the interface, i.e. indicating PET to the lower viscosity polymer, despite rheological evidence to the contrary.

The reclaim cycle of coated film article was simulated in the laboratory and on an industrial scale. Under thermo-oxidative conditions the PET was seen to degrade in accordance with accepted theory. The formulation of the coating was seen to influence the degradation rate of the film, with the crosslinking agent tri-methoxy methylmelamine (TMMM), exerting the strongest influence on rate of degradation. In fact the rate of chain scission was shown to be ½ order, with respect to the initial concentration of TMMM. The rate of gel formation was also increased by TMMM indicating a chain extension or branching mechanism during reclaim.

The colour of the degraded material was seen to heavily influenced by the concentration of gel (non soluble) material in the sample, and this was taken as evidence of the thermo-oxidative degradation reaction occurring in PET.

These results could be successfully extrapolated into an industrial scale experiment, where it was found that a fully formulated coating, influences the degradation of PET by a factor of one -half of the uncoated degradation rate.

7.2 Suggestion for Further Work

The degradation of PET is of critical importance in the film manufacturing industry. Hence the influence of other materials needs to be understood fully in order that product performance and the recovery of scrap material can be optimised for maximum commercial benefit. The influence of coating components on the degradation of PET films has been studied at one temperature (563K), and the next step would be extract similar information for the full PET processing temperature range, i.e. 543K - 583K. This would also allow activation energies to be calculated for the various degradation mechanisms, such as chain scission and gel formation.

The influence of a second phase on the crystallisation of PET needs to be investigated further, as the variability in crystallinity across a ~7 m wide web in a commercial manufacturing process may cause mechanical instability in the film leading to splitting and loss of production. The same argument is true for the presence of 'gel' in

the polymer, which we have seen can be created by the presence of a second phase. The exact nature of PET PMMA graft copolymer and its dependence on temperature and time and concentration of PMMA and PET is important and needs to be investigated thoroughly. This analysis needs to be extended to the interaction with other non condensation polymers which may be used as coating materials.

An independent verification of the Flory - Hugins interaction parameter would be useful in extracting the extent to which the amorphous PET / PMMA interface is broadened by capillary waves. It seems plausible that this could be accomplished by a measurement of the interfacial tension between the two polymers or by further analysis of the interface between the two polymers. Extending the PET/PMMA interfacial broadening to account for different molecular weights and the effects of polydispersity would also be useful in the context of an industrial coating operation. A knowledge of the interface between PET and other polymers used in coating formulations, e.g. polystyrene, would also be useful. The adhesion between these polymers needs to be fully understood in order that the formulation of coatings can be optimised with respect to their subsequent performance and their reclaimability. An interesting area for investigation is the formation of an interface under dynamic conditions, i.e. when the two polymers forming the interface are subjected to lateral force or flow, such as a transverse draw in a commercial stenter process. Such experiments are currently been considered by DuPont Teijin Films inc.

The marker movement experiment also needs to be conducted at lower temperatures and longer times to eliminate the possibility of PMMA degradation and utilising A-PET copolymer to eliminate PET crystallisation, hence the interfacial movement (or not) could be monitored unambiguously.